THE HONG KONG
POLYTECHNIC UNIVERSITY
香港理工大學
Pao Yue-kong Library
包玉剛圖書館

Copyright Undertaking

This thesis is protected by copyright, with all rights reserved.

By reading and using the thesis, the reader understands and agrees to the following terms:

1. The reader will abide by the rules and legal ordinances governing copyright regarding the use of the thesis.
2. The reader will use the thesis for the purpose of research or private study only and not for distribution or further reproduction or any other purpose.
3. The reader agrees to indemnify and hold the University harmless from and against any loss, damage, cost, liability or expenses arising from copyright infringement or unauthorized usage.

If you have reasons to believe that any materials in this thesis are deemed not suitable to be distributed in this form, or a copyright owner having difficulty with the material being included in our database, please contact lbsys@polyu.edu.hk providing details. The Library will look into your claim and consider taking remedial action upon receipt of the written requests.

Pao Yue-kong Library, The Hong Kong Polytechnic University, Hung Hom, Kowloon, Hong Kong

http://www.lib.polyu.edu.hk

CFD Simulation of Floor Level Air Supply Method and Evaluation of System Energy Savings

Xu Hongtao

A thesis submitted in partial fulfillment of the requirements for the Degree of Doctor of Philosophy

Department of Building Services Engineering
The Hong Kong Polytechnic University

July 2005

Pao Yue-kong Library
PolyU · Hong Kong

CERTIFICATE OF ORIGINALITY

I hereby declare that this thesis is my own work and that, to the best of my knowledge and belief, it reproduces no material previously published or written, nor material that has been accepted for the award of any other degree or diploma, except where due acknowledgement has been made in the text.

Xu Hongtao

Department of Building Services Engineering

The Hong Kong Polytechnic University

Hong Kong SAR, China

July, 2005

ABSTRACT

Abstract of thesis entitled: CFD Simulation of Floor Level Air Supply Method and Evaluation of System Energy Savings

Submitted by : Xu Hongtao

For the degree of : Doctor of Philosophy

at The Hong Kong Polytechnic University in July, 2005

The supply diffuser influences air flow patterns in the space with the heating, ventilating and air-conditioning (HVAC) system. How to accurately quantify its impact is essential for the proper design of air distribution systems. Some simplified CFD (Computational Fluid Dynamics) modeling methods are available. Among them, the box and momentum methods are the most popularly used. Different from the mixing system, the underfloor air distribution (UFAD) system employs the supply diffuser in the occupied zone and takes advantage of room air stratification for thermal comfort and energy saving. The design of this system is more sophisticated but requires practical tools, and the objective of this thesis is to develop such tools based on the supply diffuser simulation and air temperature stratification models.

The box method cannot be employed where the buoyancy force dominates indoor air flow, as is the case with the UFAD system. In this thesis, the fully represented geometry method (FRGM) was proposed to model the supply diffuser. The aim is to reveal the influence of diffuser configurations on the air flow pattern near the supply diffuser. This method was validated with the experimental data from a

precombustion chamber. Employing the standard $\kappa - \varepsilon$ turbulence model, the FRGM presented more accurate results near the supply diffuser than the momentum method. With this method, the need to measure the input conditions near the supply diffuser can potentially be eliminated, which is difficult and inaccurate to do due to the large gradients. The RNG $\kappa - \varepsilon$ turbulence model was also investigated with this method and it was found more suitable for predicting flow patterns in the downstream recirculation zone.

With the FRGM, two supply diffusers, named the swirling and square diffusers, were employed in UFAD systems for different thermal environment investigations. It was found that indoor air temperature stratification can be maintained with both supply diffusers, but the thermal environment in the occupied zone was greatly influenced by the configuration of the supply diffuser. The swirling diffuser generated a more uniform thermal environment than the square diffuser due to the 'swirling' characteristic. Furthermore, the effects of the vane declining angles of the swirling diffuser were investigated, and it was found that two different flow patterns can be created, the horizontal and vertical flows. The horizontal flow is preferable for better thermal comfort.

Indoor air temperature stratification in the UFAD system offers an opportunity for cooling load reduction and energy saving potential, as compared with the mixing system. Most energy simulation programs should be revised to take into account the stratification in the UFAD system. In this thesis, a numerical method by which the energy analysis program ACCURACY is coupled with the CFD technique was presented. The dimensionless temperature coefficient was defined and obtained through the CFD simulation with the boundary conditions calculated by

ACCURACY. In conditions where the indoor heat sources dominated the whole cooling load in an office room, it was concluded that, for a constant air volume (CAV) supply, the dimensionless temperature coefficient was affected by the elevation of the electronic equipment when other heat sources were fixed. For a variable air volume (VAV) supply, the supply air flow rate dominated the dimensionless temperature coefficient when all heat sources were fixed. When compared with the mixing system, the UFAD system derives its energy saving potential from the following three factors: an extended free cooling time, a reduced ventilation load, and increased Coefficient of Performance (COP) for chillers.

The cooled ceiling (CC) is a representative of HVAC systems. When it was combined with a DV (displacement ventilation) or UFAD system, the typical indoor air temperature stratification was suppressed and the indoor air temperature at head level (1.1m) was almost equal to the exhaust air temperature in a small office room, signifying that the uniform indoor air temperature model can be employed for the energy analysis of the combined systems, CC/DV and CC/UFAD. Based on the same thermal sensation index (PMV=0) at head level, the combined systems presented a more uniform thermal environment in the occupied zone as a result of the employment of CC. Compared with the CC/DV and CC/UFAD system, the mixing system offers a longer free cooling time due to the larger air flow rate, when the economizer operation is assisted by a constant speed supply fan. The higher temperature required by the ceiling panel in the combined system makes it possible to have a separate chiller system running at much higher evaporator temperature conditions for the chiller energy saving.

PUBLICATIONS ARISING FROM THE THESIS

I. Journal Papers

- **Xu H.T.** and J.L. Niu. Numerical model for predicting energy consumption of the underfloor air distribution system compared with the conventional mixing system. *Energy and Buildings*. (*Article in Press*) (based on Chapter 5)

- **Xu H.T.** and J.L. Niu. 2004. Numerical simulation and experimental validation of the swirling turbulent airflow and mixing processes. *Numerical Heat Transfer*, Part A, 46(6): 571-586. (based on Chapter 3)

Ⅱ. Conference Papers

- **Xu H.T.** and J.L. Niu. A numerical method for energy consumption prediction of the underfloor air distribution system. *Proceedings of Indoor Air 2005*, 4-9 September, Beijing, China. (based on Chapter 5)

- Niu J.L., C.W. Tung and **H.T. Xu.** 2005. Study of inter-flat airflow dispersion for airborne diseases transmission in residential buildings. *Symposium on Advanced Technology for Health Care and Hygiene Control*, 27 May, Hong Kong SAR.

- **Xu H.T.** and J.L. Niu. 2004. CFD analysis of two different supply diffusers in underfloor air distribution systems. *Proceedings of Roomvent2004 for Indoor Air Quality*, 5-8 September, Coimbra, Portugal. (based on Chapter 4)

- **Xu H.T.** and J.L. Niu. 2003. CFD simulation of airflow characteristics of swirling floor diffusers. *Proceedings of the 8th International IBPSA*

Conference, 3:1429-1433, 11-14 August, Eindhoven, Netherlands. (based on Chapter 4)

- Niu J.L. and **H.T. Xu.** 2003. Potential IAQ and energy benefits achievable with personalized air. *The 2nd Conference of New Technologies of HVAC Systems*, 19-22 November, Shanghai, China.

Ⅲ. Journal Papers in Preparation

- **Xu H.T.** and J.L. Niu. A method to generate cooling load reduction factor for floor level supply air distribution system. *International Journal of HVAC&R*.
- **Xu H.T.** and J.L. Niu. How to quantify two factors for annual energy consumption of the under-floor air distribution system: supply strategy and return air location. *Energy and Buildings*.

ACKNOWLEDGEMENTS

There are many people who deserve recognition for their support and guidance during my Ph. D studies. First and foremost among these people is my supervisor, Dr. Niu Jianlei. I am grateful not only for his patience and guidance, but also for his advice that cheered me up, cooled me down, and encouraged me to persevere. He kept me pointed in the right direction.

I wish to extend my gratitude to the technicians in our department of Building Services Engineering (BSE), for their enthusiasm and support of my research. Special thanks are given to Mr. Lau Waipang for helping me to solve the FLUENT operation problems during my CFD simulation work.

I wish to express my appreciation to Dr. Cao Jing and Dr. Sui Hongtao of Shanghai Hi-Key Technology Corporation Ltd. for their assistance in user-defined function (UDF) inspections and suggestions for my written programs.

I also wish to thank Prof. Yao Qiang of Tsinghua University for his help in obtaining the dimensions of the swirling diffuser for the validation work of the numerical simulation method.

Finally, a very special thank is given to my parents and relatives for their ongoing patience, understanding and support during my Ph. D studies.

TABLE OF CONTENTS

LIST OF FIGURES

LIST OF TABLES

NOMENCLATURE

Variable	Description	Unit
A	Van Driest constant	ND
Ar	Archimedes number	ND
B	Constant in the demensionless velocity equation	ND
c_1, c_2, c_μ	Constants in the turbulence model	ND
C	Species concentration in energy equation	ND
$C_{2\varepsilon}^{RNG}$	Constant in RNG κ – ε turbulence model	ND
C_p	Specific heat of air	J/(kg·k)
COP	Coefficients of performance	ND
d	Air humidity	kg/kg
d_e	Air humidity of the exhaust air	kg/kg
d_h , d_1,	Diameters of the supply channel	mm
d_o	Air humidity of the outdoor air	kg/kg
D_1,D_2,D_3	Diameters of the pre-combustion chamber	mm
D_e	Hydraulic diameter	m
f	Instantaneous variable	ND
f_1	Mixture fraction of stream one	ND
f_{cl}	Ratio of man's surface area while clothed, to man's surface area while nude	ND
g_i	Gravitational acceleration in the direction x_i	gm/s^2
h_c	Convective heat transfer coefficient	W/m^2·℃
h_e	Enthalpy of the exhaust air	J/kg
h_o	Enthalpy of the outdoor air	J/kg
I	Turbulence intensity	ND
I_{cl}	Thermal resistance of clothing	m^2·℃/W
k	Von Karman constant	ND
κ	Turbulent kinetic energy	J/kg

l	Mixing length of turbulent motion	m
L , L_1	Lengths of the pre-combustion chamber	mm
L_{sq}	Length of the pipe for the square diffuser	mm
L_{sw}	Length of the pipe for the swirling diffuser	mm
m	Mass flow rate of supply air	kg/s
m_f	Mass flow rate of the fresh air	kg/s
m_1	Mass fraction of stream one	ND
M	Metabolic rate of body	W/m^2
p	Instantaneous static pressure	Pa
P_a	Partial water vapor pressure	Pa
p_s	Static pressure	Pa
Pr	Prandtl number	ND
PD	Percentage of people dissatisfied due to draft	ND
PMV	Predicted mean vote	ND
q_W	Heat flux density	$W/(m^2 \cdot s)$
$Q_{chiller}$	Total coil load removed by the chiller	W
Q_{ch1}	Coil load removed by the air-side chiller	W
Q_{ch2}	Coil load removed by the water-side chiller	W
$Q_{equipment}$	Heat gain from indoor electronic equipment	W
$Q_{lighting}$	Heat gain from indoor lighting	W
$Q_{occupied}$	Cooling load in the occupied zone	W
Q_{space}	Cooling load in the conditioned zone	W
$Q_{unoccupied}$	Cooling load in the unoccupied zone	W
Re	Reynolds number	ND
R_{sq}	Radius of the pipe for the square diffuser	mm
R_{sw}	Radius of the pipe for the swirling diffuser	mm
R_ε	An additional term in ε equation of the RNG κ – ε turbulence model	ND
Sc	Schmidt number	ND

S_Φ	Source term of Φ transport equation	ND
t_a	Local air temperature	℃
t_{ch}	Chiller water temperature	℃
t_{cl}	Surface temperature of clothing in PMV model	℃
t_e	Exhuast air temperature	℃
t_s	Supply air temperature	℃
T^+	Dimensionless temperature	ND
T_u	Local turbulence intensity in PD model	ND
T_W	Temperature on the boundary wall	K
T, T_1, T_2	Temperatures of supply air stream	K
T_0	Reference air temperature	K
u_W	Velocity on the boundary wall	m/s
u^+	Dimensionless velocity	ND
u_i	Velocity component in direction x_i	m/s
u'	Instantaneous velocity component in direction x_i	m/s
$\vec{U}$	Velocity vector	m/s
v	Local mean air velocity in PD model	m/s
$\bar{v}$	Mean velocity	m/s
v'	Instantaneous velocity component in direction y_i	m/s
v^*	Tangential stress velocity in wall functions	m/s
V	Air velocity of supply diffuser in chamber	m/s
V_a	Air volumetric flow rate	m^3/h
V_{axial}	Axial velocity of supply diffuser in chamber	m/s
$V_{tangential}$	Tangential velocity of supply diffuser in chamber	m/s
w'	Instantaneous velocity component in direction z_i	m/s
W	Radium of the square diffuser	mm
x_i	Velocity component direction	ND
y^+	Dimensionless distance	ND

Greek Symbols

β	Coefficient of gas thermal expansion	K^{-1}
Γ_t	Turbulent diffusivity	m^2/s
Γ_Φ	Generalized diffusion coefficient	m^2/s
Δp	Fan total pressure rise	Pa
$\delta_{i,j}$	Kronecker delta	ND
ε	Dissipation rate of turbulence energy	W/kg
ε_t	Dimensionless temperature coefficient	ND
θ	chamber construction angle	Degree
θ_w	obliquity of the side-wall	Degree
η	Molecular viscosity	m^2/s
η_f	Fan efficiency	ND
η_t	Turbulent viscosity	m^2/s
λ	Heat conductivity coefficient	W/(m·k)
λ_t	Hydraulic conductivity coefficient	W/(m·k)
υ	Motion viscosity	m^2/s
ρ	Air density	kg/m^3
ρ_0	Reference air density	kg/m^3
σ_l	Molecule Prandtl numbers	ND
$\sigma_k, \sigma_t, \sigma_\varepsilon$	Constants in the turbulence model	ND
τ_w	Tangential stress in wall functions	Pa
Φ	Universal transport variables	ND
ϕ	Instantaneous flow variable	ND
$\overline{\phi}$	Time average of the instantaneous flow variable	ND
ϕ'	Fluctuating quantity of the flow variable	ND

Note: ND = No Dimensions

SUBSCRIPTS

e	Exhaust
a	Air
f	Fresh (Chapter 5)
f	Fan (Chapter 5)
c	Convective
s	Supply (Chapter 5)
s	Static (Chapter 2)
o	Outdoor
P	Pressure
cl	Clothing
sq	Square
sw	Swirling
ch	Chiller
*ch*1	Chiller one
*ch*2	Chiller two
w	Wall
t	Temperature (Chapter 5)
t	Turbulence (Chapter 2)
k	Kinetic
ε	Energy dissipation rate
Φ	Universal transport variables

CHAPTER 1 INTRODUCTION

1.1 Background

The origin of heating, ventilating and air-conditioning (HVAC) systems can be traced back to the beginning of the last century. In the year of 1902, Mr. W.H. Carrier first developed a system for humidity control (McQuiston and Parker 1994). Since then, the HVAC system has become one of the most important building systems to provide thermal comfort environments. The energy crisis in the early 1970's made people aware of the need to save energy. As a result, the airtight envelope design and insulation materials were employed to reduce heat loss in winter, heat gain in summer and the infiltration of outdoor air.

The purpose of HVAC systems is to provide the conditions for human thermal comfort, which is defined as the condition of the mind expressing satisfaction with the thermal environment (ASHRAE 1992). Early occupant surveys have found that a thermal comfort environment is among the most important attributes of an office, however, the provision of such an environment has not been very successful (Harris and Associates 1980). Recent research has found that building occupants who have no individual control capabilities are twice as sensitive to changes in temperature as are occupants who do have individual thermal control (Bauman 1998). In fact, the lack of individual control was identified as the single attribute contributing most to occupant dissatisfaction (Loudermilk 2003). Since worker productivity is related to satisfaction (Brill and Margulis 1984), thermal comfort deserves serious inquiry. A review of relevant research has concluded that a 0.5% to 5% increase in productivity

is possible when the quality of the indoor thermal and lighting indoor environments is enhanced (Fisk 2000). In the hot and humid regions like Hong Kong, over fifty percent of supplied electricity is used in commercial buildings for air conditioning, and a large fraction of this is used to provide comfort, so the efficiency with which comfort is provided is quite important (Yik et al. 1998).

Presently, some new indoor environmental factors have emerged that will affect the development of HVAC systems. Firstly, in modern businesses, the churn rate is a fact of life. It is defined as the percentage of workers per year and their associated work places in a building that are reconfigured or undergo significant changes. A recent survey in the US found the national average churn rate to be 44% (Benchmark 1997). True flexibility, for expansion or alteration, is preferably achieved with plug-in ease, as cost savings in building service reconfiguration is a main concern of building owners. Secondly, in Hong Kong, it is very common that advanced or flexible interior furnishings are used to partition a variety of individual and team work spaces. For occupants, the significant variations in comfort preference exist in 'micro-' environments due to the differences in their clothing, activity levels (metabolic rate), and individual preferences. Many complaints arise due to the ignorance of individual thermal comfort preferences in mixing HVAC systems (Schiller et al. 1988). Thirdly, the greater number of personal computers, engineering workstations, mainframes, etc. generates a large quantity of heat. How to discharge such heat loads and air-conditioning rooms efficiently have become the major issues for HVAC engineers. Today, people spend almost 90% of their time indoors, raising concerns about indoor air pollutants. The reduced supply air from a mixing system causes an increase in the concentration of indoor pollutants and the incidence of so-called sick building syndrome (SBS) (Godish and Spengler 1996).

The mixing HVAC system has changed little since the variable air volume (VAV) system was first introduced in the 1960's. Given the above mentioned new indoor environments, the development of new effective and economical HVAC systems is necessary. The concept of an underfloor air distribution (UFAD) system was developed to solve many of the problems outlined above. The UFAD strategy was first introduced at the beginning of the 1960's in the Federal Republic of Germany in rooms with large heat production (Sodec and Craig 1990). The air was supplied to the room via floor outlets in the form of highly turbulent air jets. The return air was withdrawn at ceiling level. The strong buoyancy movement was supported by the air flow from the bottom to the top. At that stage, the UFAD system was primarily used for equipment cooling, not for people cooling. Consequently, the first floor diffusers were not designed to be easily adjustable. Later, in the middle 1970's, this system was adopted in general offices in West Germany mainly due to the modernization of the general office, the impact of automated electronic equipment and the excess heat it transferred to the office. In these buildings, the comfort of office workers had to be considered, giving rise to the development of occupant-controlled local supply diffusers to provide task air conditioning (TAC).

The potential economic benefits of using UFAD technology to achieve greater satisfaction within the workforce are believed to be very large. These benefits include increased work productivity, employee retention, thermal comfort, ventilation efficiency, indoor air quality, greater market value of facilities and reduced operating costs (Arnold 1990; Sodec and Craig 1990; Bauman and Webster 2001; Loudermilk 2001; Fukao et al. 2002). UFAD systems have now achieved considerable acceptance in Europe, North America and Japan.

The cooled ceiling (CC) technique is a HVAC alternative and has been popular in many European countries since the early 1990's (Mertz 1992; Wilkins and Kosonen 1992; Krühne 1993). Lacking a ventilation function and humidity control, the CC technique is seldom used on its own and usually combined with other HVAC systems. Such a combination separates the cooling and ventilation tasks of a building air-conditioning system, by employing the cooled ceiling to treat a sensible cooling load and using an independent HVAC system for the ventilation and humidity control.

Various ventilation systems can be combined with the cooled ceiling system to provide the required outside air and latent cooling. The cooled ceiling system has certain unique characteristics. A portion of radiant heat will be absorbed by the chilled panels and directly converted into the cooling load without the delay and attenuation that usually occurs in a mixing HVAC system. On the other hand, the existence of the cooled panel surface lowers the radiation temperature in a room. The radiation temperature should be taken into account, in addition to the room air temperature, for indoor air design temperature. It is believed that such a combined system provides better thermal comfort in terms of the draft risk and reduces vertical temperature gradients in the occupied zone (Busweiler 1993; Loveday et al. 1998, 2002).

1.2 Problem Statements

Despite its advantages, barriers still exist to the widespread adoption of the UFAD system. For the majority of building owners, developers, facility managers,

architects and engineers, the UFAD system represents a relatively new and unfamiliar technology. No standardized design guidelines exist at present for the reference purpose. In addition, there are some important gaps in our fundamental understanding of the UFAD system. Key areas where information is lacking are: the impact of air diffuser characteristics on stratification, the behavior of thermal plumes near solar-heated windows, the interaction between thermal plumes and diffuser air flows, ventilation efficiencies, the thermal performance of underfloor air supply plenums, and health and comfort benefits (Bauman 2003).

The UFAD system has been designed with distribution in access floor plenums for more than three decades, using floor-level air supply diffusers. This system is an effective method for dealing with unevenly distributed heat loads in a room as the supply diffusers can be precisely allocated based on the locations of the heat loads, which is much different from the supply diffusers employed in mixing HVAC systems. On the other hand, for thermal comfort, the air flow patterns near floor level can cause discomfort because the supply air flows upward and passes human bodies directly. Draft complaints usually mean incorrectly placed air terminals or placements that are too close to workstations (Shute 1992). For example, surveys indicate that women, with lighter clothing, are more bothered by incorrect air terminal placement. The conclusion is that the influence of floor level supply diffusers for thermal comfort is of much concern to occupants.

There are many types of supply diffusers used in UFAD systems. Vivian et al. (2002) concluded that the swirling diffuser could be used to ensure effective thermal mixing near the floor and while maintaining the stratifications between the occupied space and the upper space in order to conserve energy. To investigate the behavior of

supply diffusers, either experimental measurements or Computational Fluid Dynamics (CFD) simulations are employed. For the CFD simulation technique, it is necessary to know the boundary conditions that describe the inlet jet from a supply diffuser. It is believed that the modeling of the air flow supplied by diffusers is a major limitation on the application of CFD to indoor air flow (Moser 1991; Vogel et al. 1993). For complex air diffusers, some researchers (Chen and Jiang 1996; Emvin and Davidsen 1996; Srebric and Chen 2001a) have proposed two simplified methods, the box and the momentum methods, as the most appropriate for use in CFD simulations. The box method is not recommended for the diffusers used in the UFAD and DV (displacement ventilation) systems, because the buoyancy force dominates jet development (Jacobsen and Nielsen 1993; Lai and Naser 1998). The momentum method neglects the inlet swirl in the flow for the swirling diffusers and results in somewhat large discrepancy near the supply diffuser, as compared with the experimental data (Xu and Niu 2004).

The effective employment of the UFAD system relies on the proper consideration, quantification, and treatment of indoor air temperature stratification. Unfortunately, most available load calculation programs and procedures, such as ACCURACY (Chen and Kooi 1988; Niu and Kooi 1993; Niu et al. 1995; Niu and Burnett 1998), BLAST (Fontoynont et al. 1984; Akbari et al. 1987; BSL 1999; Ke and Mumma 1999; Schibuola 1999), DOE-2 (Diamond et al. 1981, 1986; Meldem and Winkelmann 1995; Winkelmann et al. 2003), and EnergyPlus (Crawley et al. 2001), do not differentiate air temperature stratification because the mixing system is assumed. Nielsen (1988) investigated the gradient of the vertical air temperature in upward ventilation and found that, in a room with a constant cooling load from a concentrated heat source, the temperature gradient decreases slightly as the

Archimedes number increases. The gradient is strongly related to the surface temperature of the heat sources (Nielsen 1992a).The vertical linear temperature gradient assumption is widely used in designs for upward ventilation (Skistad 1994). It is difficult to predict the nonlinear temperature profile due to the large number of variables, which include ventilation rate, heat source type and position, wall temperature and wall radiative characteristics, space height, and diffuser type (Yuan et al. 1998).

In the combined system, comprising a cooled ceiling (CC) and a HVAC system, both of the advantageous features of CC with respect to thermal comfort and favorable air quality characteristics of the displacement flow pattern are expected. However, adding together two favorable characteristics does not necessarily result in a combination that provides both advantages in their entirety. Alamdari and Eagles (1996) concluded that the combination of a chilled ceiling with a displacement ventilation system could destroy displacement flow at low ceiling temperatures (14℃-16℃). At higher ceiling temperatures (18℃-21℃), the stratification boundary layer was strongly suppressed. Loveday et al. (1998) have shown that as the ceiling temperature was reduced, the stratified boundary layer was suppressed, disrupting the displacement flow pattern. The characteristics of radiant cooled ceilings influence the displacement flow in such a way that the typical flow pattern of the displacement ventilation may vanish and be replaced by a mixing flow pattern instead (Martin 1999). The thermal environment and energy consumption of the combined system are much different from the mixing HVAC system and are in need of investigations.

1.3 Aims of the Present Work

Supply diffusers are necessary for proper indoor air distributions to generate acceptable thermal environments. However, research on this aspect is insufficient in the UFAD system, as stated above. This thesis aims at follows:

1. Propose a fully represented geometry method (FRGM) for supply diffuser simulation with the validation work.
2. Investigate different thermal environments influenced by two supply diffusers with the employment of FRGM in the UFAD system.
3. Model indoor air temperature stratification in the UFAD system with the swirling supply diffuser to inspect energy saving potential of this system.
4. Inspect the different thermal environments and energy consumption among different HVAC system, due to the employment of the cooled ceiling.

1.4 Organization of This Thesis

Since the late 1970's, the numerical simulation technique for turbulence flows has advanced greatly due to the rapid development of computation capacity and the availability of several engineering turbulence models. State-of-the-art of the computer techniques has motivated us to use the computer as a powerful tool in the investigations of HVAC thermal environments and energy consumption.

Chapter 2 provides a review of the numerical simulation method for supply diffusers. In this chapter, the standard $\kappa - \varepsilon$ turbulence model is first introduced. Then, several simplified modeling methods for supply diffuser simulations are reviewed.

Chapter 3 investigates the fully represented geometry method (FRGM) for the swirling diffuser simulation in order to consider the effects of the diffuser configuration on overall flow parameters, especially near the supply diffuser. The experimental data from a pre-combustion chamber are used for the validation work. The detailed experimental setup and measurements are presented. Two inlet boundary condition specifications, the momentum method and FRGM, are first compared with the standard $\kappa - \varepsilon$ turbulence model. Then, the RNG $\kappa - \varepsilon$ model is further investigated for this method.

Chapter 4 discusses the classification of diffusers in the UFAD system. Employing the numerical method FRGM, two supply diffusers, the swirling and square diffusers, are investigated for thermal comfort environments in a small office room.

Chapter 5 first presents the conventional simulation method for energy analysis in HVAC systems and then reviews some popular programs and procedures. Great effort is devoted to the numerical modeling method, considering indoor air temperature stratification in the UFAD system. Compared with the mixing system, the energy saving potential of the UFAD system is discussed in detail.

Chapter 6 investigates the combinations of cooled ceiling with the DV and the UFAD systems for thermal environments and energy consumption and the results are compared with the mixing system.

Chapter 7 summarizes the conclusions drawn from the present work and provides suggestions for future research.

CHAPTER 2 NUMERICAL SIMULATION OF INDOOR AIR FLOWS AND SUPPLY DIFFUSERS

2.1 Introduction

Accurate predictions of air flow information such as velocity, temperature, etc. in a room are indispensable for designing high-quality HVAC systems from the viewpoint of comfort, health, and energy savings. For indoor air flow investigations, experimental measurement and computer simulation are the two basic approaches. Direct measurements provide the most accurate information on indoor air. However, complete measurements may require many months of work to conduct the full-scale tests. When necessary, tests have to be performed on geometrically reduced-scale models to estimate the performance of a design. Due to the conflicting requirements of Reynolds number (*Re*) similarity and Archimedes number (*Ar*) similarity, an undistorted similitude scaled-down model is not possible for rooms with internal heat sources (Zhang et al. 1990). The measurement results are highly dependent on the precision of the experimental equipment and the setup and conduct of the experiments requires experience with HVAC systems.

Due to the limitations of the experimental approach and the increase in performance and affordability of high-speed computers, the Computational Fluid Dynamics (CFD) technique can greatly improve our knowledge about the performance of indoor environment designs. Through this method, detailed information about velocity, temperature, contaminant distributions etc. can be obtained, which is in generally very difficult and time consuming to obtain using scale-models or full-scale field

measurements but very important for the evaluation of indoor air quality (IAQ) and thermal comfort. The CFD technique is a cost-effective way to conduct a parameter study or a trade-off study for different ventilation configurations in early design stages, for innovative ventilation system design and ventilation system optimization. When appropriately used, the CFD technique can be a very powerful design tool, but it has not yet developed to the stage where it can be used as a foolproof design tool. Much effort and expertise are required to properly conduct a simulation of practical ventilation flows. The results must be validated by experimental data and the predicted results need to be judged with the engineering insight.

This chapter first summarizes the standard $\kappa - \varepsilon$ turbulence model for the numerical simulation of indoor air flows. Then, a review of different numerical modeling methods for supply diffusers is presented. The fully represented geometry method (FRGM) was the method used in the author's simulation work.

2.2 Conservation Laws

Basically, indoor air flow can be viewed as turbulence flow. Turbulence is defined in terms of irregularity, diffusivity, large Reynolds numbers, three-dimensional vorticity fluctuations, dissipation and continuum (Tennekes and Lumley 1972). In the turbulence flow, almost all fluid physical parameters (such as the velocity component, pressure, temperature, density, enthalpy etc.) fluctuate and interact with each other over time and across space. Tennekes and Lumley (1977) pointed out that turbulence is viewed as a fluid flow consisting of a highly disordered array of eddies with widely different sizes. Eddies are stretched in a preferred direction by the mean flow and in a random direction by each other. This process is called the energy

cascade which means that only eddies of comparable size can exchange energy with one another. Large eddies obtain kinetic energy from mean motion and this energy is then transferred to eddies of smaller size and continues to smaller and smaller scales until the eddies lose energy by the direct action of viscous stresses. At the final stage, the energy is converted into internal thermal energy. Due to its complexity, turbulence flow is not yet fully understood.

In order to study the impact of turbulent mixing on thermal comfort and indoor air quality, partial differential equations governing turbulent flow must be solved. Indoor air flow can be viewed as the incompressible turbulent flow of a Newtonian fluid and the numerical governing differential equations of air flow are based on the conservation laws, i.e., those of mass conservation, momentum conservation and energy conservation. These three conservation equations can illustrate the necessity of each parameter and show how they are combined to describe the total flow field.

Continuity equation:

$$\frac{\partial u_i}{\partial x_i} = 0 \tag{2.1}$$

Momentum equation:

$$\rho_0\left(\frac{\partial u_i}{\partial t} + \frac{u_k \partial u_i}{\partial x_k}\right) = -\frac{\partial p}{\partial x_i} + \frac{\partial}{\partial x_k}\left[\eta\left(\frac{\partial u_i}{\partial x_k} + \frac{\partial u_k}{\partial x_i}\right)\right] + g_i(\rho - \rho_0) \tag{2.2}$$

Energy/species equation:

$$\frac{\partial \Phi}{\partial t} + \frac{\partial \Phi u_i}{\partial x_i} = \frac{\lambda}{\rho C_p} \frac{\partial^2 \Phi}{\partial x_i \partial x_i} + S_\Phi \tag{2.3}$$

where u_i is the instantaneous velocity component in the direction x_i, p is the modified instantaneous static pressure, i.e., $p = p_s - \rho_0 g_i x_i$, where p_s is the static pressure. Φ is a scalar quality which may stand for either temperature T or species concentration C. S_Φ is a volumetric source term expressing, for example, heat generation due to chemical reactions. η and λ are the molecular (kinematic) viscosity and air heat conductivity coefficients respectively. The Boussinesq assumption (Tritton 1988) has been used in the above equations so that the influence of variable density appears only in the buoyancy term on the right hand side of Equation (2.2), involving the reference density ρ_0 and the gravitational acceleration g_i in the direction x_i. Together with an equation relating the local density ρ to the local value of T, e.g., $(\rho - \rho_0)/\rho_0 = \beta(T_0 - T)$, Equations (2.1) to (2.3) form a closed set of equations and, in principle, describe all the details of the turbulent motion. β is the coefficient of gas thermal expansion. Unfortunately, the above equations, at present, are difficult to solve directly for turbulent flows due to the practical complex natures of turbulence in theory and the available computation capacity restrictions in practice.

Therefore, in the following sections, a statistical approach which was used in the 1890's (Reynolds 1895) and forms the basis of the turbulence models will be presented. To date, the turbulence models that have provided the most practical

contributions in engineering applications are those based upon Boussinesq's eddy-viscosity concept (Boussinesq 1877).

2.3 Standard κ – ε Turbulence Model

2.3.1 Time Average Definition

Because turbulence flow consists of random fluctuations of various flow properties, a statistical approach (Reynolds average) is used. In this approach, all quantities are expressed as the sum of mean and fluctuating parts. In general, the Reynolds average assumes a variety of forms involving either an integral or a summation. The term used to describe these averaging processes is 'mean'. In the turbulence model, the 'time' average is used.

Time average is appropriate for stationary turbulence, i.e., a turbulent flow that, on the average, does not vary with time, such as the flow in a pipe which is driven by a constant-speed blower. For such flow, we express the instantaneous flow variable as ϕ. Its time average, $\bar{\phi}$, can be defined as

$$\bar{\phi} = \frac{1}{\Delta t}\int_{t}^{t+\Delta t} \phi(t)dt \tag{2.4}$$

The instantaneous value of the variable ϕ can be separated into the mean $\bar{\phi}$ and the fluctuating ϕ' quantity

$$\phi = \bar{\phi} + \phi' \tag{2.5}$$

Assuming f is another instantaneous variable, we obtain the following equations:

$$\left.\begin{array}{l}
\overline{\phi}' = 0;\ \overline{\overline{\phi}} = \overline{\phi};\ \overline{\overline{\phi} + \phi'} = \overline{\phi} \\
\overline{\overline{\phi} f} = \overline{\phi} \overline{f};\ \overline{\overline{\phi} f'} = 0;\ \overline{\overline{\phi} f} = \overline{\phi} \overline{f};\ \overline{\phi f} = \overline{\phi}\,\overline{f} + \overline{\phi' f'} \\
\dfrac{\overline{\partial \phi}}{\partial x_i} = \dfrac{\partial \overline{\phi}}{\partial x_i};\ \dfrac{\overline{\partial \phi}}{\partial t} = \dfrac{\partial \overline{\phi}}{\partial t};\ \dfrac{\overline{\partial^2 \phi}}{\partial x_i^2} = \dfrac{\partial^2 \overline{\phi}}{\partial x_i^2} \\
\dfrac{\overline{\partial \phi'}}{\partial x_i} = 0;\ \dfrac{\overline{\partial^2 \phi'}}{\partial x_i^2} = 0
\end{array}\right\} \tag{2.6}$$

Introducing Equation (2.5) into Equations (2.1) to (2.3) and doing the average calculations again in the same way yields the following equations:

$$\frac{\partial \overline{u_i}}{\partial x_i} = 0 \tag{2.7}$$

$$\rho_0\left(\frac{\partial \overline{u_i}}{\partial t} + \frac{\overline{u_k}\partial \overline{u_i}}{\partial x_k}\right) = -\frac{\partial \overline{p}}{\partial x_i} + \frac{\partial}{\partial x_k}\left(\eta\left(\frac{\partial \overline{u_i}}{\partial x_k} + \frac{\partial \overline{u_k}}{\partial x_i}\right) - \rho_0 \overline{u_i' u_k'}\right) + g_i\left(\rho - \rho_0\right) \tag{2.8}$$

$$\frac{\partial \Phi}{\partial t} + \frac{\partial \Phi \overline{u_i}}{\partial x_i} = \frac{\partial}{\partial x_i}\left(\frac{\lambda}{\rho_0 C_{\mathrm{p}}}\frac{\partial \Phi}{\partial x_i} - \overline{u_i' \Phi'}\right) + S_\Phi \tag{2.9}$$

where, $\overline{u_k' u_j'}$ and $\overline{u_i' \Phi'}$ are turbulence correlations which are defined in a manner similar to that in Equation (2.4):

$$\overline{u_i' u_k'} = \frac{1}{\Delta t}\int_t^{t+\Delta t} u_i' u_k' d\tau\ ,\ \overline{u_i' \Phi'} = \frac{1}{\Delta t}\int_t^{t+\Delta t} u_i' \Phi' d\tau \tag{2.10}$$

Equations (2.7), (2.8) and (2.9) are known as Reynolds average equations and can be solved for the mean values of velocity, pressure and temperature or concentration only when the turbulence correlations $u_i' u_k'$ and $u_i' \Phi'$ can be determined in some way. For the purpose of equation closure, different turbulence models are proposed, which approximate the correlations $u_i' u_k'$ and $u_i' \Phi'$ either in terms of the mean flow quantities or by introducing the transport equations for the correlations.

2.3.2 Turbulence Viscosity

Most turbulence models today are still based on the oldest proposal for modeling turbulence or Reynolds stresses $-\rho u_i' u_j'$, in which the eddy-viscosity concept was first proposed by Boussinesq (1877). In fact, the term $-\overline{u_i' u_j'}$ may be considered as the effect of turbulence on the averaged flow and may be interpreted as additional shear stress. It is written as the Reynolds stress, $\left(\tau_{i,j}\right)_t$, viz.

$$\left(\tau_{i,j}\right)_t = -\rho \overline{u_i' u_j'} \tag{2.11}$$

Boussinesq (1877) assumed that, analogous to the viscous stresses in laminar flows, turbulence stresses are proportional to the mean velocity gradients. For general flow simulations, this concept can be expressed as

$$-\rho \overline{u_i' u_k'} = \left(\tau_{i,j}\right)_t = \eta_t \left(\frac{\partial u_i}{\partial x_k} + \frac{\partial u_k}{\partial x_i} \right) - \frac{2}{3} \rho \kappa \delta_{i,k} \tag{2.12}$$

where η_t is the turbulence or eddy viscosity which, in contrast to the molecular viscosity η, is not a fluid property but strongly depends on the state of turbulence. $\delta_{i,j}$ is the so-called Kronecker delta in tensor notation ($\delta_{i,k} = 1$ for $i = k$ and $\delta_{i,k} = 0$ for $i \neq k$). κ is the turbulent kinetic energy of the fluctuating motion:

$$\kappa = \frac{1}{2}\left(\overline{u'^2} + \overline{v'^2} + \overline{w'^2}\right) \tag{2.13}$$

where u', v' and w' are fluctuating velocity components in three different directions.

2.3.3 Turbulence Diffusivity

Turbulence heat or mass transport is assumed to be related to the gradient of the average transported quantity,

$$-\rho\overline{u_i'\Phi'} = \Gamma_t \frac{\partial \Phi}{\partial x_i} \tag{2.14}$$

where Γ_t is the turbulent diffusivity of heat or mass and is closely related to η_t:

$$\Gamma_t = \frac{\eta_t}{\sigma_t} \tag{2.15}$$

σ_t is called the turbulent Prandtl number (*Pr*) for heat transfer and Schmidt number (*Sc*) for mass transfer.

Although η_t and Γ_t are not fluid physical properties and are strongly dependent on fluid turbulence intensity, from experimental investigation, the ratio σ_t is assumed to be a constant (0.6 in free stream and 0.9 in attached wall flow).

Substituting Equations (2.14), (2.15) for Equations (2.8) and (2.9), the momentum and energy equations can be rewritten as:

$$\rho_0\left(\frac{\partial \overline{u_i}}{\partial t}+\frac{\overline{u_k}\partial \overline{u_i}}{\partial x_k}\right)=-\frac{\partial \overline{p}}{\partial x_i}+\frac{\partial}{\partial x_k}\left(\eta\left(\frac{\partial \overline{u_i}}{\partial x_k}+\frac{\partial \overline{u_k}}{\partial x_i}\right)+\frac{\eta_t}{\sigma_t}\frac{\partial \overline{u_k}}{\partial x_i}\right)+g_i(\rho-\rho_0) \qquad (2.16)$$

$$\frac{\partial \Phi}{\partial t}+\frac{\partial \Phi \overline{u_i}}{\partial x_i}=\frac{\partial}{\partial x_i}\left(\frac{\lambda}{\rho_0 C_p}\frac{\partial \Phi}{\partial x_i}+\frac{\eta_t}{\rho\sigma_t}\frac{\partial \Phi}{\partial x_i}\right)+S_\Phi \qquad (2.17)$$

In order to obtain the value of Γ_t, obtaining the proper η_t is essential and is the emphasis of research. For numerical simulations of indoor air flows, the standard $\kappa-\varepsilon$ turbulence model is the most widely used.

2.3.4 κ and ε Equations

By far, the most popular turbulence model is the standard $\kappa-\varepsilon$ turbulence model. The earliest development efforts based on this model were those of Chou (1945), Davidov (1961), and Harlow and Nakayama (1968). However, the key paper, by Jones and Launder (1972), has nearly reached the same status as the Boussinesq and Reynolds papers in the turbulence modeling community. This model is so well known that it is referred to as the standard $\kappa-\varepsilon$ model and the reference to the Jones-Launder's paper is often omitted. Actually, Launder and Sharma (1974)

"retuned" the model's closure coefficients and most researchers use the form of the model presented in the 1974 paper.

The standard $\kappa - \varepsilon$ turbulence model is a semi-empirical model based on model transport equations for the turbulence kinetic energy κ and its dissipation rate ε. The model transport equation for κ is derived from an exact equation, while the model transport equation for ε was obtained using physical reasoning and bears little resemblance to its mathematically exact counterpart. In the derivation of the standard $\kappa - \varepsilon$ model, it was assumed that the flow was fully turbulent.

The final κ and ε equations can be written as (Tao 2001):

$$\rho \frac{\partial \kappa}{\partial t} + \rho \overline{u}_j \frac{\partial \kappa}{\partial x_j} = \frac{\partial}{\partial x_j}\left[\left(\eta + \frac{\eta_t}{\sigma_k}\right)\frac{\partial \kappa}{\partial x_j}\right] + \eta_t \frac{\partial \overline{u_i}}{\partial x_j}\left(\frac{\partial \overline{u_i}}{\partial x_j} + \frac{\partial \overline{u_j}}{\partial x_i}\right) - c_D \rho \frac{\kappa^{3/2}}{l} \qquad (2.18)$$

$$\rho \frac{\partial \varepsilon}{\partial t} + \rho \overline{u}_j \frac{\partial \varepsilon}{\partial x_j} = \frac{\partial}{\partial x_j}\left[\left(\eta + \frac{\eta_t}{\sigma_\varepsilon}\right)\frac{\partial \varepsilon}{\partial x_j}\right] + \frac{c_1 \varepsilon}{\kappa} \eta_t \frac{\partial \overline{u_i}}{\partial x_k}\left(\frac{\partial \overline{u_i}}{\partial x_k} + \frac{\partial \overline{u_k}}{\partial x_i}\right) - \frac{c_2 \rho \varepsilon^2}{\kappa} \qquad (2.19)$$

2.3.5 Closure

The standard κ – ε turbulence model is closed as

$$
\left.
\begin{aligned}
&\frac{\partial u_i}{\partial x_i} = 0 \\
&\rho_0\left(\frac{\partial u_i}{\partial t} + \frac{u_k \partial u_i}{\partial x_k}\right) = -\frac{\partial p}{\partial x_i} + \frac{\partial}{\partial x_k}\left(\eta\left(\frac{\partial u_i}{\partial x_k} + \frac{\partial u_k}{\partial x_i}\right) + \frac{\eta_t}{\sigma_t}\frac{\partial u_k}{\partial x_i}\right) + g_i(\rho - \rho_0) \\
&\frac{\partial \Phi}{\partial t} + \frac{\partial \Phi u_i}{\partial x_i} = \frac{\partial}{\partial x_i}\left(\frac{\lambda}{\rho_0 C_p}\frac{\partial \Phi}{\partial x_i} + \frac{\eta_t}{\rho_0 \sigma_t}\frac{\partial \Phi}{\partial x_i}\right) + S_\Phi \\
&\rho_0 \frac{\partial \kappa}{\partial t} + \rho_0 u_j \frac{\partial \kappa}{\partial x_j} = \frac{\partial}{\partial x_j}\left[\left(\eta + \frac{\eta_t}{\sigma_k}\right)\frac{\partial \kappa}{\partial x_j}\right] + \eta_t \frac{\partial u_i}{\partial x_j}\left(\frac{\partial u_i}{\partial x_j} + \frac{\partial u_j}{\partial x_i}\right) - \rho_0 \varepsilon \\
&\rho_0 \frac{\partial \varepsilon}{\partial t} + \rho_0 u_j \frac{\partial \varepsilon}{\partial x_j} = \frac{\partial}{\partial x_j}\left[\left(\eta + \frac{\eta_t}{\sigma_\varepsilon}\right)\frac{\partial \varepsilon}{\partial x_j}\right] + \frac{c_1 \varepsilon}{\kappa}\eta_t \frac{\partial u_i}{\partial x_k}\left(\frac{\partial u_i}{\partial x_k} + \frac{\partial u_k}{\partial x_i}\right) - \frac{c_2 \rho_0 \varepsilon^2}{\kappa} \\
&\eta_t = \frac{c_\mu \rho_0 \kappa^2}{\varepsilon}
\end{aligned}
\right\} \quad (2.20)
$$

For brevity, the overbars indicating the mean values are dropped from Equation (2.20). Six equations include six variables: $u_i (i = 1,3)$, Φ , κ and ε . Also three coefficients (c_1 , c_2 , c_μ) and three constants (σ_κ , σ_ε , σ_t) are shown in Equation (2.20). They have the default values shown in Table 2.1.

Table 2.1 Coefficients in the standard κ – ε turbulence model

c_1	c_2	c_μ	σ_κ	σ_ε	σ_t
1.44	1.92	0.09	1.0	1.3	0.9~1.0

In summary, all equations in the standard κ – ε turbulence model can be represented in a general form:

$$\frac{\partial(\rho\Phi)}{\partial t} + div\left(\rho\vec{U}\Phi\right) = div\left(\Gamma_\Phi grad\Phi\right) + S_\Phi \qquad (2.21)$$

where Φ represents different variables and $\vec{U}$ is the velocity vector.

2.3.6 Boundary Conditions

In order to apply the standard $\kappa - \varepsilon$ turbulence model to wall-bounded flows, boundary conditions must be specified appropriately to a solid bound for the velocity and two turbulence parameters. For this purpose, the logarithmic law wall function (White 1974) was used (Tao 2001).

The logarithmic wall function was initially developed for forced convection boundary layers. The flow close to the wall is considered as consisting of a laminar sublayer ($0< y^+ \leq 5$), buffer zone ($5< y^+ \leq 30$), and inertial sublayer ($30< y^+ \leq 130$), where y^+ is the dimensionless distance to the wall. The wall has a damping effect on the turbulent flow, and the layer closest to the wall has predominant viscous forces. In the buffer zone, viscous forces and Reynolds stresses have the same order of magnitude and neither can be neglected. Finally, the inertial sublayer is dominated by turbulent flows.

The wall functions give expressions for laminar and turbulent sublayers while the buffer zone is neglected. A near wall flow is considered laminar if $y^+ \leq 11.63$, and if

y^+ >11.63 the flow is turbulent. The dimensionless velocity profile in a forced convection boundary layer, with zero pressure gradients, is approximated:

$$u^+ = \frac{u}{v^*} = \frac{1}{k}\ln\left(\frac{yv^*}{\upsilon}\right) + B = \frac{1}{k}\ln y^+ + B \tag{2.22}$$

where u^+ is the dimensionless velocity, υ is the motion viscosity. $v^* = \sqrt{\tau_w / \rho}$ is the tangential stress velocity (τ_w is the tangential stress). k is the von Karman constant. $k = 0.4 \sim 0.42$ and $B = 5.0 \sim 5.5$. In order to show the influence of turbulence flows, the definitions of y^+ and u^+ should be rewritten as:

$$y^+ = \frac{y\left(c_\mu^{1/4}\kappa^{1/2}\right)}{\upsilon} \tag{2.23}$$

$$u^+ = \frac{u\left(c_\mu^{1/4}\kappa^{1/2}\right)}{\tau_w / \rho} \tag{2.24}$$

Introducing the dimensionless temperature:

$$T^+ = \frac{\left(T - T_W\right)\left(c_\mu^{1/4}\kappa^{1/2}\right)}{\left(q_W / \rho c_p\right)} \tag{2.25}$$

where q_W is the heat flux density. The logarithmic law wall functions of the velocity and temperature can be rewritten as:

$$u^+ = \frac{1}{k}\ln\left(Ey^+\right) \tag{2.26}$$

$$T^+ = \frac{\sigma_t}{k}\ln\left(Ey^+\right) + \sigma_t\left(\frac{\pi/4}{\sin\left(\pi/4\right)}\right)\left(\frac{A}{k}\right)^{1/2}\left(\frac{\sigma_l}{\sigma_t}-1\right)\left(\frac{\sigma_l}{\sigma_t}\right)^{-1/4} \tag{2.27}$$

where σ_l and σ_t are molecule and turbulence Prandtl numbers. A is the Van Driest constant. Employ $B = \ln(E)/k$ and $k = 0.4$, then $\left(\frac{\pi/4}{\sin\left(\pi/4\right)}\right)\left(\frac{A}{k}\right)^{1/2} = 8.955 \cong 9$. For CFD simulation, the first internal node P should be placed in the strongly turbulent flow, where the logarithmic law is reasonable. The hydraulic viscosity coefficient η_t and conductivity coefficient λ_t can be defined as:

$$\tau_W = \eta_t \frac{u_P - u_W}{y_P} \tag{2.28}$$

$$q_W = \lambda_t \frac{T_P - T_W}{y_P} \tag{2.29}$$

where u_W and T_W are the velocity and temperature on the boundary wall. Then, using the logarithmic law, Equations (2.26) and (2.27) can be rewritten as:

$$\frac{u_P\left(c_\mu^{1/4}\kappa_P^{1/2}\right)}{\tau_w/\rho} = \frac{1}{k}\ln\left[Ey_P\frac{\left(c_\mu^{1/2}\kappa_P\right)^{1/2}}{\nu}\right] \tag{2.30}$$

$$\frac{(T_P - T_W)\left(c_\mu^{1/4}\kappa_P^{1/2}\right)}{\left(q_W / \rho c_p\right)} = \frac{\sigma_t}{\kappa}\ln\left[E\frac{y_P\left(c_\mu^{1/2}\kappa_P\right)^{1/2}}{\upsilon}\right] + \sigma_t P_\sigma \tag{2.31}$$

where $P_\sigma = 9\left(\frac{\sigma_l}{\sigma_t} - 1\right)\left(\frac{\sigma_l}{\sigma_t}\right)^{-1/4}$. Combining Equations (2.28) and (2.30), we get

$$\eta_t = \left[\frac{y_P\left(c_\mu^{1/4}\kappa_P^{1/2}\right)}{\upsilon}\right]\frac{\eta}{\ln\left(Ey_P^+\right)/k} = \frac{y_P^+}{u_P^+}\eta \tag{2.32}$$

Similarly, combining Equations (2.29) and (2.31), we get

$$\lambda_t = \frac{y_P^+\eta c_P}{\frac{\sigma_t}{k}\ln\left(Ey_P^+\right) + P_\sigma\sigma_t} = \frac{y_P^+\eta c_P}{\sigma_t\left[\ln\left(Ey_P^+\right)/k + P_\sigma\right]} = \frac{y_P^+}{T_P^+}\Pr\lambda \tag{2.33}$$

The boundary conditions for κ can be taken as $\left(\frac{\partial\kappa_P}{\partial y_P}\right)_W = 0$ (y is vertical to the boundary wall). The κ equation of the first node P can be calculated as Equation (2.18). The boundary conditions for ε can be specified as the following algebraic equation (Ozoe et al. 1978):

$$\varepsilon_P = \frac{c_\mu^{3/4}\kappa_P^{3/2}}{\kappa y_P} \tag{2.34}$$

2.3.7 Discretization of the Transport Equations

In order to convert the differential equations into algebraic equations that can be solved numerically, some discretization strategies must be employed. To date, the two most common discretization methods have been the finite element method and the finite volume method.

The finite element method represents the extension of matrix methods (Rockey et al. 1983) for skeletal structures to the analysis of continuum structures. In this method, the continuum is idealized as a structure consisting of a number of individual elements connected only at nodal points. The particular advantage of this method is to apply an irregular grid which can be selectively refined and chosen to match the boundaries of the domain. The finite element method also tends to employ direct simultaneous solution of the continuity equation, the momentum equation, and the remaining dependent variables rather than adopting a sequential approach to achieve more rapid convergence. Examples of the application of the finite element method in turbulent air flows were presented recently (Keresteciogl u et al. 1989; Katzarov 1999). This method is extremely powerful since it enables continua with complex geometrical properties and loading conditions to be accurately analyzed. One limitation of this method is that it requires more computing time due to the direct solutions (Patankar 1980).

The finite volume method divides space into a finite number of control volumes. The transport equations are then applied to each of the control volumes, integrating the governing equations and yielding discrete equations that conserve each quantity on a control-volume basis (Versteeg and Malalsekera 1995). This method can employ the

advanced grid generation techniques such as unstructured grid and body-fitted coordinates, and has become the most widely used discretization method. Manole and Lage (1993) found that forty seven percent of the papers, published in the International Journal of Heat and Mass Transfer and ASME Journal of Heat Transfer in the three years from 1990 to 1992, employed the finite volume method. In this thesis, the following numerical simulation work below also used this method.

2.3.8 Methods for Flow Field Calculations

The real difficulty in the calculation of the velocity field lies in the unknown pressure (Equation (2.16)). Patankar and Spalding (1972) presented an algorithm, known as the Semi-Implicit Method for Pressure Linked Equations (SIMPLE), to overcome this problem. Subsequently, this method has formed the basis of many flow simulation computer codes. For the detailed employment of the SIMPLE algorithm, an initial pressure distribution is first assumed, and substituted into the momentum equation to evaluate an initial velocity distribution. A pressure correction term is then applied and the consequent new pressure distribution and velocity distributions are valued. Other transport equations, which influence the flow field, are similarly solved. The iteration process is continued until the continuity equation is satisfied. This procedure is essentially a sequential approach.

The SIMPLE algorithm has been successfully used in many cases. The great simplicity of this algorithm lies in its neglecting the terms that couple neighboring velocity values in the equation of the velocity correction (Shyy and Mittal 1998). It has been found that this neglect tends to overpredict the pressure correction in such a way that an under-relaxation factor for pressure correction has to be resorted to

stabilize the iterative procedures. The factor should be positive and smaller than one. Convergence can be checked by two criteria: the change in field values between two successive iterations becoming very small and the decrease in the residuals of the discretised conservation equations (Patankar 1980).

Because the influence of the neighboring velocity corrections is ignored in the calculation of pressure correction, slow convergence occurs due to the severe pressure corrections in the SIMPLE algorithm. In order to solve this problem, some improved algorithms, such as SIMPLER (Patankar 1980) and SIMPLEC (Van Doormaal and Raithby 1984), have been proposed. The former solves the pressure equation to obtain the pressure field and solves the pressure-correction equation only to correct the velocities. The later incorporates the temperature correction suitable for buoyancy-driven flows. Another algorithm, SIMPLEX (Van Doormaal and Raithby 1985; Raithby and Schneider 1988), takes into account the effects of dropping the neighboring grids and solves a set of algebraic equations for the coefficients in the velocity correction equation. In 1985, the Pressure-Implicit with Splitting of Operators (PISO) pressure-velocity coupling method was proposed to implement two or more correction steps for pressure correction (Issa 1985).

Recently, a new segregated algorithm named CLEAR (Coupled and Linked Equations Algorithm Revised) has been proposed which deals with the coupling between velocity and pressure in fully implicit nature (Tao et al. 2004a, 2004b). This new algorithm completely discards two basic assumptions of the semi-implicit SIMPLE series algorithms which are widely used in the CFD and CHT (Computational Heat Transfer) community. It differs from all SIMPLE-like algorithms in that it solves the improved pressure directly, rather than by adding a

correction term, and no term is dropped in the derivation of the pressure equation. Thus the effects of the neighboring velocity values are fully taken into account, and the coupling between velocity and pressure is fully guaranteed, greatly enhancing the convergence rate of the iteration process. Its robustness is improved by introducing a second relaxation factor (Tao et al. 2004b).

2.4 Numerical Modeling Methods for Supply Diffusers

For mechanically ventilated rooms, the air distribution is highly dependent on the performance of air supply diffusers, especially those used in displacement ventilation (DV) and underfloor air distribution (UFAD) systems. The prediction of diffuser flow characteristics is challenging since the jet flow from the diffuser is complicated due to the complex diffuser geometry and the effects of the confined space.

The CFD technique can save us much time and effort in the investigations of indoor thermal environments, when it is used properly. The reliability and accuracy of CFD simulation depends on several factors, including the turbulence model, the numerical scheme, the boundary condition modeling, etc. Nielsen (1974) pioneered the employment of the CFD technique in ventilation flows. Since that time, CFD has gained widespread application in analyzing indoor air flows and heat or mass transfers. A major bottleneck in this modeling technique is the small size of most diffusers as compared to the size of the room and their high flow velocities. To model the air flow in a room, it is necessary to know the boundary conditions that describe the inlet jet air flow from a supply diffuser. In fact, the method of modeling the air flow supplied by diffusers is believed to be a major limitation in CFD application (Chen and Moser 1991; Heikkinen 1991; Moser 1991; Skovgaard and

Nielsen 1991; Vogel et al. 1993).

Due to the complex geometries that air supply diffusers often have, the aim of simplified diffuser modeling methods is to provide the boundary conditions for supply diffusers without modeling the detailed diffuser geometry. The first detailed investigation work on supply diffusers is the well known international research project IEA Annex-20, organized by the International Energy Agency (IEA 1993). In that project, a HESCO-type nozzle was investigated and different diffuser modeling methods were evaluated for their prediction of air flow patterns and their applicability as design tools, when compared with the experimental data. Although each nozzle can be rotated freely, this study fixed all nozzles in one position: 40^{o} towards the ceiling. Figure 2.1 shows the visualized air flow pattern by smoke in the symmetry plane (Heikkinen 1991). Different modeling methods are described in the following sections.

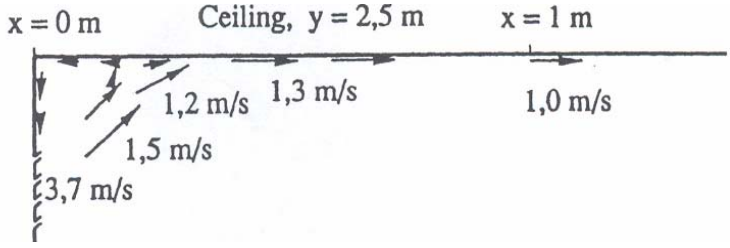

Figure 2.1 Airflow pattern visualized by smoke in the symmetry plane

2.4.1 Simple Opening Method

In the simple opening model the diffuser input boundary is represented by a simple rectangular or circular surface on a wall. The complex diffuser configuration and air flow path in the diffuser are ignored. In the ANNEX-20 project, the simple opening

model of the HESCO-type nozzle was classified into three variants: the basic model, the wide slot model and the multiple slot model, shown in Figure 2.2.

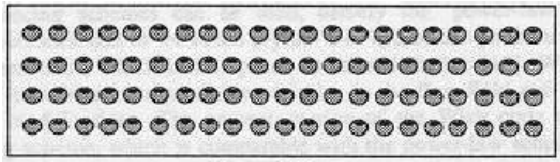

(a)

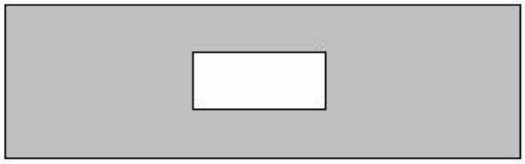

(b)

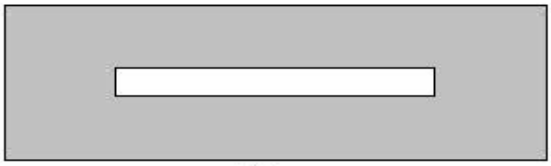

(c)

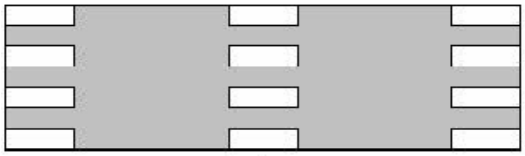

(d)

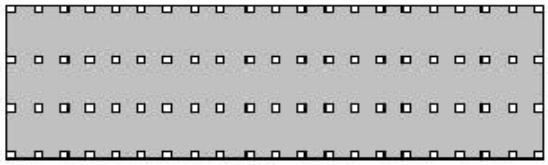

(e)

Figure 2.2 Sketch of the HESCO-type nozzle diffuser and simulation models
(a) The diffuser picture, (b) The basic model, (c) The wide slot model,
(d) The multiple slot (12) model, and (e) The multiple slot (84) model.

In the basic model the complicated diffuser is replaced by a simple opening which has the same effective area as the small nozzles. It was found that this method could reasonably predict the room air flow distributions. However, the small area of nozzles resulted in large inlet velocities, which penetrated too far into the room

(Heikkinen 1991; Skovgaard and Nielsen 1991). Due to the jet spread, the recirculation in the left upper corner (Figure 2.1) was smaller than in real conditions (Heikkinen 1991). In order to overcome this limitation, the wide slot model was developed. Employing this model, mixing was increased within small distances as compared with the basic model, resulting in fast velocity decay near the supply opening. Heikkinen (1991) found that the mixing in the core region and jet penetration were still over-predicted. Chen and Moser (1991) used another multiple slot model and the prediction of air flow was somewhat better than the single slot model, but the predicted result was still not satisfactory.

Heikkinen (1990) found the basic method was unsuitable for non-isothermal air flows. At present, many different diffusers are used in different HVAC systems. The simple opening model is limited to very few of them.

2.4.2 Momentum Method

The momentum method is one promising method, first developed by Chen and Moser (1991). In this method, the supply diffuser is represented as an opening of the same size as the real diffuser, which can be regarded as evenly distributed infinite jets, as shown in Figure 2.3 (Chen and Srebric 2000).

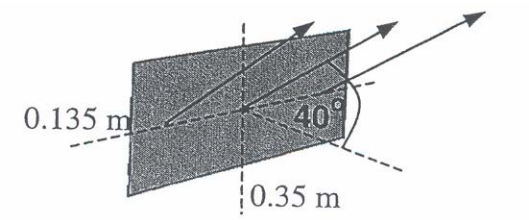

Figure 2.3 Simulation of the nozzle diffuser with the momentum method

This method imposes the initial jet momentum as a boundary condition in CFD simulation. It is easy to use as the initial momentum is normally available. Since the area of the real diffuser is larger than the sum of the areas of the nozzles, the mass flow is not based on nozzle velocity. To ensure the correct mass and momentum flows from the diffuser, the mass and momentum flows need to be decoupled and specified separately. The momentum method requires data on air flow rate, discharge jet velocity or effective diffuser area, supply air turbulence properties, supply air temperature and contaminant concentrations.

This method predicted air velocity and temperature distributions similar to the experimental data (Chen and Moser 1991). However, Heikkinen (1991) found the momentum loss measured in front of the diffuser was approximately 14% of the total momentum and he recommended using a somewhat smaller diffuser area for CFD simulation. Another difference with the experimental observation was no recirculation computed in the upper left corner (Srebric and Chen 2001b) (Figure 2.4). Emvin and Davidson (1996) pointed out that this method was a dangerous way of circumventing the resolution because the entrainment could not be represented properly.

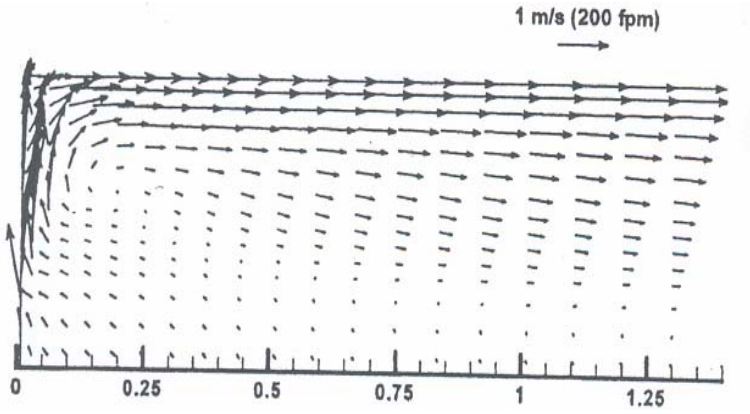

Figure 2.4 Simulated flow field with the momentum method

Recently, Luo and Roux (2004) found that the momentum method together with the RNG $\kappa - \varepsilon$ turbulence model (Chen 1984; Gan 1998) and local mesh refinement can yield good predictions for the HESCO nozzle diffuser. The more detailed research work for the momentum method was finished by Srebric and Chen (2002). They investigated this method for eight different diffusers and compared it with the box method, presented below.

2.4.3 Box Method

The box method is another promising method first developed by Nielsen (1974). This method uses an imaginary box surface to represent the supply diffuser boundary conditions and the flow pattern inside the box is ignored, as presented in Figure 2.5 (Sretric and Chen 2002).

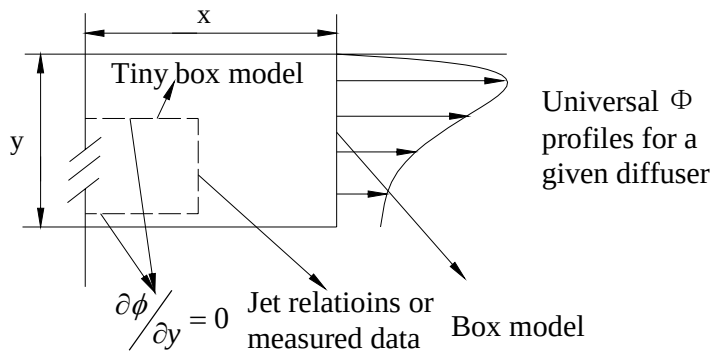

Figure 2.5 Box and tiny box models for the nozzle supply diffuser

The box method needs information on the distributions of the air velocity, turbulence properties, and temperature and contaminant concentrations. To specify the boundary conditions, either suitable jet formulae or measured data should be applied. As described below, the jet relations can be applied only in some special cases, such as fully developed free or attached diffuser jets, assuming that formulae are available

for those types of diffusers. Unfortunately, in many applications, diffuser jets are neither free nor attached, and the transition region tends to be large. Furthermore, the main region of the jet is influenced by room air flow.

Another limitation of this method is the determination of the box size. The box should be large enough to have its boundaries in the fully developed jet region where the velocity and temperature profiles are similar. On the other hand, the box has to be small enough to avoid the impact of room air recirculation and thermal plumes on the jet. Srebric and Chen (2001) pointed out that the box method is not suitable for low Reynolds number flows, in which the buoyancy force strongly influences jet development from its discharge. However, if the buoyancy force is negligible compared to the momentum force at the box surface, the box data gathered under isothermal conditions could be applicable for non-isothermal conditions. They presented a method to determine the critical distance where jet velocities are predominately influenced by momentum forces. The box should be smaller than this distance from the jet origin in the discharge direction. The validation work showed that the box method resulted in good agreement with the experimental data (Nielsen 1997).

In the IEA Annex-20 project, the box method was investigated and found to overpredict the maximum jet velocity more than other simplified methods (Heikkinen 1991). Srebric and Chen (2002) proposed the tiny box method for a slot diffuser simulation, which is slightly different from the box method, and shown in Figure 2.6.

(a) (b)

Figure 2.6 Simulation of the nozzle diffuser
(a) Box method and (b) Tiny box method

In the tiny box method, the box was so small that the temperature and trace-gas concentration at the box surface could be estimated without measurements of the energy and species balance. Srebric and Chen (2001b) also showed details on how to determine the tiny box size and corresponding flow and thermal boundary conditions. One difference between the box and the tiny box methods is that the tiny box does not contain any recirculation flow. When compared with the experimental data, the tiny box method could not predict the jet flow due to the flat velocity profile used at the supply surface. To improve the results, measured data are still needed.

Table 2.2 shows the summary of eight supply diffusers used in different HVAC systems, which were investigated by Srebric and Chen (2002) using the momentum and the box methods.

Table 2.2 Summary of simplified diffuser modeling methods

Diffusers	Box method	Momentum method	Recommend
Nozzle	Good	Poor	Box
Slot (linear)	Good	Poor	Box
Valve	Good	Poor	Box
Displacement	Poor	Good	Momentum
Square ceiling	Good	Good	Momentum
Round ceiling	Good	Good	Momentum
Vortex ceiling	Good	Good	Momentum
Grille	Good	Good	Momentum

2.4.4 Prescribed Velocity Method

In this model, boundary conditions are given at a simple opening and also in the flow field as in the box model. The idea is to minimize the necessary measurements by giving only the most important variables in the most important locations in the jet and to compute the rest, as shown in Figure 2.7 (Nielsen 1992a). This method is easy to use and it is only necessary to measure the velocity parameters in the jet from the actual diffuser used in the predictions. It may also be necessary to update the temperature distribution and the contaminant distribution in the cases of non-isothermal flow and flow with tracer gas distribution, respectively.

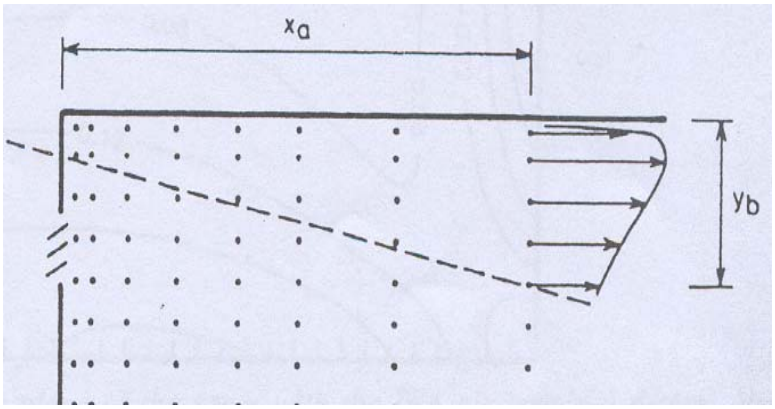

Figure 2.7 Prescribed velocity fields close to the supply opening

For the HESCO-type nozzle in IEA Annex-20, Heikkinen (1991) found that the velocity decay with this method was close to the measured decay. However, the profile in the vertical and horizontal directions was not very good. This was partly due to the prescribed velocity profile, which had a minimum in the symmetry plane. As it requires a minimum amount of measured information, the prescribed velocity method seems to be the most promising one for practical use when the momentum of the jet is not well known. When applying this method, measurements for each diffuser studied are still needed. Additionally, the description of the boundary conditions for the complicated supply diffuser cannot be avoided.

2.4.5 Jet Formulae

Depending on the type of diffuser, ASHRAE (1993) classified diffuser air jets as follows: Linear jets, Compact jets, Radial Jets, Incomplete radial jets, Conical jets and Swirling jets. Air jets have different characteristics depending on the type of diffuser by which they are supplied or the conditions (initial air velocity, temperature, supply air direction, etc.). Some researchers (Nottage 1951; Kostel and Tuve 1955;

Baturin 1972; Miller and Nevins 1972) pioneered the development of the jet formulae.

Theoretically, jet formulae are most appropriate for supply air jet predictions. However, jet formulae have mainly been developed for the main jet region in an empty room. The room should be large enough in order not to interfere with the jet development. Li et al. (1993) reviewed the previous research findings on the characteristics of diffuser air jets and air flow in occupied regions as well as their relationships. They concluded that it is possible to predict the velocity and temperature characteristics of the jets at the point where they enter the occupied zone using current jet theory. Further research, however, is needed to relate the jet characteristics to the air flow and temperature in the occupied zone. The effects of diffuser types and locations, internal heat loads, and obstructions need to be studied and built into prediction models. Srebric (2000) pointed out that indoor air temperature stratification was neglected in jet formulae. In fact, however, air temperature stratification can influence a jet's trajectory (Murakami et al. 1991). These limitations to jet formulae reduce their reliability and accuracy for designing room air distribution systems. Huo et al. (2000) proposed a relatively new method which transfers the specification of complicated air terminal device boundary conditions to the specification of a volume around the diffuser. This method was developed based on the box method.

2.4.6 Fully Represented Geometry Method (FRGM)

Emvin and Davidson (1996) simulated the detailed diffuser geometry used in the IEA Annex-20 project and found that a full representation of the inlet diffuser was

accurate but expensive. This is true due to detailed diffuser geometry requiring millions of grid cells thus needing a large computer capacity. Chen and Jiang (1996) investigated a complex diffuser, shown in Figure 2.8, where similar velocity distributions were achieved by flow visualization. Recently, Abanto et al. (2004) presented numerical simulation results of air flow in a complex computer room with the detailed four-way ceiling supply diffuser geometry modeled (Figure 2.9). They emphasized that the boundary conditions, including real-world geometries, have a strong influence on overall fluid flow behavior. However, no experimental data are provided for comparison with their simulation results. The detailed investigation of this method is presented in Chapter 3, and validated by experimental data.

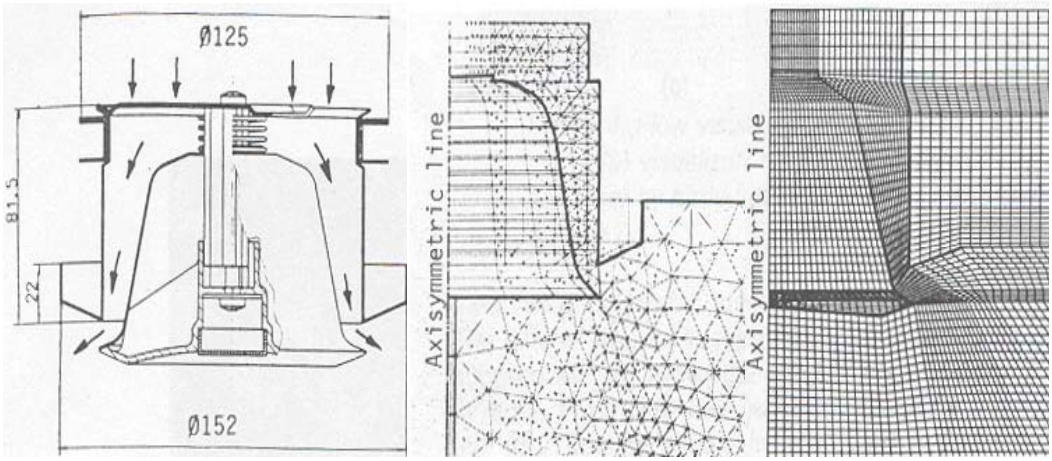

(a) (b) (c)

Figure 2.8 Diffuser sketch and grid systems

(a) Sketch of the diffuser, (b) Unstructured grids, and (c) Body-fitted coordinate

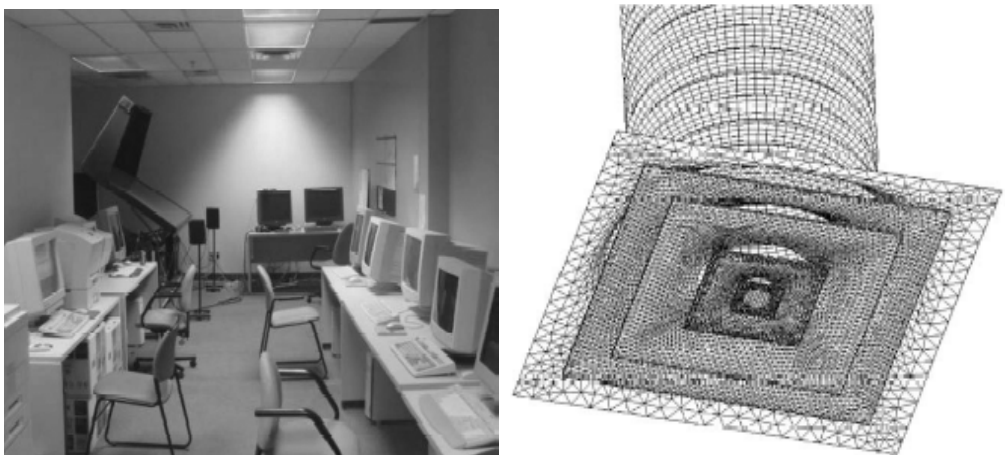

(a) (b)

Figure 2.9 Simulated computer room and one four-way diffuser

2.5 Summary

This chapter presented an overview of the turbulence assumptions for indoor air flows. The main numerical model for indoor air information simulations is the standard $\kappa - \varepsilon$ turbulence model. When it is employed, the following factors should be considered carefully: the boundary conditions, discretization strategies, flow field calculations, etc.

The CFD technique can generally provide reasonable predictions of indoor air flow information. For HVAC systems, the main difficulty lies in the supply diffuser boundary conditions, which describe the supplied air jet from an inlet diffuser into the conditioned space. Some simplified numerical methods, ignoring the complex diffuser geometry, have been proposed. Among them, the box and momentum methods are the most popularly used. Theoretically, jet formulae can determine the decay and profiles of velocity and temperature, which can be used as the flow and thermal boundary conditions for the supply diffuser. However, jet formulae ignore the following factors: the influence of room confinement on air distribution, internal

heat sources (distribution, temperature stratification), internal partitions and obstacles. The fully represented geometry method (FRGM) is believed to present more accurate results near the supply diffuser zone.

In underfloor air distribution (UFAD) systems, swirling diffusers are commonly used. No suitable jet formulae for this type diffuser are presently available. Due to the strong buoyancy force driven flow, the box method mentioned above can not be employed. The momentum method can be used if the momentum loss near the supply diffuser is ignored.

CHAPTER 3 NUMERICAL INVESTIGATION AND EXPERIMENTAL VALIDATION OF FRGM

3.1 Introduction

Leschziner and Rodi (1984) found that, for the swirling jet involving recirculation, the sensitivity of the calculations to the inlet conditions of the nozzle exit is fairly strong. This sensitivity makes the assessment of turbulence model performance a difficult task since the disagreement between predicted results and experimental data may not be so much due to the turbulence model faults as due to the use of inappropriate inlet conditions. Hwang et al. (1993) also found that the solution was sensitive to even small changes in the inlet conditions. In specifying inlet conditions, most of the numerical studies either assume uniform inlet velocities and temperatures, or use the measured data near the swirling diffuser. Owing to the difficulties in obtaining reliable measurements close to the swirling diffuser and to the assumption that the inlet swirl in the flow can be neglected, relatively large differences exist between the numerical predictions and the experimental data for the area near the supply diffuser (Rao et al. 1983; Tekriwal 1994).

This chapter investigates the fully represented geometry method (FRGM) in the swirling diffuser simulation. Due to the difficulties in finding the available dimensions of supply diffusers and detailed experimental data for the area near the supply diffuser used in HVAC systems, the experimental data (Niu and Xu 1988) from a precombustion chamber is employed for the validation work. The standard $\kappa - \varepsilon$ turbulence model was first used, then the RNG $\kappa - \varepsilon$ turbulence model was

investigated and finally the simulation results were compared with the standard $\kappa - \varepsilon$ turbulence model.

3.2 Multi-Domain Interface Information Transfer

The main limitation associated with supply diffusers in CFD simulations is the different dimension scales between the room and the supply diffuser. If the same mesh grid size is employed, the quantity of needed computer memory is very large, requiring a great deal of time. In the fully represented geometry method (FRGM), the CFD calculation domain is extended into the supply air duct and different grid sizes are employed for the room space and diffuser air flow channels. The detailed air flows between the supply diffuser and air-conditioned space should be linked together. FRGM critically depends on the treatment of the interface information transfer between the supply diffuser and the room. The accuracy and efficiency of information transfer and the synchronization of the solution process among adjacent domains affects the stability and convergence characteristics of this method. Some researchers (Kallinderis 1992; Liu and Shyy 1996; Thakur et al. 1998) have presented the detailed algorithm for this method. Figure 3.1 shows the information transfer in a two-dimensional, two-block grid (Thakur et al. 1998).

Through the information transfer between the multi-domain interfaces, the effects of swirling diffusers on overall flow parameters can be more rigorously simulated. Using the well-established flow qualities of a fully developed turbulent flow in a circular or rectangular duct as the incoming boundary conditions, turbulence generation due to the presence of diffuser vanes can be taken into account.

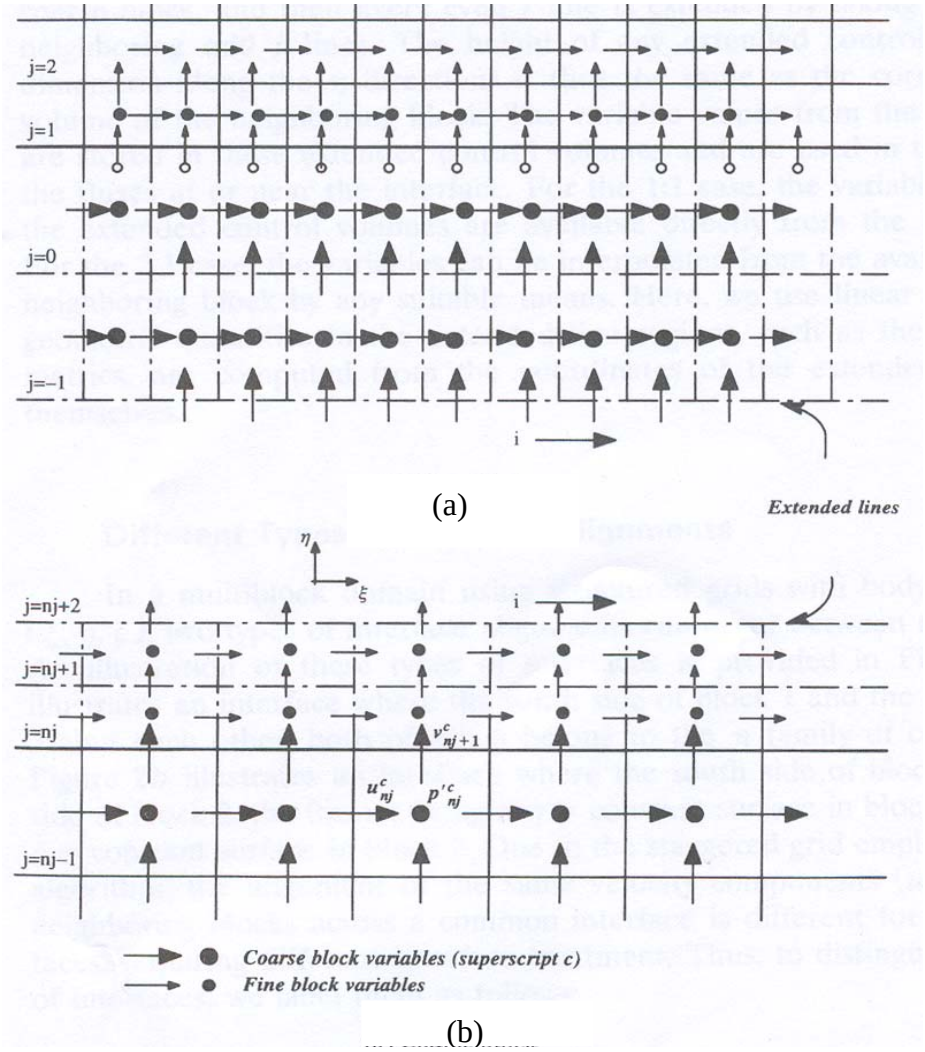

Figure 3.1 Schematic of a multi-domain interface showing extended lines and the variables stored in them: (a) Fine block, and (b) Coarse block

3.3 Employment of Swirling Flow in Engineering Fields

3.3.1 In Combustions and Burners

Kreith and Margolis (1959) first proved that the use of a swirling flow in tube flows could augment surface heat transfer rates relative to flows without swirl. In combustions and burners, swirling flows were extensively used in flame stabilization, due to the enhanced mixing processes between the supplied air and the recirculated high-temperature gas (Davies and Beer 1971; Zhou et al. 1993). A variety of devices

and geometries were developed to induce swirl in internal flows. Date (1974) and Hong and Bergles (1976) employed twisted tape inserts. Sampers et al. (1992) and Li and Tomita (1994) used rotating vanes, propellers, or honey combs near tube entrances in adiabatic flows. A swirling flow can be influenced by different diffuser angles and swirl numbers (Singer 1981; Visser and Plessis 1992).

Hedlund et al. (1999a, 1999b, 2000) reviewed a variety of devices and geometries to induce swirl in internal flows. They proposed another swirl chamber, which employed tangential jets from wall slots or ducts to induce large-scale swirling in internal tube flows. The changes in the local Nussel number in this swirl chamber were inspected for variable Reynolds numbers and ratios of inlet temperature to wall temperature. The aim was to show the important changes in surface heat transfer and flow structural characteristics through infrared imaging in order to find better schemes for cooling turbine components located just downstream from the combustion chamber.

3.3.2 In HVAC Systems

Turbulent, swirling flows are also used as air static mixers in air-conditioning systems. When the mixing between two airstreams is not complete, large differences in temperature, velocities and other properties will exist across the plenum. These large differences can create many problems, some of which include frozen oils (Delaney et al. 1984), an inadequate amount of outdoor air (EPA 1991) and inaccuracies in the control system (Kao 1985). One method commonly used to reduce this stratification is including a static air mixer in the air-handling unit (AHU). The static air mixer can create additional turbulence in air streams and, as a result,

increase mixing between the return and outdoor airstreams and achieve a uniform combined air stream (Haines 1980).

Swirling diffusers are used in the UFAD system to ensure effective thermal mixing near the floor while maintaining the stratifications between the occupied space and the upper space of a room to conserve energy (Vivian et al. 2002). A preliminary CFD simulation indicates that the swirling flow near the floor level can result in a well-mixed air flow pattern, potentially reducing the PD (percentage dissatisfied due to draft) value in the occupied zone due to the raised temperature combined with the increased air movement (Xu and Niu 2003).

3.4 Numerical Models for Swirling Flow Investigations

In order to better understand the complicated characteristics of swirling flows, many turbulence models have been introduced. The standard $\kappa - \varepsilon$ turbulence model (Launder and Spalding 1974) has been the most widely used (Favaloro et al. 1991; Chuang et al. 1999; Zhou et al. 1999; Niu and Chuk 2001; Feng 2002). Some commercial codes were also employed for complicated swirling flow simulations (Eastwick et al. 1999; Ma et al. 2001; Stockwell 2001; Fan et al. 2002). In specifying inlet conditions, all of the above numerical studies either assumed uniform velocities and temperatures, or used the measured data near the swirling diffuser.

The following sections investigated in detail the fully represented geometry method for the swirling supply diffuser. Due to the lack of experimental data for the area near the swirling diffuser in HVAC systems, the validation work was based on the experimental data from a precombustion chamber. In this chamber, three air streams

were mixed. A swirling diffuser was used for the primary air supply, which is similar to the diffuser used in the underfloor air distribution system. The detailed experimental setup and measurements were carried out by Niu and Xu (1988).

3.5 Experiment Setup

Figure 3.2 shows the configuration of the precombustion chamber. The primary air flow is distributed into the chamber along an axial fixed inlet swirling diffuser. Two concentric axial air flows, named the secondary and the tertiary air flows, are supplied downstream from the chamber.

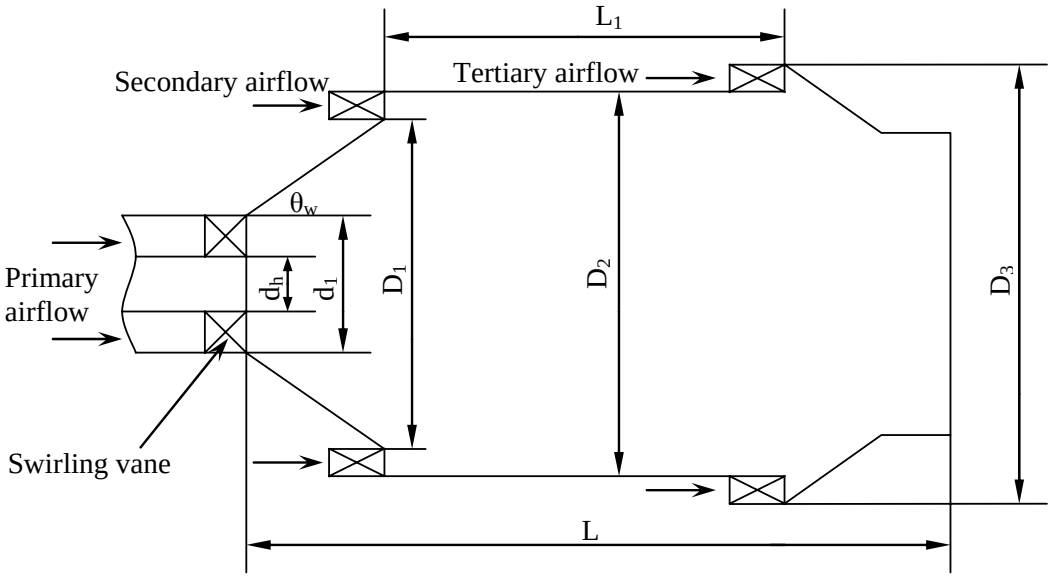

Figure 3.2 Configuration of the precombustion chamber
L=425mm, L_1=270mm, d_h=62mm, d_1=111mm,D_1=278mm, D_2=300mm, D_3=350mm, θ_w=45^o

The Reynolds numbers of the three supply air streams are 1.51×10^5, 6.0×10^4 and 7.3×10^4, respectively. The schematic test system for this precombustion chamber is given in Figure 3.3. Electrical heaters with a maximum power of 30 kW are installed in the primary and tertiary ducts to control the supply air temperature. Through the

controlled electrical heaters, the temperature differences among the three air streams could be maintained at approximately 15°C. Valves were used to control the supply air flow rates, which were measured by three flow meters.

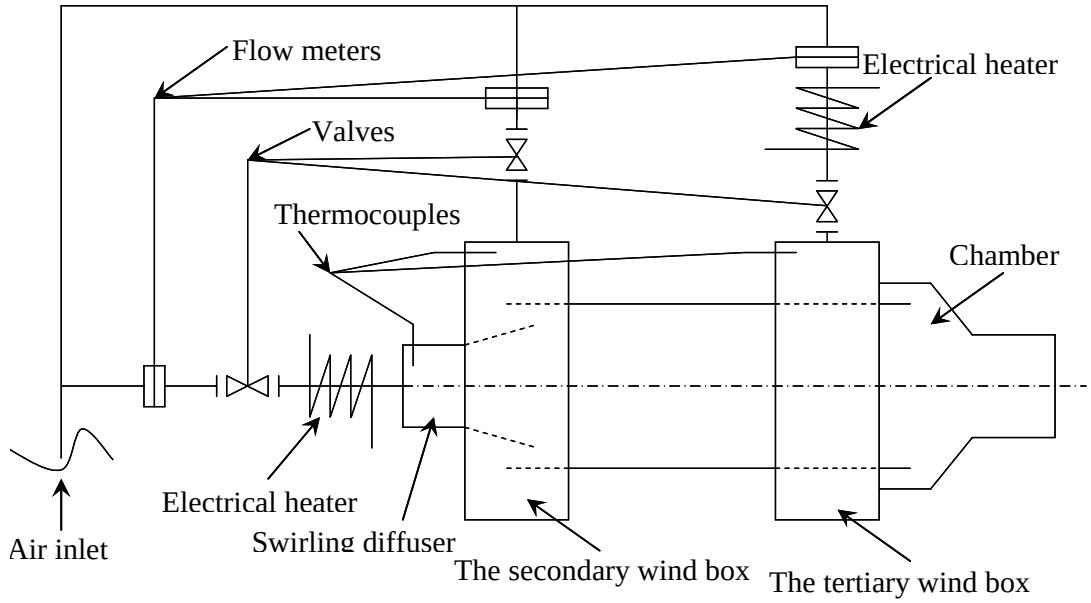

Figure 3.3 Schematic test system of the experimental plant

The temperature distributions in the chambers are measured simultaneously by thermocouples at eight axial positions at a radial distance every 2.5mm, as shown in Figure 3.4(a). During the measurements, the thermocouples are moved along the radial direction, and temperatures at radial points of every 2.5mm distance are recorded. Figure 3.4(b) is the coordinate system for subsequent numerical simulations. A three-hole pitot probe is used to measure the axial and tangential velocity components of the three-dimensional flow of the swirling jet on eight axial positions at radial positions of every 2.5mm distance. Manual adjustments are made according to the static pressure differences from two static pressure holes so that the total pressure hole is maintained facing the flow direction. Thus, the low radial

velocity component is not measured in this chamber, and it is expected that its effects on the accuracy of the two major components are minimal.

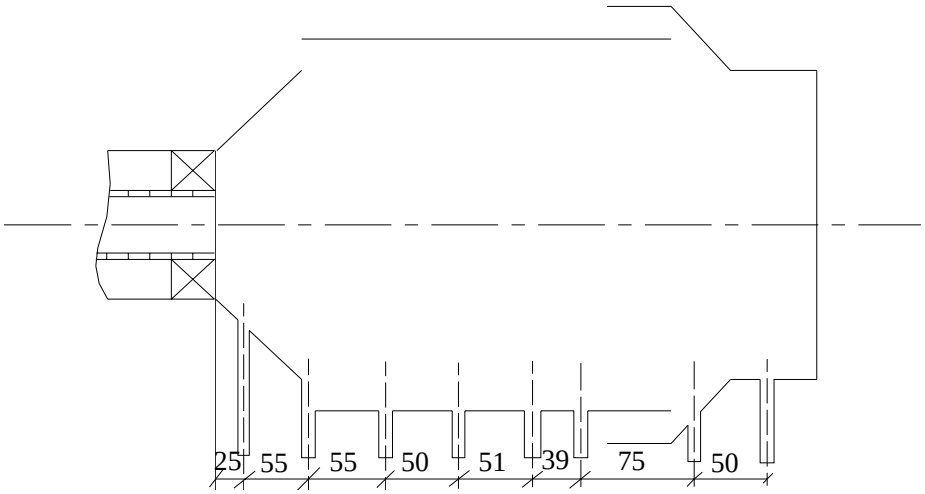

(a)

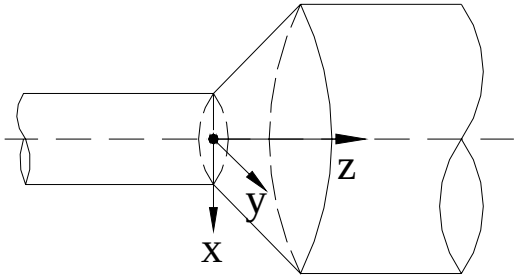

(b)

Figure 3.4 Axial measurement positions of the precombustion chamber
(a) Measurement positions, and (b) Coordinate system for numerical simulation

The local mixing fractions of the primary, secondary and tertiary air cannot be measured directly, but can be indirectly induced from the measured temperature. Figure 3.5 illustrates the adiabatic mixing processes of two air streams with the same physical properties.

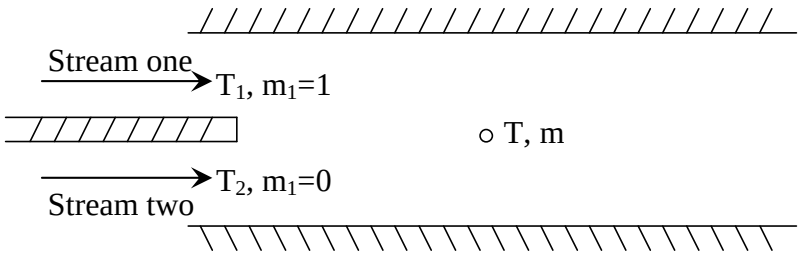

Figure 3.5 Sketch map of two combined air streams

Both local enthalpy and the concentration of a stream in the mixture can be described by the following equation:

$$div(\rho\vec{U}\phi - \Gamma_{\phi} grad\phi) = 0 \tag{3.1}$$

where ϕ can be the temperature or mass fraction of the air stream.

The boundary conditions for the temperature T and mass fraction m_1 for stream one can be described as follows:

$$\left.\begin{array}{ll} \text{At stream one inlet:} & T = T_1, m_1 = 1 \\ \text{At stream two inlet:} & T = T_2, m_1 = 0 \\ \text{At the wall surface:} & \partial T/\partial n = 0, \partial m/\partial n = 0 \end{array}\right\} \tag{3.2}$$

$f_1 = \dfrac{T - T_2}{T_1 - T_2}$ is defined; Equation (3.1) is also suitable for f_1. The boundary conditions for f_1 are as follows:

$$\left.\begin{array}{ll} \text{At stream one inlet:} & T = T_1, m_1 = 1 \\ \text{At stream two inlet:} & T = T_2, m_1 = 0 \\ \text{At the wall surface:} & \partial T/\partial n = 0, \partial m/\partial n = 0 \end{array}\right\} \tag{3.3}$$

The flow in this precombustion chamber is assumed to be strong turbulence with a high Reynolds number and low temperature difference. Based on the similarity relations between the heat flow equation and mass transfer equation, the turbulence heat and mass diffusion coefficients were almost equal (Eckert 1959). With the same conservation equation and boundary conditions, f_1 and m_1 have the same expressions. Then we get:

$$m_1 = f_1 \tag{3.4}$$

; i.e.,

$$m_1 = \frac{T - T_2}{T_1 - T_2} \tag{3.5}$$

Therefore, from the measured air supply temperatures T_1, T_2 and the local temperature T, the local mixing fraction of the primary air can be calculated. Similarly, the mass fraction distribution of other air streams can also be found experimentally.

3.6 Numerical Simulation Characteristics

The standard $\kappa - \varepsilon$ turbulence model was employed and solved using the SIMPLE-C algorithm (Van Doormaal and Raithby 1984). In the combustion chamber, the swirling jet was generated by a fixed-vane swirl-generating device, as shown in Figure 3.6. The vane declining angle was 20^o, relative to the axial direction. The

number of the swirling vanes was 12. The detailed dimensions of the supply diffuser vane are shown in Table 3.1.

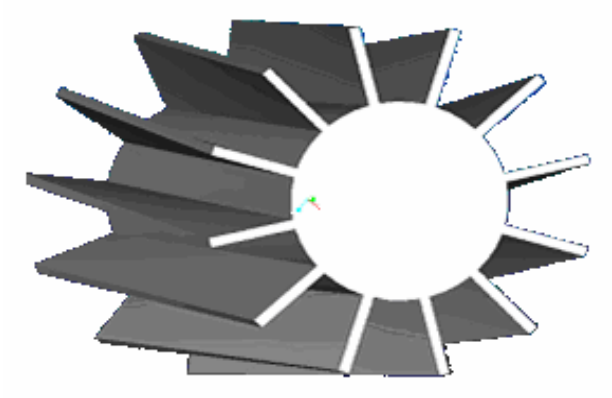

Figure 3.6 Configuration of the inlet swirling diffuser

Table 3.1 Detailed vane dimensions of the fixed-swirling diffuser

	Vane length	Vane thickness	Inner diameter	Outer diameter
Dimension (mm)	150	3	62	111

For the purpose of comparisons, the momentum method to specify the inlet conditions was also tested. Figure 3.7 shows the velocity vector graph of the momentum method. In this method, the supply velocity (V) was decomposed to the axial component (V_{axial}) and the tangential component ($V_{tangential}$), which were determined by either measured data or assumed uniform supply velocities. No radial velocity component exists for the momentum method.

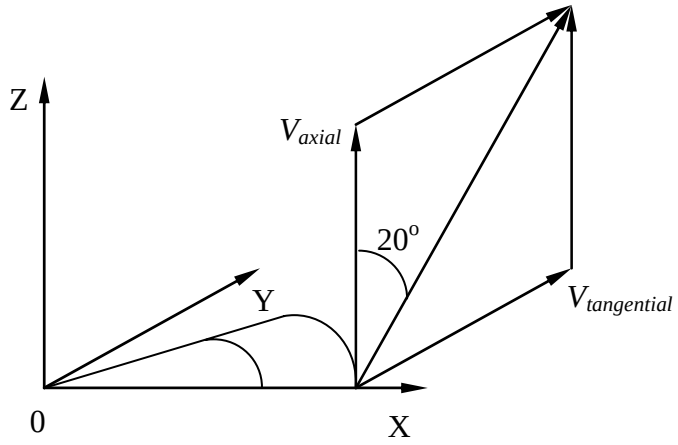

Figure 3.7 Velocity vector graph of the inlet velocity (momentum method)

The swirling diffuser configuration was generated by the CAD software Pro/Engineering and imported into Gambit (FLUENT 2001) for the grid mesh. The swirling diffuser vanes were actually removed and the left is the flow channel space in the simulation domain. In cylindrical coordinates, due to periodicity, only 1-12th of the 3-D zone was chosen in the simulation domain to cover one whole swirling vane, as shown in Figure 3.8. Figure 3.8(b) presents the interfaces for flow information transfer between the supply swirling diffuser and the precombustion chamber. Figure 3.9 shows the mesh grids in the interfaces and partial side walls. Using the multi-grid technique, the flows between the swirling diffuser outlet and chamber inlet were linked together (Xu and Niu 2003).

The present numerical model employed the following facts, features and assumptions:

1. The geometry and flow conditions are periodic along the tangential direction, and only 1-12th of the chamber zone is discretized for computational economy. There are a total of 1,408,470 cells in the simulation chamber zone. In the swirling diffuser zone, the number of cells is 467,024.

2. The inlet conditions for the three air jets were assumed to be fully developed turbulence conditions. The turbulence intensity ($I = 0.16(R_e)^{-1/8}$) and turbulence length scale ($l = 0.07D_e$) (FLUENT 2001) were set as the inlet conditions for the standard $\kappa - \varepsilon$ turbulence model (Table 3.2).
3. In order to avoid reversed flows at the outlet of the calculation domain, the simulated domain was extended to 0.6m downstream from the chamber inlet, and a zero-gradient exit condition was used at this domain outlet, where the simulated results indicated that no recirculation occurred when the simulation results were converged.
4. During the numerical simulation, the buoyancy effect was neglected, and the density of air was assumed to be uniform. This is based upon the high Reynolds number and small temperature difference, and therefore small Archimedes number conditions.
5. The near-wall grid size had a significant effect on the accurate simulation of heat transfer when the standard wall function approach was used. Due to the high velocity near the wall and the relatively low velocity in the middle zone of the precombustion chamber, the successive ratio scheme (FLUENT 2001) was used to mesh the simulated zone. Near the wall, the radial cell size was 0.2mm and near the central line the radial cell length was 2.0 mm. In the axial direction, the cell length was 2.0mm.

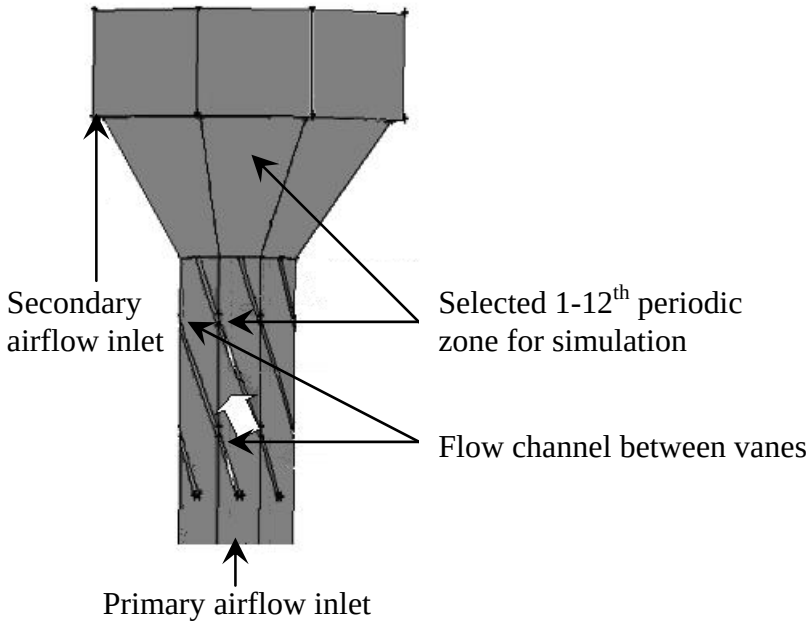

(a)

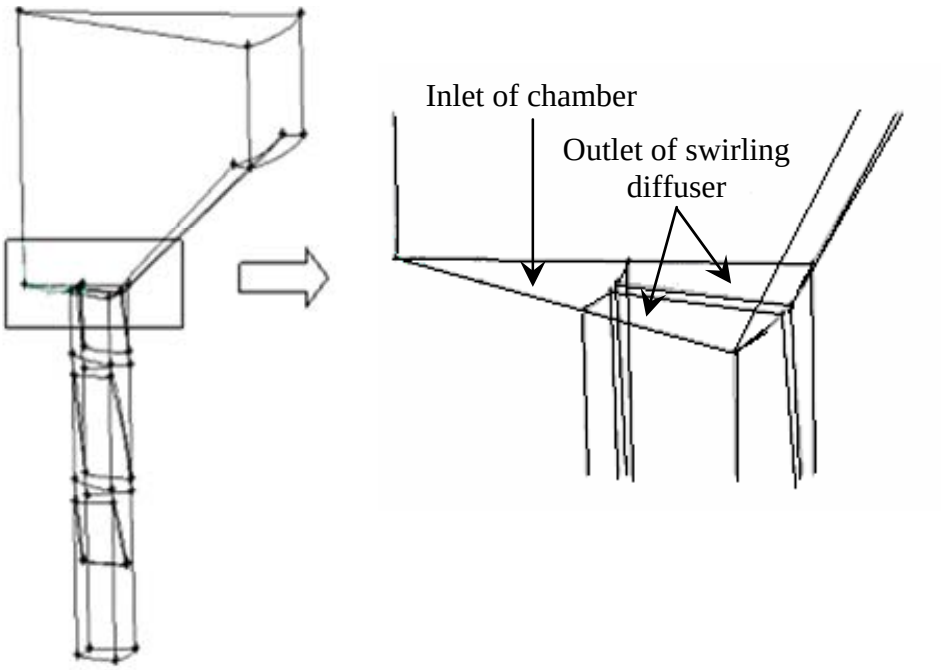

(b)

Figure 3.8 Simulated 1-12th periodic zone (including one whole vane)
(a) 1-12th periodic zone for simulation, and (b) Interfaces between the swirling diffuser and precombustion chamber

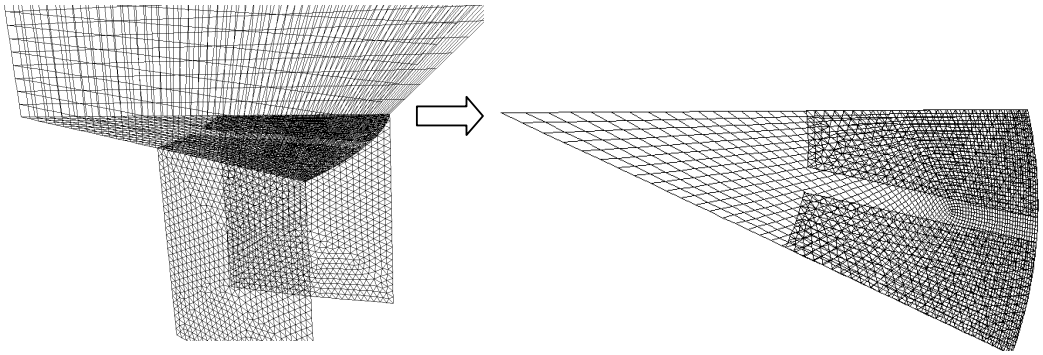

Figure 3.9 Interface and partial wall mesh grids in the precombustion chamber

Table 3.2 Boundary conditions of the simulation

	Boundary conditions
Primary air	T=318K; V= 49.37m/s; I = 3.6%; l = 0.00343m.
Secondary air	T=303K; V= 43.31m/s; I= 4%; l = 0.00154m.
Tertiary air	T=303K; V= 23.26m/s; I= 3.9%; l = 0.0035m.
Wall	T=300K
Outlet	Outflow

3.7 Simulation Results Compared with the Experimental Data

During the following simulations, the near-wall cell was adapted in order to place the y+ (dimensionless distance) value in the range of 10-70 to ensure the validity of the standard wall function. The typical computation time for a convergent solution of the whole simulation was approximately 24 hours in the academic UNIX machine composed of 16 PCs with 1.2 GHz processor (HKPU22). The simulated field distributions are illustrated in Figure 3.10 to Figure 3.15. Taking advantage of the symmetrical shape of the chamber, only half of the configuration is shown in these figures.

3.7.1 Velocity Distributions

Figure 3.10(a) shows the assumed uniform inlet air tangential velocity distribution of the momentum method at the surface of the precombustion chamber inlet.

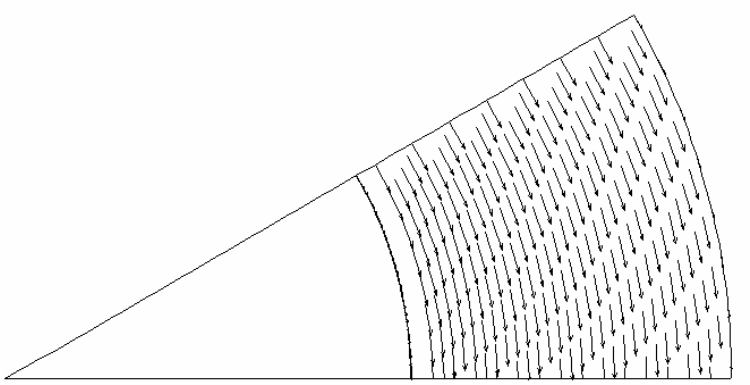

(a)

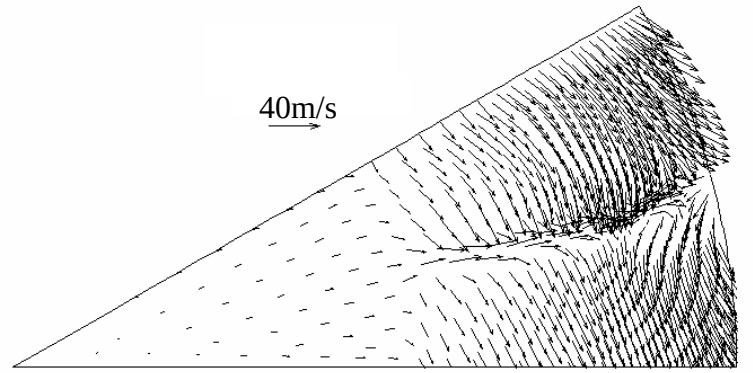

(b)

Figure 3.10 Velocity vector distributions on the inlet plane of the precombustion chamber (Z=0.0m)
(a) Momentum method, and (b) FRGM

Obviously, the momentum method uses constant tangential velocity distributions at the supply inlet and no radial velocity exists. However, for the fully represented geometry method (FRGM), the simulated velocity vectors show fairly large variations (Figure 3.10(b)). Also, a higher radial direction flow can be observed, which may indicate the combined effects of the centrifugal force and the

entrainments of the concentric annular secondary air jet. These effects appear to have an impact on the outflow of the primary air upstream much sooner than usually thought. It is expected that these effects cannot be represented by the momentum method.

3.7.1.1 Axial Velocity Distributions

The velocity vector distributions of FRGM in the axial direction plane are presented in Figure 3.11. The simulated velocity distribution within this chamber is fairly unique. It shows that the velocity near the chamber wall is much higher than the internal zone. It can also be seen that the swirling jet flows along the wall and immediately adjacent to the outlet of the primary air, while the reversed flow appears to penetrate right to the primary air inlet. Within the reversed flow zone, the magnitude of the velocity is quite small compared with the inlet velocity, which is very important from the perspective of the flame stabilization (Zhao and Chan 2000).

In the core zone of the cylindrical chamber in Figure 3.11(b), the axial velocity vector shows that the flow is along the negative z direction. This zone is also called the reversed flow zone. With the distance of the flow increasing from the inlet, the radius of the reversed zone first increases and then decreases. The axial velocity distributions in the precombustion chamber show the typical ‘M’ shape. Beyond the recirculation zone along the axial direction, there is a tendency for the magnitude of the axial velocity to decrease with the increasing *z*, which is due to the flattening of the velocity profiles and the effect of jet spread. The simulated results are in good agreement with the experimental results (Niu and Xu 1988).

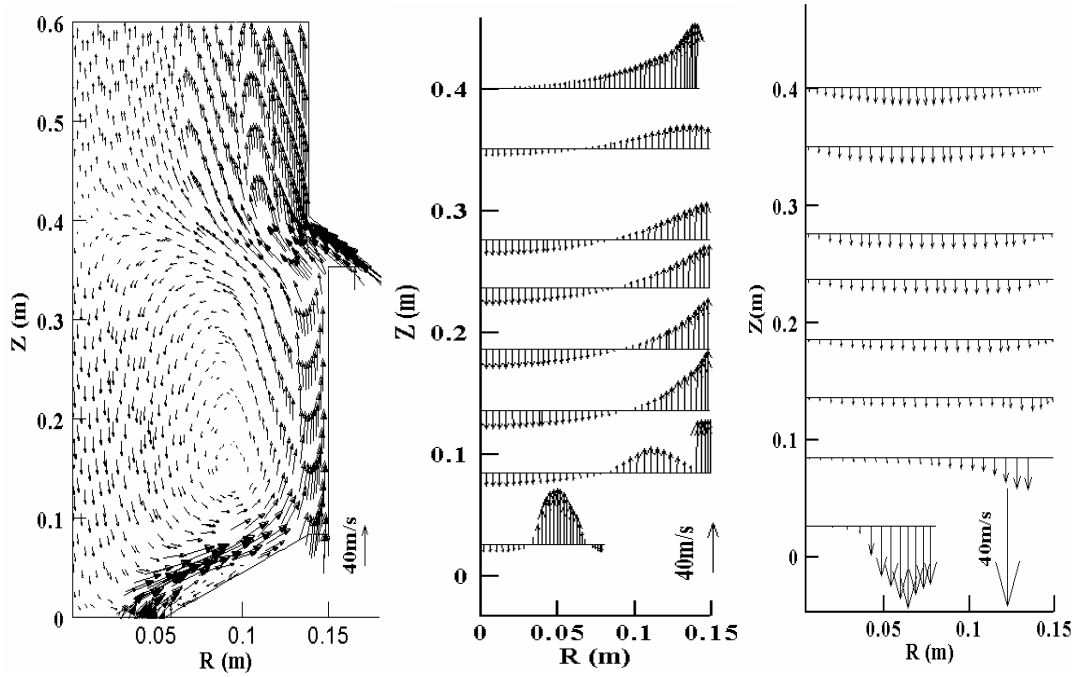

(a) (b) (c)

Figure 3.11 Vector distributions of air flow velocities in plane R-Z (FRGM)
(a) Vectors, (b) Axial velocity vectors, and (c) Tangential velocity vectors

In order to compare the different results of axial velocity distributions between the momentum method and FRGM, closer comparisons of the simulation results with the experimental data are illustrated in Figure 3.12. Due to the lack of experimental data near the supply swirling diffuser, only simulated results from the two methods are presented (Figures 3.12(a) and 3.12(b)). Shown in Figure 3.12(c) is the comparison of the predicted and experimental axial velocity profiles. It can be seen that the predicted axial velocity using FRGM is in better agreement with the measured data than that with the momentum method. However, we can also see that two peaks of the axial velocity profile predicted by these two methods are very different from the experimental data. The predicted reversed flow occurs between the primary air and the secondary air flow, which was not borne out in the experimental measurement. The velocity peaks predicted by the momentum method are obviously related to the assumed inlet velocity profile. The predicted primary air

flow penetrates more deeply into the reversed flow, while in the experiment the primary air tends to be more attached to the chamber wall. The mixing of the primary air, which in combustion applications is actually laden with pulverized coal, with the reversed flow would have a greater impact on the combustion processes. This would indicate that, for a full simulation, including the combustion process, the inlet condition specification might be more significant.

It appears that, farther downstream from the swirling diffuser, the predicted simulation velocity profiles from the two methods become similar (Figures 3.12(d-f)). However, FRGM can more accurately predict the size of the recirculation zone. Both methods overpredict the peak axial velocity near the chamber wall down-stream from the tertiary air inlet (Figure 3.12(g)), which may be attributed to the deficiencies of the $\kappa - \varepsilon$ turbulence model. This aspect will be further examined using other improved turbulence models.

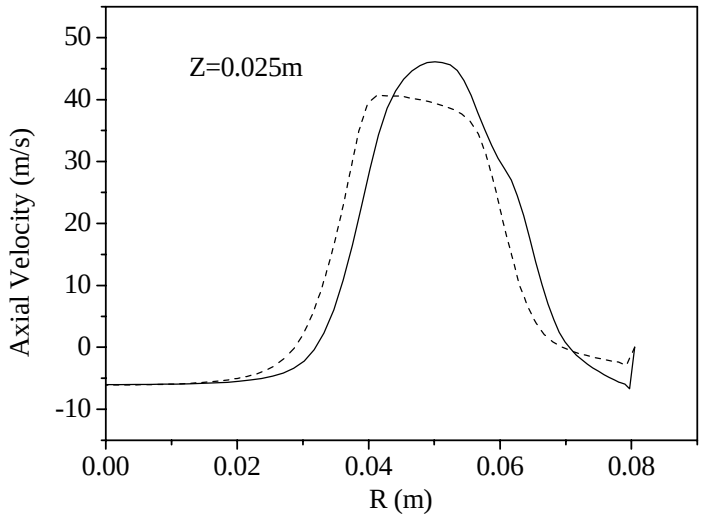

(a)

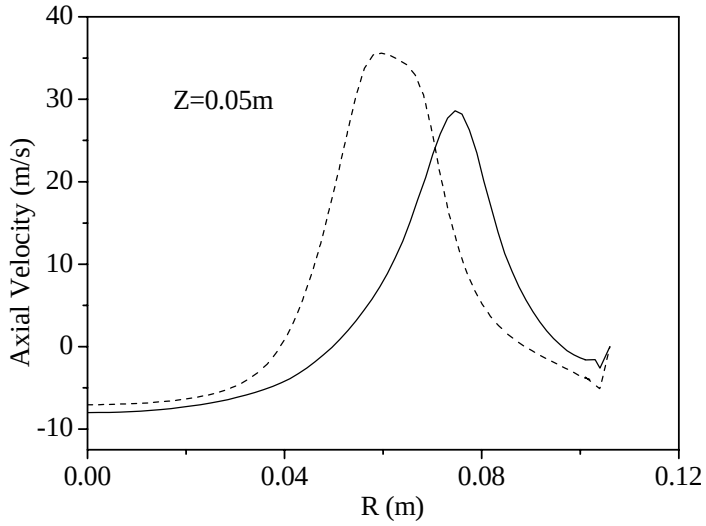
Z=0.05m
Axial Velocity (m/s)
R (m)
40
30
20
10
0
-10
0.00
0.04
0.08
0.12

(b)

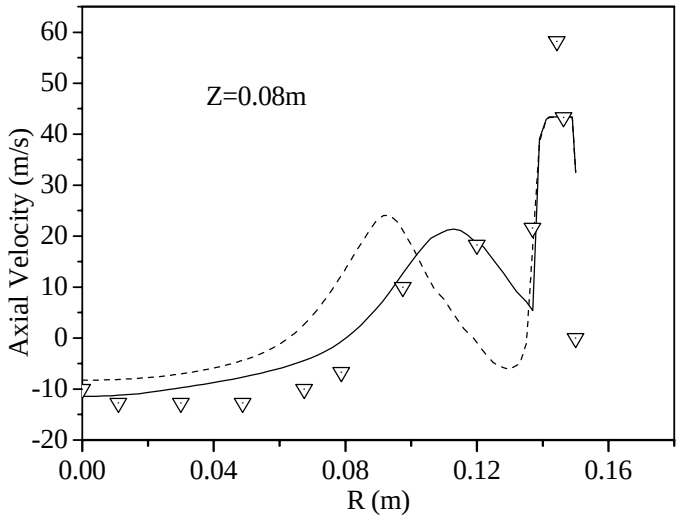
Z=0.08m
Axial Velocity (m/s)
R (m)
60
50
40
30
20
10
0
-10
-20
0.00
0.04
0.08
0.12
0.16

(c)

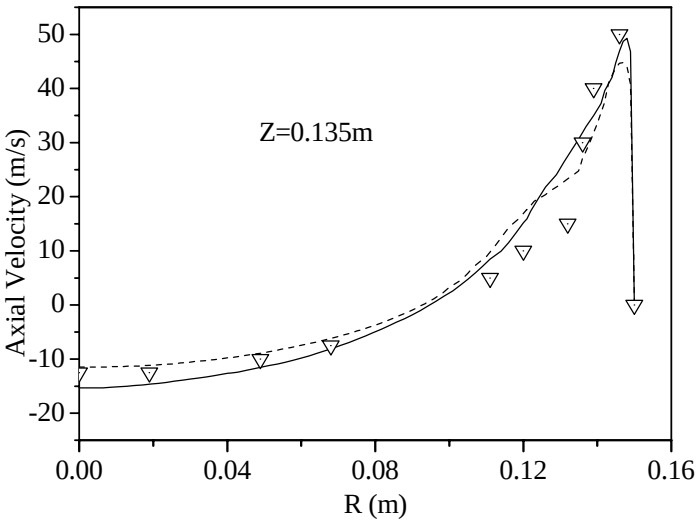
Z=0.135m
Axial Velocity (m/s)
R (m)
50
40
30
20
10
0
-10
-20
0.00
0.04
0.08
0.12
0.16

(d)

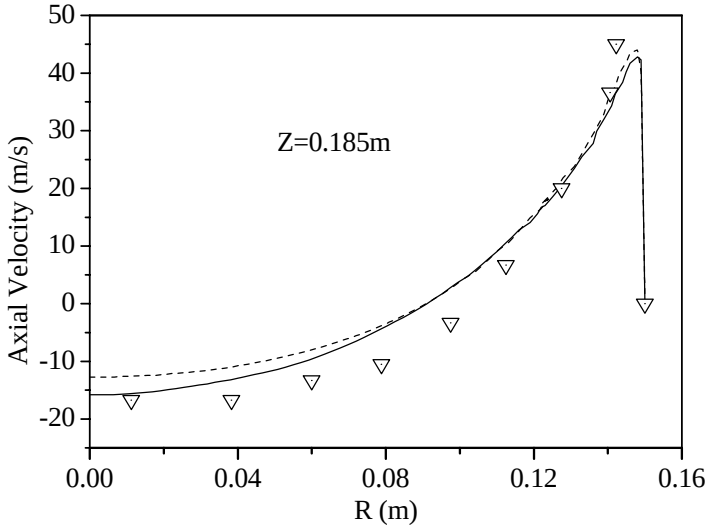

(e)

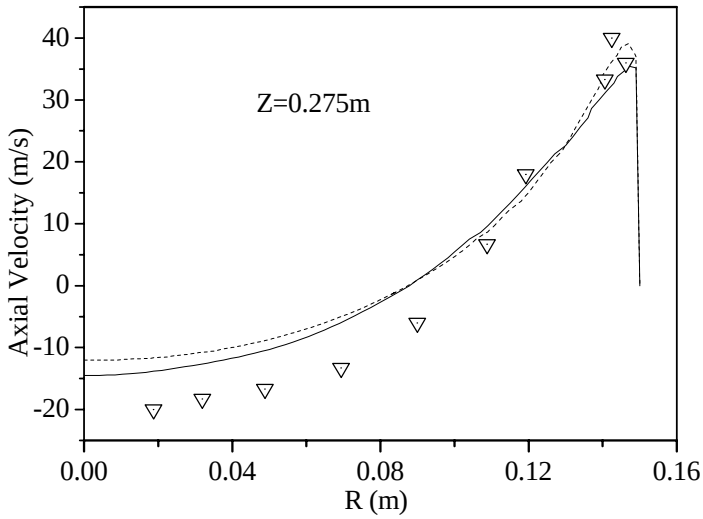

(f)

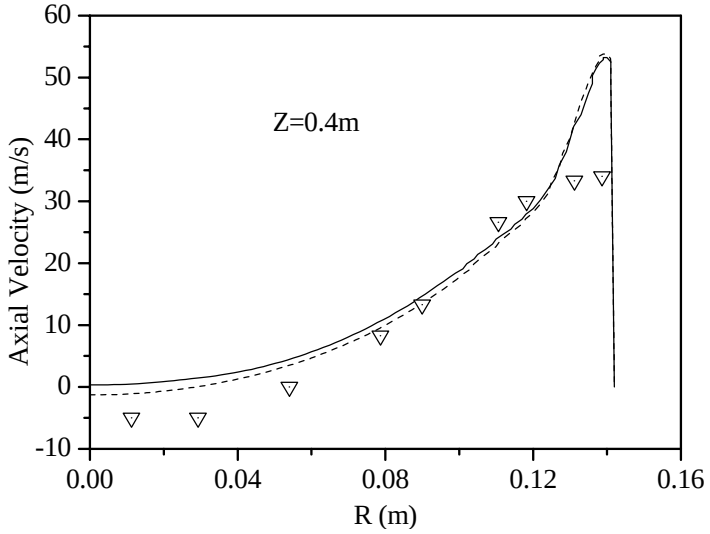

(g)

Figure 3.12 Axial velocity distribution comparisons

(FRGM: ——, Momentum method: - - - -, Experimental data: ▽)

3.7.1.2 Tangential Velocity Distributions

Generally, the tangential velocities are much lower than the axial velocity, increasing along the radius *R* from zero on the cross-sections (Figure 3.11(c)). This indicates the presence of a forced-vortex type of motion. With *R* further increased, the profiles become flat, and the tangential velocity decreases towards the wall. For tangential velocity comparisons, only three groups of experimental data are available on cross sections (Z=0.08m, 0.135m and 0.185m). Just like the axial velocity distribution, near the swirling diffuser, the tangential peak velocity from the simulation results using FRGM is closer to the side wall (Figures 3.13(a) and 3.13(b)), but both methods overpredict the peak tangential velocity of the primary air stream near the chamber wall, as compared with the experimental data (Figures 3.13(c) and 3.13(d)). In the downstream zone, there are no obvious differences between these two methods, as shown in Figures 3.13(e-g).

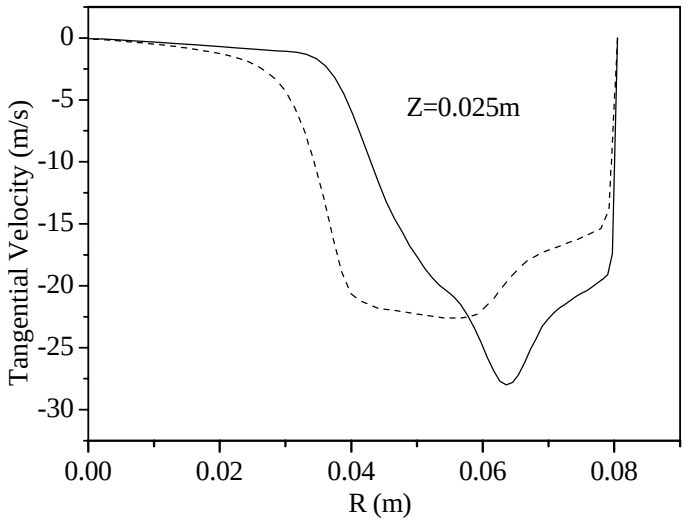

(a)

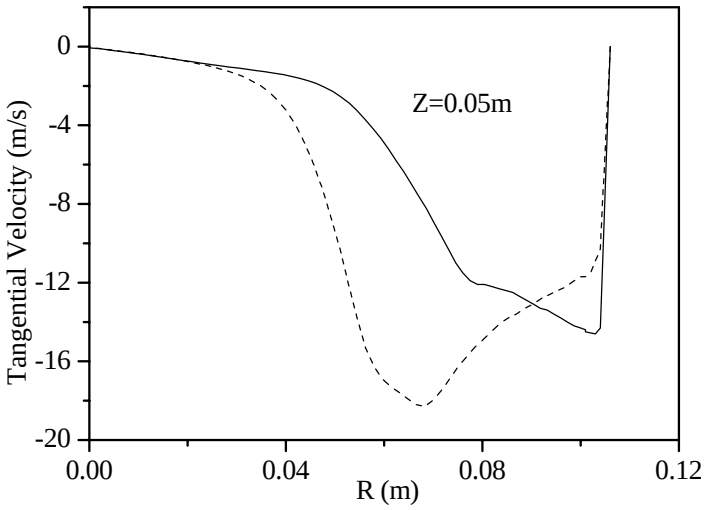
Z=0.05m
Tangential Velocity (m/s)
R (m)
0
-4
-8
-12
-16
-20
0.00
0.04
0.08
0.12

(b)

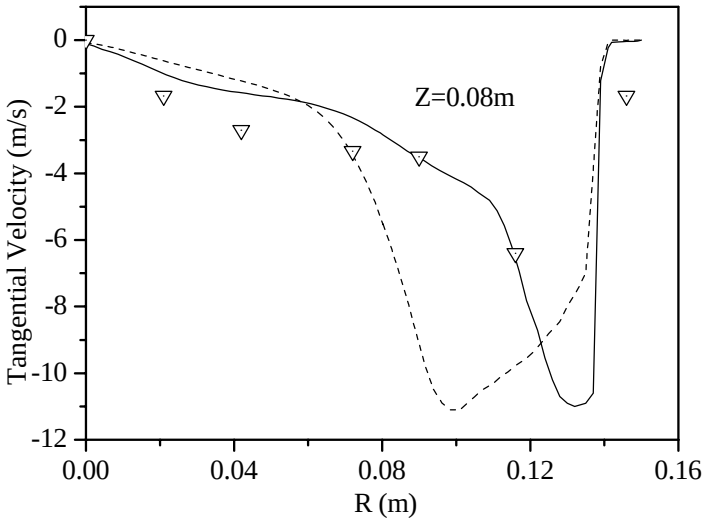
Z=0.08m
Tangential Velocity (m/s)
R (m)
0
-2
-4
-6
-8
-10
-12
0.00
0.04
0.08
0.12
0.16

(c)

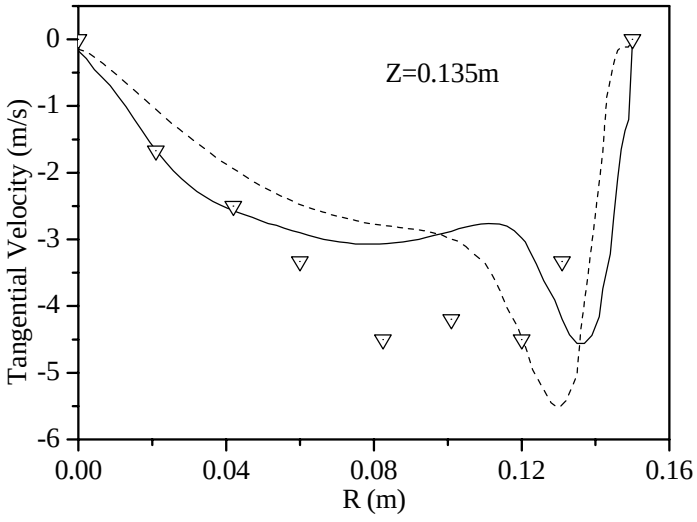
Z=0.135m
Tangential Velocity (m/s)
R (m)
0
-1
-2
-3
-4
-5
-6
0.00
0.04
0.08
0.12
0.16

(d)

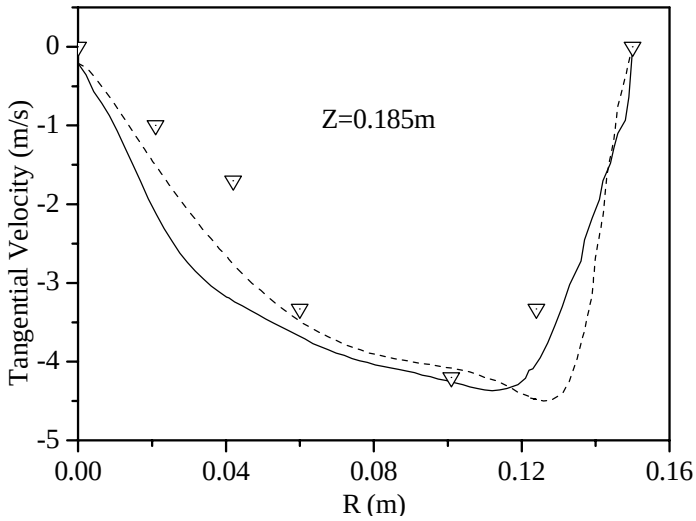

(e)

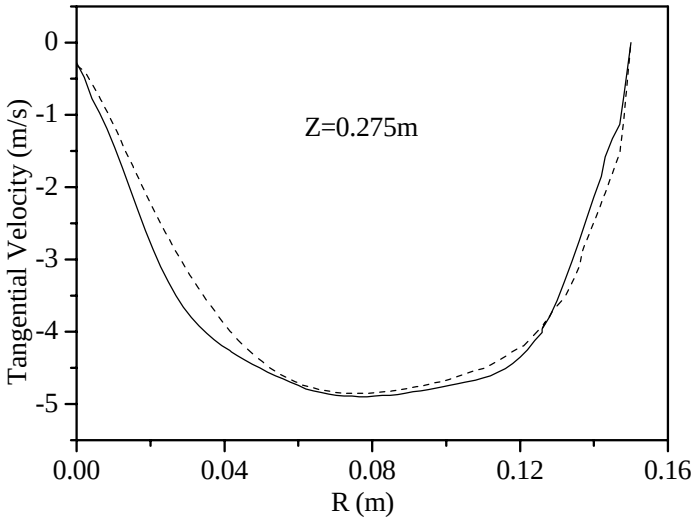

(f)

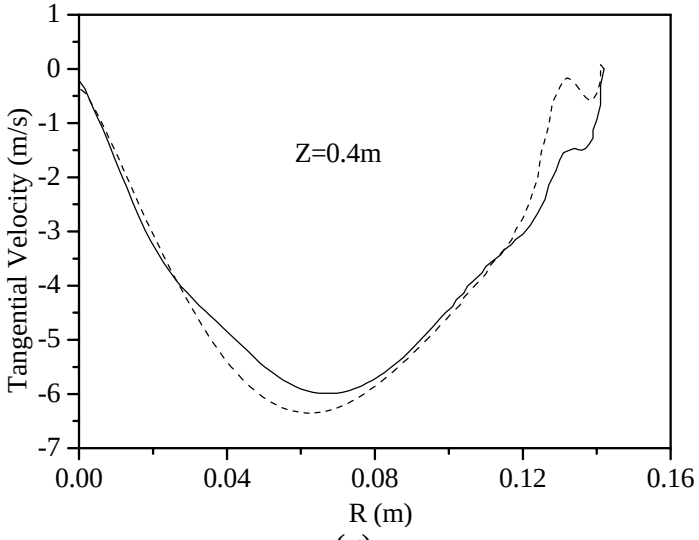

(g)

Figure 3.13 Tangential velocity distribution comparisons

(FRGM:——, Momentum method: - - - -, Experimental data: ▽)

3.7.2 Contours of Mass Fraction

3.7.2.1 Primary Air Flow Mass Fraction

Figure 3.14(a) is the simulation result of the primary air mass fraction contours from the fully represented geometry method. It shows that the primary air flow is distributed into the precombustion chamber along the gradually enlarged wall. The concentration of primary air flow increases with the increasing radius *R*. The typical 'M' shape is shown, which indicates that the primary air flow is combined with two other streams as the annular jet forms: the outside is combined with the secondary air flow and the inside is combined with the reversed streams. Near the outlet of the chamber, the mass fraction becomes uniform, indicating that the primary air flow is fully mixed with the secondary air flow.

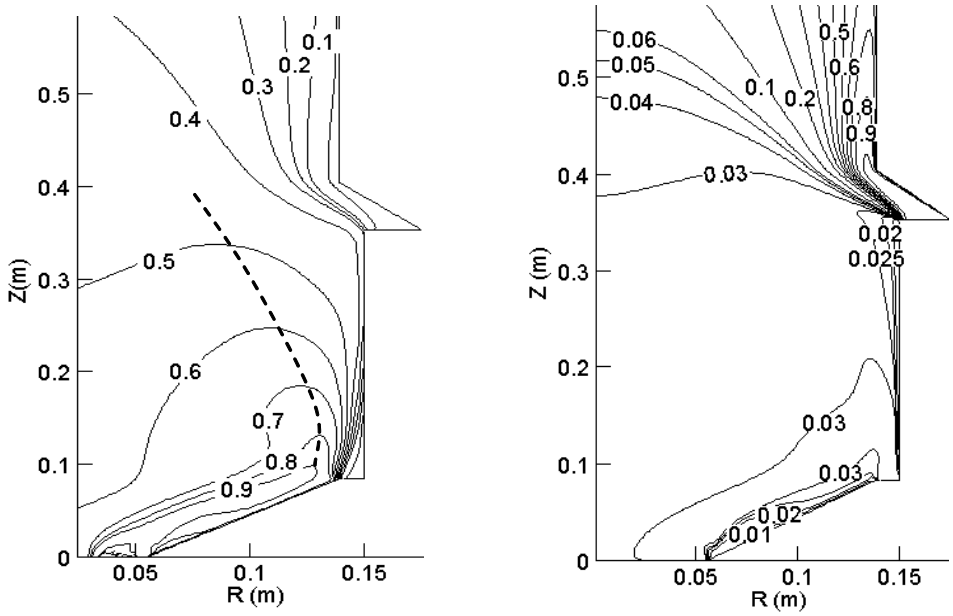

(a) (b)

Figure 3.14 Simulated mass fraction contours of air streams (FRGM)
(a) The primary air stream, and (b) The tertiary air stream.

Figure 3.15 shows the mass fraction comparisons of the primary air stream at eight axial positions. The mass fractions are chosen from experimental data only for the area near the precombustion chamber wall due to the large concentration gradient. The predicted simulation mass fractions from these two methods are very similar in the core zone of the chamber, where the mass concentration is very uniform. In Figure 3.15(b), the mass fraction peak from the FRGM is closer to the chamber wall than the momentum method, due to the combined effects of the centrifugal force at the outlet of the swirling primary air. Near the combustion wall, the two methods show a little difference in mass fraction distributions. At the same space locations near the chamber wall, the primary air mass concentration from the FRGM is larger than that from the momentum method (Figures 3.15(c-h)).

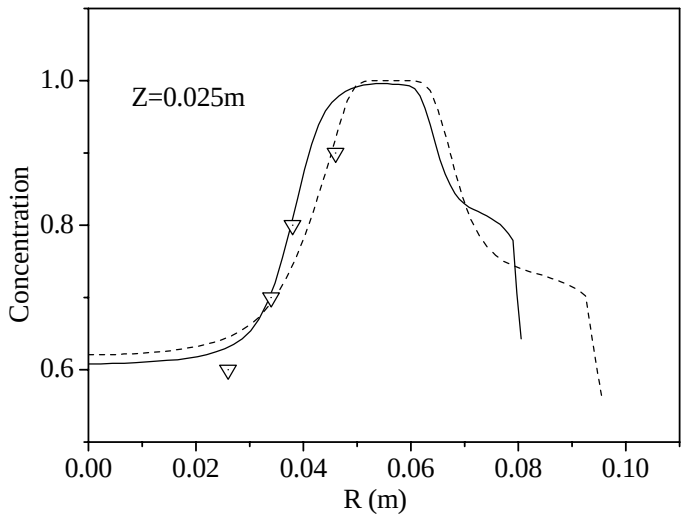

(a)

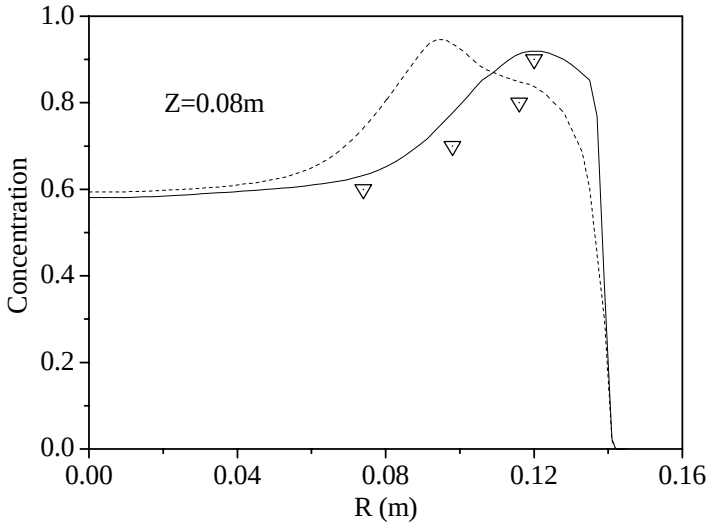
Z=0.08m
Concentration
R (m)
1.0
0.8
0.6
0.4
0.2
0.0
0.00
0.04
0.08
0.12
0.16

(b)

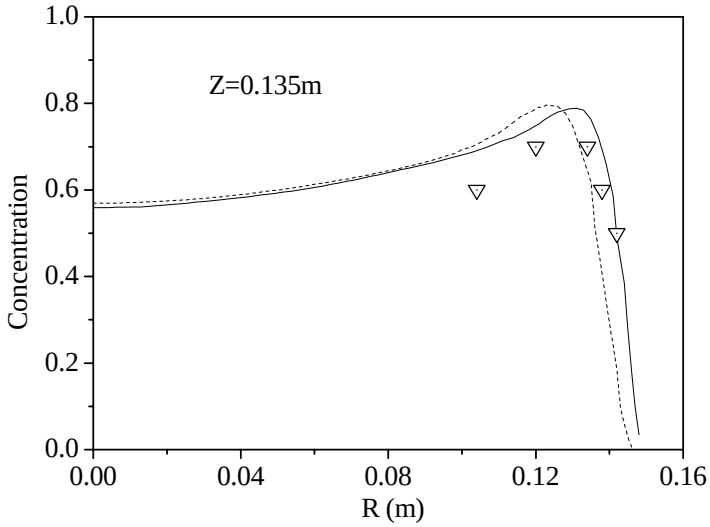
Z=0.135m
Concentration
R (m)
1.0
0.8
0.6
0.4
0.2
0.0
0.00
0.04
0.08
0.12
0.16

(c)

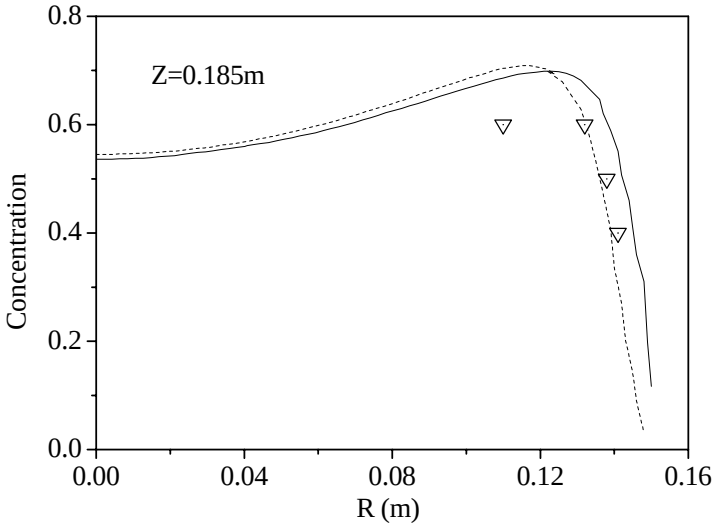
Z=0.185m
Concentration
R (m)
0.8
0.6
0.4
0.2
0.0
0.00
0.04
0.08
0.12
0.16

(d)

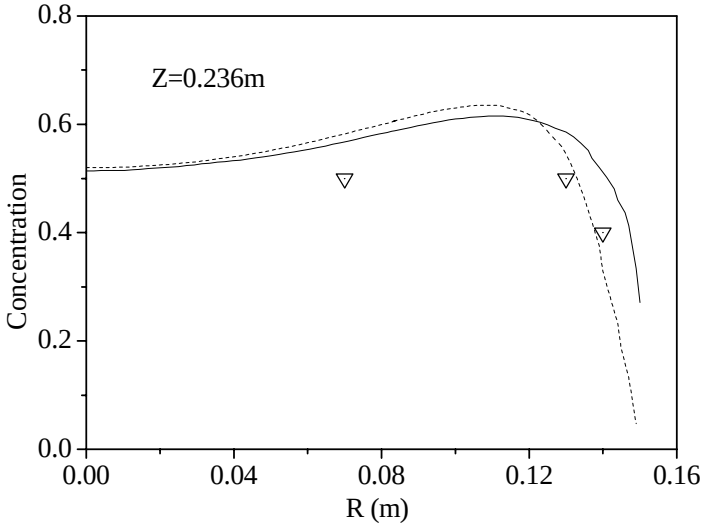
Z=0.236m
Concentration
R (m)
0.0
0.2
0.4
0.6
0.8
0.00
0.04
0.08
0.12
0.16

(e)

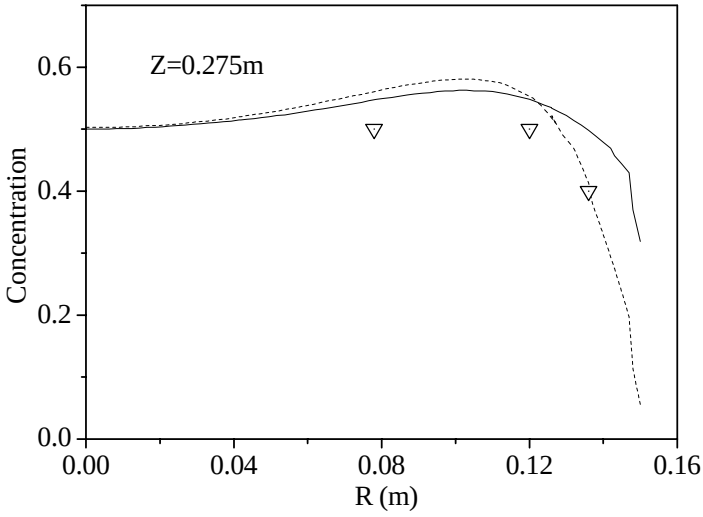
Z=0.275m
Concentration
R (m)
0.0
0.2
0.4
0.6
0.00
0.04
0.08
0.12
0.16

(f)

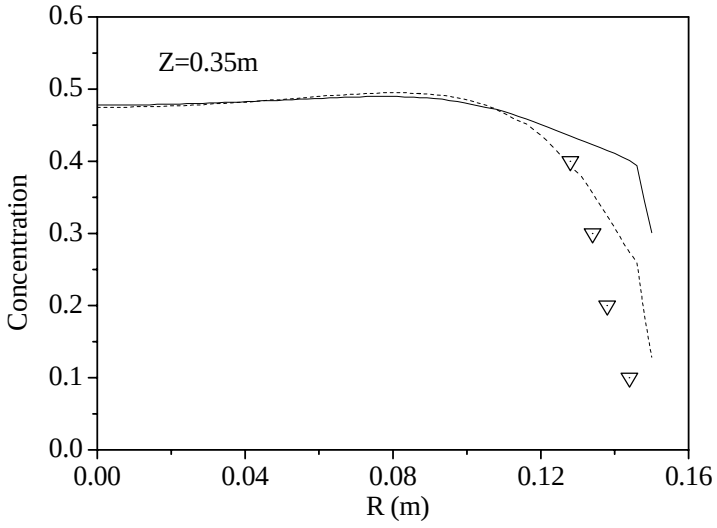
Z=0.35m
Concentration
R (m)
0.0
0.1
0.2
0.3
0.4
0.5
0.6
0.00
0.04
0.08
0.12
0.16

(g)

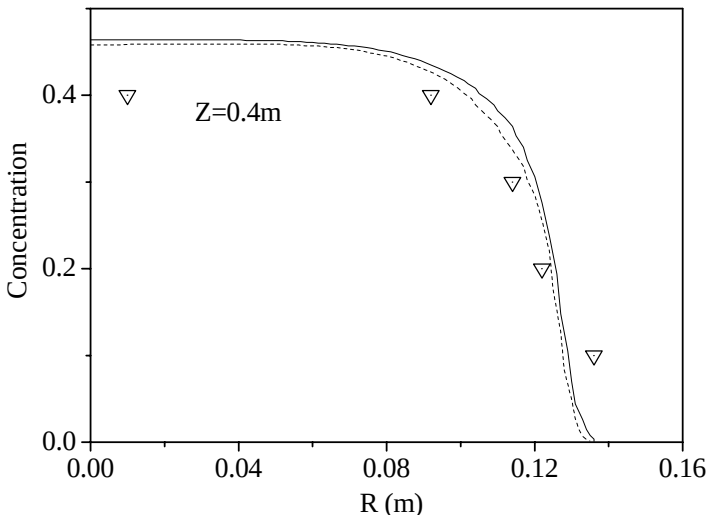

(h)

Figure 3.15 Comparisons of mass fraction distribution of the primary air stream (FRGM: ——, Momentum method: - - - -, Experimental data: ▽)

3.7.2.2 Tertiary Air Flow Mass Fraction

The tertiary air flow is located downstream, close to the exit of the precombustion chamber. The tertiary air flow first mixes with the primary air flow and secondary air flow, and then penetrates into the recirculation zone through convection. From Figure 3.14(b), we can see that in most parts of the recirculation zone, the concentration of the tertiary air flow is only about 3%, which indicates that it contributes very little to the combustion processes upstream. It is in fact difficult to measure in experimental tests. However, the main effect may be on the recirculation rate, which would affect the upstream mixing process. The combined tertiary air flow can raise the temperature near the precombustion chamber exit, which promotes further combustion of the pulverized coal.

3.8 Comparisons of Two Turbulence Models with FRGM

In order to obtain more accurate predictions of swirling air flow information, engineers in this field have begun to apply more advanced models. One of them is the RNG κ – ε turbulence model (Yakhot and Orzag 1986), which was found to be able to more accurately predict the backward-facing step turbulent flow pattern than the standard κ – ε turbulence model (Speziale and Thangam 1992; Papageorgakis and Assanis 1999). Improved prediction was also achieved using the RNG κ – ε model for the turbulent buoyancy flow (Gan 1998). However, Papageorgakis and Assanis (1999) found that the RNG κ – ε turbulence model cannot enhance the predictions of two-dimensional shear flows. In this section the standard κ – ε model and RNG κ – ε model are compared to investigate the applicability of the fully represented geometry method to 3-D confined concentric swirling air flows.

3.8.1 Differences between the two Turbulence Models

The RNG theory, when applied in Navier-Stokes equations, attempts to formulate a universal law for small scales, using an equation that incorporates a Gaussian random force and an assumption that this equation describes small-scale properties of turbulent flow in the inertial range (Yakhot and Orzag 1986).

The RNG κ – ε model has a similar form to the standard κ – ε model. The most visible difference between the RNG κ – ε model and the standard κ – ε model is that the RNG model typically leads to reduced eddy viscosity and higher effective Reynolds number. Firstly, the reduced value of $C_{2\varepsilon}^{RNG} = 1.68$, compared with the standard ε equation coefficient $C_{2\varepsilon}^{STANDARD} = 1.92$ (Table 2.1), has the main effect of decreasing the rate of dissipation of ε, thus increasing ε and producing smaller eddy

viscosities. Secondly, the RNG $\kappa - \varepsilon$ model has an additional term R_ε in its ε equation that significantly improves accuracy for rapidly strained flows. Equation 3.6 shows the latest coefficients of the RNG $\kappa - \varepsilon$ model (Speziale and Thangam 1992).

$$\left.\begin{aligned} c_\mu = 0.085;\ c_1 = 1.42 - \frac{\tilde{\eta}\left(1 - \tilde{\eta}/\tilde{\eta}_0\right)}{1+\beta\tilde{\eta}^3};\ c_2 = 1.68 \\ \sigma_k = 0.7179;\ \sigma_\varepsilon = 0.7179;\ \tilde{\eta} = S\kappa/\varepsilon \\ S = \left(2S_{i.j}S_{i,j}\right)^{1/2};\ \eta_0 = \tilde{4.38};\ \beta = 0.015 \\ S_{i,j} = \frac{1}{2}\left(\frac{\partial u_i}{\partial x_j} + \frac{\partial u_j}{\partial x_i}\right) \end{aligned}\right\} \quad (3.6)$$

3.8.2 Comparison of Velocity Distributions

The simulated velocity vectors are shown in Figure 3.16 (R_o=150mm) for planes of Z=0.05m and Z=0.135m. In Figure 3.16 (a), near the swirling diffuser zone, no negative radial velocity occurs in the standard $\kappa - \varepsilon$ model. Negative radial velocity exists between the primary flows, where the velocity peak value occurs, and the expanded wall in the RNG $\kappa - \varepsilon$ model (Figure 3.16(b)). In the downstream zone (Z=0.135m), the RNG $\kappa - \varepsilon$ model predicts much larger radial velocities, as shown in Figure 3.16(d). Accordingly, a stronger radial direction flow can be observed. In the planes vertical to the axis, these obviously different flow patterns much influence the tangential velocity distributions. Both models predict the radial eddies, which were not measured in the planes vertical to the axis in Niu and Xu's (1988) experimental study.

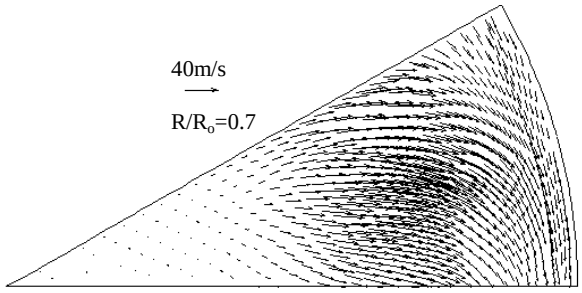

(a)

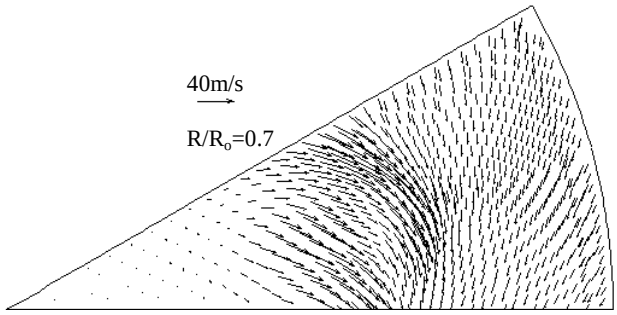

(b)

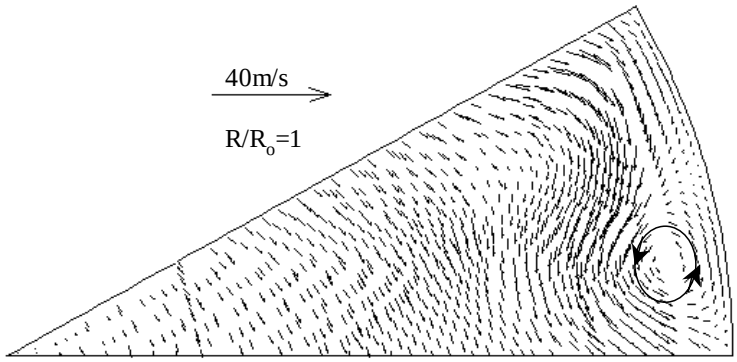

(c)

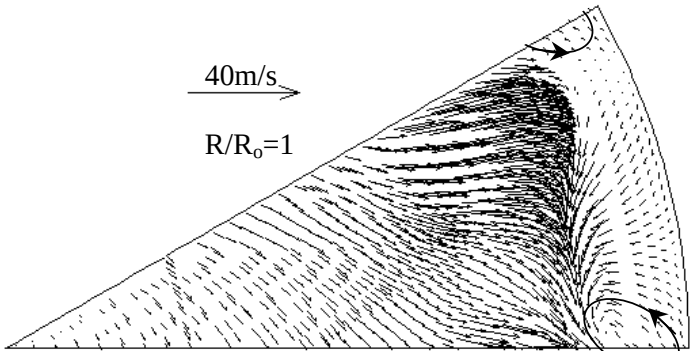

(d)

Figure 3.16 Velocity vector distributions at two different axial planes
(a) Standard κ –ε model (Z=0.05m), (b) RNG κ –ε model (Z=0.05m),
(c) Standard κ –ε model (Z=0.135m), and (d) RNG κ –ε model (Z=0.135m)

3.8.2.1 Comparison of Axial Velocities

Figure 3.17 presents the detailed comparisons between the predicted and measured axial velocity distributions. In Figure 3.17(c), the predicted axial velocity using the standard $\kappa-\varepsilon$ model is in better agreement with the measured data than the RNG $\kappa-\varepsilon$ method. On the axial cross section Z=0.08m, where the secondary wind is distributed into the chamber and combined with the primary wind, the two methods predict two peaks of the axial velocity profile which are different from the experimental data. The RNG $\kappa-\varepsilon$ model presents a larger separately reversed flow between the primary air and the second air flow, which was not found in the experiment. The primary air flow in the RNG $\kappa-\varepsilon$ model penetrates more deeply into the reversed flow, while in the experiment the primary air tended to be more attached to the chamber wall, which better agrees with the standard $\kappa-\varepsilon$ model prediction. The velocity peaks predicted by these two models are obviously related to the velocity profile near the swirling diffuser (Figure 3.16) These discrepancies with experimental data for the zone near the swirling diffuser mean that some improved turbulence models are still needed to deal with the near wall conditions.

From Figure 3.17(e) to Figure 3.17(g), it can be seen that further downstream from the swirling diffuser, the velocity profiles of the two methods become similar. However, the simulated axial velocities from the RNG $\kappa-\varepsilon$ turbulence model show better agreement with the experimental data for the recirculation zone, as indicated in Figures 3.17(f) and 3.17 (g). These two models still overpredict the axial peak velocity near the chamber wall downstream from the tertiary air inlet (Figure 3.17(g)).

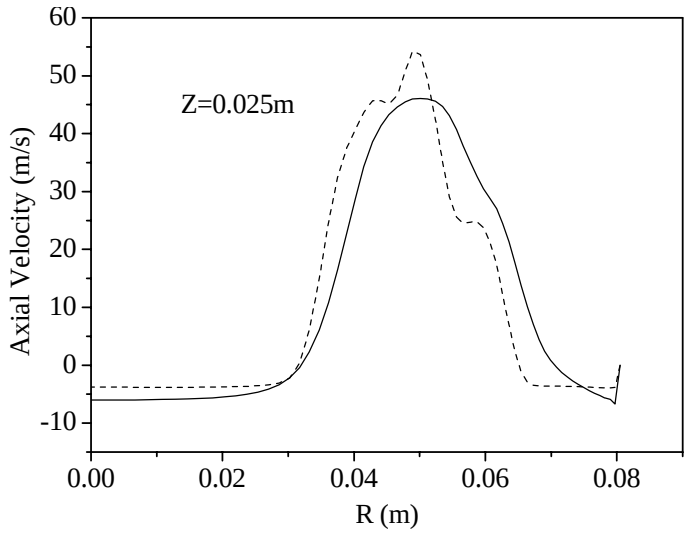
Z=0.025m
Axial Velocity (m/s)
R (m)
60
50
40
30
20
10
0
-10
0.00
0.02
0.04
0.06
0.08

(a)

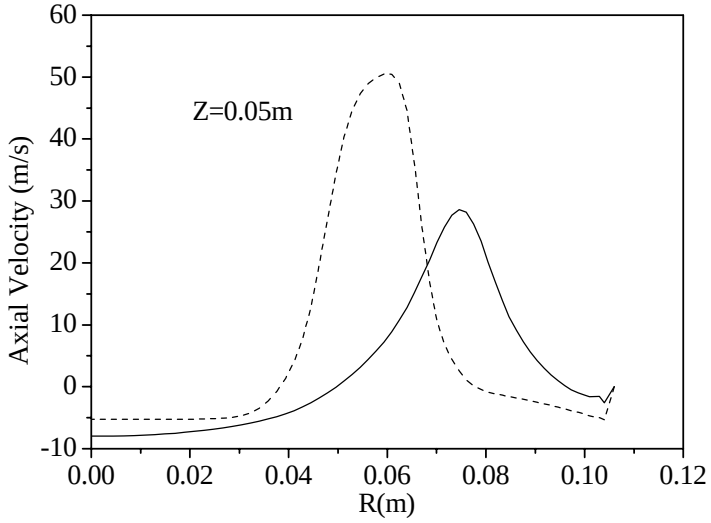
Z=0.05m
Axial Velocity (m/s)
R(m)
60
50
40
30
20
10
0
-10
0.00
0.02
0.04
0.06
0.08
0.10
0.12

(b)

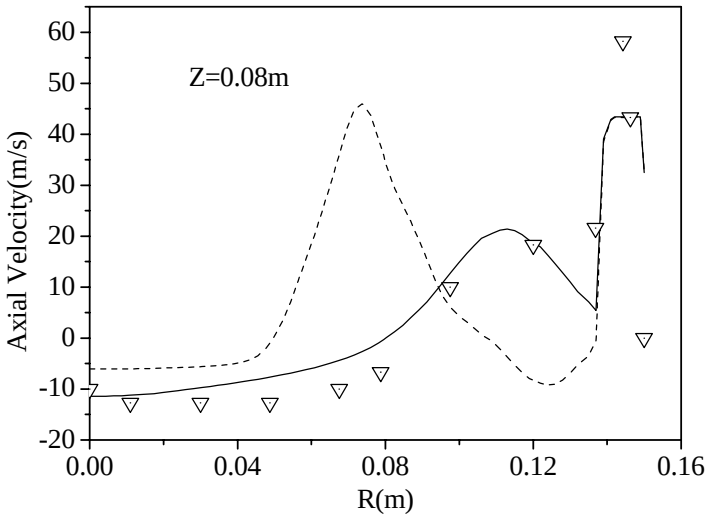
Z=0.08m
Axial Velocity(m/s)
R(m)
60
50
40
30
20
10
0
-10
-20
0.00
0.04
0.08
0.12
0.16

(c)

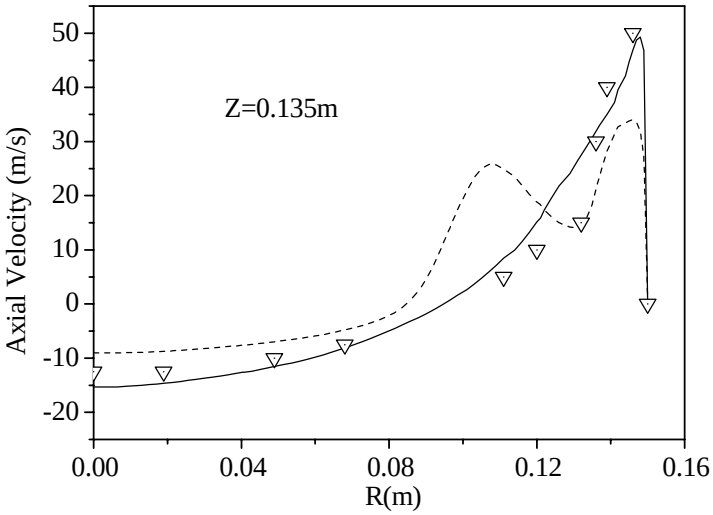
Z=0.135m
Axial Velocity (m/s)
R(m)
50
40
30
20
10
0
-10
-20
0.00
0.04
0.08
0.12
0.16

(d)

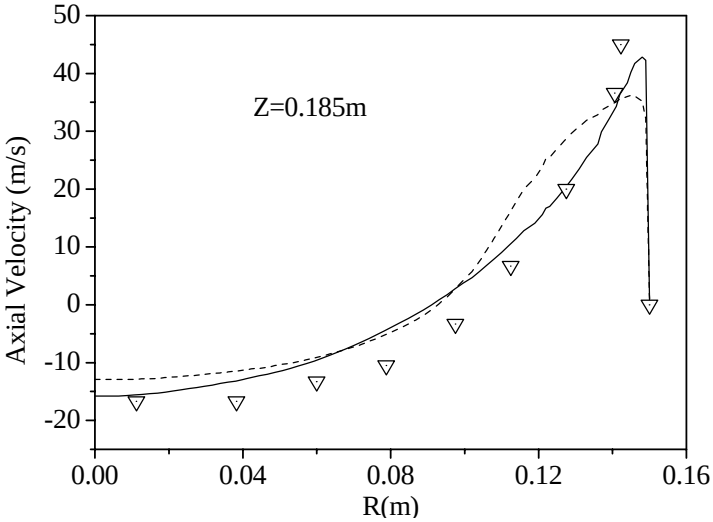
Z=0.185m
Axial Velocity (m/s)
R(m)
50
40
30
20
10
0
-10
-20
0.00
0.04
0.08
0.12
0.16

(e)

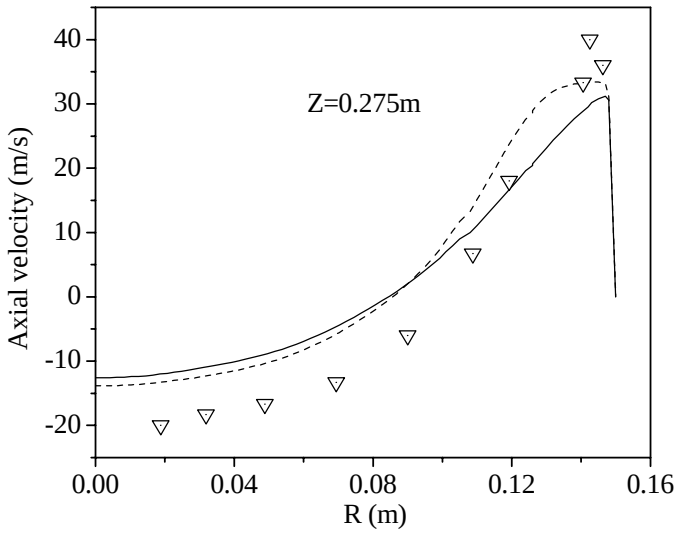
Z=0.275m
Axial velocity (m/s)
R (m)
40
30
20
10
0
-10
-20
0.00
0.04
0.08
0.12
0.16

(f)

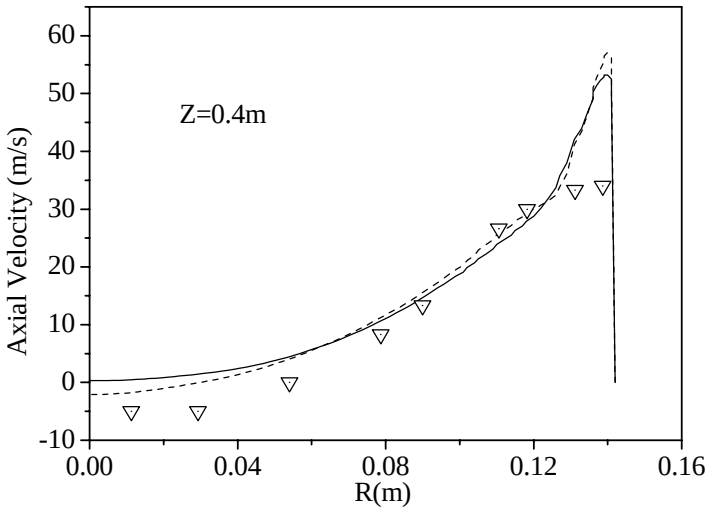

(g)

Figure 3.17 Axial velocity distribution profiles at seven axial planes

(Standard κ –ε model: ____, RNG κ –ε model: ----, Experimental data: ▽)

3.8.2.2 Comparison of Tangential Velocities

Just like the axial velocity distributions in the region between the primary swirling diffusion and the secondary air diffusion, the tangential peak velocity predicted by the standard κ – ε turbulence model is closer to the wall than that predicted by the RNG model (Figures 3.18(a-c)). The RNG κ – ε turbulence model predicts steeper tangential velocity profiles, a fact that can essentially be attributed to the smaller dissipative nature of this model as compared to the standard κ – ε model (Papageorgakis and Assanis 1999). In the RNG κ – ε model (Figures 3.18(d) and 3.18(e)) the positive tangential velocity occurs near the wall. The predicted locations of radial eddies are different in the two models (Figure 3.16), which contributes to the different tangential vector. In the weak swirling turbulence zone, far from the swirling diffuser, the RNG κ – ε model predicts a better sign of the reversed zone.

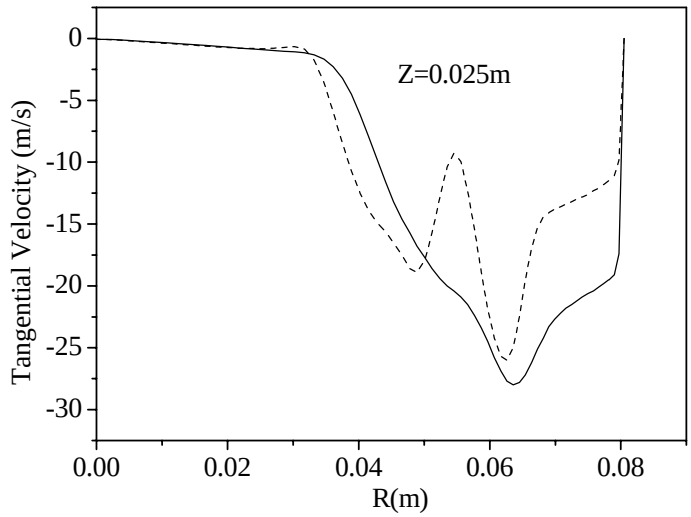
Z=0.025m
Tangential Velocity (m/s)
R(m)
0
-5
-10
-15
-20
-25
-30
0.00
0.02
0.04
0.06
0.08

(a)

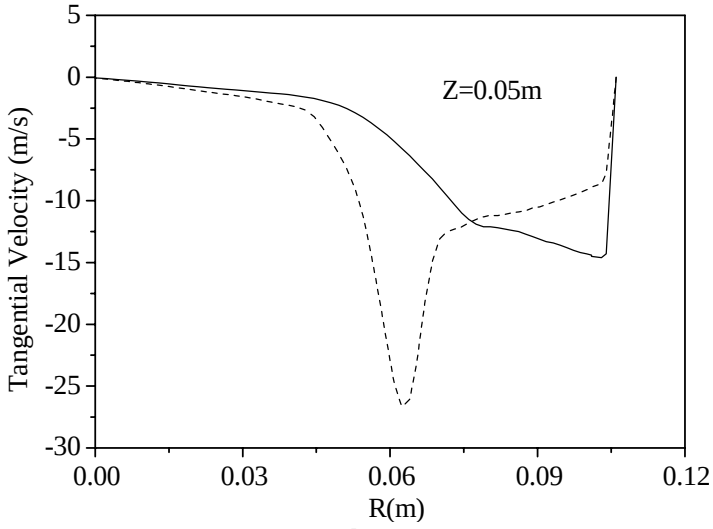
Z=0.05m
Tangential Velocity (m/s)
R(m)
5
0
-5
-10
-15
-20
-25
-30
0.00
0.03
0.06
0.09
0.12

(b)

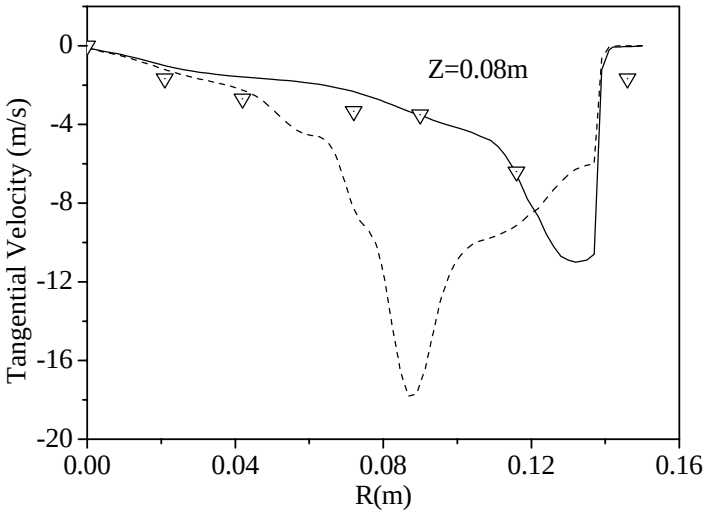
Z=0.08m
Tangential Velocity (m/s)
R(m)
0
-4
-8
-12
-16
-20
0.00
0.04
0.08
0.12
0.16

(c)

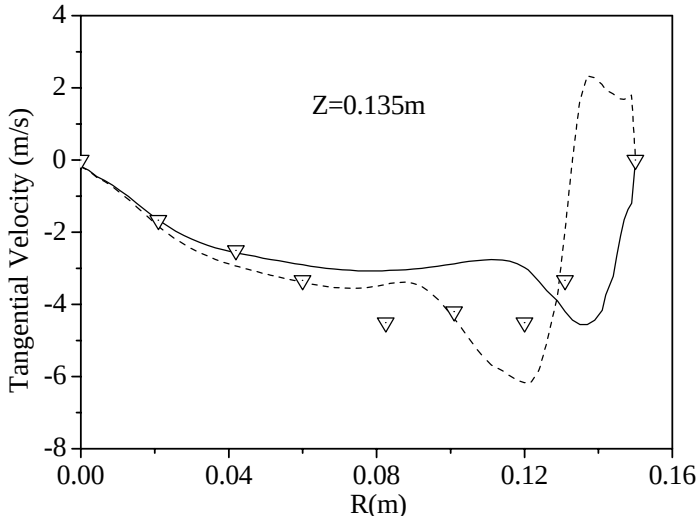

(d)

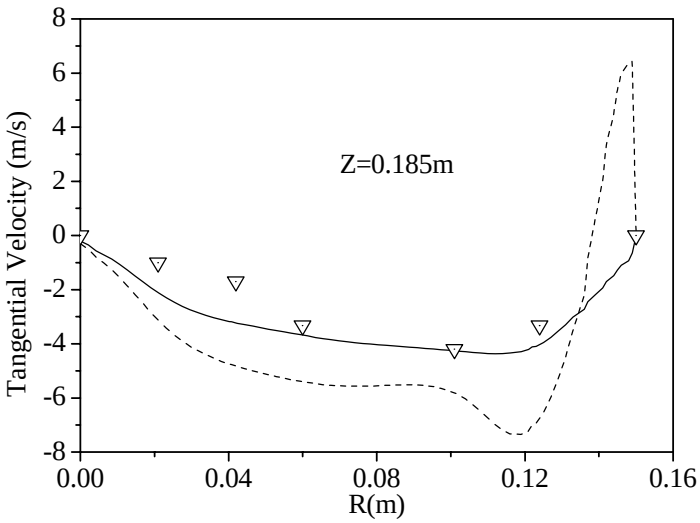

(e)

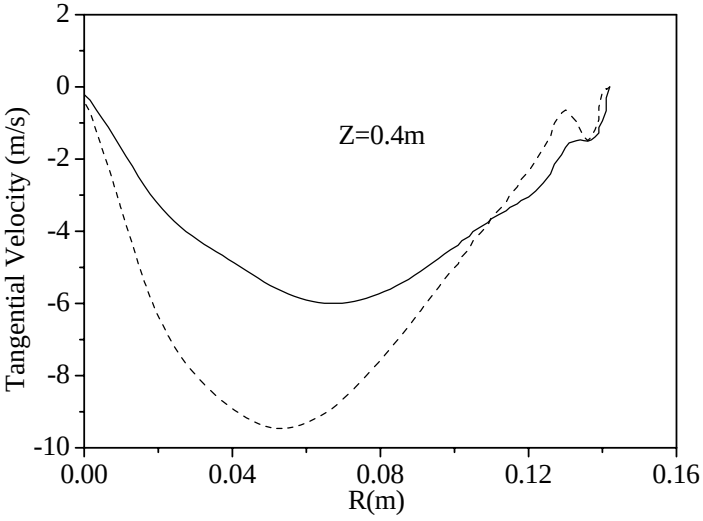

(f)

Figure 3.18 Tangential velocity distribution profiles at six axial planes (Standard κ –ε model: ____, RNG κ –ε model: ----, Experimental data: ▽)

3.9 Application of the Supply Diffuser Outlet Boundary Conditions from the Standard κ –ε Model to the RNG κ –ε Model

In the above studies, the simulation results show that the RNG κ –ε model inaccurately predicts air flow patterns near the swirling diffuser due to the unreasonable results for the outlet surface of the swirling diffuser. This section further investigates the employment of the RNG κ – ε model in the momentum method, named Case-3. Case-1 employs the standard κ – ε model and Case-2 uses the RNG κ – ε model with FRGM, as presented in Sections 3.8 and 3.9. Case-3 uses the simulated results of the supply diffuser outlet from case-1 as the primary air inlet conditions.

3.9.1 Axial Velocity Distributions

Figure 3.10 (b) shows the velocity vector distributions on the inlet plane of the precombustion chamber with the standard κ – ε model. Case-3 employs this velocity distribution as the primary air inlet condition with the RNG κ – ε model. The turbulence kinetic energy κ and its dissipation rate ε are also exported from Case-1 as the inlet conditions.

Figure 3.19 shows the detailed comparisons between the predicted and measured axial velocity distributions at different axial cross sections for three cases. Employing the simulation results from Case-1 as the primary air inlet conditions, Case-3 shows axial velocity distributions near the swirling diffuser are very similar to Case-1 (Figures 3.19(a-c)). From Figure 3.19(d) to Figure 3.19(g), it can be seen

that the predicted velocity profiles of the three cases become similar. However, further downstream from the swirling diffuser, the simulated axial velocities of case-3 show better agreement with the experimental data for the recirculation zone, as indicated in Figures 3.19(f) and 3.19(g).

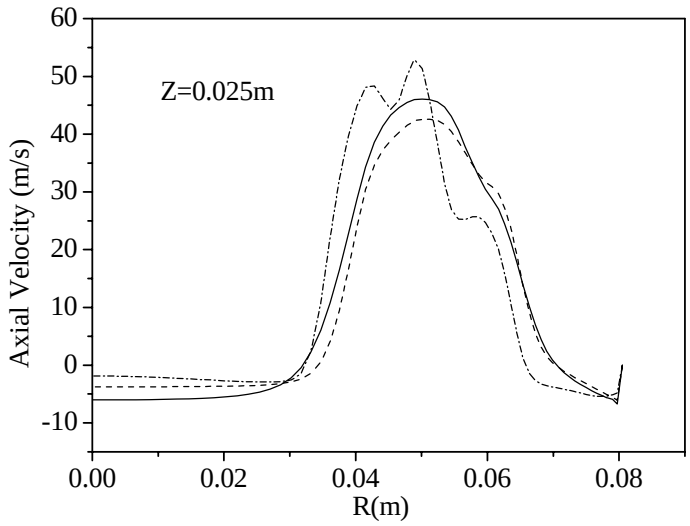

(a)

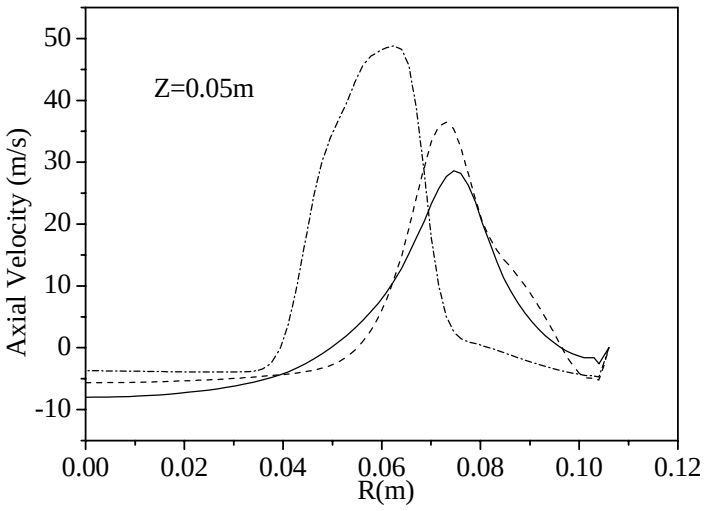

(b)

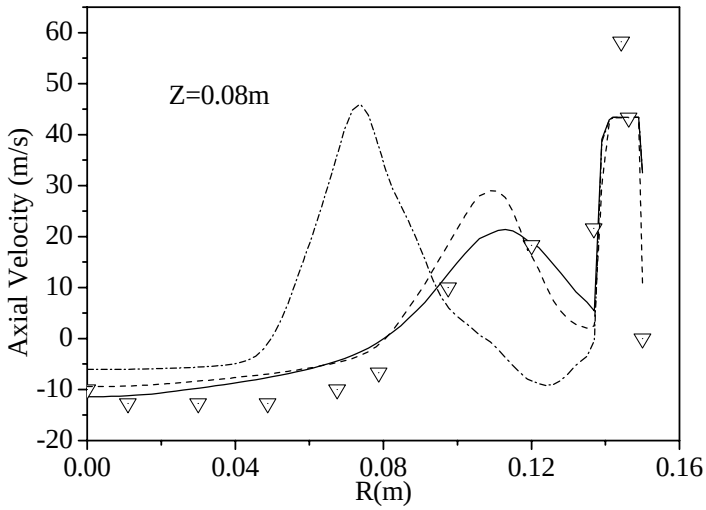
Z=0.08m
Axial Velocity (m/s)
R(m)
60
50
40
30
20
10
0
-10
-20
0.00
0.04
0.08
0.12
0.16

(c)

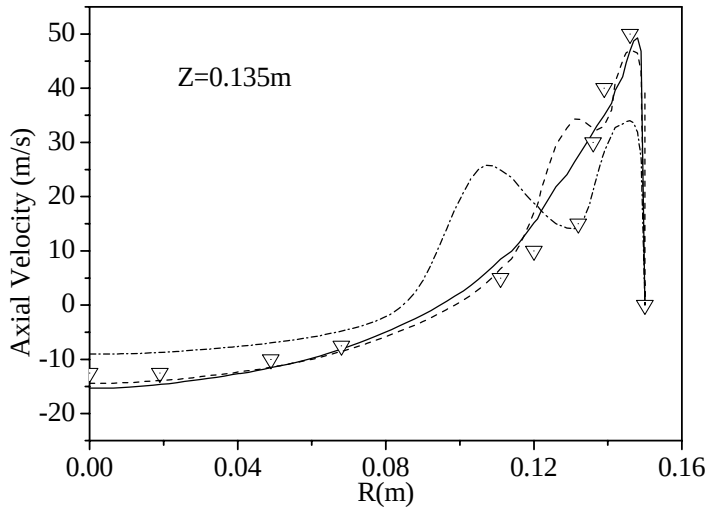
Z=0.135m
Axial Velocity (m/s)
R(m)
50
40
30
20
10
0
-10
-20
0.00
0.04
0.08
0.12
0.16

(d)

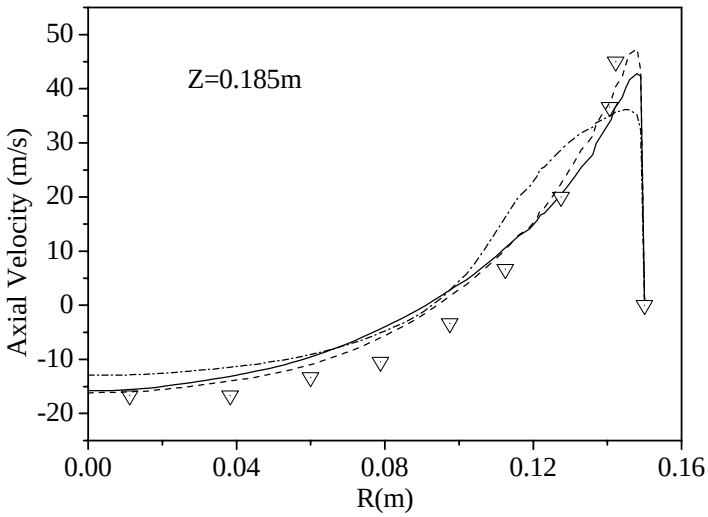
Z=0.185m
Axial Velocity (m/s)
R(m)
50
40
30
20
10
0
-10
-20
0.00
0.04
0.08
0.12
0.16

(e)

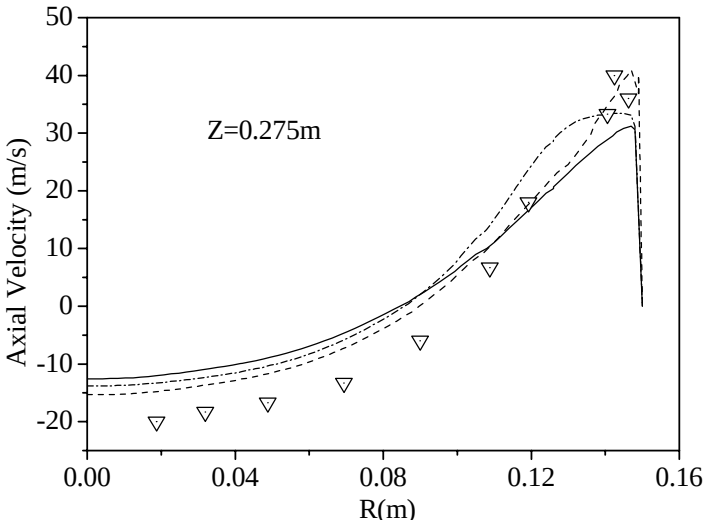

(f)

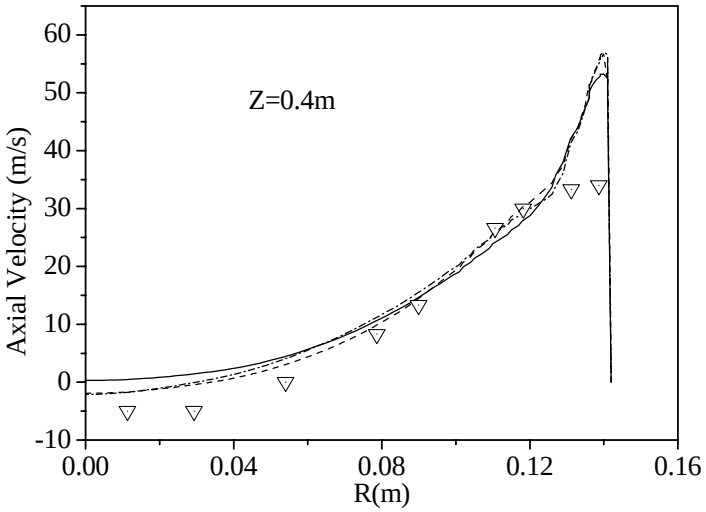

(g)

Figure 3.19 Axial velocity distribution comparisons

(Case-1: ——, Case-2: -.-.-, Case-3: - - - -, Experimental data: ▽)

3.9.2 Tangential Velocity Distributions

Figure 3.20 presents the tangential velocity comparisons. Employing the supply diffuser boundary conditions from the standard $\kappa - \varepsilon$ turbulence model with FRGM, the RNG $\kappa - \varepsilon$ turbulence model predicts almost the same results as the momentum method. It emphasizes again that the inlet boundary conditions are crucial for accurately predicting downstream flow fields.

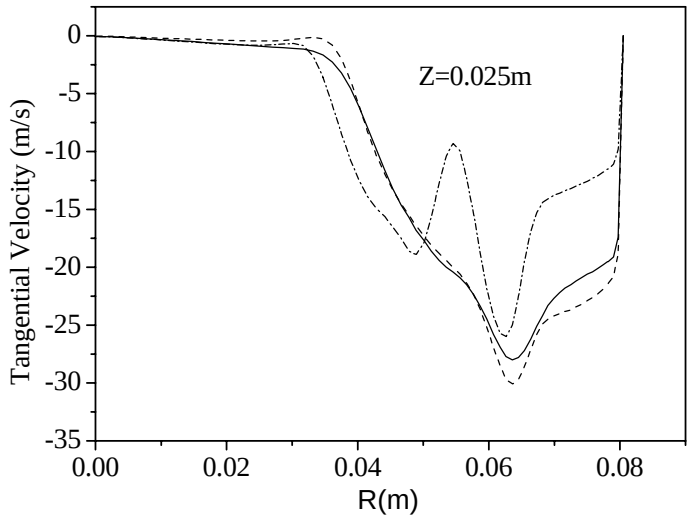
Z=0.025m
Tangential Velocity (m/s)
R(m)
0
-5
-10
-15
-20
-25
-30
-35
0.00
0.02
0.04
0.06
0.08

(a)

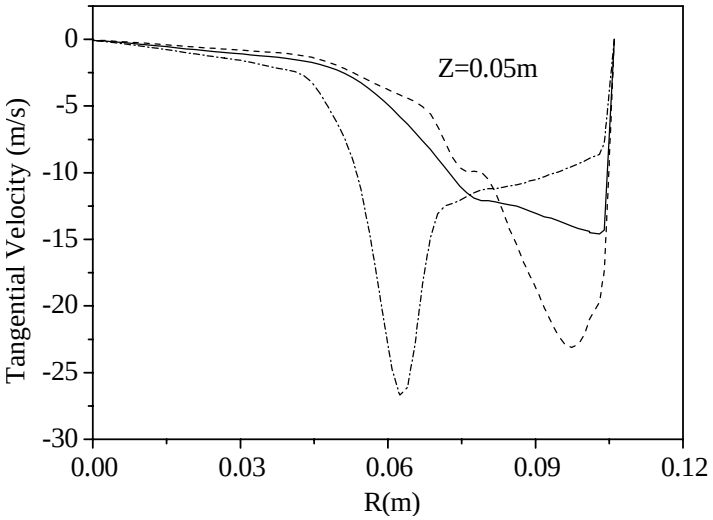
Z=0.05m
Tangential Velocity (m/s)
R(m)
0
-5
-10
-15
-20
-25
-30
0.00
0.03
0.06
0.09
0.12

(b)

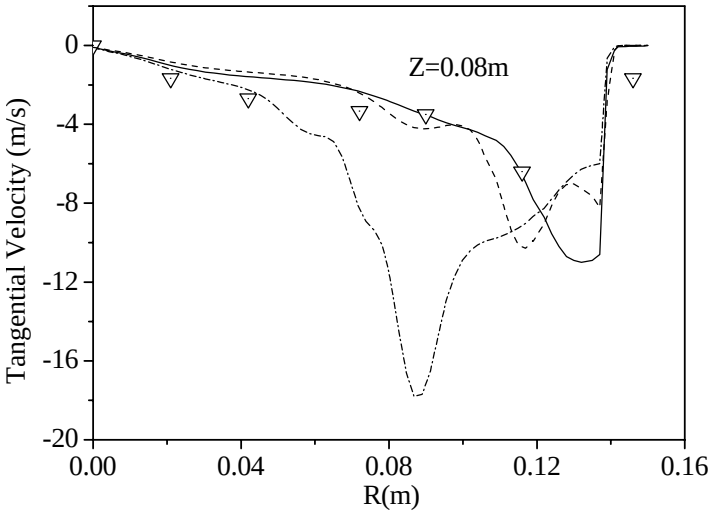
Z=0.08m
Tangential Velocity (m/s)
R(m)
0
-4
-8
-12
-16
-20
0.00
0.04
0.08
0.12
0.16

(c)

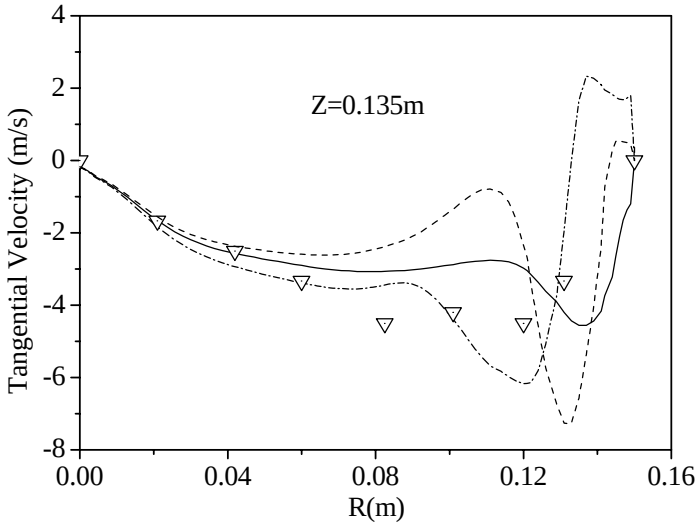
Z=0.135m
Tangential Velocity (m/s)
R(m)
4
2
0
-2
-4
-6
-8
0.00
0.04
0.08
0.12
0.16

(d)

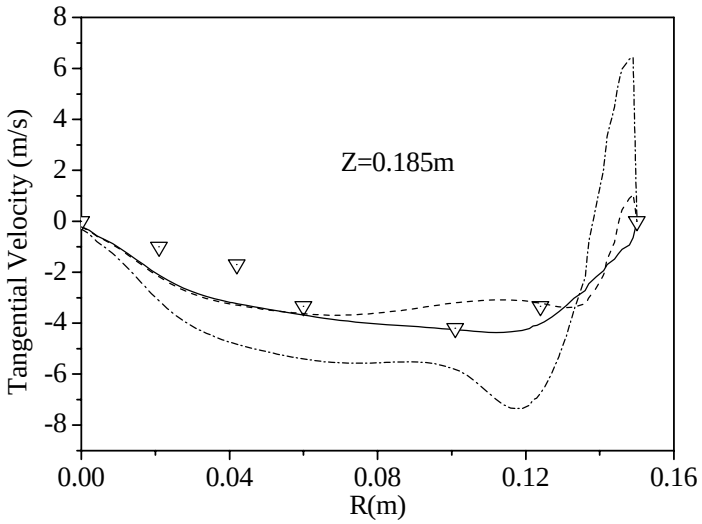
Z=0.185m
Tangential Velocity (m/s)
R(m)
8
6
4
2
0
-2
-4
-6
-8
0.00
0.04
0.08
0.12
0.16

(e)

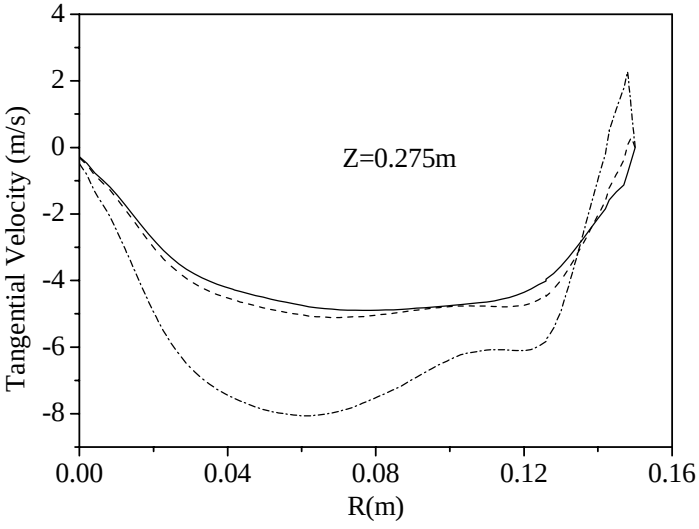
Z=0.275m
Tangential Velocity (m/s)
R(m)
4
2
0
-2
-4
-6
-8
0.00
0.04
0.08
0.12
0.16

(f)

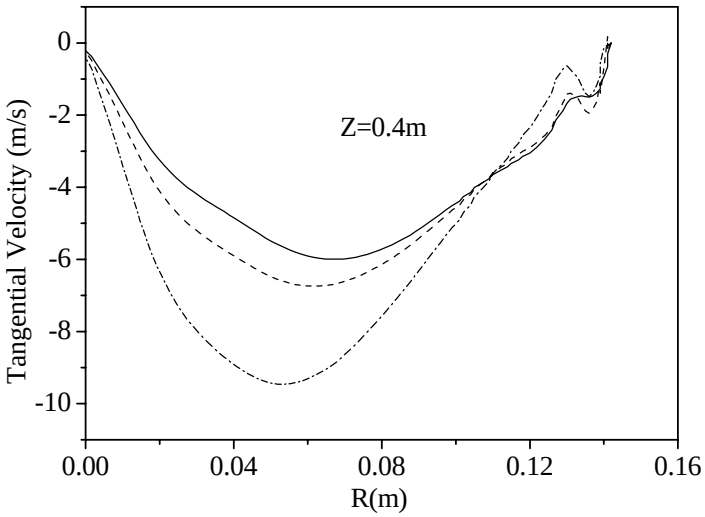

(g)

Figure 3.20 Tangential velocity distribution comparisons

(Case-1: ——, Case-2: _._._, Case-3: _ _ _ _, Experimental data: ▽)

3.9.3 Contours of the Primary Air Mass Fraction

Figure 3.21 presents the simulation results of the primary air flow mass fraction contours. Near the combustion wall, Case-1 and Case-3 show small different mass fraction distributions.

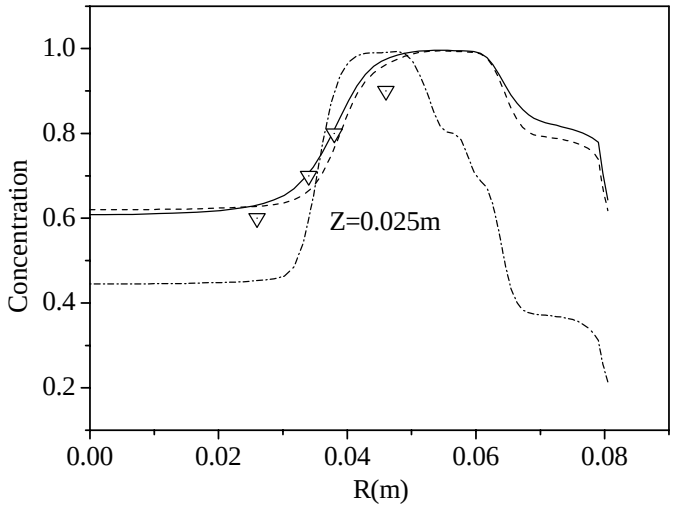

(a)

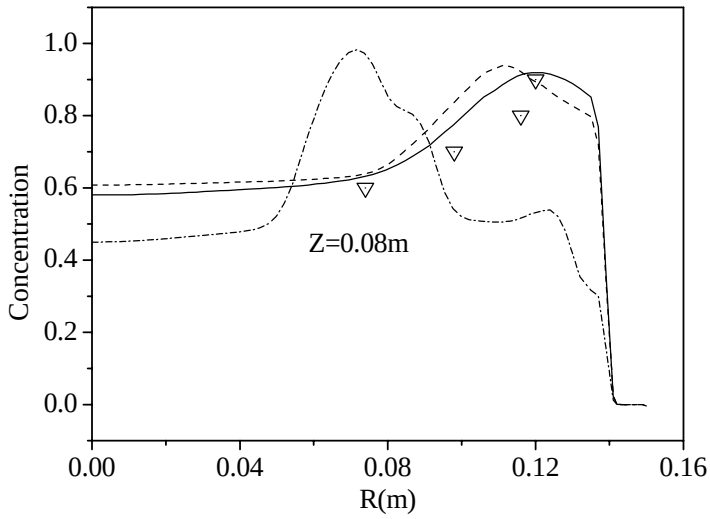
Concentration
R(m)
Z=0.08m
1.0
0.8
0.6
0.4
0.2
0.0
0.00
0.04
0.08
0.12
0.16

(b)

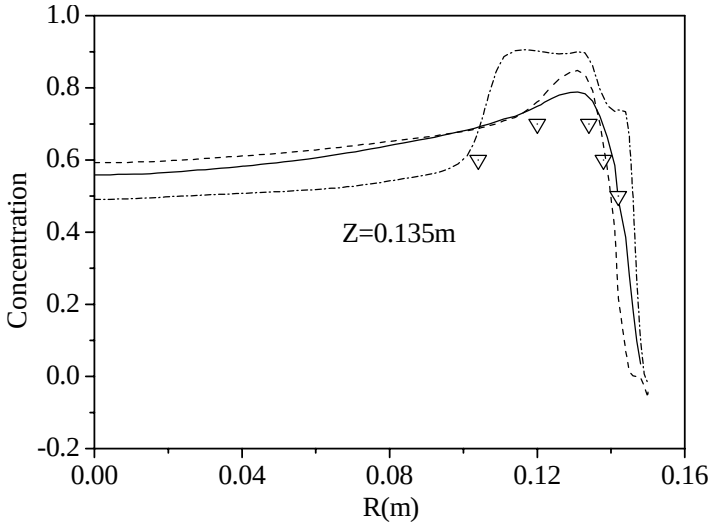
Concentration
R(m)
Z=0.135m
1.0
0.8
0.6
0.4
0.2
0.0
-0.2
0.00
0.04
0.08
0.12
0.16

(c)

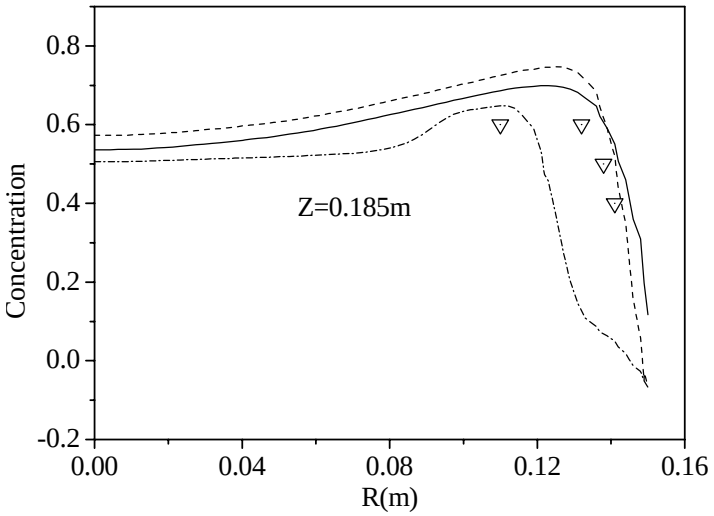
Concentration
R(m)
Z=0.185m
0.8
0.6
0.4
0.2
0.0
-0.2
0.00
0.04
0.08
0.12
0.16

(d)

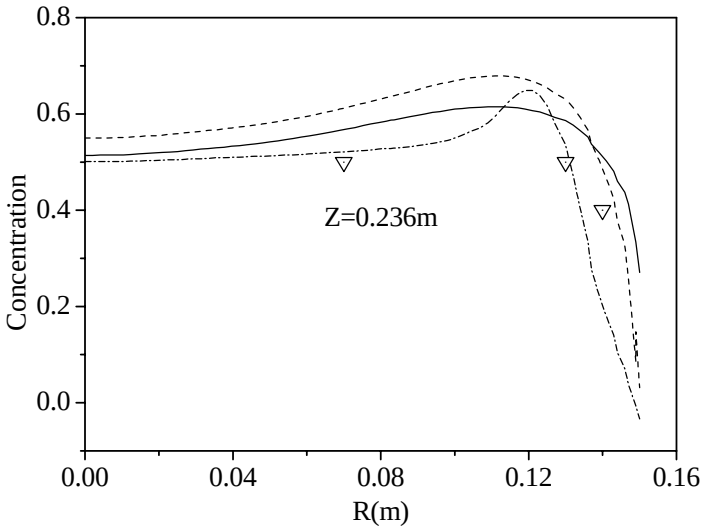
0.8
0.6
0.4
0.2
0.0
Concentration
Z=0.236m
0.00
0.04
0.08
0.12
0.16
R(m)

(e)

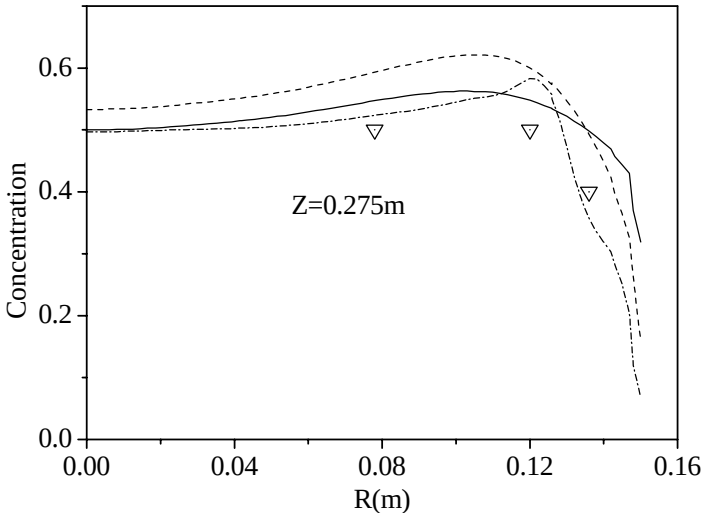
0.6
0.4
0.2
0.0
Concentration
Z=0.275m
0.00
0.04
0.08
0.12
0.16
R(m)

(f)

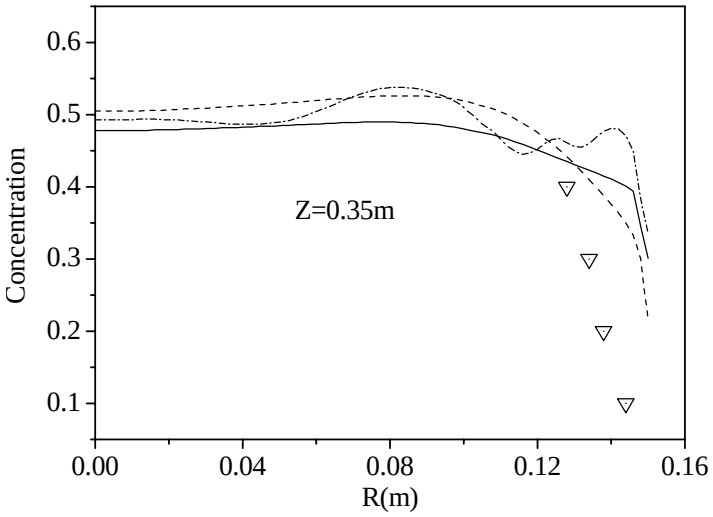
0.6
0.5
0.4
0.3
0.2
0.1
Concentration
Z=0.35m
0.00
0.04
0.08
0.12
0.16
R(m)

(g)

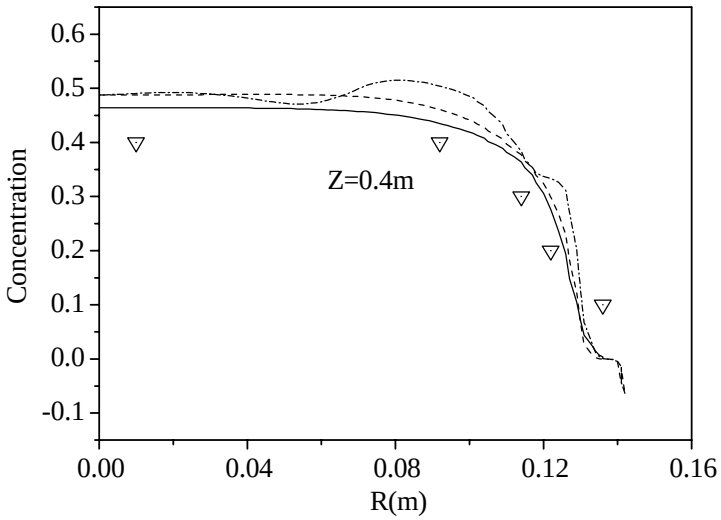

(h)

Figure 3.21 Comparisons of mass fraction distribution of the primary air stream (Case-1: ——, Case-2: _._._, Case-3: _ _ _ _, Experimental data: ▽)

3.10 Discussion and Summary

This chapter investigated the fully represented geometry method (FRGM) for the swirling supply diffuser. Knowledge of information transfer in multi-domain interfaces is necessary.

It is generally believed that the swirling flow with recirculation cannot be properly simulated using the standard $\kappa - \varepsilon$ turbulence model. The author simulation indicates that the proper inlet conditions are essential in the case of a swirling inlet, although there remain some discrepancies between the simulation results and the experimental data. Through the comparisons between the axial velocities and the tangential velocities in a combustion chamber, FRMG with the standard $\kappa - \varepsilon$ turbulence model predicts more accurate flow information in the area near the supply diffuser than the momentum method. With this method, the necessity of measuring the input

conditions near the supply diffuser can potentially be eliminated, which is difficult and inaccurate due to the large gradients.

Employing the FRGM, The RNG $\kappa - \varepsilon$ turbulence model did not appropriately predict air flow patterns near the swirling diffuser. Yakhot et al. (1992) pointed out that the current version of the dissipation rate transport equation has only been modeled to account for the effects of irrotational strains. Incorporation of the effects of rotational strains, which can be important in turbulent flows involving curvature or a system rotation, is a difficult task that has not yet been achieved and needs future study. It was found that the RNG $\kappa - \varepsilon$ model predicted more accurate recirculation zone than the standard $\kappa - \varepsilon$ model with the FRGM.

One disadvantage of the FRGM is that more powerful computer capacities are needed due to the large number of meshed cells, as compared with some simplified modeling methods. With the rapid development of computer technology, this disadvantage will eventually disappear. The mesh technique is also important for the complicated geometry of the supply diffusers. Presently, many commercial preprocessing software programs are available, such as ICEMCFD, TrueGrid, Gambit, etc., which will further stimulate the actualization of this method.

CHAPTER 4 NUMERICAL INVESTIGATIONS OF TWO SUPPLY DIFFUSERS IN THE UFAD SYSTEM

4.1 Introduction

It is well known that air distributions are mainly dependent on the jet flow from supply diffusers, especially in the underfloor air distribution (UFAD) system, because the supply opening is installed in the occupied zone. There are many types of diffusers, available from different companies including TITUS (1946) and TROX (1951). Based on the configurations and locations where they are installed, supply diffusers can be classified as ceiling diffusers, side-wall diffusers, floor diffusers, jet nozzles, low velocity displacement diffusers, etc.

In UFAD systems, the supply diffuser can be classified into two types: active and passive diffusers (Bauman 2003). Active diffusers are defined as air supply outlets that rely on a local fan to deliver air from either a zero-pressure or pressurized plenum through the diffuser into the conditioned space of a building (Figure 4.1(a)). Passive diffusers are defined as air supply outlets that rely on a pressurized underfloor plenum to deliver air from the plenum through the diffuser into the conditioned space of a building (Figure 4.1(b)). Fixed or adjustable vanes are usually used to control air flow directions (Figure 4.2). In mixing HVAC systems, the supply diffusers are installed in the ceiling far away from the occupants, so the thermal environments near the supply diffusers are of less concern. However, in UFAD systems, an uncomfortable situation may arise when the cold inlet jet hits a person in the occupied zone.

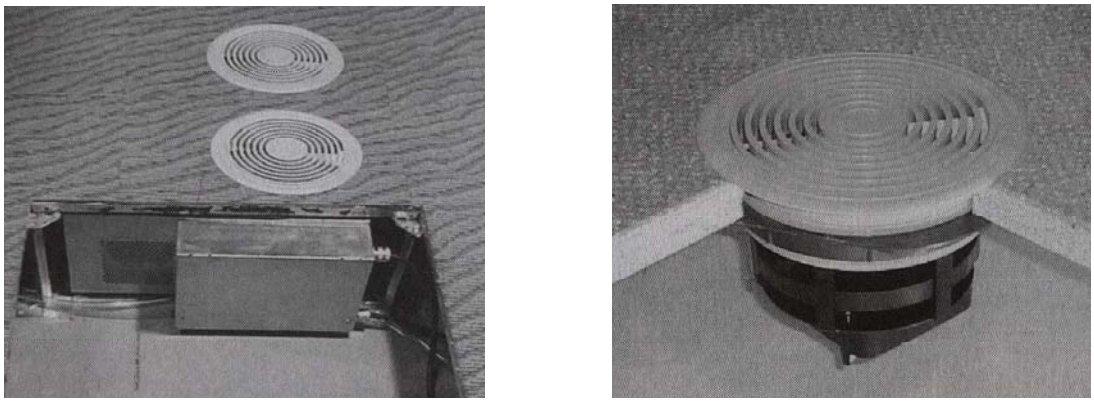

(a) (b)

Figure 4.1 Supply units (Trox 2002)

(a) Active diffuser, and (b) Passive diffuser

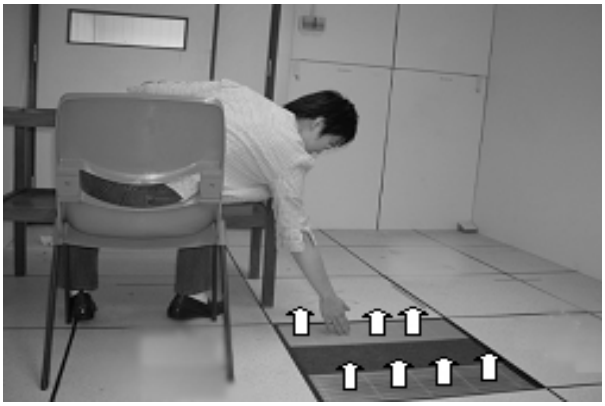

Figure 4.2 Personal manual controls for air flow directions

Different supply diffusers in UFAD systems result in different thermal environments in the occupied zone. The simplified numerical simulation methods for diffusers cannot present the detailed air flow patterns near the supply diffuser zone, discussed in Chapter 3. In this section, the swirling and square supply diffusers (Figure 4.3) are investigated for thermal environments in the UFAD system using the validated modeling method FRGM. An overview of the UFAD system is first presented.

(a) (b)

Figure 4.3 Pictures of two supply diffusers (from TROX Company)
(a) Swirling diffuser, and (b) Square diffuser

4.2 Overview of UFAD System

4.2.1 Description of UFAD System

The UFAD system was first introduced at the beginning of the 1960's for equipment cooling in the Federal Republic of Germany (Sodec and Craig 1990). Later, in the mid-1970's, this system was adopted in the general offices due to the modernization of general offices, the impact of automated electronic equipment and the excess heat it transferred to the office. Over the past three decades, research on this system has increased rapidly (Matsunawa et al. 1995; McCarry 1995; Loudermilk 1999; Bauman and Webster 2001; Fukao et al. 2002; Loudermilk 2003). At present, the UFAS system has achieved considerable acceptance in Europe, North America, and Japan.

The UFAD system is similar to the mixing system in terms of the types of overhead equipment used at the cooling and heating plants and the primary air-handling units (AHU). Key differences include the use of an underfloor air supply plenum, warmer supply air temperature, localized air distribution (with or without individual control),

and the resulting floor to ceiling air flow pattern. Figure 4.4 presents the configuration of an office room with a UFAD system. For large spaces, the outlet can be installed either in the ceiling or in the occupied zone. Chapter 5 investigates the same configuration as that in Figure 4.4 for system energy consumption. In the UFAD system, the supply openings can directly deliver the conditioned air into the occupied zone which, given the sensitivity of the occupants to the thermal environment change, means the correct selection of supply diffuser if very important.

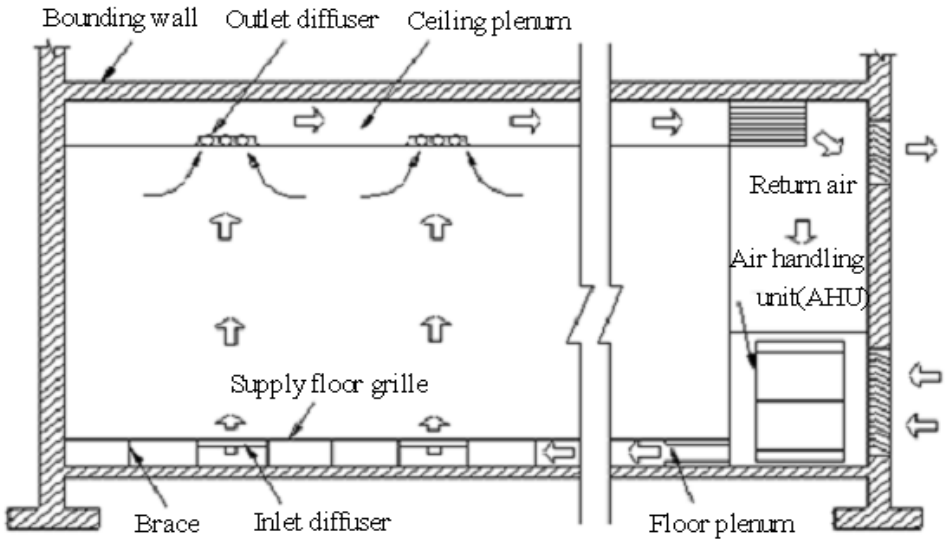

Figure 4.4 Configuration of a building with a UFAD system

The UFAD system employs buoyancy driven air flow patterns for air-conditioning space, which results in thermal stratification (Akimoto et al. 1995; Loudermilk 1999). The theoretical stratification behavior of the UFAD system is derived from the plume theory for the displacement ventilation (DV) system. In the DV system, the cool supply air is heated as it flows across the floor and then drawn upward primarily through entrainment by thermal plumes that develop over heat sources in the room. Stratification that divides the room into two zones is established. The lower zone, below the stratification level, has no circulation and is close to the

displacement flow. The upper zone, above the stratification level, is characterized by the recirculating air flow producing a fairly well-mixed region. The stratification height (SH) plays an important role in determining thermal, ventilation, and energy performance. The height of this stratification level primarily depends on the room air flow rate relative to the magnitude of the heat sources, not the vertical throw of the diffusers (Nielsen 1994; Webster et al. 2002).

In the UFAD system, Loudermilk (1999) defined the stratification height as the height at which the supply out discharge velocity is reduced to 0.25m/s (50fpm). This stratification height divides the room into two zones with distinct air flow conditions: the lower mixed zone and the upper displacement zone. Bauman (2003) employed the concept of throw height (TH) to identify a middle stratified zone if the throw height is lower than the stratification height, as shown in Figure 4.5. He contended that the upper zone was mixed, in contrast to the description by Loudermilk (1999). At present the stratification height remains a key gap related to comfort energy and energy performance in UFAD system design (Bauman 2003). Chapter 5 presents the numerical model for indoor air temperature stratification in the UFAD system.

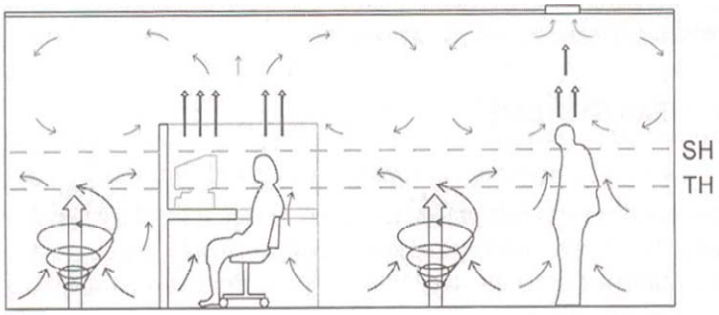

Figure 4.5 Underfloor air distribution system with diffuser throw below the stratification height

4.2.2 Benefits and Barriers of UFAD System

The UFAD system has many advantages over mixing systems. The potential economic benefits of using this system to achieve greater satisfaction within the workforce are believed to be very large. They can be summarized as follows:

1. Building churn cost reductions

   Bauman and Webster (2001) pointed out that this benefit is based upon the fact that the churn rate is a fact of life. It is defined as the percentage of workers and their associated work spaces in a building that are reconfigured or undergo significant changes per year. The supply grilles and the electrical boxes can easily be moved to suit new layouts by simply relocating the floor panel (McCarry 1995). By integrating a building's HVAC and cable management systems into one easily accessible underfloor plenum, the cost associated with reconfiguring building services is greatly saved.

2. Ventilation efficiency and indoor air quality improvement

   The UFAD system can provide much more effective gaseous contaminant removal in the lower occupied zone than the ceiling-based mixing system (Chao and Wan 2004). Indoor air quality improves due to a greater supply of fresh air to the occupied zone, and a lower concentration of air pollutants (Sodec and Craig 1990).

3. Thermal comfort improvement

   Hanzawa and Nagasawa (1990) investigated supply diffusers and concluded that the swirl flow produced little draft risk in the occupied zone. This Chapter emphasizes the detailed thermal comfort investigations of two different supply diffusers.

4. Energy consumption reduction

Bauman and Webster (2001) contended that fan energy saving is associated with reduced static pressure requirements and the potential for reduced air volumes. Chapter 5 inspects the energy saving potential of the UFAD system.

5. Productivity and health improvement

Research evidence indicates that occupant satisfaction and productivity can be increased by giving individuals greater control over their local environment and by improving the quality of indoor environments (thermal, acoustical, ventilation, and lighting) (Bauman and Webster 2001).

Despite the advantages of the underfloor air distribution system, barriers still exist to the widespread adoption of UFAD systems. Lack of familiarity can result in some problems in the entire building design, construction, and operation process, including higher cost estimates, incompatible construction methods, and incorrect building energy consumption estimates, etc (Bauman and Webster 2001). Due to the lack of standards and codes for the UFAD technology, ASHRAE has funded the development of a design guide through ASHRAE research project 1064-RP. In addition, a public web site on UFAD technology has recently been developed (Bauman et al. 2000).

4.3 Thermal Environment Investigations for Two Supply Diffusers

4.3.1 Previous Investigations of the Swirling and Square Diffusers

When the swirling diffuser is used in the mixing system, it discharges a swirl jet that entrains more room air than the square diffuser and the higher entrainment results in

faster jet velocity decay (Shakerin and Miller 1996). The detailed investigation results of swirling and square diffusers were presented in ASHRAE report *RP-1009* (Chen and Srebric 2000). Figure 4.6 shows the smoke visualization results from a manufacturer's catalogue (Chen and Srebric 2000).

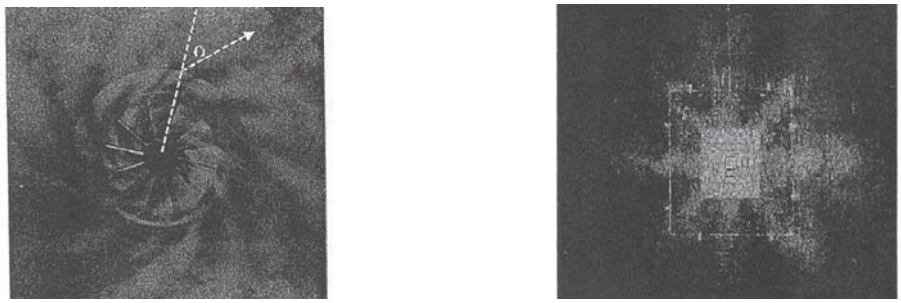

(a) (b)

Figure 4.6 Smoke visualizations
(a) Swirling diffuser and (b) Square diffuser

The momentum method was applied to these two diffusers, as shown in Figure 4.7 (Chen and Srebric 2000). For the swirling diffuser, the tangential angle is very important, because it is used to set the boundary conditions for the CFD simulation of the swirl jet. For the square diffuser, the momentum method used a discharge velocity on the entire diffuser surface as the momentum source. The discharge velocity is an averaged maximum velocity measured at the perimeter of the diffuser. The flow direction specified in the momentum method was obtained from the smoke visualization (Figure 4.6). The air temperature used is the same as the supply air temperature in the duct. Although the diffusers have complicated geometries, the momentum method can reasonably represent the diffuser for numerical simulations (Chen and Srebric 2000).

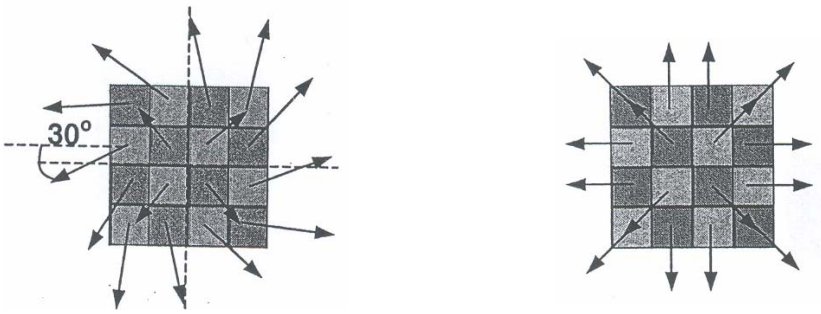

(a) (b)

Figure 4.7 Momentum method
(a) Swirling diffuser and (b) Square diffuser

The box method was investigated by Srebric and Chen (2002) for the square diffuser. Figure 4.8 shows the box size for the square diffuser. The box method requires much labor as it specifies flow information on four surfaces, whereas the momentum method requires only the flow information on one surface. The above investigations were all conducted on a mixing HVAC system, in which the supply diffusers were installed in the ceiling. The buoyancy force can be ignored.

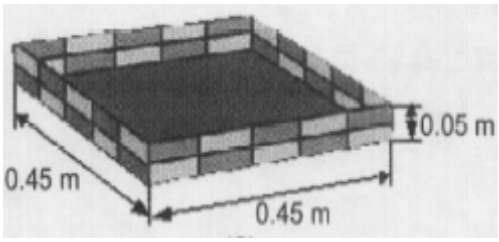

Figure 4.8 Box method for the square diffuser

Different diffusers result in different room air distributions and accordingly different thermal environments in the occupied zone. In this section, the diffuser modeling method FRGM, presented in Chapter 3, is employed to investigate the air flow patterns from two supply diffusers (Figure 3.1) and their effect on the thermal environments in the occupied zone.

4.3.2 Criteria of Environmental Indexes for Thermal Sensations

4.3.2.1 Fanger's PD Model

Cold draft is defined as "an undesired cooling of the human body caused by air movement" (ASHRAE 2001), and is argued to be a common problem in office buildings (Fanger 1992). In addition to occupant discomfort, draft can have implications for indoor air quality and energy use, as occupant who feel a draft sometimes react by increasing the room air temperature or covering air outlets (Fanger et al. 1988; ASHRAE 2001).

To assess the risk of draft to occupants, the most popular model used is that developed by Fanger et al. (1988) on the basis of laboratory experiments. This model combines three physical parameters, air temperature, mean air velocity and turbulence intensity, to predict the percentage of occupants dissatisfied due to a draft (PD). This equation can be defined as

$$PD = (34 - t_a)(v - 0.05)^{0.62}(0.37 \times v \times T_u + 3.14) \qquad (4.1)$$

where

PD is the percentage of people dissatisfied due to the draft

t_a is the local air temperature(℃)

v is the local mean air velocity (m/s)

T_u is the local turbulence intensity

4.3.2.2 Fanger's PMV Model

Fanger's Predicted Mean Vote (PMV) model was developed in the 1970's from laboratory and climate chamber studies. In these studies, participants were dressed in standardized clothing and completed standardized activities, while exposed to different thermal environments. The PMV model combines four physical variables (air temperature, air velocity, mean radiant temperature, and relative humidity) and two personal variables (clothing insulation and activity level) into an index that can be used to predict thermal comfort. The index provides a score that corresponds to the ASHRAE thermal sensation scale, and represents the average thermal sensation felt by a large group of people in a space (Fanger 1970; ASHRAE 2001). Table 4.1 shows the ASHRAE thermal sensation scale for PMV.

Table 4.1 ASHRAE thermal sensation scale

-3	-2	-1	0	1	2	3
cold	cool	slightly cool	neutral	slightly warm	warm	hot

PMV is expressed as follow:

$$\begin{aligned} PMV = &\left[0.303e^{(-0.36M)} + 0.28\right] \times \{M - 3.05 \times 0.001(5733 - 6.99M - P_a) \\ &- 0.42(M - 58.18) - 1.7 \times 0.0001M(5867 - P_a) - 0.0014M(34 - t_a) \\ &- 3.96 \times 10^{-8} f_{cl}\left[(t_{cl} + 273)^4 - (t_{mr} + 273)^4\right] - f_{cl} h_c (t_{cl} - t_a)\} \end{aligned} \quad (4.2)$$

where

$$t_{cl} = 35.7 - 0.028M - I_{cl}\left\{\left[(t_{cl}+273)^4 - (t_{mr}+273)^4\right] + f_{cl}h_c(t_{cl}-t_a)\right\}$$

$$h_c = 2.38(t_{cl}-t_a)^{0.25} \quad \text{if } 2.38(t_{cl}-t_a)^{0.25} > 12.1\sqrt{v_a}$$

$$= 12.1\sqrt{v_a} \quad \text{if } 2.38(t_{cl}-t_a)^{0.25} < 12.1\sqrt{v_a}$$

$$f_{cl} = 1.00 + 1.29I_{cl} \quad \text{if } I_{cl} \le 0.078\,\text{m}^2\text{℃/W}$$

$$= 1.05 + 0.645I_{cl} \quad \text{if } I_{cl} > 0.078\,\text{m}^2\text{℃/W}$$

M is the metabolic rate of the body (W/m^2)

I_{cl} is the thermal resistance of clothing (m^2·℃/W)

f_{cl} is the ratio of a clothed man's surface area to a nude man's surface area

t_a is the air temperature (℃)

v_a is the air velocity (m/s)

P_a is the partial water vapor pressure (Pa)

h_c is the convective heat transfer coefficient (W/ m^2·℃)

t_{cl} is the surface temperature of clothing (℃)

4.3.3 Descriptions of CFD Simulation Cases

From the investigations in Chapter 3, we can see that the diffuser modeling method plays a very important role for air flow simulation. The air flow information near the supply diffuser is a concern for occupied zone thermal comfort in the underfloor air distribution system. Due to the difficulties to obtain the credible experimental data near the supply diffuser and the validation work in Chapter 3, here only the simulation work are presented.

For the cooling load or heat extraction calculations, only one room is picked for analysis in the numerical study. The room is assumed to be a south-facing office room in Hong Kong (22^{o}N, 114^{o}E) with identical rooms adjacent, above and below. The façade is south facing with a 35% double glazing area. The window is fitted with venetian blinds. This room is 5.1m in length, 3.6m in width and 2.64m in height (Figure 4.9).

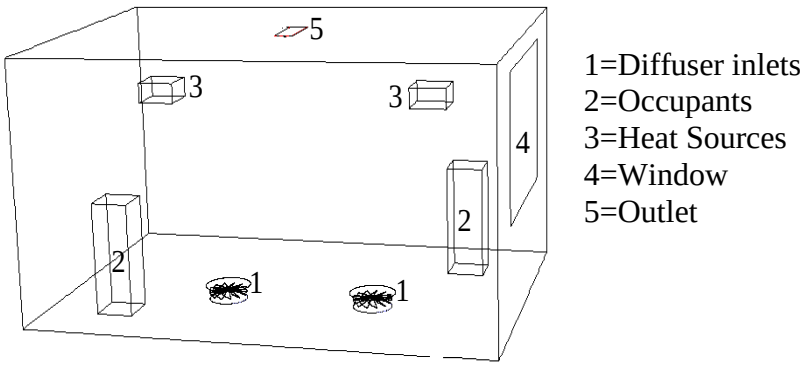

Figure 4.9 Configuration of the simulation room

This simulation work is focused on the indoor air thermal comfort, not on the heat transfer through walls or window, so no carpet is assumed on floor. The heat gain from south wall is not significant. During ACCURACY simulation, the external wall consists of three layers: 180mm (7.09in) thick concrete slab inside and a 100mm (3.94in) thick brick layer outside with 60mm (2.36in) insulation in between. The floor (also the ceiling) has a 320mm (12.6in) thick concrete slab base with another 70mm (2.76in) thick cement layer.

The building is occupied only during working hours. From 9:00am to 6:00pm there are two occupants (each occupant generating a convective heat gain of 50 watts and radiant heat gain of 25 watts). Heat gains also come from other internal heat sources in convective and radiative forms. The total emitted heat from two large electronic

appliances is assumed to be 256 watts. Half is assumed to be convection heat. In the calculation of cooling load, no air infiltration occurs. The room operative temperature for simulation is set at 24℃.

During the following numerical simulation, a method of estimating the thermal comfort conditions by combining a room-simulation with 3D air flow modeling is presented. An enhanced dynamic cooling load program ACCURACY (Chen and Kooi 1988; Niu and Kooi 1993; Niu et al. 1995; Niu and Burnett 1998), which is based on the ASHRAE Room Energy Balance Method, is used to calculate the room cooling load at the desired operative temperature (24℃). In order to include the transient heat storage behaviors of the concrete floor and the façade wall and external heat gains from solar radiation, the Hong Kong weather data for the year 1989 were used as the external conditions of the simulated room.

ACCURACY provides the room surface temperatures and convective heat fluxes as boundary conditions for CFD simulation. The surface temperatures are used to calculate the room radiant temperature and the convective heat fluxes are used as the input boundary conditions (Table 4.2) for the room air flow simulations. The real south wall in CFD simulation is composed of the defined window, two facades and south wall, so we can see that the wall surface temperatures are almost the same for facades and south wall.

Table 4.2 Boundary conditions calculated by ACCURACY (1:00pm, July 15, 1989)

	Convective heat flow (W)	Wall surface temperature (°C)
Rear wall	74.16	25.5
Floor	119.25	25.6
Ceiling	15.40	25.4
South wall	36.96	27.0
Facade 1	15.41	27.1
Facade 2	7.74	27.0
Window	198.13	36.6

Figure 4.10 shows the basic scheme for the data exchange and the calculation procedure between ACCURACY and CFD simulation.

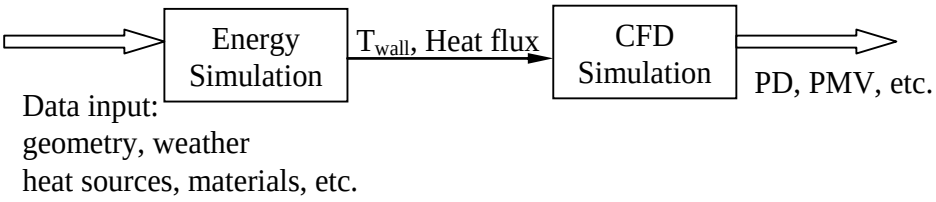

Figure 4.10 Data transfer from energy simulation to CFD simulation

Case-1 and Case-2 correspond to swirling and square diffuser applications in the UFAD system. Figure 4.11 shows the diffuser mesh grids and dimensions. In the UFAD system, it is generally believed that the supply outlet temperature should be maintained at or above 17°C -18°C (63^{o}F – 64^{o}F) to avoid uncomfortably cold conditions for the nearby occupants due to draft (Shute 1992, 1995; Matsunawa et al. 1995). In the following CFD simulations, the supply air flow rate was set at 133.5 l/s, or an air change (ACH) rate of 10 times per hour. The calculated inlet supply air

temperature from ACCURACY was 17.6 °C.

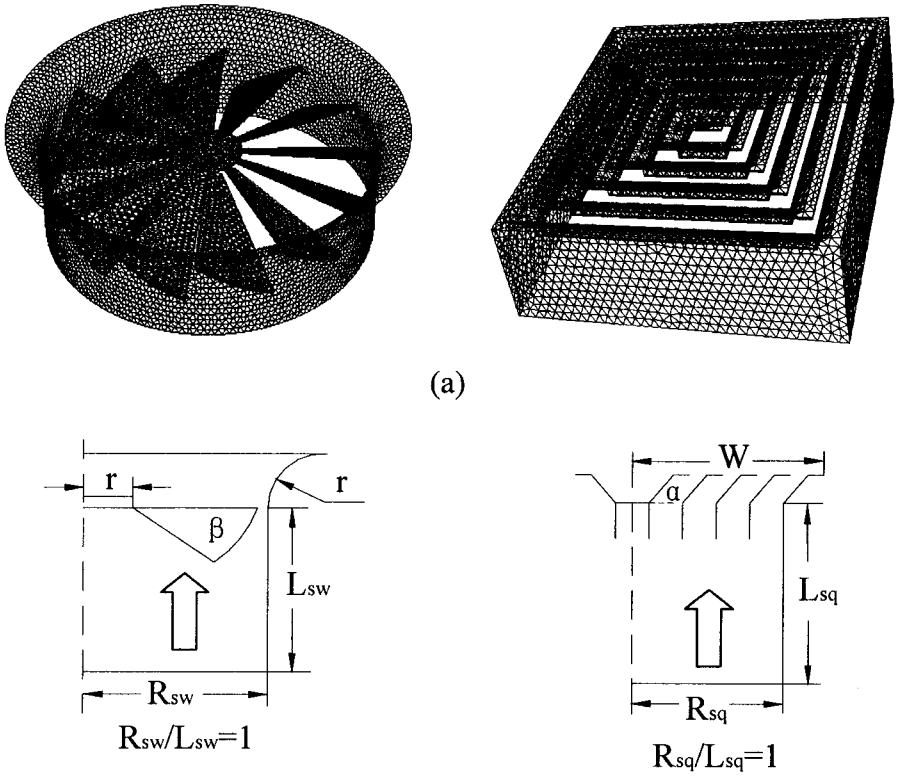

Figure 4.11 Configurations of two different diffusers
(a) Meshed by FLUENT (2001), and (b) Dimensions (Table 4.3)

Table 4.3 Dimensions of two different diffusers

Diffuser	Dimension
Swirling diffuser:	$R_{sw}=L_{sw}=216$mm; r=40mm; $\beta=30^{o}$
Square diffuser:	$R_{sq}=L_{sq}=175$mm; W=200mm; $\alpha=45^{o}$

4.3.4 Numerical Simulation Characteristics

The standard $\kappa-\varepsilon$ turbulence model (Launder and Spalding 1974; Chen and Jiang 1992) was chosen and the Boussinesq assumption (Tritton 1988) was used to account

Pao Yue-kong Library
PolyU • Hong Kong

for the buoyancy effects resulting from heat sources in the UFAD system. The SIMPLE-C algorithm (Van Doormaal and Raithby 1984) was used for pressure-velocity coupling calculations. The discrete ordinates (DO) radiation model for the air radiation temperature was employed. The second order upwind scheme (Leonard 1981) was used for energy, momentum, κ and ε equation discretizations.

Unstructured grids are employed to represent the complicated geometries of two supply diffusers, as shown in Figure 4.11(a). Figure 4.12 presents the partial linked grids between the room and supply diffuser. It can be seen that the diffuser mesh size is much smaller than that of the indoor space due to the different size scales. A 10 mm grid size is employed to mesh the swirling and square diffusers. For the room space, three internal sizes, 40mm, 60mm and 80mm, are investigated. Because grid independence was found with a grid size of 60mm or finer, the results with this resolution are presented. The inlet conditions for air jets were assumed to be fully developed turbulence conditions. The turbulence intensity (I) and turbulence length scale (l) can be calculated and set as inlet boundary conditions for the standard $\kappa - \varepsilon$ turbulence model.

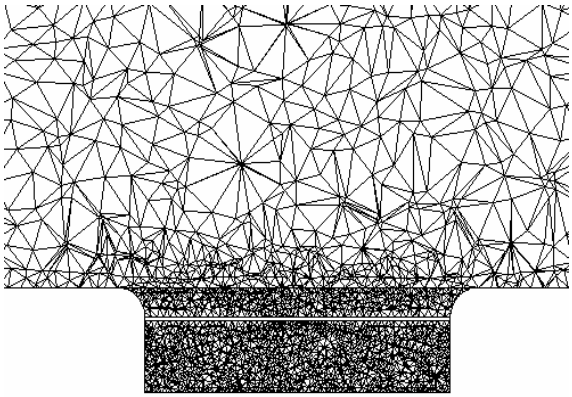

Figure 4.12 Partial linked grids between the room and the supply diffuser

The UNIX machine HKPU22 was used for my simulation work. During the following simulations, the near-wall cells were adapted in order to place the y+ (dimensionless distance) value in the range of 5 to 25 to ensure the validity of the standard wall function. The UDF (user defined functions) of PD and PMV, shown in the appendix, were written by the author and compiled into the CFD code FLUENT.

4.3.5 Velocity Characteristics of Different Diffusers

Figure 4.13 shows the velocity path line characteristics of the two diffusers. They are dominated by the different diffuser configurations.

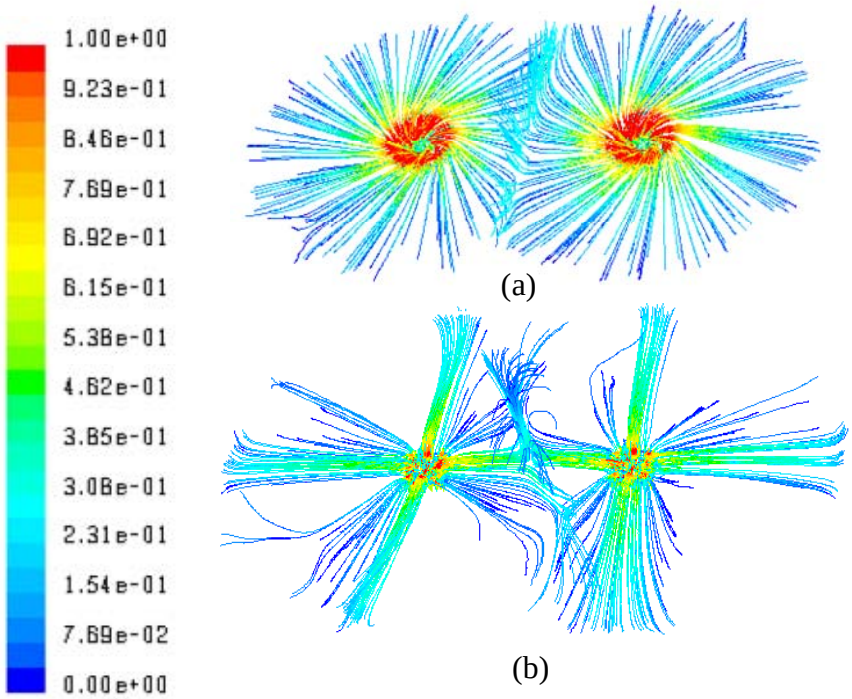

Figure 4.13 Air flow path lines around the outlets
(a) Swirling diffuser, and (b) Square diffuser

Figure 4.14 presents velocity vector distributions in the office room. Due to the low temperature and large velocity near the floor, the cool supply air travels a distance

enough for mixing with room air by entrainment before spreading upward to the occupied zone. With the “swirling” characteristic, supplied air from the swirling diffuser can more quickly combine with room air than that from a square diffuser and generates a uniform velocity field near the floor level. Above the floor, the upward flow patterns are typically characterized by the convection flow and buoyancy force.

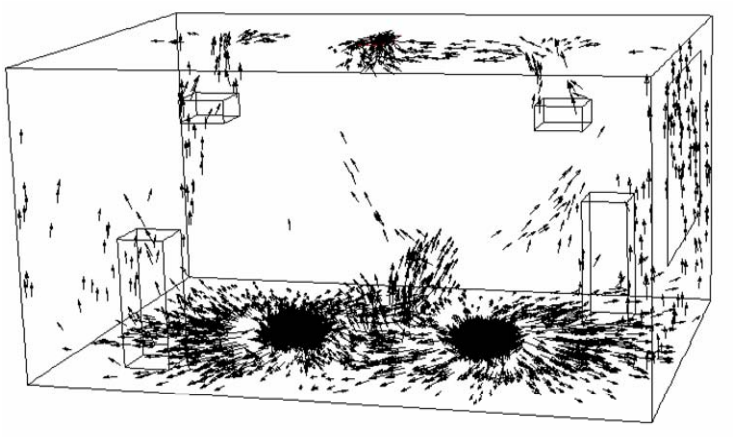

(a)

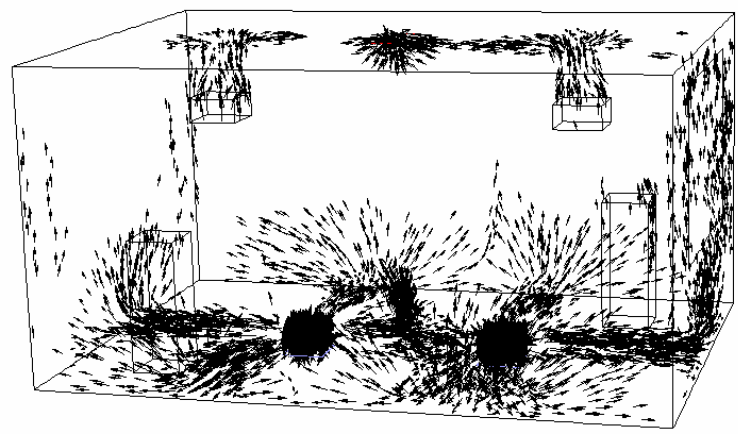

(b)

Figure 4.14 Velocity vector distributions in the simulation room (>0.15m/s)
(a) Case-1, and (b) Case-2

The velocity vectors at the middle vertical plane (Y=0.0m) are shown in Figure 4.15. It can be seen that the supply air spreads out near the floor, reaches the vertical walls

and then flows upward due to the Coanda effect. Above the floor, room air is introduced to the supply air stream and mixed in order to rapidly reduce the velocities of the supply air. In the occupied zone, Case-1 shows more uniform air velocities than those of Case-2 due to the rapid mixing property of the swirling diffuser. Above the height of the heat sources (1.9m), room air flows upward, as a result of natural buoyancy (heat) forces.

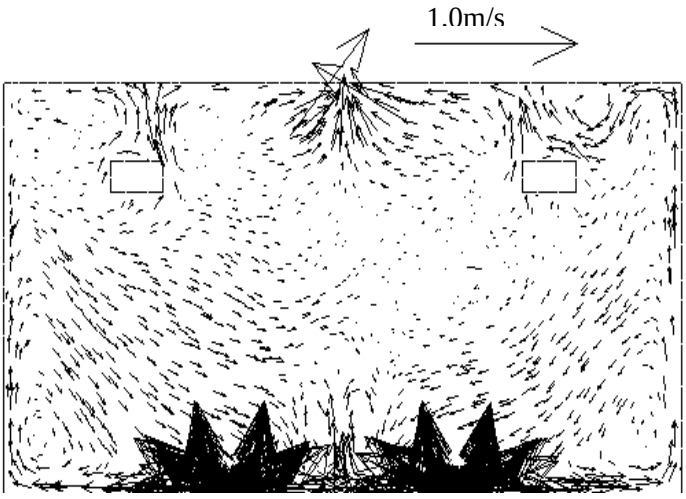

(a)

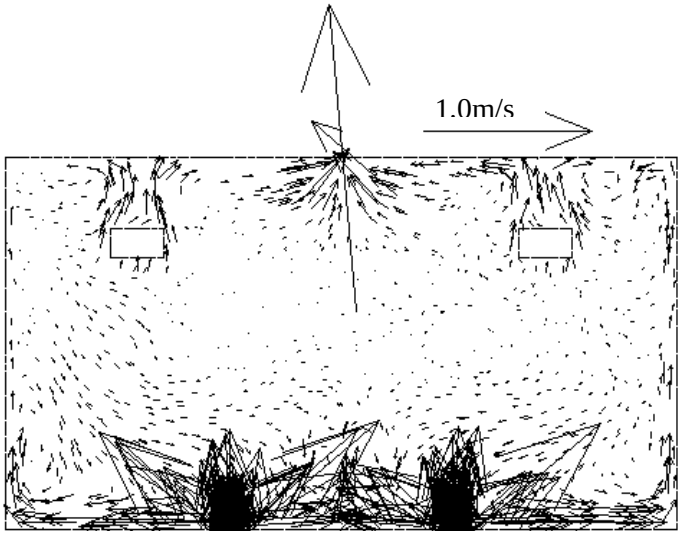

(b)

Figure 4.15 Velocity vector at the middle planes (Y=0)
(a) Case-1, and (b) Case-2

4.3.6 Temperature Profiles of Different Diffusers

The key design objective of UFAD systems is to satisfy thermal comfort issues. One limitation is the vertical temperature rise in the occupied zone. The largest allowed temperature difference should not exceed 3°C at heights between 0.1m and 1.1m in order to maintain thermal comfort environments (ISO 7730 1984). The temperature contours in the middle vertical plane are shown in Figure 4.16. It indicates that there exists vertical temperature stratification, which is a criterion for the successful design and operation of UFAD systems.

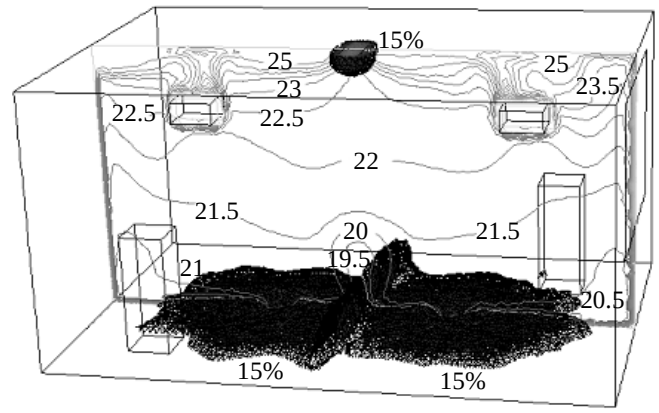

(a)

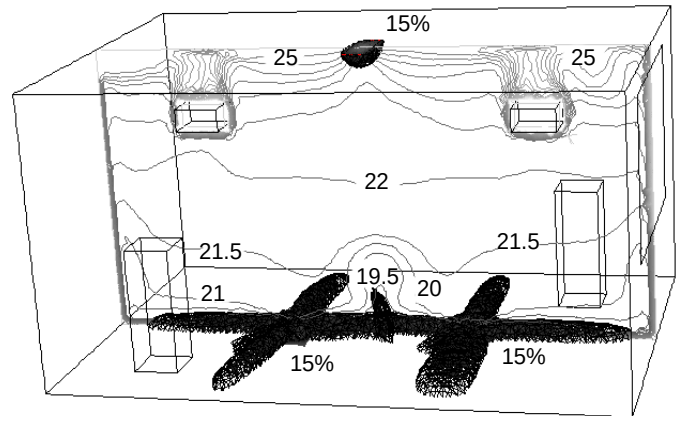

(b)

Figure 4.16 PD due to draft (iso-surface of 15%) and temperature contours (°C) in the middle planes (Y=0)
(a) Case-1, and (b) Case-2

In order to present more detailed thermal environments influenced by two different supply diffusers, thirteen vertical locations were selected on the floor (Figure 4.17). Due to symmetries, only five locations: A0, C0, C1, D1 and E1 were chosen to represent most of the locations in the simulated office room.

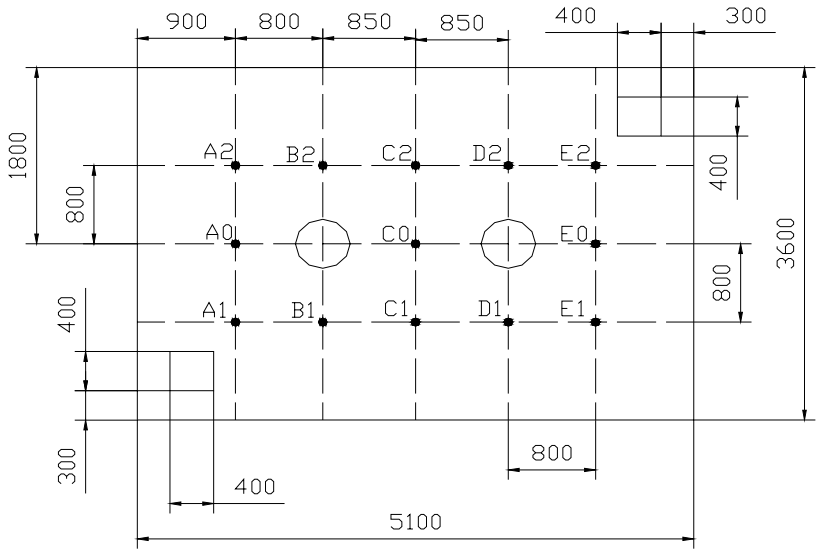

Figure 4.17 Thirteen vertical locations at floor level

Figure 4.18 shows the temperature profiles at four locations: C1, D1, E1 and C0. The temperature gradient below foot level is very large, which means that occupants will not feel much cold before the supplied cool air reaches their ankles. Between these two diffusers, the greatest difference in vertical temperature gradients occurs below the height of 1.1m. At locations D1 and C0, the temperature differences from the square diffuser were about 0.43°C and 0.74°C larger than those from the swirling diffuser. Since there is very uniform entrainment of the supply air stream from the swirling diffuser and the room air, the temperature tends to be higher at foot level than that found for the square diffuser. At other locations: C1 and E1, where no

direct supplied air flow passes from the square diffuser, the temperature differences of the swirling diffuser were 0.38°C and 0.65°C larger, respectively. This is due to the fact that no direct airflow passes these two locations from the square diffuser and the mixing between the supply air and room air is very weak. The largest temperature difference is 2.34°C at location C0 in Case-2. However, it is possible to deduce that the square diffuser has the potential for generating larger temperature differences exceeding 3°C at some locations, due to the inconsistent combinations between the supply air and room air.

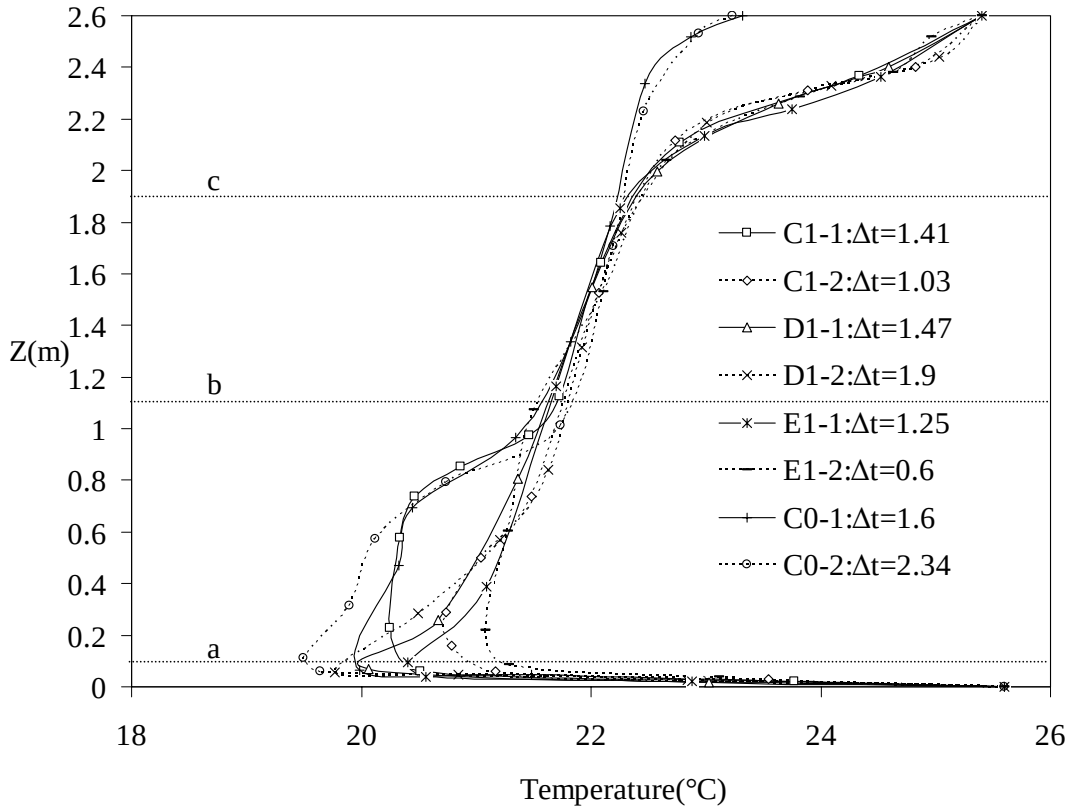

Figure 4.18 Temperature profiles (℃) at four locations (-1: Case-1, -2: Case-2)

Temperature stratification is very important for energy savings because convective heat sources located in the upper displacement zone can be isolated from the

conditioned air reservoir and may be neglected in the calculation of space supply air requirements (Webster et al. 2002; Loudermilk 2003). Chapter 5 investigated the influence of temperature stratification on system energy consumption.

4.3.7 PD Comparisons

The shadow regions in Figure 4.16 are PD iso-surfaces, within which the local percentage dissatisfied due to draft (PD) was higher than 15%. Around the supply diffuser, PD tended to be high. This is due to the combined effects of low temperature, relatively large velocity, and the existence of turbulence. At a certain distance away from the supply diffusers, the draft risk normally diminishes. Such discomfort draft environments are also characterized by diffuser configurations, which means that diffuser designs are very important in creating a thermal comfort environment with the UFAD system. Near the room outlet, relative large air velocities exist and may cause a draft if it is occupied, although this unoccupied zone is of little concern.

Figure 4.19 shows comparison results of PD at five locations. It shows that, near the floor, PD is relatively large and decreases dramatically below foot level (0.1m). Above the height of 0.1m, at location C0 where two supply air streams meet, occupants may feel a cold draft, which is mainly dependent on the distance between two supply diffusers (as indicated in zone B). In these two cases, in zone A, a more uniform PD field is presented and no draft complaint exists if PD is less than 15%. It can be said that, in such case, the thermal environment is acceptable.

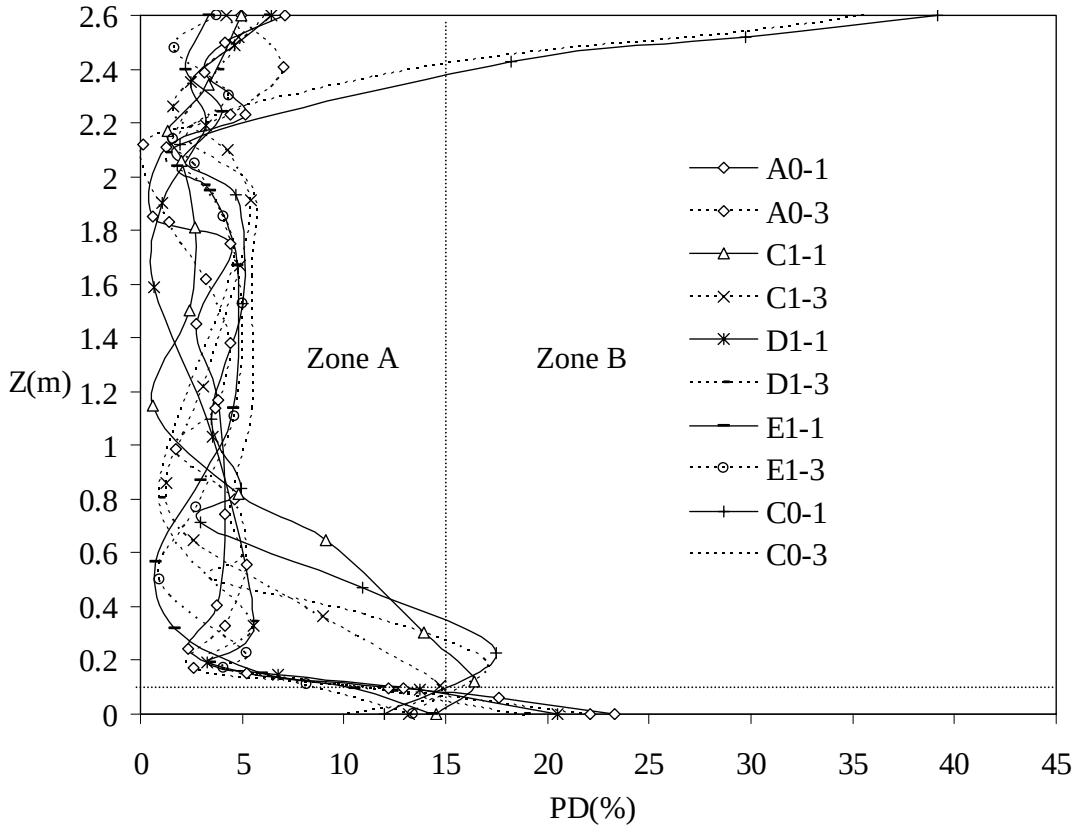

Figure 4.19 PD profiles (%) at five vertical locations (-1:Case-1, -2:Case-2)

4.4 Vane Declining Angle Investigations for the Swirling Diffuser

Due to measurement difficulties and the instability of air flows near the supply diffuser, the most practical method to achieve flow information is to use smoke visualization (Chen and Jiang 1996) or infrared visualization (Sun and Smith 2005). The flow currents can be seen with the above methods, but the detailed flow information cannot be compared numerically. Different supply air stream directions result in different thermal sensations near the diffuser zone. The thermal environment changes resulting from changes in the swirling diffuser vane declining angles are investigated in this section for the UFAD system using the CFD technique. The declining angle of the swirling diffuser in Case-1 is 30^{o}. In Case-3 the corresponding angle is 60^{o}, the only difference from Case-1.

4.4.1 Velocity Path Line

Figure 4.20 shows the velocity path line characteristics of Case-1 and Case-3. For Case-1, with a vane declining angle of 30^{o}, the supplied air from the swirling diffuser spreads near the floor just as in displacement ventilation (DV) systems, which can be called a horizontal discharge strategy. For Case-3, the simulated upward flow path line is typically called the vertical discharge strategy.

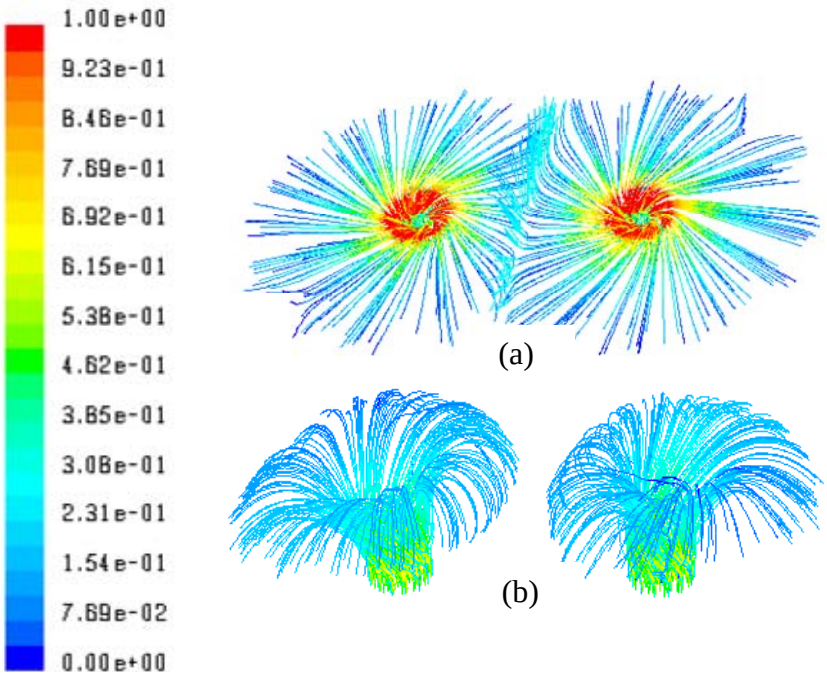

Figure 4.20 Velocity path lines of Case-1 (a), and (b) Case-3

The supply air flows like a fountain (Bergstrom 1994), flowing upward and then spreading downward due to the relatively low air temperature that result in a large air density. The decay in supply velocity occurs mainly in the vertical direction with the larger vane declining angle of 60^{o}.

4.4.2 Temperature Profiles

Figure 4.21 presents temperature profiles at four locations: C1, D1, E1 and C0. It can be seen that increasing vane inclining angle from 30^{o} to 60^{o} for the swirling diffuser significantly lowers the average temperature of the occupied zone.

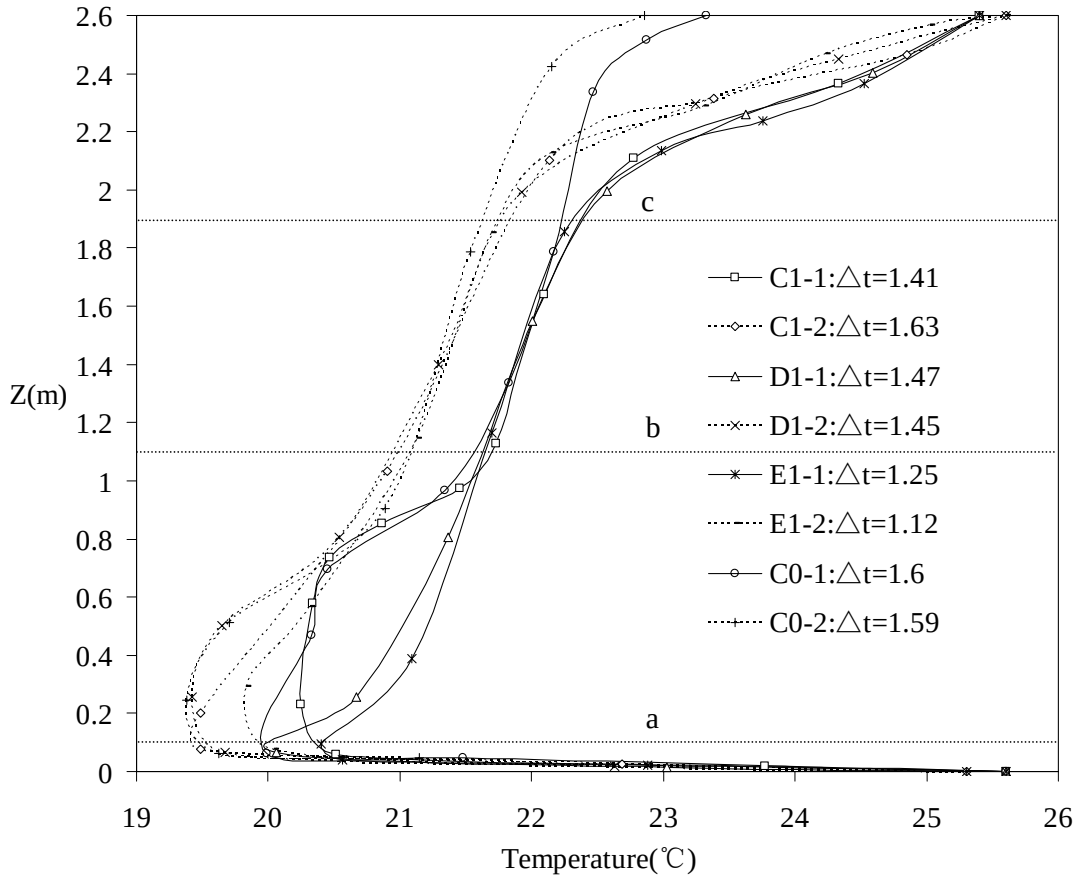

Figure 4.21 Temperature profiles at four vertical locations (-1: Case-1, -2: Case-3)

4.4.3 PD Comparisons

PD index larger than 15% in Case-1 is like a tile covering the floor, as shown in Figure 4.16(a). For Case-3, the PD index (>15%) is concentrated in a limited vertical space, as presented in Figure 4.22. Obviously, this discomfort draft environment is due to different swirling diffuser vane declining angles. Air temperature stratification

can still be observed. Figure 4.23 shows comparisons of PD index at five locations. In these two cases, in zone A, there is no draft complaint if PD is less than 15% and it can be said that the thermal environment is acceptable. No distinct differences exist between these two cases.

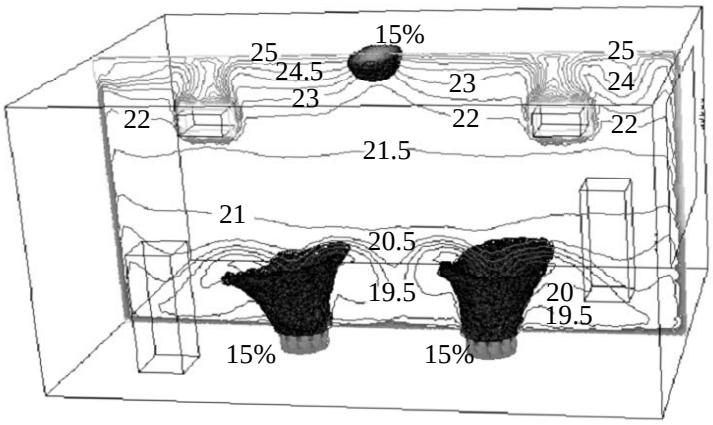

Figure 4.22 PD (iso-surface of 15%) and temperature contours (°C) for Case-3

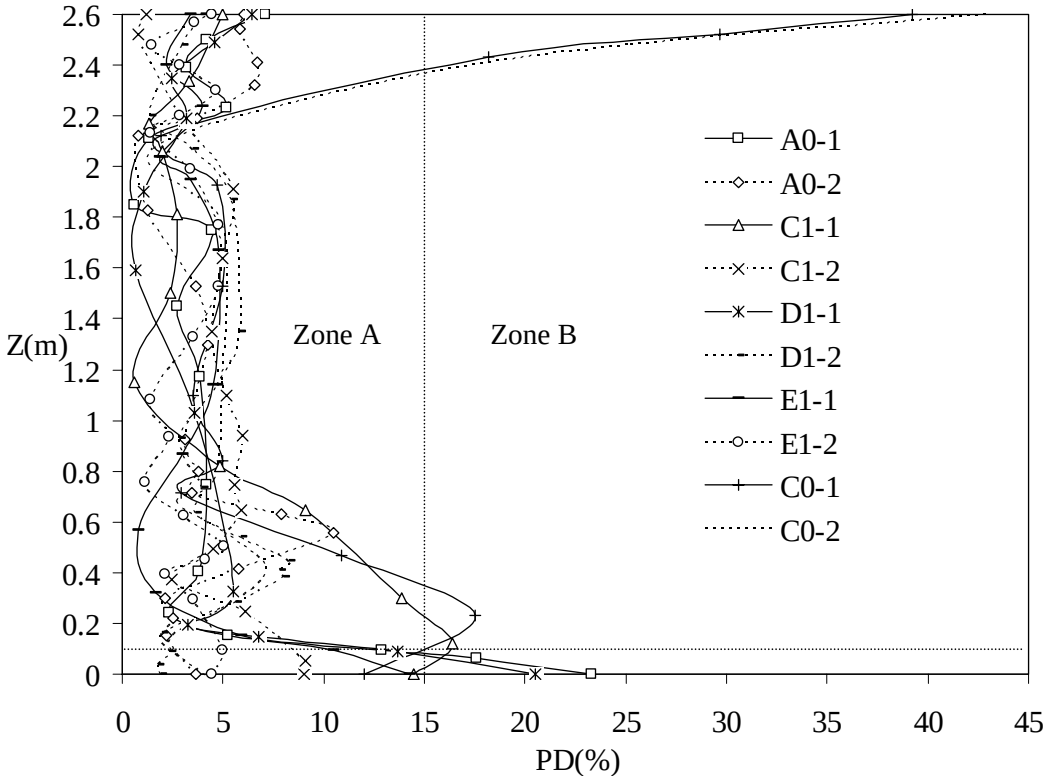

Figure 4.23 PD profiles at five vertical locations (-1: Case-1, -2: Case-3)

4.4.4 PMV Comparisons

During PMV simulations, the metabolic rate of bodies is assumed to 1.0met and the thermal resistance of clothing equals to 0.7clo. The partial water vapor pressure is assumed to be 1500Pa and the rate of mechanical work accomplished equals zero. In Case-1, shown in Figure 4.24(a), it is slightly cool at foot level while it is warm at the heat source level according to the PMV scale. Near the floor, this may primarily be attributed to the lower air temperature and larger air velocity. In Case-3 (Figure 4.24(b)), the difference in PMV from Case-1 is mainly found at locations around the swirling diffusers, mainly due to different vane declining angles. Figure 4.24(c) and 4.24(d) are the simulated results at the vertical plane of Y=-1.2m, where occupants are seated. The vertical PMV difference between angle level and head level is about 0.6 in these two cases. It can be seen that different vane declining angles result in almost the same PMV at the occupied location, which is about 1.4m far away from the supply diffuser.

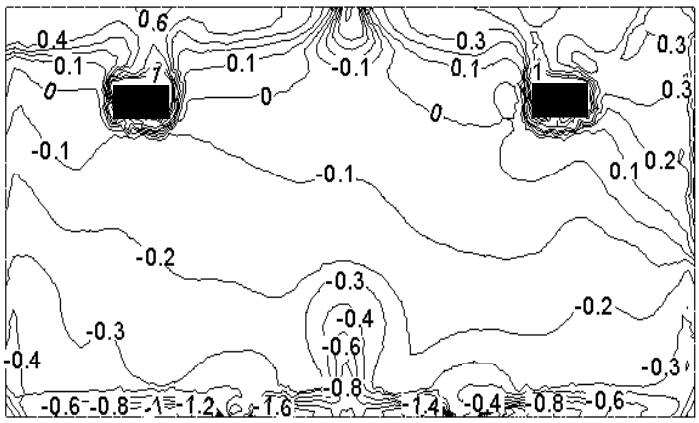

(a)

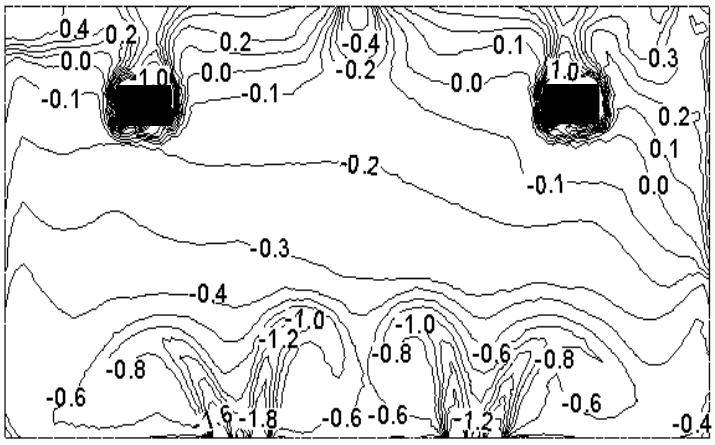

(b)

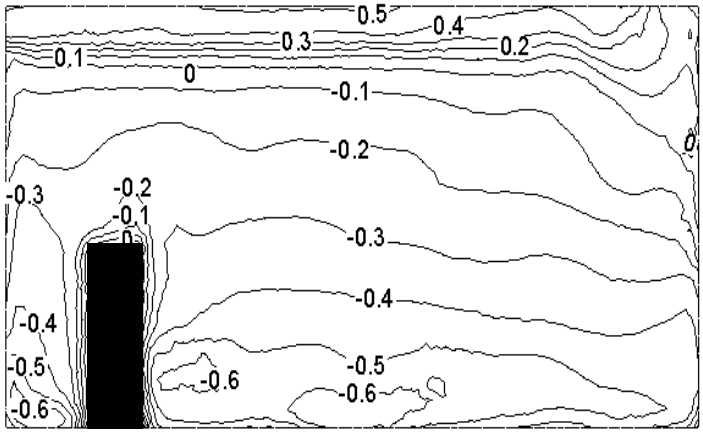

(c)

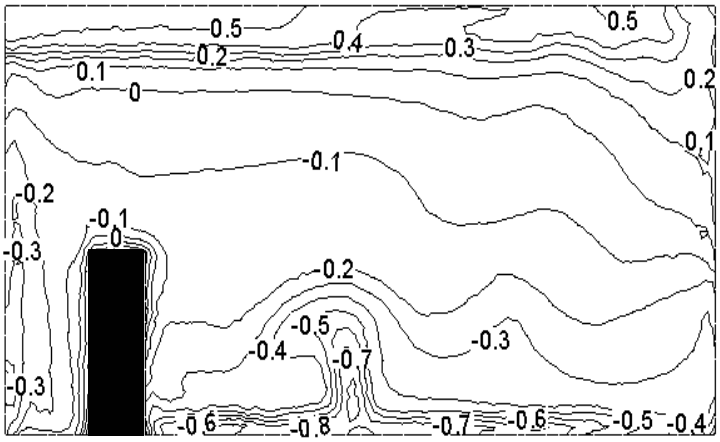

(d)

Figure 4.24 PMV distributions in two planes

(a) Case-1 at Y=0.0m, (b) Case-3 at Y=0.0m,

(c) Case-1 at Y=-1.2m, and (d) Case-3 at Y=-1.2m.

4.5 Discussion and Summary

This chapter focused on the influences that supply diffusers have on indoor thermal environments. The investigation approach was based on the CFD method due to its easier applications. The fully represented geometry method FRGM, validated in Chapter 3, was used for the supply diffuser simulation in a small office room. The CFD simulations were carried out based on the boundary conditions from ACCURACY.

Firstly, two different diffusers, a swirling diffuse and a square diffuser, were investigated for thermal environments. It was found that both swirling and square diffusers can successfully maintain vertical air temperature stratification in the UFAD system. The primary air flow from a swirling diffuser can be more quickly combined with the room air than that from a square diffuser. Between foot and head levels, the vertical temperature difference produced by the swirling diffuser is smaller than that of the square diffuser at locations where intercrossed supply air passes (for the square diffuser). At other locations, where no direct air flow passes from the square diffuser, the temperature difference produced by the swirling diffuser is larger that that of the square diffuser. Draft risk is much influenced by the different configurations of the supply diffusers. For the two diffusers, the PD index changes inconspicuously with high inlet temperature and low inlet velocity in the occupied zone, and both thermal environments acceptable.

Secondly, two supply strategies, horizontal and vertical supply, were studied for different diffuser vane declining angles of the swirling diffuser. It was found that the fundamental indoor air temperature profiles were similar. However, the vertical

supply strategy showed a lower temperature at the same height. In terms of the thermal comfort environments, the zone near the supply diffuser is much influenced by the supply strategy. With the supply air direction changed from horizontal to vertical, the PD index (>15%) changed from the floor cover form to the fountain form. PMV is also affected by diffuser configuration and a larger PMV gradient occurs near the supply diffuser.

CHAPTER 5 INDOOR TEMPERATURE STRATIFICATION AND ENERGY SAVING POTENTIAL OF UFAD SYSTEM

5.1 Introduction

Lam and Chan (1994) carried out a survey on electricity use in both hotel and office buildings in Hong Kong. They found that the largest electricity consumer was the HVAC system (49.9% in office buildings, 51.7% in office/shopping complexes, 56.8% in hotel buildings). The electricity requirements of HVAC systems, resulting from fuel consumption, have a direct impact on the cost of operating a building and an indirect impact on the environment, in the form of carbon emissions. Koomey et al. (1998) estimated that the current trend of carbon emissions from energy consumption in building operations could increase by 12% over 1997 levels by 2010. The energy consumption and global environmental concerns have motivated an increasing number of designers, developers and building users to propose more efficient design and operation strategies for HVAC systems.

Although the procedures for estimating energy requirements vary considerably in their degree of complexity for HVAC systems, they all have three common elements, *i.e.*, the calculation of (1) space load, (2) secondary equipment load, and (3) primary equipment energy requirements. The space load calculations determine the amount of energy that must be added to or extracted from a space to maintain thermal comfort. The secondary equipment load refers to equipment that distributes the heating, cooling, or ventilating medium to conditioned spaces, while primary

equipment energy requirements refer to central plant equipment that converts fuel or electric energy into a heating or cooling effect.

For space load calculations, the simplest procedures assume that the energy required to maintain comfort is only a function of the outdoor dry-bulb temperature. More detailed methods consider solar effects, internal gains, heat storage in walls and interiors, and the effects of wind on both building envelope heat transfer and infiltration. Basically, the energy simulation methods can be classified as steady-state and dynamic methods. In the steady-state method, degree-day (Büyükalaca et al. 2001) methods are the simplest if building use and the efficiency of the HVAC equipment are constant. When efficiency or conditions of use vary with outdoor temperature, the consumption can be calculated for different values of the outdoor temperature and multiplied by the corresponding number of hours. This approach is used in various bin methods (Hanby 1995).

When the indoor temperature is allowed to fluctuate or when interior gains vary, dynamic methods should be considered. To employ these methods, a mathematical model of the building and its energy system must represent (1) the thermal behavior of the building structure (the loads model), (2) the thermodynamic behavior of the air-conditioning delivery system (the secondary systems model), and (3) a mathematical relationship for load versus energy requirements of the primary energy conversion equipment (the primary equipment model). Figure 5.1 shows the basic function of each major model element on an input and/or output basis using ASHRAE Algorithms (ASHRAE Handbook 1993). Generally, the loads model tends to be the most complex and time-consuming; the central plant model, the least.

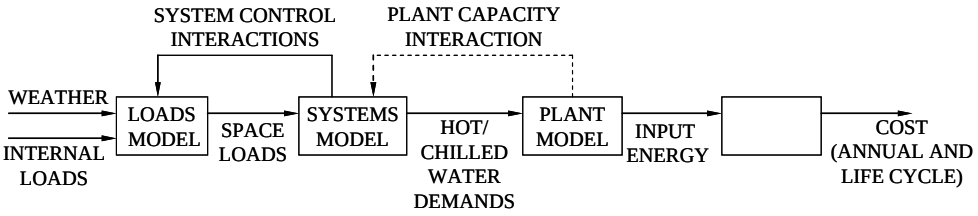

Figure 5.1 Flow diagram for calculating hourly heating cooling loads using ASHRAE Algorithms

This chapter first reviews three popular codes for dynamic energy simulations. Then, a new energy simulation method considering indoor air temperature stratification in UFAD systems is presented. The simulation result is compared with the mixing system for the different air supply strategies, CAV and VAV.

5.2 Three Programs for Dynamic Energy Simulations

5.2.1 BLAST

The U.S. Army Construction Engineering Research Laboratory (CERL) developed the Building Loads Analysis and System Thermodynamics (BLAST) program to investigate the energy performance of new or retrofitted building design options of almost any type and size (Hittle 1977). In addition to performing peak load (design day) calculations necessary for mechanical equipment design, BLAST also estimates a facility's annual energy performance, which is essential for the design of solar and total energy (cogeneration) systems and for determining compliance with design energy budgets.

The BLAST analysis program encompasses three major subprograms which compute hourly requirements of the space loads, demands (hot water, steam, gas,

electrical, chilled water) of the building and air-handling systems, and the annual fuel and electrical power consumptions. Some recent research projects employing BLAST for simulation work have been published (Fontoynont et al. 1984; Akbari et al. 1987; Ke and Mumma 1999; Schibuola 1999).

5.2.2 DOE-2

The DOE-2 program, developed by the Lawrence Berkeley National Laboratory (LBNL), Hirsch & Associates, the Consultants Computation Bureau, Los Alamos National Laboratory, the Argonne National Laboratory and the University of Paris (Winkelmann et al. 2003), provides the building construction and research communities with an up-to-date, unbiased, well-documented computer program for building energy analysis. It is a portable FORTRAN program that can be used on a large variety of computers, including PC's. Using DOE-2, designers can quickly determine building parameters which will improve energy efficiency while maintaining thermal comfort. A user can provide a simple or increasingly detailed description of a building design or alternative design options and obtain an accurate estimation of the proposed building's energy consumption, interior environmental conditions and energy operation cost.

Development of the above two software tools began in the 1970’s, when the U.S. Department of Defense began funding the software that became BLAST and the Department of Energy began funding the DOE-2 program. At that time, it was not clear which effort, if either, would produce a usable building energy analysis program. Each has hundreds of subroutines designed to solve specific building-

design problems, and each has been successfully used by building designers (Diamond et al. 1981, 1986; Meldem and Winkelmann 1995).

Though BLAST and DOE-2 are still valid tools that continue to be used in various environments, some limitations have restricted their development. Both were written in an older version of FORTRAN and use features that will eventually become obsolete in new compilers. They include a significant amount of “spaghetti code” and outdated structures that make it difficult to maintain, support and enhance them. Moreover, neither BLAST nor DOE-2 is able to correctly handle feedback from the HVAC system to the zone conditions.

5.2.3 EnergyPlus

EnergyPlus (Crawley et al. 2001) is a new Department of Energy-supported project that merges the two major building energy simulation programs, BLAST and DOE-2. The goal of EnergyPlus is to take the best features of BLAST and DOE-2 and unite them in a single program. EnergyPlus also includes many additional innovative simulation capabilities including time steps of less than an hour, modular systems and plants integrated with heat balance-based zone simulation, multi-zone air flow, thermal comfort, and photovoltaic systems.

EnergyPlus allows users to calculate the impact of different heating, cooling and ventilating equipment and various types of lighting installations and windows to maximize building energy use efficiency and occupant comfort. Users can simulate the effect of window blinds, electrochromic window glazings, and complex daylighting systems, which are features not seen in earlier DOE software. The

current version of EnergyPlus (Version 1.2.2) provides an integrated, simultaneous solution where building responses and the primary and secondary systems are tightly coupled (iteration performed when necessary). It employs the heat balance based solution technique for determining building thermal loads, allowing simultaneous calculations of radiant and convective effects on interior and exterior surfaces during each time step of a simulation. It combines heat and mass transfer models that account for moisture adsorption/desorption either as a layer-by-layer integration into the conduction transfer functions or as an effective moisture penetration depth model. Furthermore, it links to other simulation environments such as COMIS (Ren and Stewart 2003), TRANSYS (Wolf 1994) and allows more detailed analysis of other components in building environmental systems.

EnergyPlus has an improved structure to define a well organized modular concept that facilitates the addition of features and links to other programs. The key benefit of modularity is that new modules can be concurrently developed without interfering with other modules under development and with only a limited knowledge of the entire program structure. FORTRAN 90, which is a modern, modular language with good compilers on many platforms and allows C-like data structure and mixed language modules, was used for the initial release of EnergyPlus.

Another advantage of EnergyPlus that it shares with both BLAST and DOE-2 is that the source code of the program is currently available in the public domain and is open for public inspection, revision, etc. It is not intended to be a black box that is unintelligible to users and developers around the world. The hope is that this access to source code will improve the accuracy and usability of the program over the long term and allow many developers to work simultaneously on the program.

5.3 Main Limitation of Energy Simulation Programs

To date, most available programs or procedures have used the assumption of the mixing system for energy analysis (Hittle 1977; Chen and Kooi 1988; Crawley et al. 2001; Winkelmann et al. 2003). However, for UFAD and DV systems, these models may be inappropriate due to the existence of indoor air temperature stratification. It is believed that the energy saving potential of UFAD systems results from the existence of air temperature stratification in the conditioned space. Bauman and Webster (2001) has pointed out that an understanding of the controlled/optimized thermal stratification was critical to provide designers with a reliable energy-estimation tool. At present the quantification of the energy saving potential remains a barrier to the fundamental understanding of the UFAD system.

With the program EnergyPlus (Winkelmann et al. 2003), the UCSD (University of California, San Diego) displacement ventilation model was developed to consider room air temperature stratification. With this model, users can control how much of the internal gains, which are empirical estimations, to add to the occupied zone. Loudermilk (1999) described a space heat gain analysis for the UFAD system. This approach is also based on empirical estimates of heat gain factors below different space heights. Unfortunately, no research-based guidance exists to guide the assignment of loads to the occupied and unoccupied zones. Bauman (2003) presented a simplified two-zone UFAD load calculation model. It is relatively easy to employ due to its ignoring the complicated flow patterns in the space. However, he does not provide any numerical results or experimental data for further

demonstration. In fact, the stratification height can be located below or above the occupied zone.

In the following sections, the author will present a numerical model that takes into account the indoor air temperature stratification for system energy estimation. The idea of Bauman's (2003) simplified two-zone calculation model is revised. With this method, the energy consumption and thermal environment at head level (1.1m) for the UFAD and mixing systems are compared.

5.4 Modeling of Indoor Air Temperature Stratification

5.4.1 Indoor Air Dimensionless Temperature Coefficient

The simulation is based on the same office room presented in Chapter 4 (Figure 4.9). The same system operation time and human occupancy schedules were employed. The elevation of the electronic office equipment is believed to affect the cooling load in the occupied zone $Q_{occupied}$ and was varied to investigate this effect. Figure 5.2 shows the simplified two-zone model of the UFAD system.

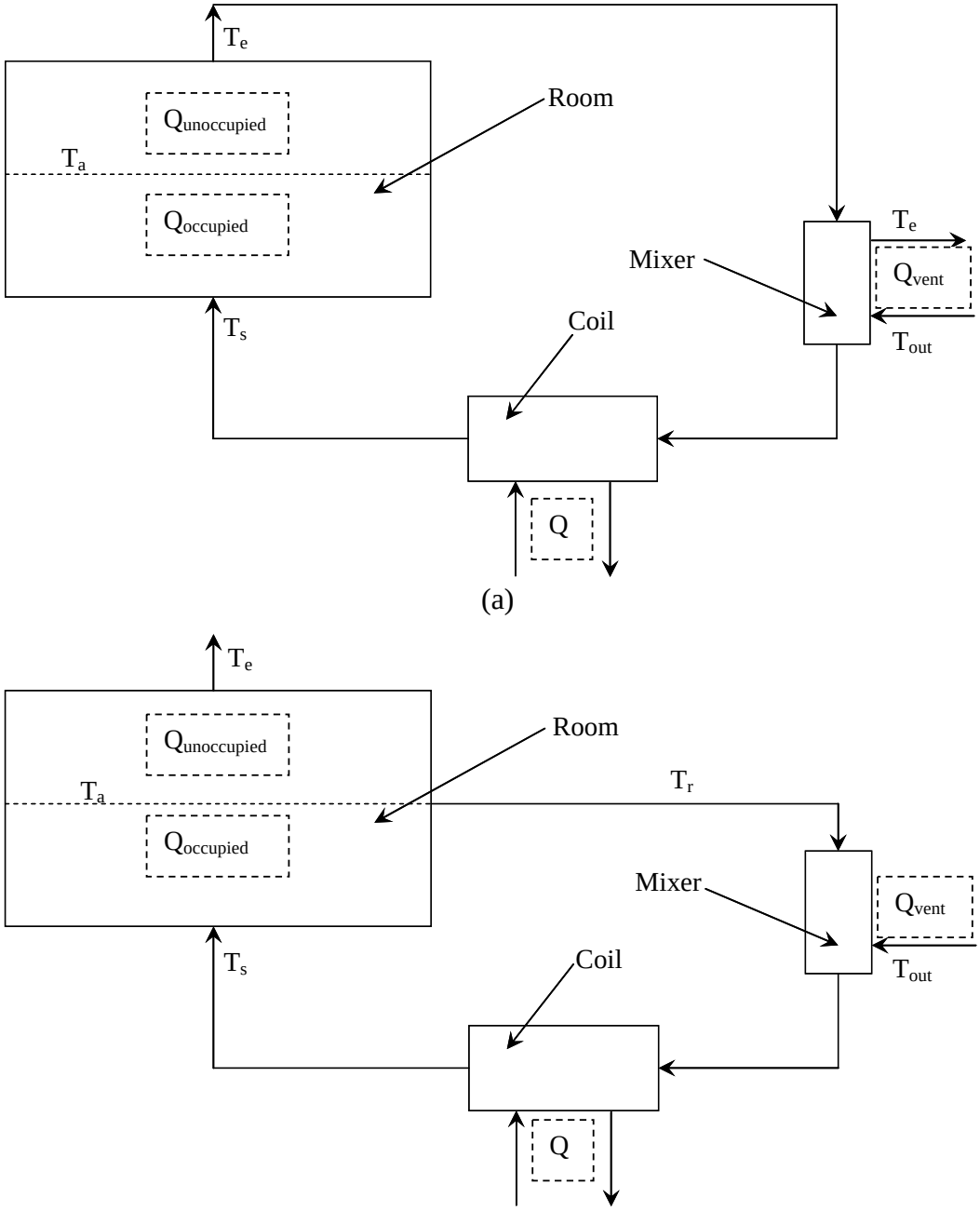

Figure 5.2 Simplified two-zone model of the UFAD system
(a) Ceiling exhaust & return, and (b) Ceiling exhaust & mid-level return

As can be seen from Figure 5.2, two alternative return air positions are possible. The following study focuses on the ceiling return and exhaust system, as in the case of the office room in Figure 5.2(a). For large spaces, a ceiling exhaust with mid-level return outlets in Figure 5.2(b) may offer further cooling load reduction, and deserves

a separate study in future. In small spaces, Yuan et al. (1999) developed a regression model to calculate the load reduction factors and estimated the cooling load in the occupied zone of DV systems. This model was developed from a database of 56 displacement ventilation conditions by using a validated CFD program (Yuan et al. 1999). Lau and Niu (2003) investigated this method in an atrium and found that different heat source grouping with heat released from the floor resulted in dramatically different reduction factors. This model still needs validation for large spaces such as theaters and atria.

The model in this section employs the assumption of two zones, divided at head level (1.1m). Based on the conservation law, the cooling load in the occupied zone $Q_{occupied}$ and unoccupied zone $Q_{unoccupied}$ can be defined as:

$$Q_{occupied} = mc_p(t_a - t_s) \tag{5.1}$$

$$Q_{unoccupied} = mc_p(t_e - t_a) \tag{5.2}$$

$$Q_{space} = Q_{occupied} + Q_{unoccupied} \tag{5.3}$$

where m is the supply air mass flow rate and c_p is air specific heat, t_s is the UFAD inlet air temperature; t_e is the exhaust air temperature, and t_a is the average air temperature at head level (1.1m). For the mixing system, t_a should be equal to t_e. The dimensionless temperature coefficient ε_t is defined as

$$\varepsilon_t = \frac{t_e - t_s}{t_a - t_s} \tag{5.4}$$

Employing Equations (5.1), (5.2), (5.3) and rearranging Equation (5.4), we get:

$$\varepsilon_t = \frac{Q_{occupied} + Q_{unoccupied}}{Q_{occupied}} = \frac{Q_{space}}{Q_{occupied}} \tag{5.5}$$

For system operation, the total coil load $Q_{chiller}$, removed by the chiller system when no heat recovery is used, can be defined as

$$Q_{chiller} = Q_{space} + Q_{vent} = Q_{space} + m_f \left(h_o - h_e\right) \tag{5.6}$$

where Q_{vent} is the cooling load due to the fresh air treatment. m_f is the fresh air mass flow rate. h_o and h_e are enthalpies of the outdoor and exhaust air, which can be defined as

$$h = 1.01t + 0.001d\left(2500 + 1.84t\right) \tag{5.7}$$

where d is air humidity in *kg/kg* dry air.

Then we get

$$Q_{vent} = m_f \left(1.01t_o + 0.001d_o\left(2500 + 1.84t_o\right) - 1.01t_e - 0.001d_e\left(2500 + 1.84t_e\right)\right) \tag{5.8}$$

From UFAD experience, in order to avoid uncomfortably cold conditions for nearby occupants due to draft, the supply air temperature should be maintained at or above 17°C -18°C (Shute 1992, 1995; Matsunawa et al. 1995), which is higher than that of the mixing system. Due to indoor air temperature stratification, a higher supply air temperature results in a higher exhaust air temperature when compared with the mixing system. From Equation (5.8), we can see that the ventilation energy saving potential is mainly due to the higher exhaust air temperature of the UFAD system. The following section will present the procedures for obtaining the exhaust air temperature. For the mixing system, it is believed that the indoor air thermal environment is very uniform, except the location of the supply diffuser, which we didn't need to consider. Therefore, in the mixing system simulation, the inlet and outlet locations of diffusers are assumed to be on a side wall, as presented in Figure 5.3.

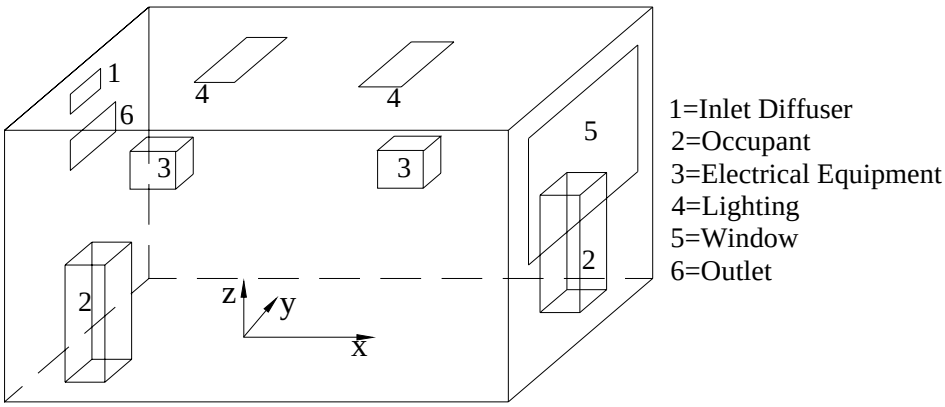

Figure 5.3 Configuration of the hypothetical office room for the mixing system

5.4.2 Equipment Models

Fan energy is an important factor in the annual energy consumption of a HVAC system. Fan performance can be characterized by its efficiency, which itself is

dependent on operational air flow rate. In general, rated volumetric flow rate, pressure rise and efficiency are available from the manufacturer. Then rated power can then be calculated as

$$\text{Fan power}=\frac{V_a \Delta p}{3600\eta_f} \tag{5.9}$$

where V_a is the air volumetric flow rate (m^3/h), and Δp is fan total pressure rise (Pa), and η_f is fan efficiency.

Chillers are used to remove the heat load from supplied air during the operation of HVAC systems. The energy performance of a water chiller is quantified by its COP (Coefficients of performance), defined as the ratio of the cooling energy to the electricity input power. For a specific system, the COP is the function of the required chilled water temperature t_{ch}, the ambient air temperature t_o, and humidity x_o, as well as the operating capacity Q, i.e.,

$$COP = f\left(t_o, x_o, Q, t_{ch}\right) \tag{5.10}$$

In this way, the performance of the cooling tower is already empirically taken into account. Subsequently, the required electric power input can be calculated according to

$$\text{Chiller power}=Q_{chiller}/COP \tag{5.11}$$

5.4.3 CAV Supply

In this investigation, the same air change rate (ACH=10) for CAV supply was used for the UFAD and mixing systems. The inlet temperature was changed to accord with the cooling load requirement. The minimum fresh air flow rate was 10 l/s·person and was about 15.1% of the total supply air.

5.4.3.1 Numerical Simulation Procedures

The supply and exhaust temperatures are the concerns for energy consumption in the UFAD system with CAV supply. Based on Equations (5.4) and (5.5), the CFD simulation is coupled with the room cooling load calculation by the dimensionless coefficient of indoor air temperature.

ACCURACY (Chen and Kooi 1988) is a FORTRAN language program, in which the source code is free and open. You can easily add yourself model in it. However, in EnergyPlus, you can only select the models in this software and you have to buy the source code if you want to define yourself numerical model in it. Take into consideration of the indoor air temperature stratification in the UFAD system, the previously validated program ACCURACY was used for cooling load simulation in following simulation work.

Based on the simulation results of the space cooling load Q_{space} from ACCURACY, the cooling load in the occupied zone can be obtained from Equation (5.5) if the dimensionless temperature coefficient ε_t is known. Again, the CFD technique is employed to calculate ε_t, using the boundary conditions obtained from ACCURACY

with the application of the hour-by-hour meteorological weather data of Hong Kong for the year 1989.

Firstly, the internal room surface temperatures of the mixing system calculated by ACCURACY were used for CFD simulation in the UFAD system and the electronic office equipment was fixed at an elevation of 0.7m. With the simulated temperature distribution and Equation (5.4), the initial value of the dimensionless temperature coefficient $\varepsilon_t^{'}$ was obtained. Secondly, using the initial $\varepsilon_t^{'}$, the indoor air vertical temperature difference was taken into account for ACCURACY revision to re-calculate the supply air temperature, wall surface temperatures at four different heat source groupings and the weather conditions in the Hong Kong climate. The updated surface temperatures from ACCURACY were used again as the input boundary conditions for indoor CFD simulations. At the end of this calculation, four dimensionless temperature coefficients were obtained, and the average value was then used for the last revision of ACCURACY to obtain the updated supply air temperature t_s. Based on Equation (5.4), the exhaust temperature t_e was obtained. At the last step, the annual year energy consumption could be predicted for the UFAD system. The detailed simulation flow chart is presented in Figure 5.4.

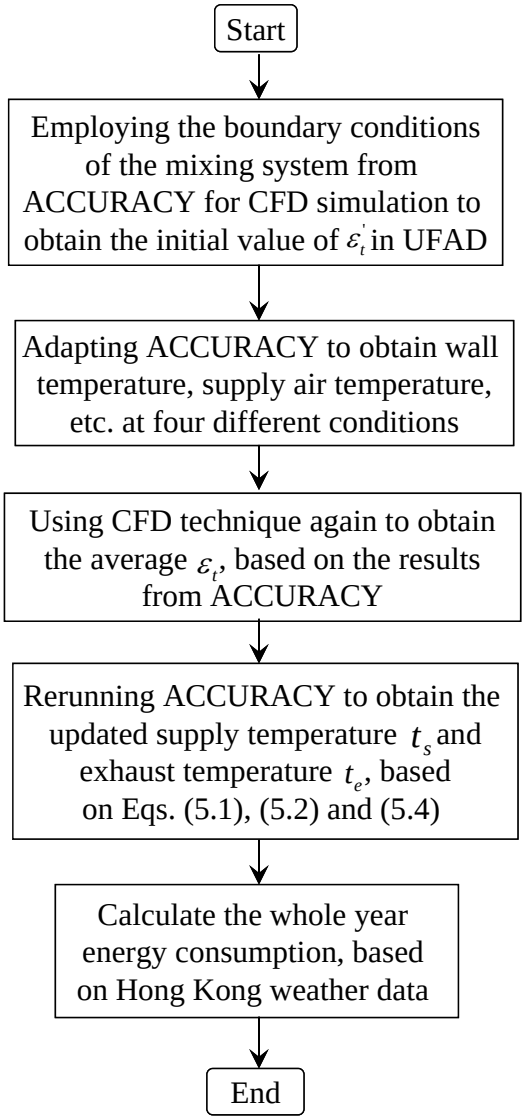

Figure 5.4 Simulation flow chart of the UFAD system (CAV)

This simulation strategy is easy for the mixing system due to its ignoring indoor air temperature stratification. Table 5.1 shows four different heat gain groupings in four cases for annual energy simulations. It can be seen that the indoor heat sources dominate the whole cooling load in the conditioned room space.

Table 5.1 Different heat gain groupings in four cases (1989)

Heat Sources (W)	Case-1	Case-2	Case-3	Case-4
$Q_{occupant}$	105	160	150	70
$Q_{equipment}$	300	250	350	250
$Q_{lighting}$	136	170	102	204
Q_{space}	837.9	1179.45	1035.8	858.1
At selected time	6 Jun. 11:00am	15 Jul. 12:00am	20 Aug. 1:00pm	25 Sep. 3:00pm

5.4.3.2 Influence of Electronic Equipment Elevation on ε_t

Three different elevations of the electronic equipment were investigated. Selected values of $\varepsilon_t^{'}$ at four times of the year 1989 are shown in Table 5.2. It is obvious that the higher the location of the electronic equipment, the larger the dimensionless temperature coefficient. At one fixed elevation of the electronic equipment, the dimensionless temperature coefficient is almost a constant under different weather conditions for CAV supply strategy, regardless of the different indoor heat source magnitudes. Thus, the average value of ε_t is assumed constant for CAV annual energy simulations conducted with the revised ACCURACY, when the arrangements of heat sources are specified.

Table 5.2 Simulated dimensionless coefficient ε_t at selected load conditions

Elevation of Electronic Equipment (mm)	Case-1	Case-2	Case-3	Case-4	Avg.
300	1.3	1.32	1.29	1.33	1.31
700	1.39	1.36	1.38	1.4	1.38
1300	1.48	1.46	1.49	1.5	1.48
Q_{space} (W)	837.9	1179.45	1035.8	858.1	
$Q_{equipment}$ (W)	300	250	350	250	

5.4.3.3 Free Cooling Hour Comparison

The economizer operation can be employed in HVAC systems when outdoor air can directly be supplied into the occupied space without treatment by the cooling coil. Because the inherent operation conditions in the UFAD system are different from the mixing system, when and how air-side economizers can be used differs from one system to the other. Two main factors that affect the use of economizers are the supply air temperature (SAT) and the return air temperature (RAT). In general, both the SAT and RAT are higher in the UFAD system than in the mixing system (Bauman 2003). Figure 5.5 presents the calculated monthly average exhaust air temperatures of the UFAD and mixing systems. It shows that the exhaust temperature in the UFAD system is higher than that in the mixing system. Figure 5.6 shows the free cooling hour comparisons between the UFAD and mixing systems. In this situation, there are six months (from November to April) with the economizer operation. In the six months, the UFAD system has more free cooling hours than the mixing system due to the higher exhaust air temperature. For annual operation, the

total percentages of free cooling hours are 29.9% for the UFAD system and 23.2% for the mixing system.

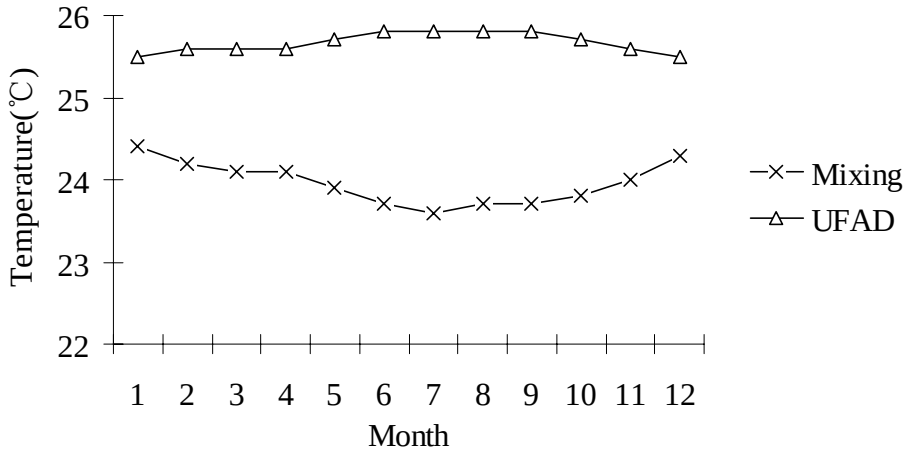

Figure 5.5 Average exhaust air temperatures

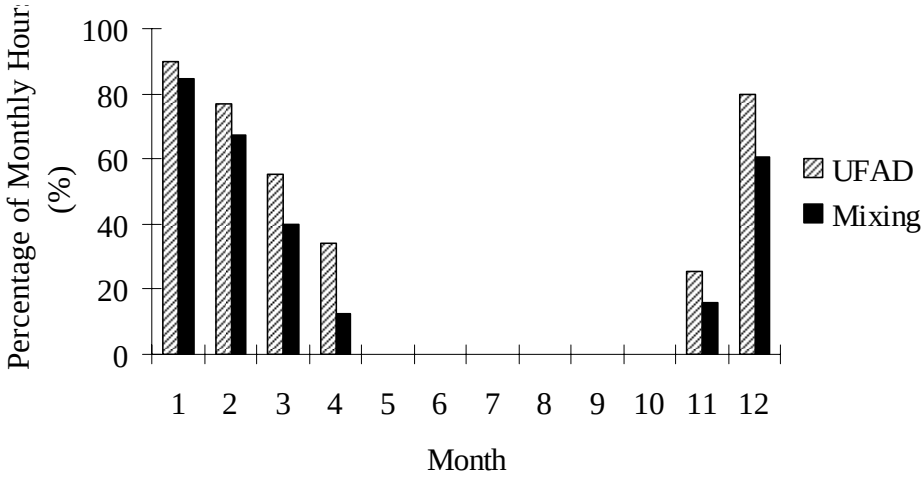

Figure 5.6 Free cooling hour comparisons

5.4.3.4 Energy Consumption Comparison

In order to put the research emphasis onto indoor air conditions for system energy consumption, some indices are simplified constantly for the two systems: fan efficiency is 60%, fan pressure rise is 1400Pa and the coefficient of performance

(COP) of the chiller system is 3.5. The energy consumption comparisons are presented in Figure 5.7.

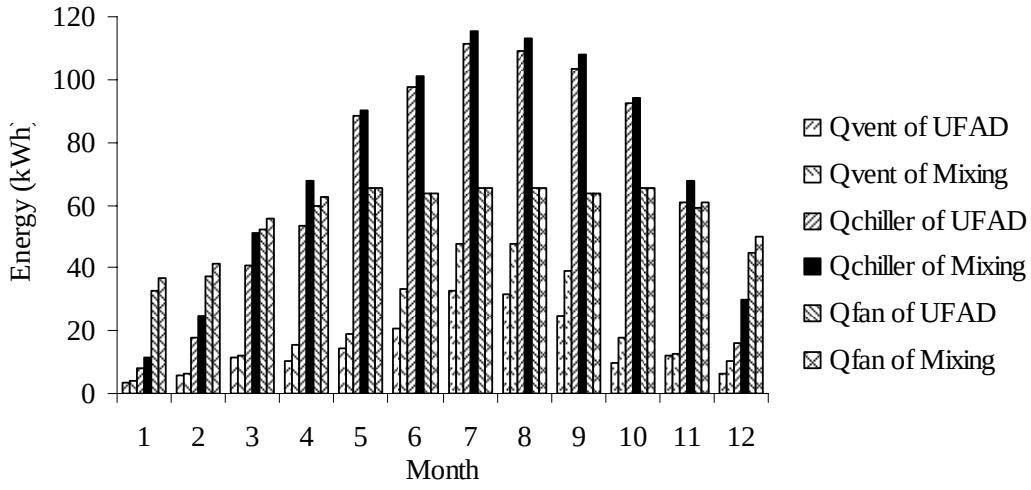

Figure 5.7 Energy consumption comparisons

Due to the higher exhaust temperature, less energy for fresh air treatment is consumed by the UFAD system than the mixing system over a year. Table 5.3 shows the detailed fresh air treatment energy comparisons between the UFAD and mixing systems. It shows that the energy saving of the fresh air treatment in the UFAD system is evident, as compared with the mixing system. The chiller energy consumption of the UFAD system is smaller than that of the mixing system due to the decreased energy consumption for fresh air treatment (Equation (5.6). Based on the assumption of CAV and the above constant fan indices, fan energy consumption is the same in the months from May to October. During the other months, the fan operates in the free cooling season. In the energy simulation program written by the author, the air flow rate is determined by the space cooling load and the air temperature difference for indoor and outdoor environment. In principle, the air flow rate vary with different weather data, so the fan energy is variable during the free cooling season, which can be seen from the above figure.

Table 5.3 Energy consumption comparisons due to the fresh air treatment (kWh)

	Jan.	Feb.	Mar.	Apr.	May	Jun.	Jul.	Aug.	Sep.	Oct.	Nov.	Dec.
Mixing	3.84	6.31	11.9	15.69	18.83	33.38	47.54	47.52	39.11	17.57	12.84	10.24
UFAD	3.17	5.63	11.75	10.44	14.26	20.53	32.7	31.6	24.42	9.76	12.22	6.38
Saving	17.4%	10.8%	1.3%	33.5%	24.3%	38.5%	31.2%	33.5%	37.6%	44.5%	4.8%	37.7%

5.4.3.5 Indoor Air Humidity Comparison

For the system operation shown in Figure 5.2, fresh air first mixes with some returned air and then passes through a cooling coil before entering the conditioned space. With the employment of the Hong Kong 1989 weather data, the simulated changes of indoor air relative humidity (RH) over two days are selected and presented in Figure 5.8.

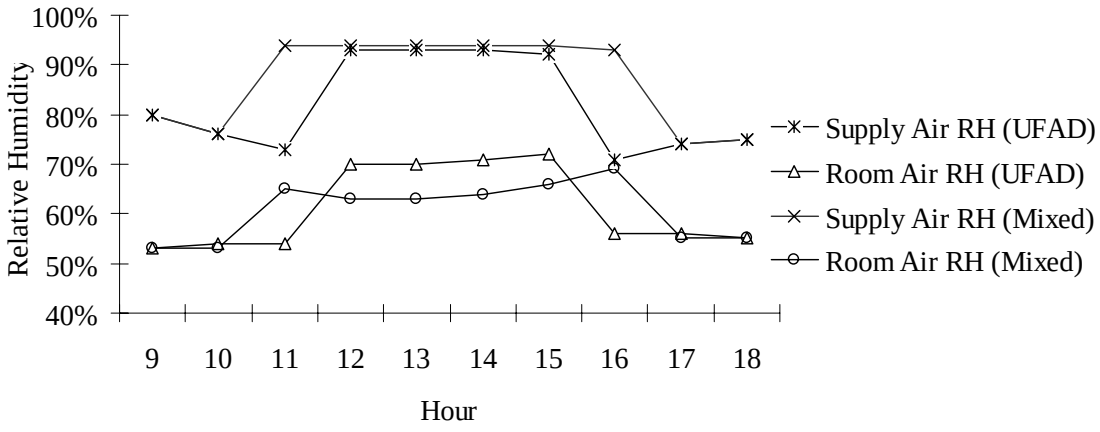

(a)

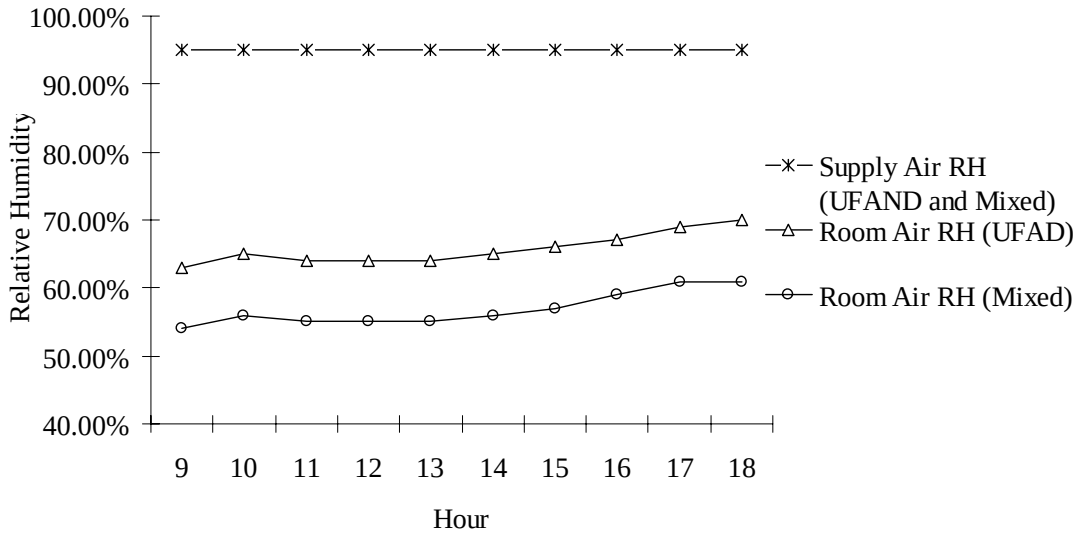

(b)

Figure 5.8 Relative humidity comparisons
(a) 20 February 1989, and (b) 15 July 1989

On the first day (20 February 1989), the economizer (free cooling) operated two hours more for the UFAD system than for the mixing system because of the higher exhaust air temperature. From 12:00am to 3:00pm, the relative humidity (RH) of the conditioned room employing the UFAD system was higher than that employing the mixing system. On the other day (15 July 1989), relative humidity 95% was assumed to represent the saturation of the supply air. From the simulation results, it can also be seen that the indoor RH with the UFAD system was higher than that with the mixing system.

5.4.3.6 PMV Comparison

In addition to the system energy consumption, indoor thermal comfort is another concern. Occupant surveys have found that a thermal comfort environment is among the most important attributes of an office, and that this comfort has not been well provided (Schiller et al. 1988). The underfloor air distribution strategy is believed to be an innovation in this regard. The thermal environments produced by the UFAD and mixing systems were compared using the mean Predicted Mean Vote (PMV) at head level (1.1m). The same heat source arrangements and air change (ACH) rates (10 times per hour) were employed in the ACCURACY program (Table 5.4).

Table 5.4 Heat sources and inlet conditions of the two systems (ACH=10)

HVAC	$Q_{occupant}$ (W)	$Q_{equipment}$ (W)	$Q_{lighting}$ (W)	V_{inlet} (m/s)	T_{inlet} (ºC)
Mixing	160	250	170	2.21	14.2
UFAD	160	250	170	0.48	17.0

Table 5.5 presents the comparisons of the PMV index from the CFD simulations. It shows that the UFAD system provides a cooler environment (PMV=-0.07) than the mixing system (PMV=0.17), at the same elevation of the electronic equipment (0.7m). Compared with the mixing system, the average temperature (21.6℃) of the UFAD system is lower and the average velocity (0.0473m/s) of the UFAD system is much smaller. As the electronic equipment was lowered, the PMV index at head level gradually increased for the UFAD system. For the mixing system, due to the employment of uniform indoor air temperature for numerical simulation, PMV did not change with the displacement of the electronic equipment. Kosonen and Tan (2004) investigated the influence of the PMV index on occupant productivity and found that an increase in PMV results in larger productivity loss. It is concluded that the UFAD system can provide a more comfortable environment than the mixing system.

Table 5.5 PMV comparisons between the two systems

HVAC	Equipment Height (m)	Temperature (ºC)	Velocity (m/s)	Vapor Pressure (Pa)	Average PMV
Mixing	0.7	23.5	0.115	1588.7	0.17
UFAD	0.3	21.8	0.0525	1667.2	-0.04
UFAD	0.7	21.6	0.0473	1646.9	-0.07
UFAD	1.3	21.2	0.0519	1606.7	-0.12

5.4.3.7 Discussion

In the above study, the initial value $\varepsilon_t^{'}$ was employed for the revision of ACCURACY. Then the simulated wall temperatures from ACCURACY were used as boundary conditions for the CFD simulation to get the average ε_t, which was used in the last step of the annual energy investigations. Table 5.6 shows that the discrepancy in the space cooling load between ACCURACY estimation and CFD simulation varies from 8.6% to 12.3%. In fact, in order to obtain more accurate results, the average ε_t should be employed again to get the updated boundary conditions through the revision of ACCURACY for CFD re-simulation. Due to the computing time limitation, only the first average dimensionless temperature coefficient was used for system energy estimation, which is one of the reasons for this discrepancy. The other reason is that during the CFD investigation the wall temperatures, not the heat fluxes, from ACCURACY were used as the wall boundary conditions.

Table 5.6 Space cooling load comparisons

	6 Jun. 11:00am	15 Jul. 12:00am	20 Aug. 1:00pm	25 Sep. 3:00pm
ACCURACY (W)	837.9	1179.5	1035.8	858.1
CFD (W)	765.8	1048.1	908.2	754.4
Discrepancy	8.6%	11.1%	12.3%	12%

In the above simulation work, the same COP (3.5) for the UFAD and mixing systems was used. Actually, in the UFAD system, the COP of the chiller increased due to the higher chilled water temperature required with the higher supply air temperature. It is believed that the higher COP results in a greater energy saving

potential. Detailed comparisons of chiller energy consumption with different COPs are presented in Table 5.7. When COP is assumed to be 3.5 for both systems, the chiller energy saving with the UFAD system is somewhat smaller from May to October due to the reduced ventilation load without economizer operation. More free cooling hours with the UFAD system mean more energy saving in the operation of the chiller. It can be concluded that when COP in the UFAD system is increased to 3.8, the energy saving potential of the UFAD system will be much larger.

Table 5.7 Chiller energy consumption comparisons with different COPs

Month	UFAD (kWh) COP=3.5	Mixing (kWh) COP=3.5	Saving	UFAD (kWh) COP=3.8	Saving
Jan.	8.536	12.565	32%	7.862	37.4%
Feb.	19.441	26.921	27.8%	17.906	33.5%
Mar.	43.949	55.746	21.2%	40.479	27.4%
Apr.	57.748	73.249	21.2%	53.189	27.4%
May	96.301	97.601	1.3%	88.698	9.1%
Jun.	106.248	109.899	3.3%	97.86	11%
Jul.	120.842	125.355	3.6%	111.302	11.2%
Aug.	118.412	122.946	3.7%	109.064	11.3%
Sep.	111.930	117.032	4.4%	103.093	11.9%
Oct.	100.099	102.339	2.2%	92.196	9.9%
Nov.	66.379	73.573	9.8%	61.139	16.9%
Dec.	17.634	32.453	45.7%	16.242	50%

5.4.4 VAV supply

This section presents the energy simulation results for the UFAD and mixing systems with the VAV supply. The supply air temperature for the mixing system was set at 14℃ and 18℃ for the UFAD system. The arrangements of the heat sources were the same as in the above CAV cases.

Table 5.8 presents the CFD calculated dimensionless temperature coefficient on the day of 15 July 1989. It shows that the variable air flow rate dominates the changes of ε_t after the HVAC system is turned on. During the energy simulation in ACCURACY, only the day setting was assumed for the indoor thermostat. As a result, excessive cooling would be encountered in the morning, resulting in a large air flow rate. At the first time, 9:00, the dimensionless temperature coefficient ε_t was larger than for the following hour values. At noon time, the largest air flow rate resulted in the smallest dimensionless.

Table 5.8 Simulated dimensionless temperature coefficient (15 July 1989)

Time	9:00	11:00	12:00	13:00	15:00	17:00
ε_t	1.41	1.38	1.35	1.34	1.4	1.44
Flow rate (kg/s)	0.171	0.163	0.166	0.168	0.151	0.13

Figure 5.9 shows the change of ε_t at six different time over a day. The ε_t values at the other hours of the day were obtained by interpolation from Figure 5.9 and are presented in Table 5.9, which was used in ACCURACY to calculate the updated air flow rates and the energy consumption investigations. It was found that a larger air

flow rate resulted in a smaller value of ε_t when indoor heat sources dominate the whole cooling load.

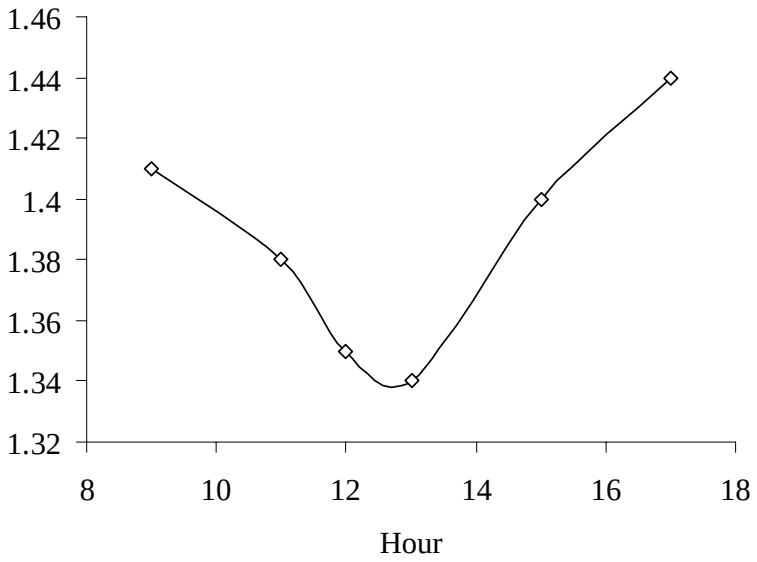

Figure 5.9 Dimensionless temperature coefficient changes in six hours

Table 5.9 ε_t used for ACCURACY revision to calculate the updated air flow rate

Time	9	10	11	12	13	14	15	16	17	18
ε_t	1.41	1.39	1.38	1.35	1.34	1.37	1.4	1.42	1.44	1.46

The flow chart for VAV simulation is shown in Figure 5.10. The major difference from CAV is that, for VAV supply, different values of ε_t were used for each hour.

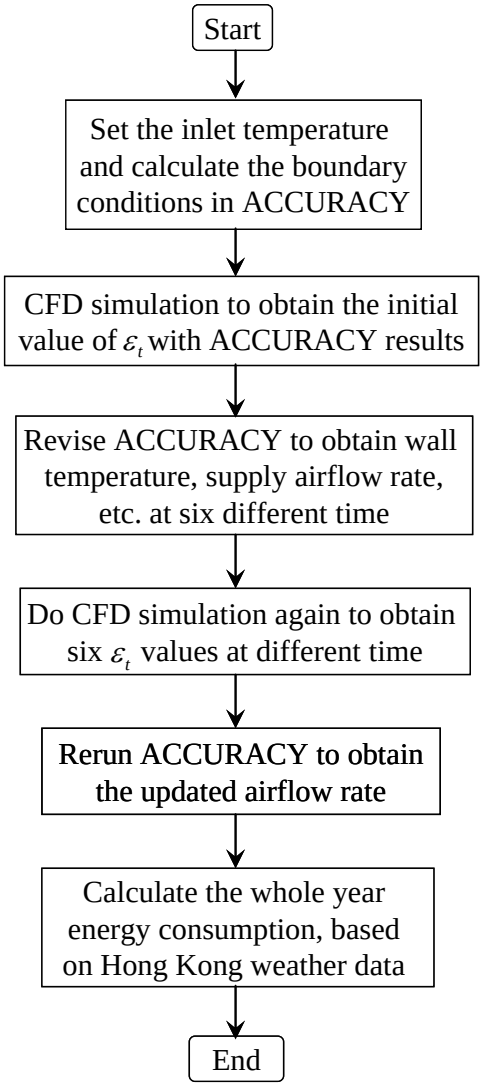

Figure 5.10 Simulation flow chart of the UFAD system (VAV)

Figure 5.11 presents the energy comparisons between the UFAD and mixing systems. On a monthly basis, the UFAD system consumes less ventilation energy than the mixing system due to the higher exhaust temperature. Based on Equation (5.6), chiller energy consumption is reduced with the UFAD system. For the UFAD system, Bauman and Webster (2001) pointed out that fan energy saving is associated with reduced static pressure requirements and the potential for reduced air volumes. Static pressures are reduced for most UFAD designs due to the elimination of most branch ductwork which allows the supply air to freely flow through the underfloor plenum at low plenum pressures. More significantly, the reduced air volume is due

to the fact that the cooling load outside the occupied zone is not included in the airside load, especially when the return air and exhaust air outlets are separately located at the mid-level and ceiling level (Figure 5.2(b)) . In the above analysis, the same static pressure was used for the UFAD and mixing system. With the assumptions of the same fan pressure rise and efficiency in the UFAD and mixing systems, larger air flow rate in the UFAD system results in larger fan energy consumption. In fact, to rigorously calculate the fan energy consumption in the UFAD system, the real pressure data for the supply fan from the manufacturer's catalogue had to be used.

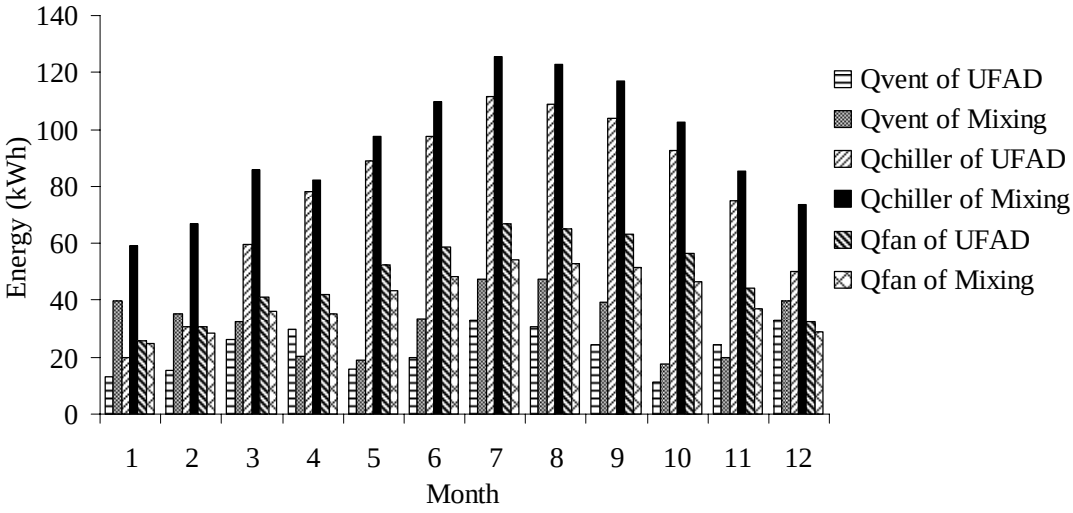

Figure 5.11 Energy comparisons between the UFAD and mixing systems

5.5 Summary

In this chapter, a numerical model was presented for energy consumption predictions, considering indoor air temperature stratification in the UFAD system. In this model, the energy simulation program ACCURACY was used for the space cooling load and boundary condition calculations and the CFD technique was employed to calculate the dimensionless air temperature coefficient. According to the

dimensionless coefficient, ACCURACY was revised to calculate the higher exhaust air temperature due to indoor air temperature stratification in the UFAD system. Using the Hong Kong weather data from 1989, annual energy consumptions of HVAC systems, i.e., a UFAD and a mixing system were compared.

With the CAV design, the indoor air dimensionless temperature coefficient was mainly affected by the elevation of the electronic office equipment, when the indoor heat sources dominated the whole indoor cooling load, and the locations of the occupants and lightings were fixed. The energy saving potential of UFAD systems with CAV is derived from three factors: the extended free cooling time, the reduced ventilation load, and increased COP of chillers. The exhaust air temperature determines the free cooling hours. With the higher exhaust temperature of the UFAD system, the energy consumed for the treatment of fresh air is much reduced. The increased COP reduces chiller energy consumption in the UFAD system. In contrast to CAV, the variable air flow rate dominates the dimensionless temperature coefficient when the locations of the heat sources are all fixed in VAV supply. A larger air flow rate results in a smaller dimensionless temperature coefficient. The variable ε_t for each hour is used for annual energy simulations. For VAV supply, fan energy saving potential comes from the decreased air flow rate.

The average thermal environments at the head level were also investigated. The relative humidity in the space conditioned by the UFAD system is slightly higher than that of the mixing system. It showed that the UFAD system can provide a somewhat cooler indoor environment than the mixing system based on the same indoor heat source arrangements and ACH. As the elevation of the office electronic

equipment increased, PMV decreased, however, in the mixing system, PMV remained the same.

During the simulation work, some simplified assumptions were employed, such as fan operation efficiency, pressure rise, etc. The predicted percentage of energy saving is subject to actual project variations, and on-site validations. The merit of this work is to be able to pinpoint three major factors and their contributing percentages to overall energy saving potential, so that design engineers can consciously take advantage of the three major factors to maximize energy saving in UFAD systems.

CHAPTER 6 THERMAL ENVIRONMENT & ENERGY CONSUMPTION COMPARISONS AMONG DIFFERENT SYSTEMS

6.1 Introduction

Most HVAC systems in operation to date have been all-air systems, which mean that air is not only employed for ventilation, but also as a heat transfer medium. Though these systems have been popular for the cooling or heating of rooms, some discomfort factors have been claimed. Besides wasting energy, these systems are likely to create uncomfortable environments due to cold drafts and large air temperature difference between head and foot levels of humans (Feustel and Stetiu 1995). The diffuser investigation in Chapter 4 was the work done to avoid these drawbacks in UFAD system designs.

Radiant cooling as an alternative air-conditioning system was first investigated in European countries in the early 1990's (Wilkins and Kosonen 1992; Krühne 1993). The radiant cooling system has three main advantages, including water pump energy saving, thermal comfort improvement and simple and effective zone control (Brunk 1993; Niu et al. 2002). This system is often combined with other HVAC systems to separate the cooling and ventilation tasks, by employing the cooled-ceiling (CC) to treat a sensible cooling load and setting up an independent HVAC system for ventilation and humidity control (Fitzner 1996). This chapter investigates different combined systems to inspect the different thermal environments and energy consumption.

6.2 Review of CC/DV System

The displacement ventilation (DV) strategy was first applied in the early 1970's as a means of improving general ventilation in industrial facilities with contamination problems (Svensson 1989). After that, this system became popular for ventilating spaces occupied by people with a low activity level (Sandberg and Sjoberg 1984). The main idea behind displacement ventilation is that the supplied fresh air displaces the polluted room air in the occupied zone without mixing thus improving the indoor air quality (IAQ). It is relatively easy to satisfy general thermal comfort requirements in the occupied zone.

Based on the definition from ISO Standard 7730 (ISO 1984) and the vertical air temperature gradient (less than 3℃), the DV system is limited to remove a convective load of up to 25W/m^2 (Sandberg and Blomqvist 1989). However, office cooling load frequently exceeds this figure, and it is necessary to specify additional cooling mechanisms and the cooled ceiling (CC) system is one of them (Mertz 1992; Wilkins and Kosonen 1992; Busweiler 1993; Laine 1993; Niu and Kooi 1993; Hodder et al. 1998; Loveday et al. 1998, 2002).

6.2.1 Energy Consumption

In comparison with the conventional all-air system, the water-panel type cooled ceiling employed with HVAC systems can be classified as an air-water system. Niu et al. (1995) investigated the annual energy consumption characteristics of the CC/DV system in the temperate Dutch climate and pointed out that the CC system

had an energy performance compatible to the all-air VAV system. In Novoselac and Srebric's (2002) review work on the CC/DV system, they found that energy consumption with the combined CC/DV system could be lower or higher than the energy consumption in an all-air VAV system, depending on cooling load, climate, room type, and system configuration in western European weather conditions.

In the combined system, the fan consumes less electrical energy due to the reduction of air flow rate. On the other hand, the electrical energy consumption increase for cooling tower and CC pump. The overall result is decrease of the total electrical energy consumption with the CC/DV system because of the high thermal capacity of water (Novoselac and Srebric 2002). Sodec (1999) compared the annual energy consumption of the CC/Mixing and CC/DV systems and found the CC/DV system has greater annual energy consumption. The reason is that to keep the air dew point temperature below CC temperature, the outdoor air is first cooled and dehumidified, and then heated to the supply temperature for DV. This process considerably increases the annual energy consumption for heating. Niu et al. (2002) employed the desiccant wheel to decouple the temperature and humidity controls and found that combining CC with desiccant cooling could save up to 44% of primary energy consumption, as compared with an all-air CAV system in Hong Kong weather conditions.

6.2.2 Thermal Environment

In a hot and humid climate like that in Hong Kong, dehumidification and ventilation are required prior to operating the cooling panels in order to reduce condensation risks (Zhang and Niu 2003). When CC is combined with DV (CC/DV), it is expected

to achieve both the advantageous features of the cooled ceiling with respect to thermal comfort and the favorable air quality characteristics of a displacement flow pattern (Külpmann 1993; Novoselac and Srebric 2002). The problem is that simply adding two such favorable characteristics does not necessarily result in a combination providing both advantages entirely. Alamdari and Eagles (1996) concluded that the combination of the CC with the DV system could destroy the displacement flow at low ceiling temperatures (14℃-16℃). At higher ceiling temperatures (18℃-21℃), the stratification boundary layer is strongly suppressed. Loveday et al. (1998) pointed out that as the ceiling temperature was reduced, the stratified boundary layer was suppressed and the displacement flow pattern was destroyed. The characteristics of the radiant cooled ceiling influence the displacement flow, so that the typical flow pattern of the displacement ventilation may vanish, becoming, instead, a near mixing flow pattern (Martin 1999).

Like the UFAD system, air temperature stratification exists in the space conditioned by a DV system. As stated above, if combined CC/DV is employed, the DV characteristic of air stratification is suppressed. It is well known that the air change rate of the DV system is very small since only fresh air is supplied. The UFAD system employs larger air flow volumes than the DV system. With the larger supply air flow rate in the UFAD system, the indoor temperature of the combined CC/UFAD system is more uniform. The numerical method of energy simulation in Chapter 5 for consideration of air temperature stratification is not necessary, which will result in different energy consumption conclusions. The following investigations were based on CAV supply. Three different systems, i.e., mixing, CC/DV, and CC/UFAD, were investigated to evaluate energy consumption among them,

considering the different thermal environments. The Hong Kong weather data for the year 1989 were used.

6.3 Mixing vs. CC/DV and CC/UFAD Systems

6.3.1 Description of the Simulated Office Room

To compare the energy consumption of the different systems, the same office room as that shown in Figure 4.9 was simulated. It was determined that about 70% of the ceiling would be covered by radial ceiling panels when the radiant ceiling panel system was employed. An occupancy pattern of two persons with a schedule from 9:00am to 6:00pm was simulated in the office. When present, each person generated 75W of sensible heat and 57.6g/h of moisture. Of the sensible heat generated, 50W was radiative and 25W was convective. The other indoor heat gains generated by the electronic equipment $Q_{equipment}$ (170W) and lighting $Q_{lighting}$ (250W) were assumed for different systems. Half of them were considered as radiative and half convective. The air-conditioning systems were also operated from 9:00am to 6:00pm. The supplied chilled water flow rate to the ceiling panels was 0.5t/h. The set point in the room was 50% RH, 24℃ of operative temperature in summer and 23℃ in winter.

6.3.2 Cooling Load Calculation in the Combined System

The simplified two-zone model for the UFAD system (Figure 5.2) in Chapter 5 was revised for the combined system. Figure 6.1 shows the simplified model for energy consumption analysis.

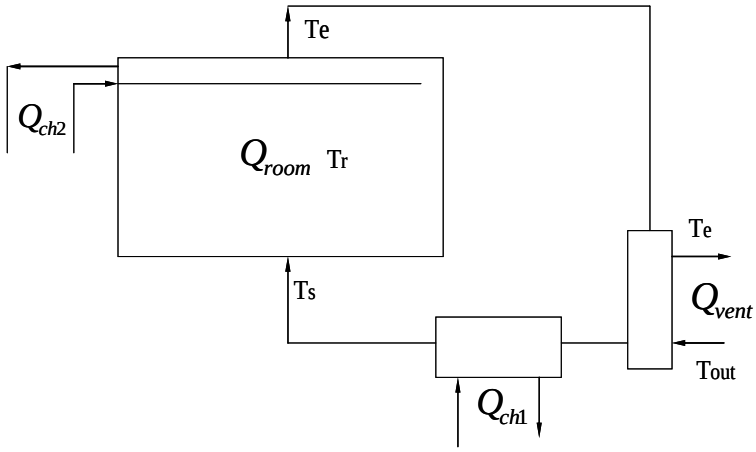

Figure 6.1 Simplified simulation model for the combined system

The space cooling load Q_{space} in the room can be defined as:

$$Q_{space} = Q_{room} = mc_p(t_e - t_s) = mc_p(t_r - t_s) \tag{6.1}$$

Due to the employment of a cooled ceiling in the DV and UFAD systems, the exhaust air temperature t_e was assumed to be equal to t_r, the average air temperature at head level (1.1m).

In the hybrid system, total coil load, removed by chiller systems, can be defined as

$$Q = Q_{ch1} + Q_{ch2} = Q_{space} + Q_{vent} = Q_{space} + m_f(h_o - h_r) \tag{6.2}$$

where Q_{ch1} and Q_{ch2} are the cooling load removed from the supply air by chillers and the chilled-ceiling. For the mixing system, Q_{ch2} is equal to zero. Q_{vent} can be calculated by Equation (5.8).

Two strategies for chiller operation were identified and investigated for the combined system, as shown in Figure 6.2. The first is the employment of a single chiller system, which means that the water used as the energy transfer medium for both the air-side and water-side was supplied by one chilled water pipe line. The other is the independent supply of chiller water to the ceiling panel and to an air handling unit (AHU), each operating at different evaporative temperatures. Since chilled-ceilings require relatively higher water-temperatures, the larger COP of the chiller can save much chiller energy (Zhang and Niu 2003).

In order to simplify the energy consumption simulation and put the emphasis on the different thermal environments among the different HVAC systems, COPs were assumed to be 3.5, 3.65 and 3.8, respectively, for the air-side chillers of the mixing, CC/DV and CC/UFAD systems due to different supply air temperatures. For water-side chiller operation, higher supply water temperatures resulted in a COP for the chiller and this COP was assumed to be 4.5. These should be based upon more detailed refrigeration cycle analysis for practical applications.

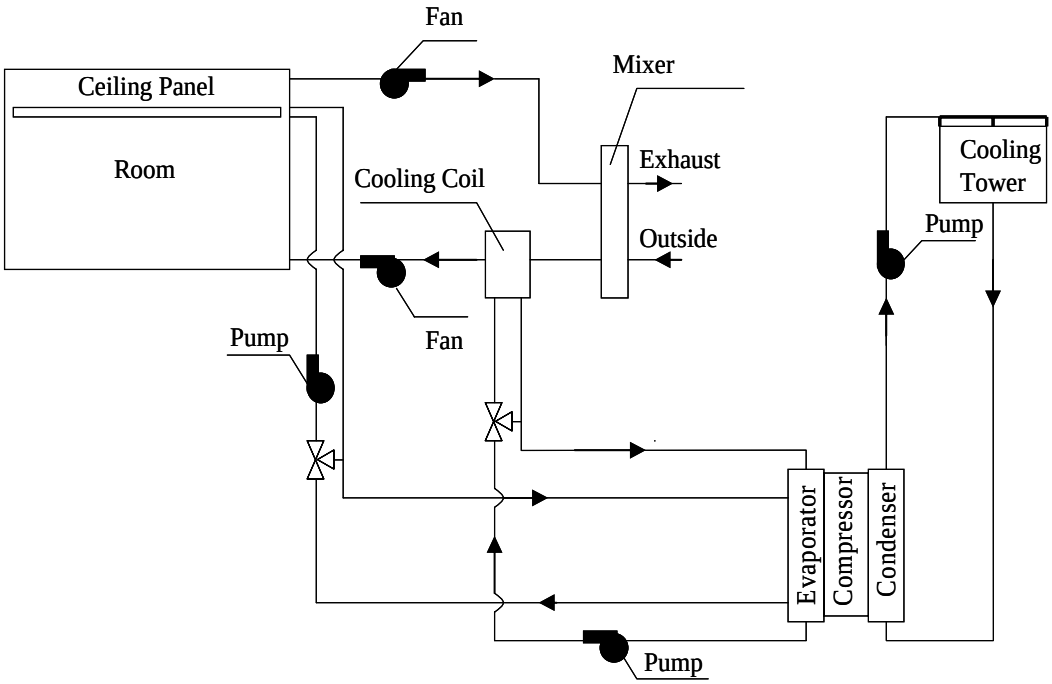

(a)

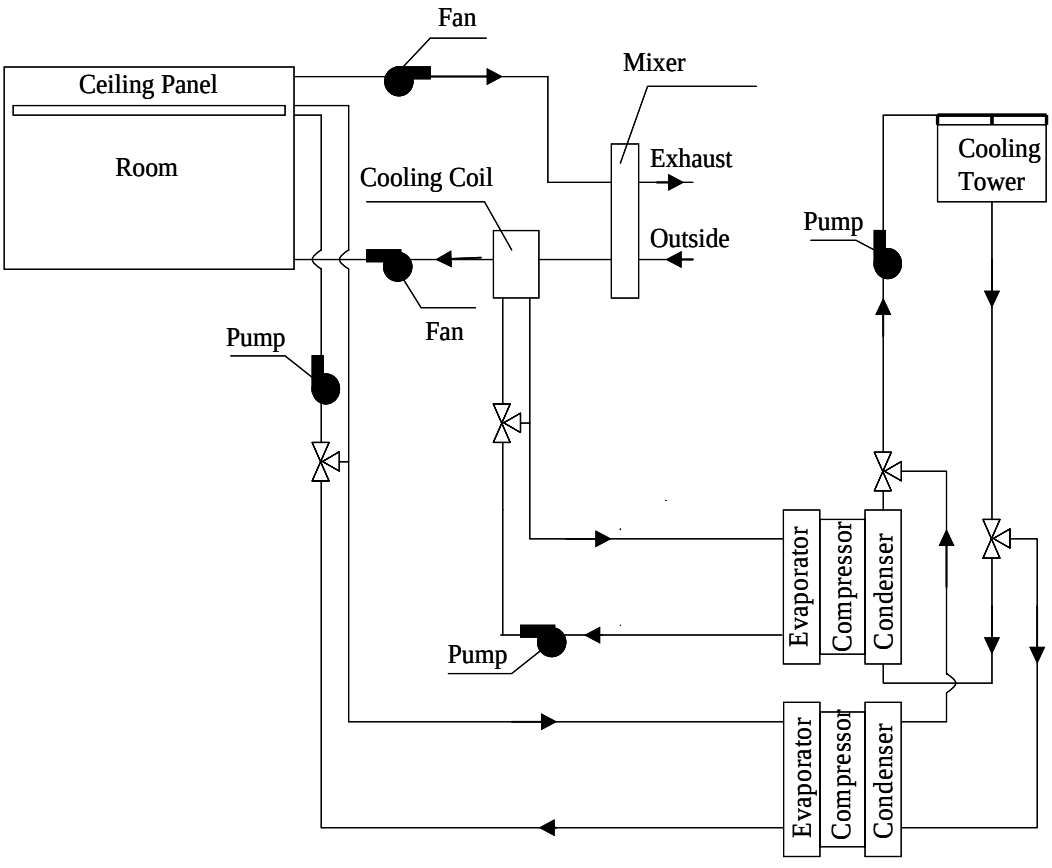

(b)

Figure 6.2 Schematic for the combined system

(a) Single chiller, and (b) Separate chiller

6.3.3 Numerical Simulation Procedures

In this section, the energy simulation program ACCURACY was first employed to calculate the necessary boundary and inlet conditions for subsequent CFD simulations of the thermal environments. The time of 12:00am, 15 July 1989 was selected for thermal environment comparisons. Occupants stood on the floor and lighting was installed in the ceiling. The elevation of the electronic equipment was 0.7m. During the CFD simulation, the basis of the mean PMV=0 at head level (1.1m) was used for the adjustment of the supply air temperature and flow rate of the mixing, CC/DV, and CC/UFAD systems. The detailed flow chart for the thermal environment investigations is shown in Figure 6.3.

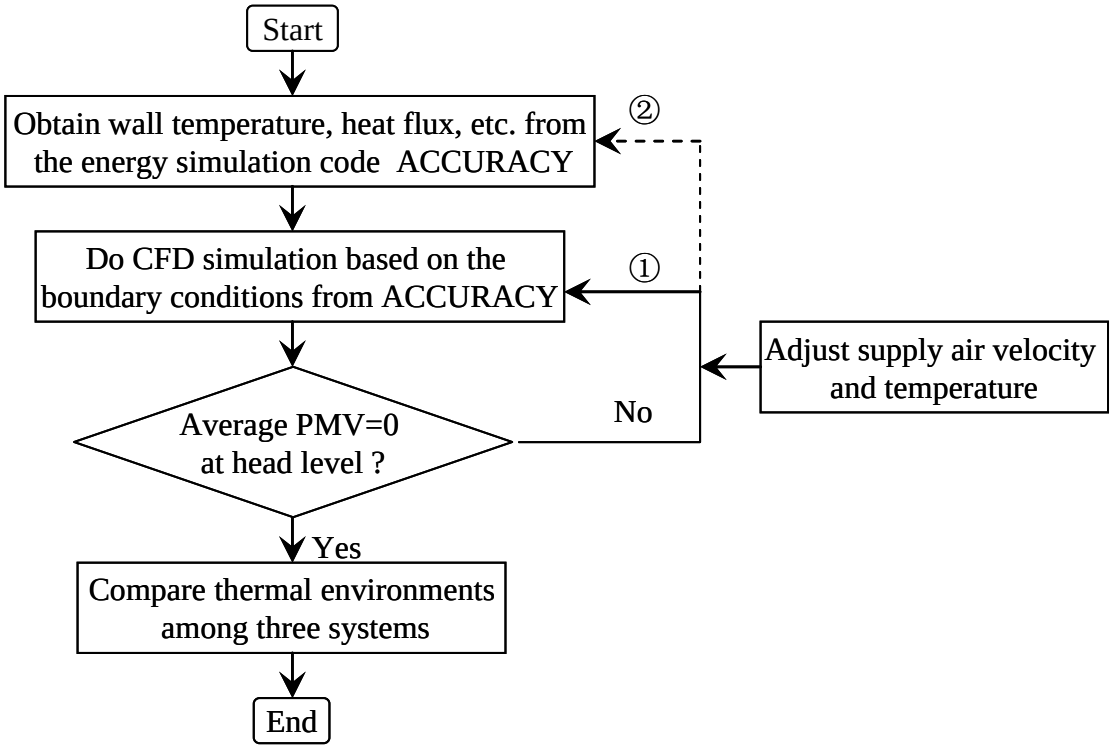

Figure 6.3 Flow chart of thermal environment comparisons

6.3.4 Thermal Environment Comparisons

The final CFD results for indoor thermal environments are presented in Table 6.1. Based on the same PMV at head level (1.1m), the mixing system showed a larger draft risk than the other systems. This was due to the lowest supply air temperature 14.5 (℃) and the largest air velocity (0.165m/s). There are no distinct differences in thermal environments between the CC/DV and the CC/UFAD systems.

Table 6.1 Supply conditions and mean indoor thermal environments at head level (12:00am, 15 July 1989)

	T_{supply}(℃)	ACH	T_{room}(℃)	Vel. (m/s)	PMV	PD (%)
Mixing	14.5	15	23.2	0.165	0.0	8.4
CC/DV	16	5	22.6	0.025	0.0	3.9
CC/UFAD	19	8.5	22.6	0.034	0.0	3.5

6.3.4.1 Velocity Distributions

The velocity vectors in the middle plane are shown in Figure 6.4. It was found that the larger velocities occurred near the surrounding walls in the mixing system and the buoyancy force could not be observed. For the CC/DV system, the supplied air underwent a free-fall causing it to accelerate before reaching the floor, just as in the DV system. The velocity near the floor level was dominated by the supply swirling diffuser in the CC/UFAD system. The “swirling” characteristic induced rapid mixing and the indoor velocity was very uniform.

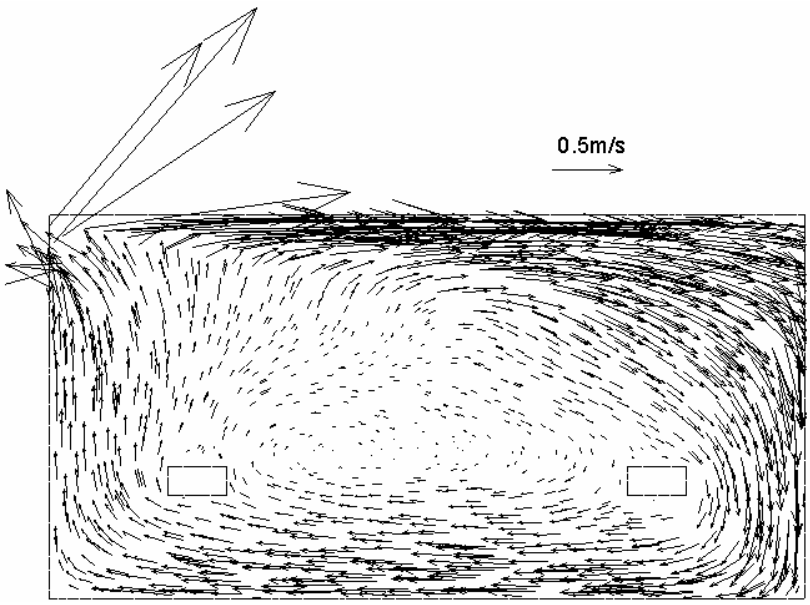

(a)

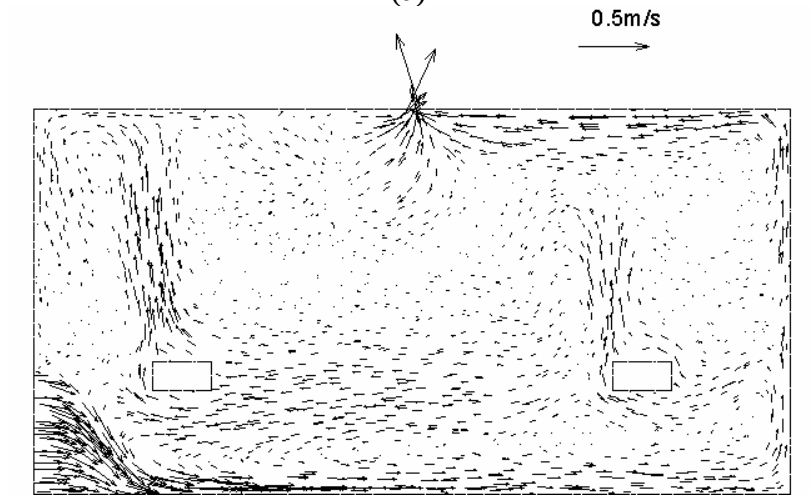

(b)

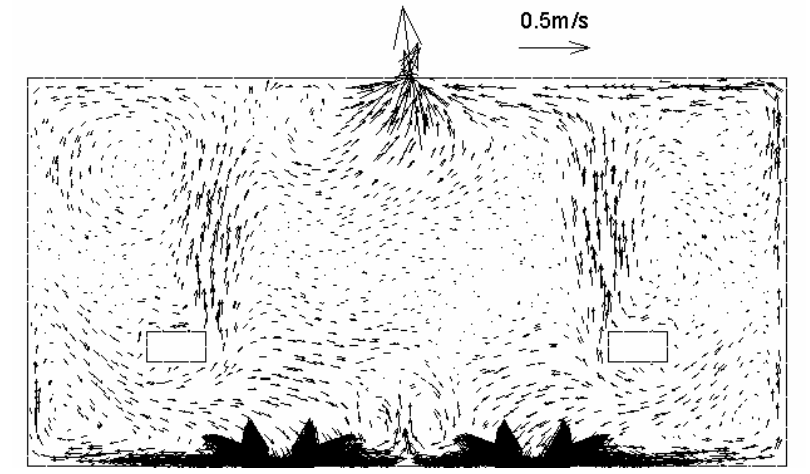

(c)

Figure 6.4 Velocity distributions in the middle plane
(a) Mixing, (b) CC/DV, and (c) CC/UFAD

6.3.4.2 Indoor Air Temperature Stratification Comparison

In Figure 6.5, it is obvious that temperature stratification did not exist in the indoor space of the mixing system. In the other two systems, CC/DV and CC/UFAD, air temperature stratification could be observed. With an increase in elevation, the indoor air temperature first increased and then decreased. It can be seen that indoor air temperature at head level was almost the same as that near ceiling level. This was due to the employment of CC, which resulted in a lower temperature near ceiling level. Based on this phenomenon, the dimensionless temperature coefficient defined in Chapter 5 was equal to 1.0 (Equation 5.4). So, the assumption of a uniform indoor air temperature model is reasonable for the energy estimation of the combined systems, CC/DV and CC/UFAD.

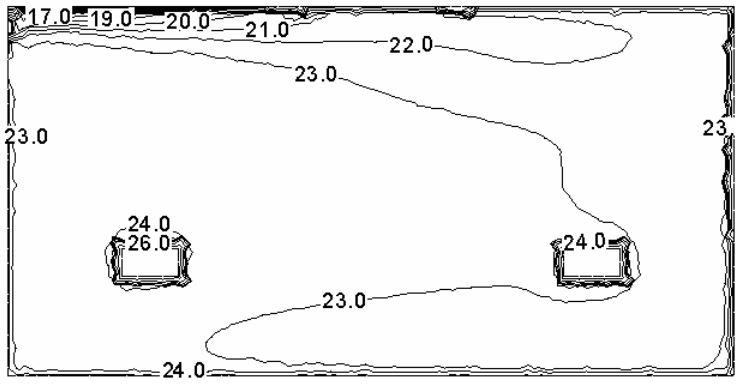

(a)

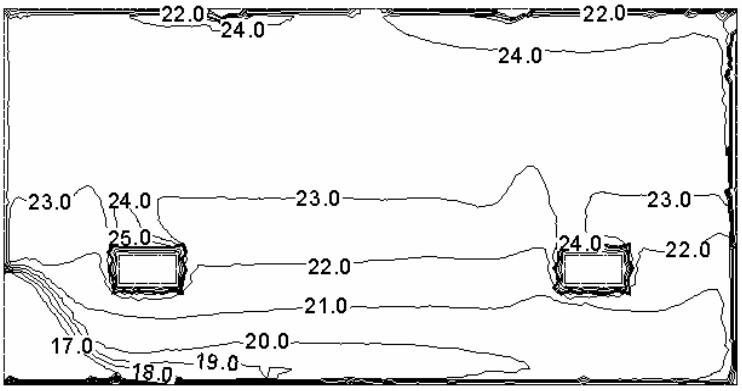

(b)

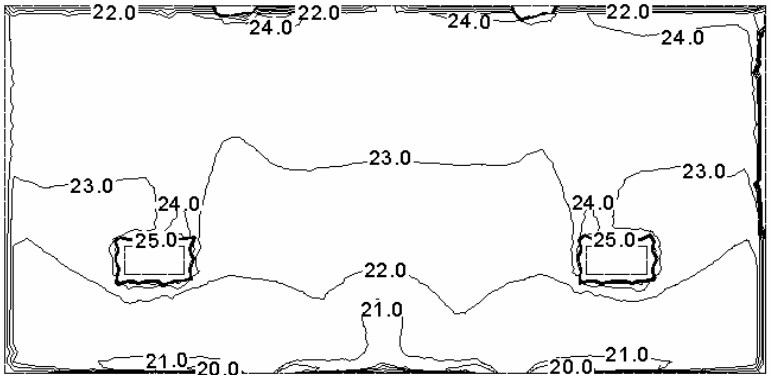

(c)

Figure 6.5 Temperature (℃) stratifications among different systems

(a) Mixing, (b) CC/DV, and (c) CC/UFAD

6.3.4.3 PD Comparison

Figure 6.6 shows the PD comparisons among the three different systems at the middle plane. The cold environment occurred near the supply inlet due to the low air temperature and large air velocity. Owing to the uniform indoor air temperature in the occupied zone, the PD gradient was mainly dominated by air velocities in the mixing system, which means that a larger draft risk occurs near the side-walls. For the CC/DV and CC/UFAD systems, the indoor draft feeling was very uniform except in those place near the supply and exhaust diffusers.

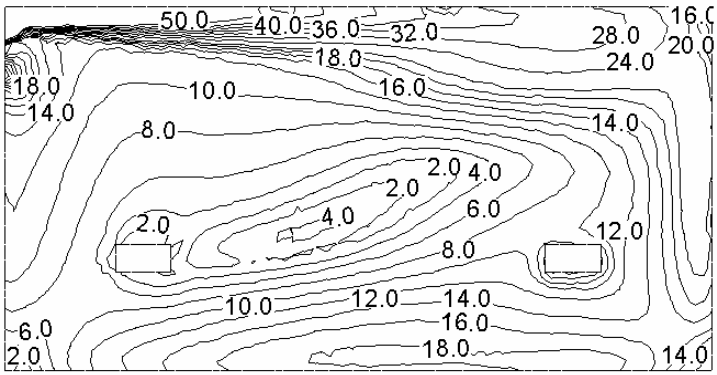

(a)

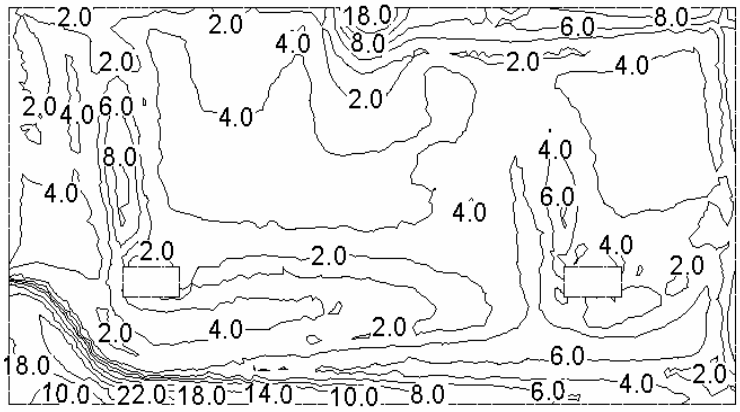

(b)

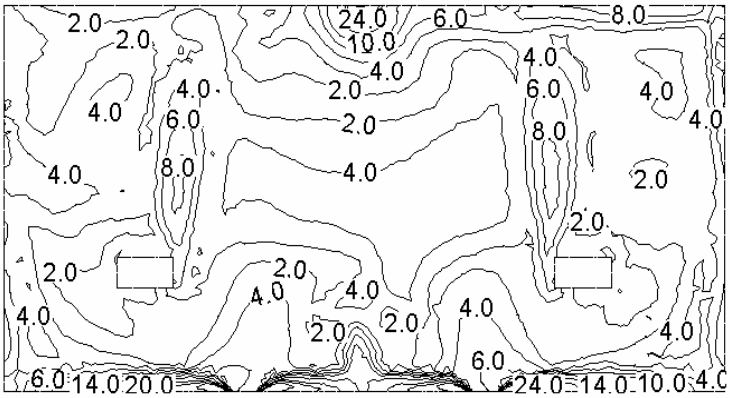

(c)

Figure 6.6 PD(%) distributions in the middle plane
(a) Mixing, (b) CC/DV, and (c) CC/UFAD

6.3.4.4 PMV Comparison

PMV was used to assess overall thermal comfort uniformity, even though it was an index originally developed for whole-body energy balance analysis. In the plotted vertical middle plane (Figure 6.7), it would appear that the zone near the supply diffuser is cool according to the PMV scale. For the three systems, head level (1.1m) is almost neutral. Above the elevation of the heat sources in Figures 6.7 (b) and 6.7 (c), the PMV gradient was small because of the employment of the cooled ceiling.

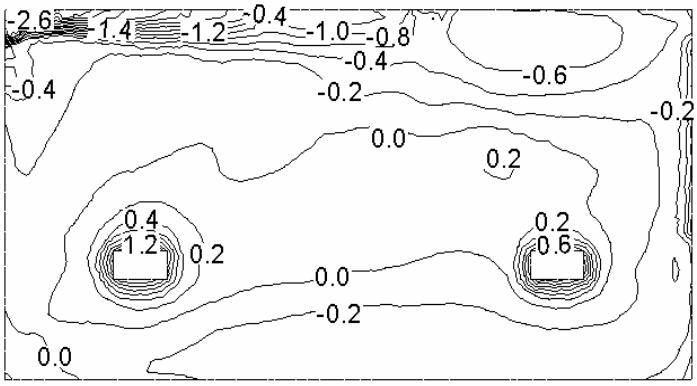

(a)

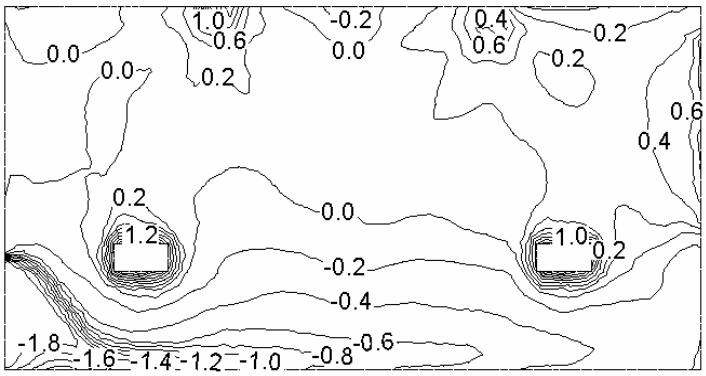

(b)

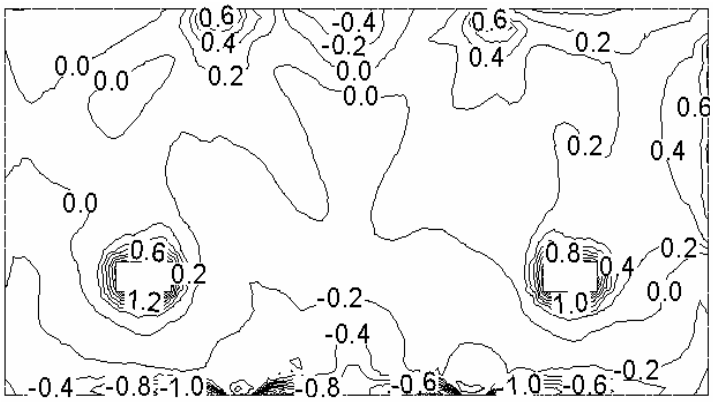

(c)

Figure 6.7 PMV distributions in the middle plane
(a) Mixing, (b) CC/DV, and (c) CC/UFAD

6.3.5 Energy Consumption Comparisons among the Different Systems

Due to indoor air temperature suppression in the combined systems, CC/DV and CC/UFAD, the procedures for the energy investigations were somewhat simpler than

those in Chapter 5. The author wrote an energy consumption program based on the simulation results (temperature and velocity) from ACCURACY.

6.3.5.1 Heat Extraction Comparison

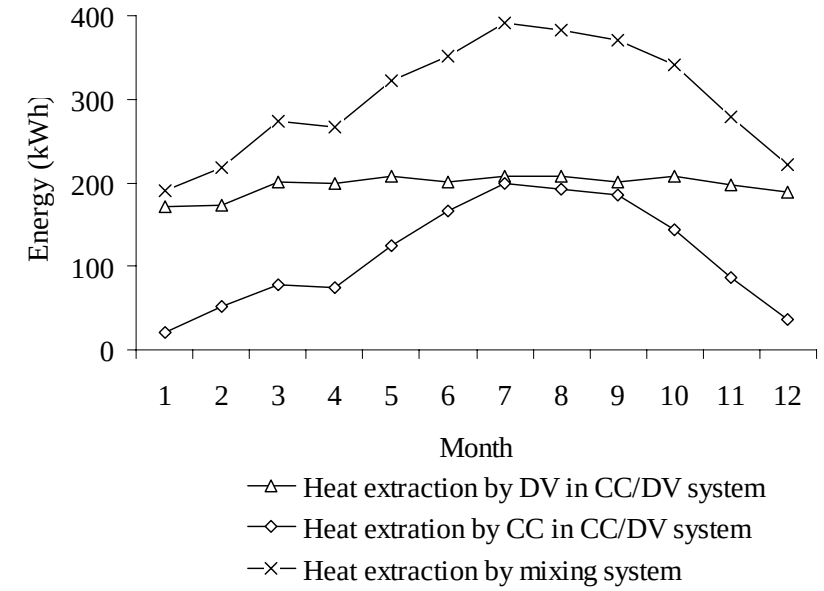

(a)

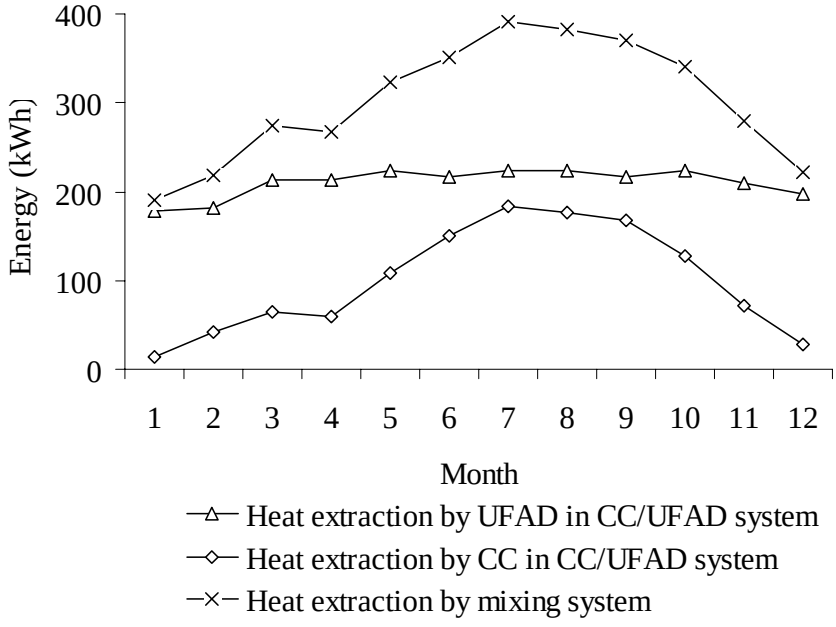

(b)

Figure 6.8 Heat extraction comparison

(a) CC/DV and mixing system, and (b) CC/UFAD and mixing system

The differences among the mixing, CC/DV, and CC/UFAD systems can be seen from the different heat extraction shown in Figure 6.8. The total heat extraction from the indoor space changed with the changes in the outdoor environments. The monthly heat extracted through ventilation was almost the same for the CC/DV and CC/UFAD systems due to the CAV supply. With the employment of the weather data for Hong Kong (1989), the required heat extraction by CC was greatest in July and least is in January in the CC/DV and CC/UFAD systems. The trends of the heat extractions by two combined systems were almost the same.

6.3.5.2 Free Cooling Hour Comparison

One advantage of the DV and UFAD systems is that the higher exhaust air temperature increases the hours of free cooing, thus reducing cooling energy consumption during economizer operation, as validated in Chapter 5. The following comparison was based on the fact that free cooling operation is assisted by a constant speed supply fan the same as Chapter 5. The air change rate (ACH) was 15, 5, and 8.5 for the mixing, CC/DV, and CC/UFAD systems, respectively (Table 6.1).

Figure 6.9 shows the free cooling hour comparisons among three systems. It shows that there are six months (from November to April) of economizer operation. During the economizer period, the mixing system had a longer period of free cooling than the CC/DV or CC/UFAD systems, in contrast to the UFAD system having greater free cooling hours than the mixing system as stated by Bauman (2003) and validated by the author in Chapter 5. With the employment of a uniform indoor air temperature, the air flow rate dominated the economizer hours due to the constant speed supply fan assisting the free cooling. The larger air flow rate resulted in greater free cooling

hours in the mixing system. Between the CC/DV and CC/UFAD systems, CC/UFAD had greater free cooling hours due to the larger air flow rate.

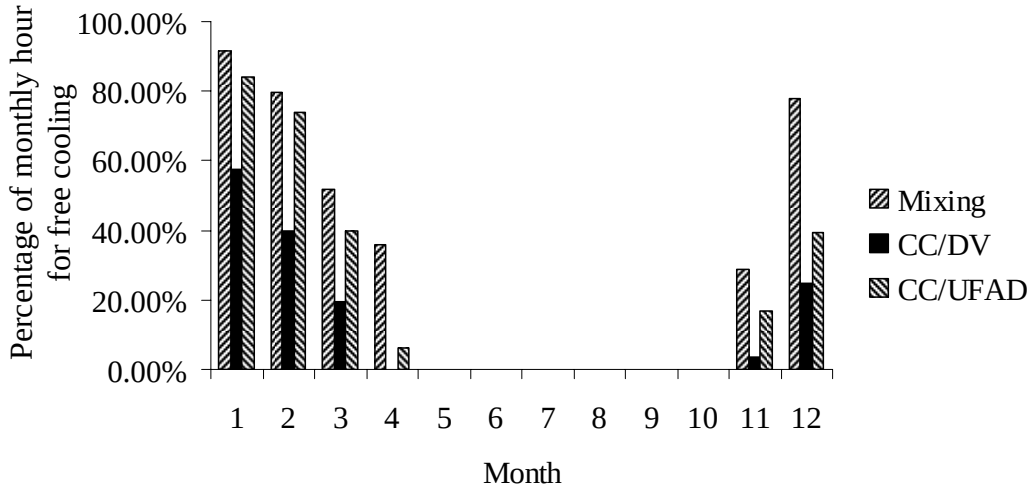

Figure 6.9 Free cooling hour comparison

6.3.5.3 Ventilation Energy Comparison

The ventilation energy is that used for heat treatment between the fresh air and exhaust air. In the CC/DV system, totally fresh air is supplied, and the exhaust air is of no concern, hence only the results from the mixing and CC/UFAD systems were compared, as shown in Figure 6.10.

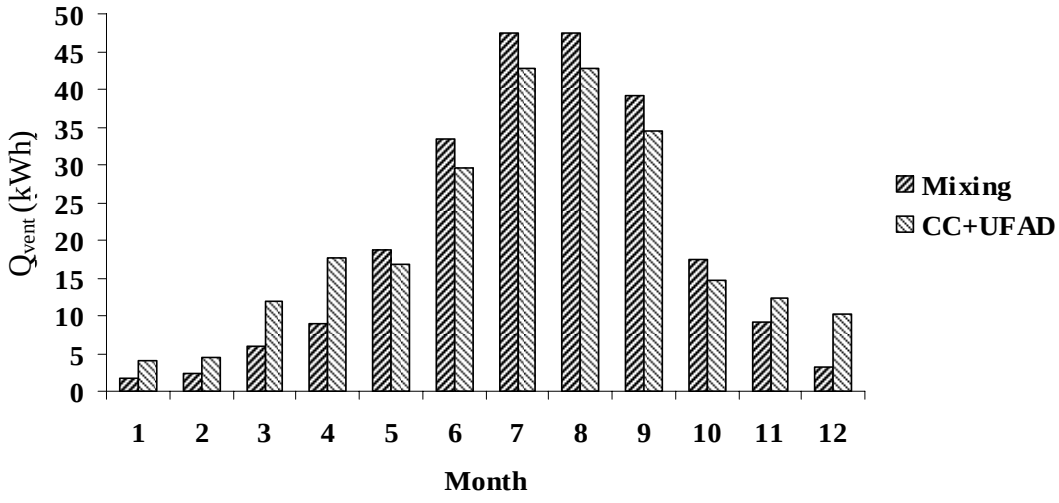

Figure 6.10 Ventilation energy comparison

Due to fewer free cooling hours, the ventilation energy consumed by the CC/UFAD system was larger during the period from November to April. From May to October, the mixing system consumed greater ventilation energy than the CC/UFAD system due to the larger operative temperature in ACCURACY, based on Equation (5.8).

6.3.5.4 Chiller Energy Comparison

Selected water and cooled panel temperatures are presented in Figure 6.11 for 15 July 1989 for the CC/UFAD system. Obviously, the supplied water temperature changed with the heat removed by the cooled ceiling (Figure 6.12). In Figure 6.11, the simulated lowest supply water temperature was about 19℃. This offered the opportunity of raising the COP of the chiller system for energy saving.

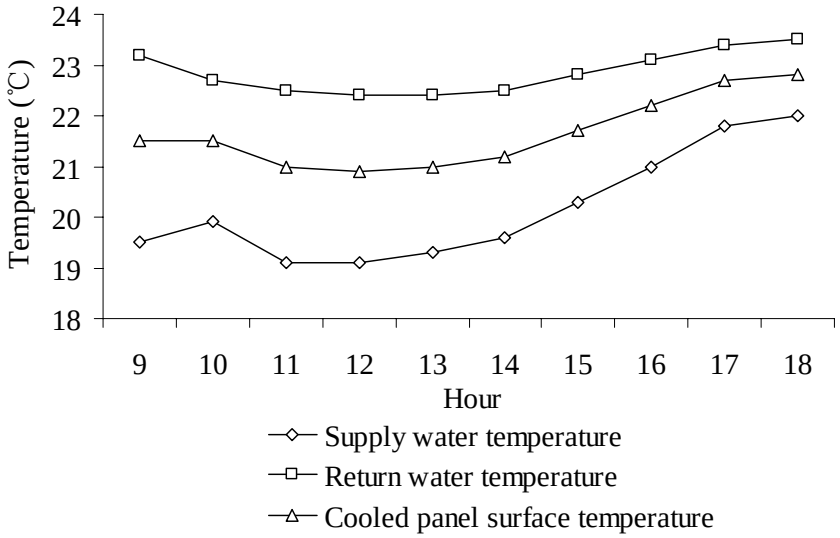

Figure 6.11 Simulated water and panel surface temperatures (15 July 1989)

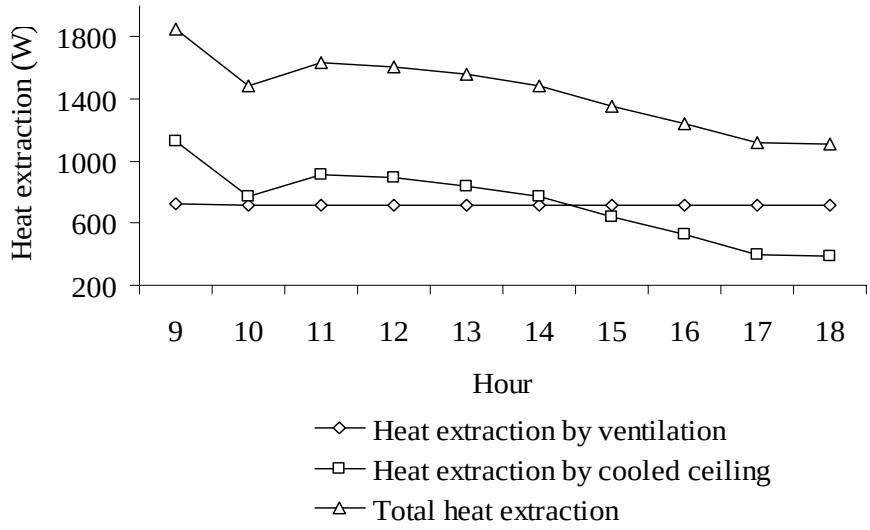

Figure 6.12 Simulated heat extractions (15 July 1989)

Figure 6.13 shows the single chiller energy comparisons among the three systems. When taking into account economizer operation, due to the reduced free cooling capacity at lower air volume (Figure 6.9), the chiller energy consumed by the CC/DV system was greatest during the period from November to April. The mixing system consumed the greatest chiller energy from May to October. This was due to the fact that the calculated monthly ventilation energy was the largest and the COP assumption (3.5) was the smallest.

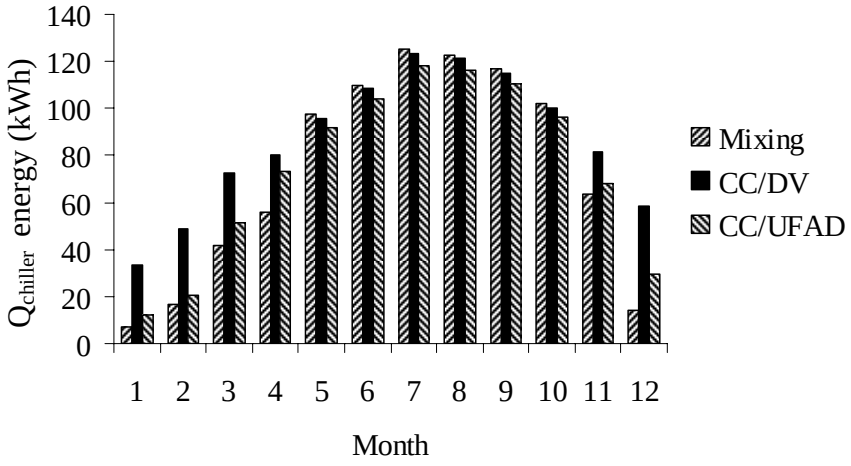

Figure 6.13 Single chiller energy comparisons among the different systems

The advantage of a separate chiller-water supply is that the higher COP on the water-side results in lower chiller power consumption due to the higher supply water temperature. Figure 6.14 presents the chiller energy comparisons between the single chiller and separate chiller employments in summer operation. Based on Equation (6.2), it can be seen that the separate chiller used for the cooling load removed by CC resulted in less energy consumption due to the higher chiller COP (4.5). With a smaller fraction of cooling load treated by CC during the economizer operation period (Figure 6.9), the difference in chiller energy consumption between single and separate chiller strategies were much smaller.

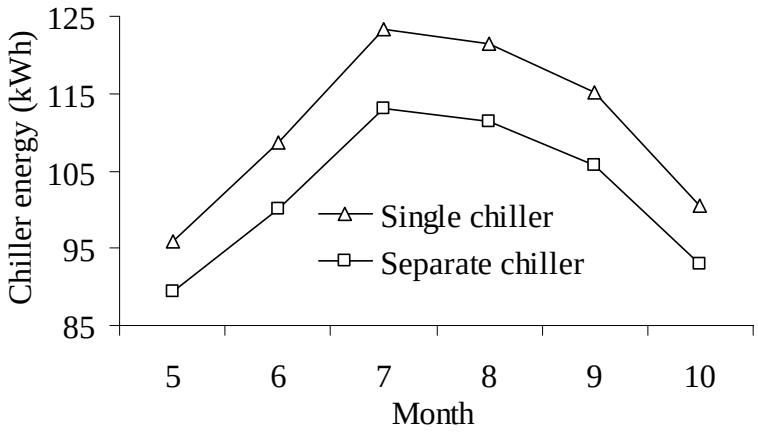

(a)

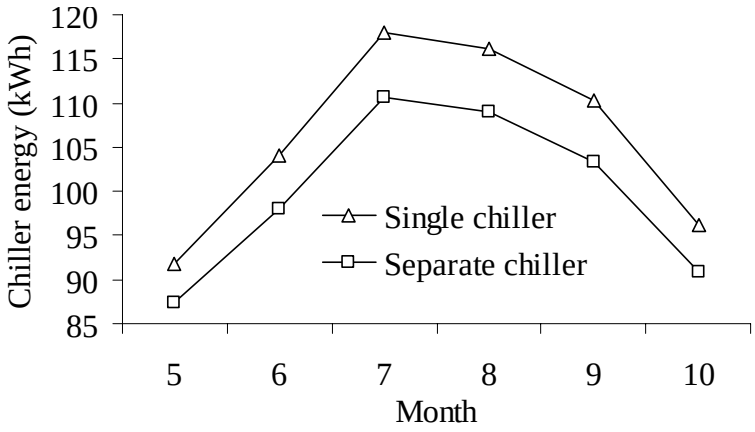

(b)

Figure 6.14 Chiller monthly energy consumption comparisons
(a) CC/DV; (b) CC/UFAD

6.3.5.5 Fan energy Comparison

For the present simulation, fan efficiency of 60% and fan pressure rise of 1400Pa were assumed. In reality, fan efficiency normally changes quite substantially as the working air flow rate is modulated in operation, depending on the method of air volume control. Fan pressure rise was also different among the different supply strategies even with the same air flow rate. Therefore, the computation of real fan power should be based on a characteristic curve, which would give the fraction of rated input power versus the fraction of rated volume. These curves can be experimentally determined or obtained from the manufacturer. Additionally, general and sufficiently accurate curves are available in the ASHRAE Handbook (ASHRAE 1993). It shows the three characteristic curves for the discharge damper control, inlet vane control and variable-speed motor control methods respectively.

6.4 Discussion and Summary

This study focused on a perimeter office room in Hong Kong, whose indoor cooling load was influenced by the outdoor environment. Although some simplified assumptions were used, the emphasis was to reveal the differences in the thermal environments resulted from the different air supply strategies used in the three systems, the mixing, CC/DV, and CC/UFAD systems.

Different supply air conditions resulted in different indoor thermal environments, which could be revealed through CFD simulation. The mixing system showed a uniform indoor thermal environment. It was found that the combined CC/DV and

CC/UFAD systems suppressed indoor air temperature stratification. Due to the employment of CC, the indoor air temperature at head level was almost equal to the exhaust air temperature in a small office room air-conditioned by the CC/DV and CC/UFAD systems. The dimensionless temperature coefficient defined in Chapter 5 is approximate to 1.0. Therefore, the indoor one-point-temperature model was used for system energy analysis. During the adjustment of the CFD simulation to obtain the same thermal sensation index (PMV=0) at head level, step ①, not step ②, was taken in Figure 6.3 due to the simulation time limitation. Theoretically, the changes in supply conditions would result in changes in the boundary conditions from ACCURACY simulation. In future work, the methodology of this paper should be improved to consider this effect.

Employing indoor air temperature stratification or not for energy analysis results in different compared results among the different systems. When a constant speed supply fan assists free cooling, Chapter 5 showed that the UFAD system had a longer free cooling time than the mixing system due to indoor air temperature stratification. However, due to the larger air flow rate in the mixing system, there are more hours of economizer operation as compared with the CC/DV and CC/UFAD systems without considering indoor temperature stratification. Based on the assumptions of constant fan pressure rise and coefficient, fan energy consumption by the mixing system was greatest in the months without economizer operation. For real fan power, the characteristic curve had to be used. In the combined systems, the chiller operation played an important role in system energy consumption with different coefficients of performance (COP) in AHU and the ceiling panel of chillers.

The energy saving potential of separate chiller operation is significant due to the larger COP resulted from the higher supply water temperature in CC.

CHAPTER 7 CONCLUSIONS AND FUTURE WORK

7.1 Concluding Remarks

This research was carried out to inspect the influence of supply diffusers on thermal environments and indoor air temperature stratification on energy consumption in the UFAD system. With the employment of the standard $\kappa - \varepsilon$ turbulence model and the diffuser simulation method FRGM, the thermal comfort environment and energy consumption of the UFAD system were investigated and compared with the mixing system. Since conclusions have been given at the end of each chapter, only some of the main points will be highlighted here.

The simplified modeling methods for supply diffusers neglect the influence of diffuser configurations on turbulent intensities near the diffuser zone, which is difficult to measure. With the powerful CAD software, the fully represented geometry method (FRGM) for the swirling supply diffuser was used in the present study and was validated against the experimental data from a pre-combustion chamber. It is concluded that proper inlet conditions from supply diffusers are essential for accurate CFD simulation using the standard $\kappa - \varepsilon$ turbulence model. The multi-domain information transfer is a numerical algorithm that is used in FRGM due to the different meshed grid sizes of the supply diffuser and conditioned space. For engineering applications, this is not a gap because this algorithm has been incorporated in most commercial codes, such as FLUENT, which was used in the author's simulation work. Operators only need to select the option in it. Due to the complicated diffuser geometries, the emphasis of the FRGM is how to generate the

exact diffuser simulation domain and yet keep the most important characteristics of the supply diffusers. Many powerful CAD (Computer Aided Design) software programs, such as Pro/Engineering, provide us with this tool.

Employing the FRGM, the need to measure the input conditions near the supply diffuser can potentially be eliminated, which is difficult and inaccurate due to the large gradients. It was found that the RNG $\kappa - \varepsilon$ turbulence model presented less accurate results near the supply diffuser with this method. The reason is that the current version of the dissipation rate transport equation has only been modeled to account for the effects of irrotational strains. Incorporation of the effects of rotational strains, which can be important in turbulent flows involving curvature or a system rotation, is a difficult task that has not yet been achieved and needs a future study. On the other hand, the RNG $\kappa - \varepsilon$ model predicts a more accurate downstream recirculation zone than the standard $\kappa - \varepsilon$ model. Such an inconsistency means that no uniform turbulence model exists for accurately solving different flow instances.

The FRGM was employed to inspect two different supply diffusers, the swirling and square diffusers, for thermal environments in the UFAD system. It was confirmed that the swirling diffuser can generate a quicker combination with the indoor air through entrainment than the square diffuser and a more uniform air flow pattern in the occupied zone. Both the swirling and square diffusers can generate air temperature stratification, which is the essential for energy saving in the UFAD system. PD is relatively larger near the floor for both supply diffusers. For the swirling diffuser, different vane angles dominated the different air flow patterns near the diffuser zone. The thermal environment was greatly influenced by the diffuser configuration in a small office room.

The accurate energy simulation of the UFAD system was based on the proper consideration and quantification of indoor air temperature stratification. How to obtain such stratification is believed to be a limitation in most energy analysis programs. A coupled method was presented in this thesis. The energy program ACCURACY was used for cooling load and wall-heat transfer calculations. CFD is used for 3D indoor air flow simulations, using ACCURACY results as the boundary conditions. Through this coupled method, the dimensionless temperature coefficient due to indoor air temperature stratification can be obtained and used for the UFAD energy estimation. In cases where the indoor heat sources dominated the whole room cooling load, for CAV supply, the dimensionless temperature coefficient mainly depended on the elevation of the electronic equipment when other heat sources were fixed. For VAV supply, this coefficient was dominated by the supply air flow rate when all heat sources were fixed. Compared with the mixing system, the energy saving potential of UFAD systems is due to three factors: more free cooling hours, smaller ventilation load, and smaller chiller energy consumption. Higher exhaust air temperature results in a longer free cooling time. Ventilation load is reduced due to the higher air exhaust temperature. Based on the higher supply water temperature, the chiller can operate at a higher evaporative temperature, thus reducing the energy consumption as compared with the mixing system.

The cooled ceiling (CC) is an attractive technique for cooling load removal in HVAC systems. For the purpose of ventilation, it is often combined with the DV system. In the combined systems, CC/DV and CC/UFAD, it was found that the typical air temperature stratification was suppressed due to the employment of CC. So, the air temperature stratification was not considered in the energy analysis of the

combined system in a small office room. Through CFD investigations, it was concluded that the employment of CC with DV and UFAD systems generated more uniform indoor thermal environments. Compared with the mixing system, the combined systems had shorter free cooling operation, assisted by a constant speed supply fan. Chiller energy consumption was decided by the different COPs of the chillers serving the AHU and ceiling panel separately. The separate chiller can save more energy due to the higher supply water temperature in the cooled ceiling.

7.2 Recommendations

Use of the fully represented geometry method (FRGM) for supply diffusers was investigated in this thesis. A disadvantage is that this method requires a large amount computer memory. In my simulation work, it was very difficult to carry out the simulations on a personal computer due to the large grid number. Further effort was focused on generating smaller grid number, while keeping the proper simulation rules. However, with the famous Moore's Law of the computer, the limitation of the personal computer memory for matching FRGM should disappear some day.

In Chapter 3, FRGM was validated by the experimental data from a precombustion chamber, employing the standard $\kappa - \varepsilon$ model. It is concluded that the type of turbulence model plays an important role in proper indoor air flow estimations, especially near the supply diffuser zone. More sophisticated models involving curvature or a system rotation deserve further study.

The previously validated energy analysis program ACCURACY was employed. FRGM was also validated in this thesis. The coupled use of the two methods for

annual energy consumption in a small office room was proposed. During employment, some simplified steps were taken. Further work should focus on solutions that more tightly couple ACCURACY and CFD. Additionally, indoor air temperature stratification in a larger space deserves investigations for system energy consumption.

In Chapters 5 and 6, some performance indices were employed to model the end energy use of the equipment, including the air fan and chiller system, to simplify the simulation work. To rigorously calculate the end energy, the specific dynamic performance curve of equipment from manufactures has to be used in future work.

REFERENCES

Abanto, J., D. Barrero, M. Reggio and B. Ozell. 2004. Airflow modelling in a computer room. *Building and Environment*, 39(12): 1393-1402.

Akbari, H., D. Samano, A. Mertol, F. Bauman and R. Kammerud. 1987. The effect of variations in convection coefficients on thermal energy storage in buildings Part II — Exterior massive walls and simulations. *Energy and Buildings*, 10(1): 29-47.

Akimoto, T., T. Nobe and Y. Takebayashi. 1995. Experimental study on the floor-supply displacement ventilation system. *ASHRAE Transactions*, 101(2): 912-925.

Alamdari, F. and N. Eagles. 1996. Displacement ventilation and chilled ceilings. Building Services Research and Information Association. Technical Note TN 2/96.

ASHRAE. 1992. Thermal environmental conditions for human occupancy. ANSI/ASHRAE Standard 55-1992.

ASHRAE. 1993. Fundamentals. Energy estimating methods. Chapter 28, USA .

ASHRAE. 1993. Fundamentals. Space air diffusion. Chapter 31, USA.

ASHRAE. 2001. Fundamentals. Thermal comfort. Atlanta, USA.

Arnold, D. 1990. Raised floor air distribution-a case study. *ASHRAE Transactions*, 96(2): 665-669.

Baturin, V.V. 1972. Fundamentals of industrial ventilation. Pergamon Press, Oxford.

Bauman, F.S. 1998. Field study of the impact of a desktop task/ambient conditioning system in office buildings. *ASHRAE Transactions*, 101(1): 1153-1171.

Bauman, F.S. 2003. Underfloor air distribution (UFAD) design guide. American Society of Heating, Refrigerating and Air-Conditioning Engineers, Inc.

Bauman, F.S., K. Powell, R. Bannon, A. Lee and T. Webster. 2000. Underfloor air technology web site: http://www.cbe.berkeley.edu/underfloorair. Center for the Built Environment, University of California, Berkeley, April.

Bauman, F.S. and T. Webster. 2001. Outlook for underfloor air distribution *ASHRAE Journal*, 43(6): 18+20-25+27.

Benchmark Ⅲ. 1997. International Facility Management Association. Houston.

Bergstrom, D.J. 1994. Numerical prediction of a turbulent fountain in a room. *ASHRAE Transactions*, 100(2): 669-676.

Boussinesq, J. 1877. Essai sur la théorie des eaux courantes. *Mem. Presentes A cad. Sci.*, Vol. 23, pp. 46. Paris.

Brill, M. and S. Margulis. 1984. Using office design to increase productivity. Buffalo, NY: Buffalo Organization for Social and Technological Innovation.

Brunk, M.F. 1993. Cooling ceilings-an opportunity to reduce energy costs by way of radiant cooling. *ASHRAE Transactions*, 99(2): 479-487.

BSL. 1999. BLAST 3.0 Users Manual. Department of Mechanical and Industrial Engineering, Building Systems Laboratory, University of Illinois, Urbana-Champaign, IL.

Busweiler U. 1993. Air-conditioning with a combination of radiant cooling, displacement ventilation and desiccant cooling. *ASHRAE Transactions*, 99(2): 503-509.

Büyükalaca, O., H. Bulut and T. Yılmaz. 2001. Analysis of variable-base heating and cooling degree-days for Turkey. *Applied Energy*, 69(4):269-283.

Chao C.Y. and M.P. Wan. 2004. Experimental study of ventilation performance and contaminant distribution of underfloor ventilation systems vs. traditional ceiling-based ventilation system. *Indoor Air*, 14(5): 306-316.

Chen Q. 1984. Comparison of different $\kappa - \varepsilon$ models for indoor air flow computations. *Numerical Heat Transfer*, Part B, 28(3): 353-369.

Chen, Q. and A. Moser. 1991. Simulation of a multiple-nozzle diffuser. *Proceedings of the 12th AIVC Conference on Air Movement and Ventilation Control within Buildings*, 2: 1-13, Ottawa, Canada.

Chen, Q. and J. Srebric. 2000. Simplified diffuser boundary conditions for numerical room airflow models. *ASHRAE RP-1009*.

Chen, Q. and J.V.D. Kooi. 1988. ACCUARCY- A computer program for combined problems of energy analysis, indoor airflow and air quality. *ASHRAE Transactions*, 94(2): 196-214.

Chen, Q. and Z. Jiang. 1992. Significant questions in predicting room air motion. *ASHRAE Transactions*, 98(1): 929-939.

Chen, Q. and Z. Jiang. 1996. Simulation of a complex air diffuser with CFD techniques. *Proceedings of the 5th International Conference on Airflow in Rooms*, 1: 227-234, Nagoya, Japan.

Chou, P.Y. 1945. On the velocity correlations and the solution of the equations of turbulent fluctuation. *Quart. Appl. Math.*, 3: 38.

Chuang S.H., C.S. Yang, and N.J. Wu. 1999. Predictions of Swirling Flow in a Sudden-Expansion Dump Combustor with Flameholder Side-Inlet Using Two-Step

Combustion Model. *The International Journal of Numerical Methods for Heat & Fluid Flow*, 9(7): 764-787.

Crawley D.B., L.K. Lawrie, F.C. Winkelmann, W.F. Buhl, Y.J. Huang, C.O. Pedersen, R.K. Strand, R.J. Liesen, D.E. Fisher, M.J. Witte, J. Glazer. 2001. EnergyPlus: creating a new-generation building energy simulation program. *Energy and Buildings*, 33(4): 319-331.

Date Q.W. 1974. Prediction of fully developed flow in a tube containing a twisted-tape. *International Journal of Heat and Mass Transfer*, 17: 845–859.

Davidov, B.I. 1961. On the statistical dynamics of an incompressible fluid. *Doklady Akademii Nauk SSSR*, 136: 47.

Davies T.W. and J.M. Beer. 1971. Flow in the Wake of a Bluff-Body Flame Stabilizer. *Proceedings of 13th International Symposium on Combustion,* 631-8, Salt Lake City.

Delaney T.A., T.M. Maiocco and A.G. Vogel. 1984. Avoiding Coil Freezeup. *Heating, Piping & Air Conditioning*, 56(12): 83-85.

Diamond S.C., B.D. Hunn and C.C. Cappiello. DOE-2 Verification Project, Phase 1, Interim Report, Group Q-11, Los Alamos National Laboratory, April 1981.

Diamond S.C., B.D. Hunn and C.C. Cappiello. DOE-2 Verification Project, Phase 1, Final Report, Group Q-11, Los Alamos National Laboratory, February 1986.

Eastwick C.N., S.J. Pickering and A. Aroussi. 1999. Comparisons of Two Commercial Computational Fluid Dynamics Codes in Modelling Pulverised Coal Combustion for a 2.5 MW Burner. *Applied Mathematical Modelling*, 23(6): 437-446.

Eckert E. R. G. 1959. Heat and Mass Transfer. 469-476. New York: McGraw-Hill.

Emvin P. and L. Davidsen. 1996. A numerical comparison of the diffuser in case EI ANNEX20. *Proceedings of the 5th International Conference on Airflow in Rooms*, 1: 219-226, Nagoya, Japan.

EPA. 1991. Building Air Quality: A Guide for Building Owners and Facility Managers. Environmental Protection Agency.

Fan X.Z., L.J. Guo, H. Guo, and J.P. Nie. 2002. Numerical Simulation of Flow and Combustion Process in the Tangentially Fired Furnace of a 200 MW Pulverized Coal Boiler, *Journal of Xi'an Jiaotong University*, 36(3): 241-245 *(in Chinese with an English abstract).*

Fanger, P.O. 1970. Thermal Comfort. Copenhagen: Danish Technical Press.

Fanger P.O., A.K. Melikov, H. Hanzawa and J. Ring. 1988. Air turbulence and sensation of draught. *Energy and Buildings*, 12: 21-39.

Fanger P.O. 1992. Efficient ventilation for human comfort. *International Symposium on Room Air Convection and Ventilation Effectiveness*, 296-306, University of Tokyo, Japan.

Favaloro S.C., A.S. Nejad and S.A. Ahmed. 1991. Experimental and Computational Investigation of Isothermal Swirling Flow in an Axisymmetric Dump Combustor. *Journal of Propulsion and Power*, 7(3): 348-356.

Feng X.P., H.Q. He and L.H. Ge. 2002. Numerical Simulation of 3-D Turbulent Flow and Combustion Process for Pre-burner (1) Model and Method. *Journal of Propulsion Technology*, 23(2): 121-125 *(in Chinese with an English abstract).*

Feustel H.E. and C. Stetiu. 1995. Hydronic radiant cooling-preliminary assessment. *Energy and Buildings*, 22(3):193-205.

Fisk, W.J. 2000. Health and productivity gains from better indoor environments and their relationship with building energy efficiency. *LBNL-45484*, Lawrence Berkeley National Laboratory, July 31.

Fitzner K. 1996. Displacement ventilation and cooled-ceiling. Results of laboratory tests and practical installations. *Proceedings of IndoorAir*, 1: 41-50, Nagoya, Japan.

FLUENT. 2001. User's Manual, Version 6.0.

Fontoynont, M., W. Place and F. Bauman. 1984. Impact of electric lighting efficiency on the energy saving potential of daylighting from roof monitors. *Energy and Buildings*, 6(4): 375-386.

Fukao, H., M. Oguro, M. Ichihara and S. Tanabe. 2002. Comparison of underfloor vs. overhead air distribution systems in an office building. *ASHRAE Transactions*, 108(1): 64-76.

Gan, G.H. 1998. Prediction of turbulent buoyant flow using an RNG k-ε model. *Numerical Heat Transfer*, Part A, 33(2): 169-189.

Godish, T. and J.D. Spengler. 1996. Relationship between ventilation and indoor air quality: a review. *Indoor Air*, 6: 135-145.

Haines R.W. 1980. Stratification. *Heating, Piping & Air Conditioning*, 52(11): 70-71.

Hanby V.I. 1995. Error estimation in bin method energy calculations**.** *Applied Energy*, 52(1): 35-45.

Hanzawa, H. and Y. Nagasawa. 1990. Thermal comfort with underfloor air-conditioning systems. ASHRAE Transactions, 96(2): 696-698.

Harlow, F.H. and P.I. Nakayama. 1968. Transport of turbulence energy decay rate. Los Alamos Sci. Lab., University of California Report LA-3854.

Harris, L. and Associates. 1980. Comfort and productivity in the offices of the ’80s. The steelcase National Study of Office Environments, No. Ⅱ. Grand Rapids, MI: Steelcase, Inc.

Hedlund C. R. and P. M. Ligrani. 2000. Local swirl chamber heat transfer and flow structure at different Reynolds numbers. *Journal of Turbomachinery, Transactions of the ASME,* 122(2): 375-385.

Hedlund C. R., P. M. Ligrani, B. Glezer and H. –K. Moon. 1999a. Heat Transfer in a Swirl Chamber at Different Temperature Ratios and Reynolds Numbers. *International Journal of Heat and Mass Transfer,* 42(22): 4081-4091.

Hedlund C. R., P. M. Ligrani, H. –K. Moon and B. Glezer. 1999b. Heat Transfer and Flow Phenomena in a Swirl Chamber Simulating Turbine Blade Internal Cooling. *Journal of Turbomachinery, Transactions of the ASME,* 121(4): 804-813.

Heikkinen, J. 1990. Modelling of the air inlet device. Working Report of International Energy Agency Annex 20.

Heikkinen, J. 1991. Modelling of a supply air terminal for room air flow simulation. *12th AIVC Conference on Air Movement and Ventilation Control within Buildings*, 3: 213-230. Ottawa, Canada.

Hittle, D.C. 1977. The Building Loads Analysis and System Thermodynamics Program, BLAST, U.S. Army Construction Engineering Research Laboratory, Champaign, Illinois.

Hodder S.G., D.L. Loveday, K.C., Parsons and A.H. Taki. 1998. Thermal comfort in chilled ceiling and displacement ventilation environments: Vertical radiant temperature asymmetry effects. *Energy and Buildings*, 27(2): 167-173.

Hong S.W. and A.E. Bergles. 1976. Augmentation of laminar flow heat transfer in tubes by means of twisted-tape inserts. *Journal of Heat Transfer, Transactions of the ASME,* 98: 251–256.

Huo, Y., F. Haghighat, J.S. Zhang and C.Y. Shaw. 2000. A systematic approach to describe the air terminal device in CFD simulation for room air distribution analysis. *Building and Environment*, 35(6): 563-576.

Hwang, C.C., G.Z. Zhu, M. Massoudi and J.M. Ekmann. 1993. A Comparison of the Linear and Nonlinear $\kappa - \varepsilon$ Turbulence Models in Combustors. *Journal of Fluids Engineering*, 115: 93-102.

IEA. 1993. Annex 20: Room Air and Contaminant Flow, Evaluation of Computational Methods, Subtask-1, Summary report. Edited by A.D. Lemaire. TNO Building and Construction Research, Delft.

ISO 7730. 1984. Moderate thermal environments-determination of PMV and PPD indices and specification of the conditions for thermal comfort, Ref. No. 7730-1984(E).

Issa, R.I. 1985. Solution of implicitly discretized fluid flow equation by operator-splitting. *Journal of Computational Physics*, 62: 40-65.

Jacobsen, T.V. and P.V. Nielsen. 1993. Numerical modeling of thermal environment in a displacement-ventilated room. *Proceedings of Indoor Air'93*: 5, Helsinki, Finland.

Jones, W.P. and B.E. Launder. 1972. The prediction of laminarization with a two-equation model of turbulence. *International Journal of Heat and Mass Transfer*, 15: 301-314.

Kallinderis Y. 1992. Numerical treatment of grid interfaces for viscous flows. *Journal of Computational Physics*, 98(1): 129-144.

Kao J.Y. 1985. Sensor errors. *ASHRAE Journal*, 27(1): 100-104.

Katzarov, I.H. 1999. Finite element method for simulation of 3-D form filling with incompressible fluid. *International Journal of Heat and Mass Transfer*, 42(17): 3331-3336.

Ke, Y.P. and S.A. Mumma. 1999. Variable air volume ventilation control strategies analysed in six climate zones. *International Journal of Energy Research*, 23(5): 371-387.

Keresteciogl u, H., M. Swami, P. Fairey, G. Lixing and S. Chandra. 1989. Modelling heat, moisture and contaminant transport in buildings: toward a new generation software. FSECPF16589, Florida Solar Energy Center, USA.

Kim, I.G. and H. Homma. 1992. Possibility for increasing ventilation efficiency with upward ventilation. *ASHRAE Transactions*, 98(1): 723-729.

Koomey, J.G., N.C. Martin, M. Brown, L.K. Price and M.D. Levine. 1998. Costs of reducing carbon emissions: U.S. building sector scenarios. *Energy Policy*, 26(5): 433-440.

Kosonen R. and F. Tan. 2004. Assessment of productivity loss in air-conditioned buildings using PMV index. *Energy and Buildings*, 36 (10): 987-993.

Kostel, A. and G.L. Tuve. 1955. Performance and evaluation of room air distribution systems. A*SHRAE Transactions*, 61:533.

Kreith F. and D. Margolis. 1959. Heat Transfer and Friction in Turbulent Vortex Flow. *Applied Scientific Research*, 8: 457-473.

Krühne H. 1993. Influence of buoyant wall-flow in rooms with displacement ventilation. *Proceedings of CLIMA-2000*, Paper No. 210, Tagungsband, London.

Külpmann R.W. 1993. Thermal comfort and air quality in rooms with cooled ceilings-results of scientific investigations. *ASHRAE Transactions*, 99(2):488-502.

Lai, J.C. and A. Naser. 1998. Two parallel plane jets: comparison of the performance of three turbulence models. *Proc Instn Mech Engrs.*, Part G J. Aerospace Engineering, 212: 379-391.

Laine T. 1993. Cool-ceiling system: for better control of office building indoor climate, *Proceedings of IndoorAir'93*, 5: 425-430, Helsinki, Finland.

Lam J. and A. Chan. 1994. Characteristics of electricity consumption in commercial buildings. *Building Research and Information*, 22(6): 313-318.

Lau J. and J.L. Niu. 2003. Measurement and CFD simulation of the temperature stratification in an atrium using a floor level air supply method. *Indoor and Build Environment*, 12(4): 280-285.

Launder, B.E. and B.I. Sharma. 1974. Application of the energy dissipation model of turbulence to the calculation of flow near a spinning disc. *Letters in Heat and Mass Transfer*, 1(2): 131-137.

Launder, B.E. and D.B. Spalding. 1974. The numerical computation of turbulent flows. *Computer Methods in Applied Mechanics and Engineering*, 3: 269-289.

Leonard B.P. 1981. A survey of finite differences with unwinding for numerical modeling of the incompressible convective diffusion equation. In: C Taylor, K Morgan, eds. Computational techniques in transient and turbulent flows, 1~35, Swansea: Pineridge Press, Limited.

Leschziner, M.A. and W. Rodi. 1984. Computation of Strongly Swirling Axisymmetric Free Jets. *AIAA Journal*, 22: 1742-1747.

Li, H. and Y. Tomita. 1994. Characteristics of swirling flow in a circular pipe. *Journal of Fluids Engineering, Transactions of the ASME*, 116(2): 370-373.

Li, Z.H., J.S. Zhang, A.M. Zhivov and L.L. Christianson. 1993. Characteristics of diffuser air jets and airflow in the occupied regions of mechanically ventilated rooms - a literature review. *ASHRAE Transactions*, 99(1): 1119-1127.

Liu J. and W. Shyy. 1996. Assessment of grid interface treatments for multi-block incompressible viscous flow computation. *Computers and Fluids*, 25(8): 719-740.

Loudermilk, K. J. 1999. Underfloor air distribution solutions for open office applications. *ASHRAE Transactions*, 105(1): 605-613.

Loudermilk, K. J. 2003. Temperature control and zoning in underfloor air distribution systems. *ASHRAE Transactions*, 109(1): 307-314.

Loveday D.L., K.C. Parsons, A.H. Taki and S.G. Hodder. 2002. Displacement ventilation environments with chilled ceilings: Thermal comfort design within the context of the BS EN ISO7730 versus adaptive debate. *Energy and Buildings*, 34(6): 573-579.

Loveday D.L., K.C. Parsons, A.H. Taki, S.G. Hodder and L. Jeal. 1998. Designing for thermal comfort in combined chilled-ceiling/Displacement ventilation environments. *ASHRAE Transactions*, 104(1): 901-911.

Luo, S. and B. Roux. 2004. Modeling of the HESCO nozzle diffuser used in IEA Annex-20 experiment test room. *Building and Environment*, 39(4): 367-384.

Luo, S. J. Heikkinen and B. Roux. 2004. Simulation of air flow in the IEA Annex 20 test room-validation of a simplified model for the nozzle diffuser in isothermal test cases. *Building and Environment*, 39(12): 1403-1415.

Ma Z., S. Tu, and S. Yao. 2001. Numerical Simulation of the Gas-Liquid Two-Phase Flow and Combustion in the Outlet of Venturi Burner. *Journal of East China Shipbuilding Institute*, 15(1): 77-81.

Manole D.M. and J.L. Lage. 1993. Nonuniform grid accuracy test applied to the natural convection flow within a porous medium cavity. *Numerical Heat Transfer*, Part B, 23: 351-368.

Martin B. 1999. Indoor air quality in rooms with cooled ceiling. Mixing ventilation or rather displacement ventilation? *Energy and Buildings*, 30(2): 155-166.

Matsunawa K, H. Iizuka and S. Tanabe. 1995. Development and application of an underfloor air-conditioning system with improved outlets for a 'smart' building in Tokyo. *ASHRAE Transactions*, 101(2): 887-901.

McCarry B.T. 1995. Underfloor air distribution systems: benefits and when to use the system in building design. *ASHRAE Transactions*, 101(2): 902-911.

McQuiston, F.C. and J.D. Parker. 1994. Heating, ventilating and air conditioning analysis and design. John Wiley & Sons, Inc., New York.

Meldem R. and F. Winkelmann. 1995. Comparison of DOE-2 with measurements in the Pala test houses. LBL-37979, Lawrence Berkeley National Laboratory, July 1995.

Mertz G. 1992. Chilled ceilings and ventilation systems -Thermal comfort and energy saving, Air Infiltration Review, 13.3, 7-10, June.

Miller P.L. and R.G. Nevins. 1972. An analysis of the performance of room air distribution systems. *ASHRAE Transactions*, 78(1): 191.

Moser, A. 1991. The message of Annex 20: air flow patterns within buildings. Proceedings of 12th AIVC conference on Air Movement and Ventilation Control within Buildings, 1: 1-26, Ottawa, Canada.

Murakami, S., S. Kato and H. Nakagawa. 1991. Numerical prediction of horizontal nonisothermal 3-D jet in room based on κ – ε model. *ASHRAE Transactions*, 97(1): 38-48.

Nielsen, P.V. 1974. Flow in air conditioned rooms, Ph.D. Thesis, Technical University of Denmark.

Nielsen, P.V. 1988. Displacement ventilation in a room with low-level diffusers. Presented at the Kaelte-Klima-Tagung, Deutscher Kaelte- und Klimatechnischer Vereine. V., Munich.

Nielsen, P.V. 1992a. Description of supply openings in numerical models for room air distribution. *ASHRAE Transactions*, 98(1): 933-971.

Nielsen, P.V. 1992b. Air distribution system-room air movement and ventilation effectiveness. *Proceedings of the International Symposium on Room Air Convection and Ventilation Effectiveness Conference*, Society of Heating, Air-Conditioning and Sanitary Engineers of Japan, Tokyo.

Nielsen P.V. 1994. Displacement ventilation-theory and design. Department of Building Technology and Structural Engineering, Aalborg University, Denmark.

Nielsen, P.V. 1997. The box method-a practical procedure for introduction of an air terminal device in CFD calculation. Institute for Bygningsteknik, Aalborg University, Denmark.

Niu, J.L. 1994. Modelling of cooled-ceiling air-conditioning systems-influences on indoor environment and energy consumption. Thesis, Delft University of Technology, Netherlands.

Niu, J.L. and J. Burnett. 1998. Integrating radiant/operative temperature controls into building energy simulation programs. *ASHRAE Transactions*, 104(2): 210-217.

Niu, J.L. and J.V.D. Kooi. 1993. A dynamic cooling load program for cooled ceiling systems and its validation in a climate room. *Proceedings of the 3rd International Congress CLIMA-2000*, November 1-3, London.

Niu, J.L., J.V.D. Kooi and H.V.D. Ree. 1995. Energy saving possibilities with cooled-ceiling systems. *Energy and Buildings*, 23(2): 147-158.

Niu J.L. and L.W. Chuk. 2001. CFD Simulation of Turbulent Combustion and Mixing Processes Upstream of Desiccant Wheel. *ASHRAE Transactions*, 107(2): 517-524.

Niu J.L., L.Z. Zhang and H.G. Zuo. 2002. Energy saving potential of chilled-ceiling combined with desiccant cooling in hot and humid climate. *Energy and Buildings*, 34(5): 487-495.

Niu J.L. and X. Ch. Xu. 1988. Calculation of Turbulent Exchange Coefficients in the Swirled-type Pre-combustion Chamber for Pulverised-coals. *Journal of Engineering Thermophysics*, 1: 20-26 *(in Chinese with an English abstract).*

Nottage, H.B. 1951. Ventilation jets in room air distribution. PhD Dissertation, Case Institute of Technology, Cleveland, Ohio.

Novoselac A. and J. Srebric. 2002. A critical review on the performance and design of combined cooled ceiling and displacement ventilation systems. *Energy and Buildings*, 34(5): 497-509.

Ozoe, H., A. Mouri, M. Hiramatsu, S.W. Churchill and N. Lior. 1984. Numerical calculation of three-dimensional turbulent natural convection in a cubical enclosure using a two-equation model. *American Society of Mechanical Engineers, Heat Transfer Division, (Publication) HTD*, 32: 25-32.

Papageorgakis, G.C. and D.N. Assanis. 1999. Comparison of Linear and Nonlinear RNG-based k-ε models for Incompressible Turbulent Flows. *Numerical Heat Transfer*, Part B, 35(1): 1-22.

Patankar S.V. and D.B. Spalding. 1972. A calculation procedure for heat mass and momentum transfer in three dimensional parabolic flows. *International Journal of Heat and Mass Transfer*, 15: 1787-1806.

Patankar, S.V. 1980. Numerical heat transfer and fluid flow. Hemisphere Publishing Corporation.

Raithby G.D. and G.E. Schneider. 1988. Elliptic system: finite difference method II, in W.J. Minkowycz, E.M. Sparrow, R.H. Pletcher, and G.E. Schneider (eds.), *Handbook of Numerical Heat Transfer*, pp. 241-289, New York.

Rao A.N., V. Ganesan, K.V. Gopalakrishnan, and R. Natarajan. 1983. Experimental and Theoretical Investigations of Vane-Generated Swirling Flows in a Circular Chamber. *Journal of the Institute of Energy*, 56(428): 137-144.

Ren, Z. and J. Stewart. 2003. Simulating air flow and temperature distribution inside buildings using a modified version of COMIS with sub-zonal divisions. *Energy and Buildings*, 35(3): 257-271.

Reynolds, Q. 1895. On the dynamical theory of incompressible viscous fluids and the determination of the criterion. *Philosophical Transactions of the Royal Society of London, Series A*, 186: 123-164.

Rockey, K.C., H.R. Evans, D.W. Griffiths and D.A. Nethercot. 1983. The finite element method: a basic introduction. Granada, London, 2nd Edition.

Sampers, W.F.J., A.P.G.G. Lamers and A.A. Van Steenhoven. 1992. Experimental and numerical analysis of a turbulent swirling flow in a tube. *Institution of Chemical Engineers Symposium Series*, **2**(129): 765–771.

Sandberg M. and C. Blomqvist. 1989. Displacement ventilation in office rooms. *ASHRAE Transactions*, 95(2): 1041-1049.

Sandberg M. and M. Sjoberg. 1984. A comparative study of the performance of general ventilation systems in evacuating contaminants. *Proceedings of Indoor Air*, 5: 59-64.

Schibuola, L. 1999. Simplified evaluation of building energy requirement for air conditioning. *International Journal of Energy Research*, 23(9): 741-750.

Schiller, G., E. Arens, F. Bauman, C. Benton, M. Fountain and T. Doherty. 1988. A field study of thermal environments and comfort in office buildings. *ASHRAE Transactions*, 94(2): 280-308.

Shakerin, S. and P.L. Miller. 1996. Experimental study of vortex diffusers. *ASHRAE Transactions*, 102(2): 340-346.

Shute, R.W. 1992. Integrated access floor HVAC. *ASHRAE Transactions*, 98(1): 730-737.

Shute, R.W. 1995. Integrated access floor HVAC: lessons learned. *ASHRAE Transactions*, 101(2): 877-886.

Shyy W. and R. Mittal. 1998. Solution methods for the incompressible Navier-Stokes equations, in R.W. Johnson (ed.), Handbook of Fluid Dynamics, 31.1-31.33, CRC Press, Boca Raton.

Singer J.G. 1981. Combustion. 4-33, Combustion Engineering, Inc., Windson.

Skistad, H. 1994. Displacement ventilation. Taunton, Somerset, England: Research Studies Press Ltd.

Skovgaard, M., P.V. Nielsen. 1991. Modelling complex inlet geometries in CFD-applied to air flow in ventilated rooms. *Proceedings of the 12th AIVC Conference on Air Movement and Ventilation Control within Buildings*, 3: 183-199, Ottawa, Canada.

Sodec, F. 1999. Economic viability of cooling ceiling systems. *Energy and Buildings*, 30(2): 195-201.

Sodec, F. and R. Craig. 1990. Underfloor air supply system-the European experience. *ASHRAE Transactions*, 96(2): 690-695.

Speziale, C. G. and S. Thangam. 1992. Analysis of an RNG Based Turbulence Model for Separated Flows. *International Journal of Engineering Science*, 30(10): 1379-1388.

Srebric, J. 2000. Simplified methodology for indoor environment design. PhD Thesis. Massachusetts Institute of Technology, USA.

Srebric, J. and Q. Chen. 2001a. Boundary conditions for diffusers in room air distribution calculations. *Proceedings of CLIMA 2000*, Napoli, Italy.

Srebric, J. and Q. Chen. 2001b. A method of test to obtain diffuser data for CFD modeling of room airflow. *ASHRAE Transactions*, 107(2): 108-116.

Srebric, J. and Q. Chen. 2002. Simplified Numerical Models for Complex Air Supply Diffusers. *HVAC and R Research*, 8(3): 277-294.

Stockwell N., C. Zhang, T. Ishii, and Y. Hino. 2001. Numerical Simulation of Turbulent Non-Premixed Combustion in a Regenerative Furnace. *ISIJ International*, 41(10): 1272-1281.

Sun Y. and T.F. Smith. 2005. Air flow characteristics of a room with square cone diffusers. *Building and Environment*, 40(5): 589-600.

Svensson, A.G.L. 1989. Nordic experiences of displacement ventilation systems. *ASHRAE Transactions*, 95(2): 1013-1017.

Tao, W.Q. 2001. Numerical heat transfer. Xi'an Jiaotong University Press, Xi'an.

Tao, W.Q., Z.G. Qu and Y.L. He. 2004a. A novel segregated algorithm for incompressible fluid flow and heat transfer problems-CLEAR (Coupled and Linked Equations Algorithm Revised) part I: mathematical formulation and solution procedure. *Numerical Heat Transfer*, Part B, 45(1): 1-17.

Tao, W.Q., Z.G. Qu and Y.L. He. 2004b. A novel segregated algorithm for incompressible fluid flow and heat transfer problems-CLEAR (Coupled and Linked Equations Algorithm Revised) part II: application examples. solution procedure. Numerical Heat Transfer, Part B, Vol. 45(1), pp. 19-48.

Tekriwal P. 1994. Heat Transfer Predictions with Extended & kappa-ε Turbulence Model in Radical Cooling Ducts Rotating in Orthogonal Mode, *Journal of Heat Transfer, Transactions of the ASME*, 116(2): 369-382.

Tennekes, H. and J.L. Lumley. 1972. A first course in turbulence, MIT Press, London.

Tennekes, H. and J.L. Lumley. 1977. A first course in turbulent shear flows, Studies in Convection, 2: 1. Academic Press, London.

Thakur S.S. and W. Shyy. 1998. Multiblock interface treatments in a pressure-based flow solver. *Numerical Heat Transfer*, Part B, 33(4): 367-396.

Tritton, D.J. 1988. Convection, Physical fluid dynamics, Clarendon, Oxford, 2nd edition, 14: 163-165.

Trox. 2002. Product information. Trox USA, Alpharetta, Ga, http://www. troxusa.com.

Van Doormaal, J.P. and G.D. Raithby. 1984. Enhancements of the SIMPLE method for predicting incompressible fluid flows. *Numerical Heat Transfer*, 7(2): 147-163.

Van Doormaal, J.P. and G.D. Raithby. 1985. An evaluation of the segregated approach for predicting incompressible fluid flow. ASME Paper 85-HT-9.

Versteeg, H.K. and W. Malalsekera. 1995. An introduction to computational fluid dynamics. The finite volume method. Essex: Longman Scientific & Technical.

Visser J.A. and J. Du Plessis. 1992. Swirling Flow in a Closed Combustion Chamber. *Proceedings of the 2nd International Conference on Advanced Computational Methods in Heat Transfer*, 2: 665-676, Milan, Italy.

Vivian L., B. Rohini, M. Michelle, V. Edward and M. Mike. 2002. Energy savings potential of flexible and adaptive HVAC distribution systems for office buildings, ARTI21-CR Research Project 605-30030, Carnegie Mellon University, Pittsburgh, PA.

Vogel P., E. Richter and M. Rosler. 1993. The effect of various inlet conditions on the flow pattern in ventilated rooms-measurements and computations. *Proceedings of the 14th AIVC Conference on Energy Impact of Ventilation and Air Infiltration*: 99-108, Copenhagen, Denmark.

Webster T., F. Bauman and J. Reese. 2002. Underfloor air distribution: Thermal stratification. *ASHRAE Journal*, 44(5): 28-30+32+34+36.

White, F. 1974. Viscous fluid flow. New York: McGraw-Hill.

Wilkins C.K. and R. Kosonen. 1992. Cool Ceiling system: A European air-conditioning alternative. *ASHRAE Journal*, 34: 41-45.

Winkelmann F.C., B.E. Birdsall, W.F. Buhl, K.L. Ellington, A.E. Erdem, J.J. Hirsch and S. Gates. 2003. DOE-2 Supplement, Version 2.1E, LBL-34947, Lawrence Berkeley National Laboratory, National Technical Information Service, Virginia, Springfield, November.

Wolf, D.M. 1994. TRANSYS - space transportation system preliminary design software. *Journal of Spacecraft and Rockets*, 31(6): 1067-1071.

Xu H.T. and J.L. Niu. 2003. CFD Simulation of Airflow Characteristics of Swirling Floor Diffusers. *Proceedings of the 8th International IBPSA Conference*, 3:1429-1433, Eindhoven, Netherlands.

Xu H.T. and J.L. Niu. 2004. Numerical simulation and experimental validation of the swirling turbulent airflow and mixing processes. *Numerical Heat Transfer*, Part A, 46(6): 571-586.

Yakhot, V. and S.A. Orszag. 1986. Renormalization group analysis of turbulence: basic theory. *Journal of Scientific Computing*, 1(1): 3-51.

Yakhot, V., S.A. Orszag, S. Thangam, T.B. Gatski and C.G. Speziale. 1992. Development of Turbulence Models for Shear Flows by a Double Expansion Technique. *Physics of Fluids*, 4(7): 1510-1520.

Yik, F.W.H., J. Burnett, P. Jones and W.L. Lee. 1998. Energy performance criteria in the Hong Kong Building Environmental Assessment Method. *Energy and Buildings*, 27(2): 207-219.

Yuan, X., Q. Chen and L.R. Glicksman. 1998. A critical review of displacement ventilation. *ASHRAE Transactions*, 104(1): 78-90.

Yuan, X., Q. Chen and L.R. Glicksman. 1999. Models for prediction of temperature difference and ventilation effectiveness with displacement ventilation. *ASHRAE Transactions*, 105(1): 353-367.

Yuan, X., Q. Chen, L.R. Glicksman, Y. Hu, and X. Yang. 1999. Measurements and computations of room airflow with displacement ventilation. *ASHRAE Transactions*, 105(1): 340-352.

Zhang, J.S., L.L. Christianson and G.L. Riskowski. 1990. Regional airflow characteristics in a mechanically ventilated room under non-isothermal conditions. *ASHRAE Transactions*, 96(1): 751-759.

Zhang, L.Z., J.L. Niu. and H.G. Zuo. 2003. Indoor humidity behaviours associated with decoupled cooling in hot and humid climate. *Building and Environment*, 38(1): 99-107.

Zhao Q.W. and C.K. Chan. 2000. Interaction between Coal-Laden Primary Air and Opposed Jets in Jet Precombustion Burner. *Annual International Pittsburgh Coal Conference*: 1915-1925.

Zhou B., X.L. Wang R.X. Li and L.X. Zhou. 1993. Swirling Gas-Particle Flows and Coal Combustion in a Spouting-Cyclone Combustor. *American Society of Mechanical Engineers, Heat Transfer Division, (Publication) HTD*, 250: 243-247.

Zhou X., Z. Sun, F. Durst, and G. Brenner. 1999. Numerical Simulation of Turbulent Jet Flow and Combustion. *Computers and Mathematics with Applications*, 38(9-10): 179-191.

APPENDIX A PD MODEL PROGRAM

```
#include "udf.h"
DEFINE_ON_DEMAND(pd)
{
   real avev,ta,u,v,w,tu;
   Domain *d;
   Thread *t;
   cell_t c;
   d = Get_Domain(1);
   thread_loop_c(t,d)
{
  if (NNULLP(THREAD_STORAGE(t,SV_UDM_I)))
{
     begin_c_loop(c,t)
{
     ta=C_T(c,t)-273.15;
     u=C_U(c,t);
     v=C_V(c,t);
     w=C_W(c,t);
     avev=sqrt(u*u+v*v+w*w);
     tu=sqrt(2.0*C_K(c,t)/3.0)/avev;
     C_UDMI(c,t,0)=(34.0-ta)*pow(fabs(avev-0.05),0.62)*(0.37*avev*tu+3.14);
 }
     end_c_loop(c,t)
 }
 }
 }
```

APPENDIX B PMV MODEL PROGRAM

```
#include "udf.h"
real RadiationTemperature(cell_t c, Thread *t)
{
   real IncRad = 0.;
   real RadTmp = 0.;
   if (sg_p1 && FLUID_THREAD_P(t))
   IncRad = C_P1(c,t);
   else if (sg_disco)
   IncRad = C_STORAGE_R_XV(c,t,SV_DO_IRRAD,0);
   else
      IncRad = 0.;
   RadTmp = pow(IncRad/(4.*SIGMA_SBC),0.25);
   return RadTmp;
}
DEFINE_ON_DEMAND(pmv)
{
   real,icl,mw,pa,eps,ww,fcl,fcic,p2,p3,tra,ta,taa,p1,p4,tcla,tcl,xn,xf,u,v,w,
   var,hcf,hcn,hc,pm1,pm2,pm3,pm4,ppmmvv;
  Domain *d;
  Thread *t;
  cell_t c;
  d = Get_Domain(1);
  thread_loop_c(t,d)
{
  if (NNULLP(THREAD_STORAGE(t,SV_UDM_I)))
{
  begin_c_loop(c,t)
{
 /*real RadiationTemperature(cell_t c, Thread *t)*/

      real IncRad = 0.;
      real RadTmp = 0.;
      if (sg_p1 && FLUID_THREAD_P(t))
          IncRad = C_P1(c,t);
      else if (sg_disco)
          IncRad = C_STORAGE_R_XV(c,t,SV_DO_IRRAD,0);
      else
          IncRad = 0.;
      RadTmp = pow(IncRad/(4.*SIGMA_SBC),0.25);

/*          The unit of RadTmp and taa is K not c        */

      m=70.0;
      icl=0.7;
      ww=0.0;
      mw=m-ww;
```

```
        pa=1500.;
        eps=0.00015;
        fcl=1.05+0.1*icl;
        if(0.155*icl<0.078) fcl=fcl-0.05+0.1*icl;
        fcic=0.155*icl*fcl;
        p2=fcic*3.96;
        p3=fcic*100;
        tra=RadTmp;
        ta=C_T(c,t)-273;
        taa=C_T(c,t);
        p1=fcic*taa;
        p4=308.7-0.028*mw+p2*pow(tra/100.,4);
        tcla=taa+(35.5-ta)/(3.5*(icl+0.1));
        xn=tcla/100.;
        xf=xn;
        u=C_U(c,t);
        v=C_V(c,t);
        w=C_W(c,t);
        var=sqrt(u*u+v*v+w*w);
        hcf=12.1*sqrt(var);
loop1:  xf=(xf+xn)/2;
        hcn=2.38*pow(abs(100.*xf-taa),0.25);
        hc=hcf;
        if(hcn>hcf) hc=hcn;
        xn=(p4+p1*hc-p2*pow(xf,4))/(100.+p3*hc);
        if(abs(xn-xf)>eps) goto loop1;
        tcl=100*xn-273;
        pm1=3.96*fcl*(pow(xn,4)-pow(tra/100.,4));
        pm2=fcl*hc*(tcl-ta);
        pm3=0.303*exp(-0.036*m)+0.028;
        pm4=0.0;
        if(mw>58.15) pm4=0.42*(mw-58.15);
        ppmmvv=pm3*(mw-3.05*0.001*(5733.-6.99*mw-pa)-pm4-
                1.7*0.00001*m*(5867.-pa)-0.0014*m*(34.-ta)-pm1-pm2);
        C_UDMI(c,t,0)=ppmmvv;
        C_UDMI(c,t,1)=100.-95.*exp(-0.03353*pow(ppmmvv,4)-
                        0.2179*pow(ppmmvv,2));
    }
   end_c_loop(c,t)
    }
    }
    }
```

APPENDIX C SYSTEM ENERGY SIMULATION PROGRAM

```
C----------------------------------WESIMULATION.FOR--------------------------------C
C---------------------------------------16, NOV. 2004-----------------------------------C
C----------------------------------THIS PROGRAM IS FOR THE WHOLE ENERGY CONSUMPTION SIMULATION, BASED ON THE CALCULATED RESULTS FROM Dr. Niu's PROGRAM ACCURACY.-----------------------------------------C
C----------------THE BASIC EQUATIONS ARE AS FOLLOWS:----------------C
C       D:          AIR VOLUME (M**3/HOUR)[10ACH]
C       ET:         THE DIMENSIONLESS TEMPERATURE COEFFICIENT
C                   FOR MIXED VENTILATION SYSTEM ET=1.0
C                   FOR DV AND UFAD SYSTEMS, ET>1.0 (STRATIFICATION)
C       MASSR:    HUMIDITY GENERATED IN ROOM (G/S)
C       MFREE:    AIR MASS FLOW RATE DURING FREE COOLING (M**3/S)
C       M1:         FRESH AIR MASS FLOW RATE (KG/S)
C       M2:         RETURN AIR MASS FLOW RATE (KG/S)
C       M3:         M1+M2 (KG/S)
C       MFRESH:  FRESH AIR MASS FLOW RATE WHEN
                    ENTH(TOUT,WOUT).LE.ENTH(TE,WE)
C       NACCUNT: THE COUNTER FOR FREE COOLING TIME
C       P:              PRESSURE RISE OF AIR FAN (N/M**2, e.g. 1400 Pa)
C      Q=QSPACE+QVENT=QSPACE+M*Cp*(TOUT-ET*TD-(1-ET)*TSUPPLY)
C      OR Q=QSPACE+QVENT=QCC+M*Cp*(TOUT-TD)
C       QSPACE:     THE CALCULATED RESULT FROM ACCURACY (W)
C       QVENT:      THE VENTILATION ENERGY CONSUMPTION (W)
C       QCC:        COOLING LOAD IN THE OCCUPIED ZONE
C       RHR:        RELATIVE HUMIDITY OF ROOM AIR (%)
C       RHS:        RELATIVE HUMIDITY OF SUPPLY AIR (%)
C       RV:         FAN EFFICIENCY ( e.g., 0.60)
C       TD:         DESIGNED ROOM AIR TEMPERATURE
C       TDEWR:      DEW POINT TEMPERATURE OF ROOM AIR (℃)
C       TDEWS:      DEW POINT TEMPERATURE OF SUPPLY AIR (℃)
C       TOUT:       OUTDOOR AIR TEMPERATURE (℃)
C       TSUPPLY:    SUPPLY AIR TEMPERATURE CALCULATED FROM
                    ACCURACY (℃)
C       WA:         HUMIDITY OF DEALT FRESH AIR (g/kg)
C       WE:         HUMIDITY OF ROOM AIR (g/kg)
C       WOUT:       HUMIDITY OF OUT AIR (g/kg)
C       WS:         HUMIDITY OF SUPPLY AIR (g/kg)
C-----------------------------------------------------------------------------------------C
      COMMON /CONSTANT/C8, C9, C10, C11, C12, C13, C14, C15, C16, C17,
     & C18
      DATA C8,C9, C10, C11, C12, C13, C14, C15, C16, C17,C18/
     &-5.800 220 6 E+03, -5.516 256 0, -4.864 023 9 E-02, 4.176 476 8
     &E-05, -1.445 209 3 E-08, 6.545 967 3,  6.54, 14.526, 0.7389
     &,0.09486, 0.4569/
      REAL M1,M2,M3,MFRESH,MASSR
```

```
      OPEN(10,FILE='For Energy Consumption Simulation-CC+DV.dat')
      OPEN(11,FILE='Energy Simulation-CC+DV.DAT')
      OPEN(12,FILE='weather.dat')
      COP=3.65
      CP=0.997
      D=5.1*3.6*2.6
      MASSR=0.032/1000
      M3=5*D/3600*1.2
      M1=M3
      M2=0
      NACCOUNT=0
      P=1400
      PATM=101300
      RV=0.65
      DO 20  I=1,8760
      READ(10,30) TOUT,QSPACE,QPANEL,TSUPPLY,TPANEL,TD,NMONTH,
     &NDAY,IHOUR
      READ(12,40) ITDEW
      TDEW=0.1*ITDEW
      IF(IHOUR.LE.8.OR.IHOUR.GE.19) THEN
        GOTO 20
      ENDIF
      RHR=0.55
      QPANEL=QPANEL/1000.
      QSPACE=QSPACE/1000.
      TE=TD
      CALL TDEW2A(TDEW,TOUT,PATM,RHOUT,WOUT)
70    CALL RH2ALL(RHR,TD,PATM,WE,TDEWE)
      IF(ENTH(TOUT,WOUT).LT.ENTH(TE,WE)) THEN
      MFRESH=QSPACE*1000./(ENTH(TE,WE)-ENTH(TOUT,WOUT))
         IF(MFRESH.LE.M3) THEN
              WS=WOUT
              TM=TOUT
              TSUPPLY=TOUT
              WE=WOUT+MASSR/MFRESH
              CALL W2ALLP(WE,TD,PATM, RHR1,TDEWR)
              IF(ABS((RHR-RHR1)/RHR).GT.0.001) THEN
                   RHR=RHR+(RHR1-RHR)*0.01
                   GOTO 70
              ENDIF
             QVENT=0.0
             Q=QSPACE+QVENT+QPANEL
             QFAN=(P*MFRESH)/(1.2*RV*1000.)
             QCHILLER=0.0
             RHS=RHOUT
             NACCOUNT=NACCOUNT+1
             NN=1
             WRITE(11,50) TOUT,TM,TSUPPLY,TPANEL,TE,NMONTH,NDAY,
     & IHOUR, NACCOUNT,QSPACE,QPANEL,QVENT,Q,QCHILLER, QFAN,
     & M1,MFRESH,RHS,RHR,NN
```

```
                GOTO 20
   ELSE
          RHS=0.95
          CALL RH2ALL(RHS,TSUPPLY,PATM,WS,TDEWS)
          WE=WS+MASSR/M3
          WM=M2/M3*WE+M1/M3*WOUT
           IF(WM.GE.WS) THEN
           CALL W2ALLP(WE,TD,PATM, RHR1,TDEWR)
           IF(ABS((RHR-RHR1)/RHR).GT.0.001) THEN
                  RHR=RHR+(RHR1-RHR)*0.01
                  GOTO 70
           ENDIF
           MFRESH=M1
           QVENT=M1*(ENTH(TE,WE)-ENTH(TOUT,WOUT))/1000.
           Q=QSPACE+QVENT+QPANEL
           QFAN=P*M3/(1.2*RV*1000.)
           QCHILLER=Q/COP
            NN=2
   WRITE(11,50) TOUT,TM,TSUPPLY,TPANEL,TE,NMONTH,NDAY,
& IHOUR, NACCOUNT,QSPACE,QPANEL,QVENT,Q,QCHILLER, QFAN,
& M1,MFRESH,RHS,RHR,NN

            GOTO 20
        ELSE
          WS=WM
          WE=WS+MASSR/M3
          CALL W2ALLP(WS,TSUPPLY,PATM, RHS,TDEWS)
          CALL W2ALLP(WE,TD,PATM, RHR1,TDEWR)
        IF(ABS((RHR-RHR1)/RHR).GT.0.001) THEN
              RHR=RHR+(RHR1-RHR)*0.01
              GOTO 70
        ENDIF
        MFRESH=M1
        QVENT=M1*(ENTH(TE,WE)-ENTH(TOUT,WOUT))/1000.
        Q=QSPACE+QVENT+QPANEL
        QFAN=P*M3/(1.2*RV*1000.)
        QCHILLER=Q/COP
        NN=3
   WRITE(11,50) TOUT,TM,TSUPPLY,TPANEL,TE,NMONTH,NDAY,
& IHOUR, NACCOUNT,QSPACE,QPANEL,QVENT,Q,QCHILLER, QFAN,
& M1,MFRESH,RHS,RHR,NN
             GOTO 20
           ENDIF
       ENDIF
     ENDIF
  RHS=0.95
  MFRESH=M1
  CALL RH2ALL(RHS,TSUPPLY,PATM,WS,TDEWS)
  WE=WS+MASSR/M3
  WM=M2/M3*WE+M1/M3*WOUT
```

```
      IF(WM.GE.WS) THEN
        CALL W2ALLP(WE,TD,PATM, RHR1,TDEWR)
          IF(ABS((RHR-RHR1)/RHR).GT.0.001) THEN
            RHR=RHR+(RHR1-RHR)*0.01
            GOTO 70
          ENDIF
          QVENT=M1*(ENTH(TOUT,WOUT)-ENTH(TE,WE))/1000.
          Q=QSPACE+QVENT+QPANEL
          QFAN=P*M3/(1.2*RV*1000.)
          QCHILLER=Q/COP
          NN=4
       WRITE(11,50) TOUT,TM,TSUPPLY,TPANEL,TE,NMONTH,NDAY,
     & IHOUR, NACCOUNT,QSPACE,QPANEL,QVENT,Q,QCHILLER, QFAN,
     & M1,MFRESH,RHS,RHR,NN
          GOTO 20
        ELSE
       WS=WM
       WE=WS+MASSR/M3
       CALL W2ALLP(WE,TD,PATM, RHR1,TDEWR)
       IF(ABS((RHR-RHR1)/RHR).GT.0.001) THEN
            RHR=RHR+(RHR1-RHR)*0.01
            GOTO 70
          ENDIF
          QVENT=M1*(ENTH(TOUT,WOUT)-ENTH(TE,WE))/1000.
          Q=QSPACE+QVENT+QPANEL
          QFAN=P*M3/(1.2*RV*1000.)
          QCHILLER=Q/COP
          NN=5
       WRITE(11,50) TOUT,TM,TSUPPLY,TPANEL,TE,NMONTH,NDAY,
     & IHOUR, NACCOUNT,QSPACE,QPANEL,QVENT,Q,QCHILLER, QFAN,
     & M1,MFRESH,RHS,RHR,NN
          GOTO 20
        ENDIF
30    FORMAT(1X,F4.1,2(1X,F7.2),3(1X,F5.1),3X,I2,1X,I3,1X,I2)
40    FORMAT(107X,I4)
50    FORMAT(5(1X,F4.1),1X,I2,1X,I3,1X,I2,1X,I4,5(1X,F6.3),1X,F7.3,
     & 2(1X,F5.3),2(1X,F4.2),1X,I1)
20    CONTINUE
      CLOSE(10)
      CLOSE(11)
      CLOSE(12)
      WRITE(*,*)'----------------THE-------------END-----------------'
      END
C-------------------------------------------------------------------------------------------C
      SUBROUTINE TDEW2A(TDEWc, TR, PATM, RHMOIS, WMOIST)
      REAL LNPW, LNPWS
      COMMON /CONSTANT/C8, C9, C10, C11, C12, C13, C14, C15, C16, C17
     &,C18
      TDEW= TDEWc + 273.15
      TDRYBL = TR + 273.15
```

```
      LNPW=C8/TDEW + C9 + C10*TDEW + C11*TDEW*TDEW + C12
     &*TDEW*TDEW*TDEW + C13 * ALOG(TDEW)
      LNPWS=C8/TDRYBL + C9 + C10*TDRYBL + C11*TDRYBL*TDRYBL +
     & C12 *TDRYBL*TDRYBL*TDRYBL + C13 * ALOG(TDRYBL)
      PW=EXP(LNPW)
      PWS =EXP(LNPWS)
      RHMOIS=PW/PWS
      WMOIST=0.622*PW/(PATM*0.001 - PW)
      RETURN
      END
C-----------------------------------EQUATIONS ARE ADAPTED FROM ASHRAE
HANDBOOK, FUNDAMENTALS-----------------------------------------------------C
      SUBROUTINE W2ALLP(WMOIST, TR, PATM, RHMOIS, TDEW)
      REAL LNPWS
      COMMON /CONSTANT/C8, C9, C10, C11, C12, C13, C14, C15, C16, C17
    &,C18
      PW=WMOIST*PATM/(0.622 + WMOIST)
      TDRYBL=273.15+TR
      LNPWS=C8/TDRYBL + C9 + C10*TDRYBL + C11*TDRYBL*TDRYBL +
    & C12 *TDRYBL*TDRYBL*TDRYBL + C13 * ALOG(TDRYBL)
      PWS=EXP(LNPWS)*1000.
      RHMOIS=PW/PWS
      ALPHAT=ALOG(PW*0.001)
      TDEW = C14 + C15* ALPHAT + C16 * ALPHAT*ALPHAT + C17*ALPHAT
    & *ALPHAT*ALPHAT + C18 * (PW*0.001)**0.1984
      RETURN
      END
C-------------------------------------------------------------------------------------------C
      SUBROUTINE RH2ALL(RH, T, PATM, AWS, TDEW)
      COMMON /CONSTANT/C8, C9, C10, C11, C12, C13, C14, C15, C16, C17
    &,C18
      REAL LNPWS
      TDRYBL=273.15 + T
      LNPWS=C8/TDRYBL + C9 + C10*TDRYBL + C11*TDRYBL*TDRYBL +
    & C12 *TDRYBL*TDRYBL*TDRYBL + C13 * ALOG(TDRYBL)
      PWS=EXP(LNPWS)*1000.
      PW = RH * PWS
      AWS = 0.622 * PW /(PATM - PW)
      ALPHAT=ALOG(PW*0.001)
      TDEW = C14 + C15* ALPHAT + C16 * ALPHAT*ALPHAT + C17*ALPHAT
    & *ALPHAT*ALPHAT + C18 * (PW*0.001)**0.1984
      RETURN
      END
C-------------------------------------------------------------------------------------------C
      FUNCTION ENTH(T,X)
     ENTH=1010*T+X*(2500+1.84*T)
     END
C-------------------------------------------------------------------------------------------C
```